RADIUM ISOTOPES AS TRACERS OF COASTAL CIRCULATION PATHWAYS IN THE MID-ATLANTIC BIGHT

by

Linda L. Rasmussen

M.S., Florida State University, 1998

Submitted in partial fulfillment of the requirements for the degree of

Doctor of Philosophy

at the
MASSACHUSETTS INSTITUTE OF TECHNOLOGY
and the
WOODS HOLE OCEANOGRAPHIC INSTITUTION

June 2003

Signature of Author

Joint Program in Oceanography/Applied Ocean Science and Engineering
Massachusetts Institute of Technology
and Woods Hole Oceanographic Institution
June 2003

Certified by

Dr. Ken O. Buesseler
Thesis Supervisor

Accepted by

Dr. Philip M. Gschwend
Chair, Joint Committee for Chemical Oceanography
Massachusetts Institute of Technology/
Woods Hole Oceanographic Institution

Abstract

Pathways of exchange between the shelf and slope in the Mid-Atlantic Bight were investigated using a combination of radiochemical tracer and hydrographic measurements. The motivation was to provide evidence of transport routes for shelfwater that could be important to the balance of shelf-slope exchange, as well as to the biogeochemical fluxes across this crucial ocean boundary. The four radium isotopes, with half-lives of 4 days to 1600 years, a coastal source, and conservative properties in seawater, were used as coastal water mass tracers. The final study was comprised of data from 5 cruises, with a total of 8 cross-shelfbreak transects. Two areas were studied, a northern Mid-Atlantic Bight transect south of Nantucket Shoals, and a southern Mid-Atlantic Bight series of transects off the coast of Delaware. In addition, data were collected from the shelfbreak at Cape Hatteras crossing the western wall of the Gulf Stream to help determine sources of anomalous ^{224}Ra enrichment which was observed on several of the shelfbreak transects. Combined with the hydrographic data, radium measurements suggested a pathway for exchange in the Mid-Atlantic Bight that was not a direct advection of shelf water toward the slope. Rather, the evidence suggested limited direct exchange of surface shelf water across the shelfbreak front. This provides observational evidence that is consistent with models (e.g., Gawarkiewicz and Chapman, 1991) which predict the shelfbreak front will impede exchange. Furthermore, ^{224}Ra activity on the upper slope points to a rapid transport pathway for bottom water from the Cape Hatteras shelf via the Gulf Stream onto the Mid-Atlantic Bight slope. The radiochemical and hydrographic evidence suggests that recirculation around the slope sea gyre may be a more important pathway than direct cross-shelf transport.

Acknowledgements

This work was supported by funding from the Woods Hole Oceanographic Institution Academic Programs office, the Woods Hole Oceanographic Institution Ocean Ventures Fund, National Science Foundation grant OCE-0097232, and Civilian Research and Development Foundation grant UGI-2432-SE-02.

Contents

List of Figures

List of Tables

Chapter 1

Introduction

The focus of this dissertation project has been to help determine pathways of exchange between the shelf and slope in the Mid-Atlantic Bight using a combination of radiochemical tracer and hydrographic measurements. The motivation was to provide evidence of transport routes for shelfwater that could be important to the balance of shelf-slope exchange, as well as to the biogeochemical fluxes across this crucial ocean boundary. The four radium isotopes, with half-lives of 4 days to 1600 years, a coastal source, and conservative properties in seawater, were ideal candidates to conduct such a study.

Although research has been intensive in this area for the past 15-20 years, still only "crude estimates" of cross-shelf exchange rates exist (Loder et al. 1998). Physical observations and modeling of exchange across the shelfbreak over the past 15 years have clarified some of the processes operating there (Chapman and Lentz 1994; Gawarkiewicz and Chapman 1991; Pickart 2000; Houghton and Visbeck 1998), but exact mechanisms are still unclear. Loder et al. note that the estimates that do exist do not identify the mechanisms of exchange, where the exchange takes place, and how seasonal or longer variability affects the estimates. Gulf Stream ring effects on the slope and outer shelf have been noted along with other processes that are suspected to play some role (frontal eddies, flow through

canyons, wind forcing) but the magnitude to which each contributes to cross-shelf exchange is considered to be "poorly known in general."

1.1 New uses for radium tracers

Previous work with radium tracers had observed smooth, exponential distributions across the South Atlantic Bight shelf that were used to estimate horizontal eddy diffusivity and groundwater inputs (Moore 1997; Moore 1996). I set out to expand this line of inquiry in several respects. First, short-lived radium tracers had not been used in the shelfbreak region. Preliminary measurements suggested that activities up to 200 km from shore were still high enough to make useful observations of shelfwater exchange across the shelfbreak front.

Secondly, physical circulation in the Mid-Atlantic Bight is characterized by processes which are highly energetic, episodic, small scale, and of short duration (Gawarkiewicz et al. submitted 2002; Gawarkiewicz et al. 1996b; Gawarkiewicz et al. 1990; Churchill and Cornillon 1991; Garvine et al. 1988; Garvine et al. 1989; Beardsley et al. 1985). These include many advective processes, such as Gulf Stream ring intrusion, entrainment of shelfwater streamers, wind forcing, bottom boundary layer transport, and effects of frontal eddies. Because of the nature of the circulation in the Mid-Atlantic Bight it appeared that short-lived radium could possibly be more useful as a tracer of small-scale events than of large-scale mixing. Previously, methods for determining mixing coefficients have assumed steady-state conditions with no advection, and thus were of limited use under realistic shelfbreak conditions. However, mechanisms of physical exchange such as shelfwater streamers or other small-scale advective mechanisms might be reasonably examined using radium isotopes.

Radiotracers have the potential to provide an internal "clock" in these situations to help determine water mass ages and transport times.

1.2 Importance of Continental Shelves in Global Fluxes

The total area of continental shelves comprises only about 10% of the global ocean, yet biological activity is high enough to account for nearly half of ocean productivity (Eppley and Peterson 1979). The ocean margins are thus extremely important both economically and evironmentally. High production and sedimentation rates make ocean margins a potentially signficant location for removal of atmospheric carbon into deep ocean burial and circulation cycles. However, many questions still remain about the mechanisms and magnitude of export, as well as how nutrients are supplied to support this system. During the 1980's, the Shelf Edge Exchange Processes program conducted the SEEP I and SEEP II experiments on the eastern continental shelf of North America. SEEP II sediment trap fluxes and species composition analysis indicated on offshelf C flux which was equal to about 6% of estimated shelf primary production (Falkowski et al. 1994), while measurements of bacterial remineralization in the water column and in the sediments of the shelf and slope pointed to a lateral downslope C flux of about 7-15% of primary production (Kemp 1994). Both studies concluded that the requirement for nutrient and carbon import onto the shelf to balance the export was small, and that recycling of nutrients on the shelf must be large to support the high productivity. ^{210}Pb measurements by Bacon (1994) also indicated a small particle export to the shelf, as well as a long residence time of material on the shelf. Several of the SEEP investigators also found evidence that export events were highly episodic (Falkowski et al. 1994; Biscaye et al. 1994a).

The SEEP program uncovered or left unresolved many key questions. Among these are how nitrogen is supplied to support high levels of shelf productivity (Biscaye et al. 1994b). Import of nitrate rich deeper slope water implies a corresponding export of surface water from the shelf, but little was observed in this or subsequent studies. This problem is magnified by the results of Seitzinger & Giblin (1996) who estimated denitrification on the North Atlantic shelf via direct measurements and empirical relationships with sediment oxygen demand and surface productivity. Their results indicate that shelf sediments are a large sink for nitrogen which is not balanced by inputs from rivers and atmospheric deposition. They and Michaels et al. (1996) in a companion study on nitrogen cycling in the North Atlantic gyre, suggest the deficit is most likely balanced by the onwelling of nitrate-rich slope water. However this is contradicted by the SEEP results which indicate movement of deep shelfbreak water is downslope (offshelf), with little offshore surface advection to compensate for any onwelling of slope water (Biscaye et al. 1994a). Observational and modeling studies of circulation and shelfbreak processes in the Mid-Atlantic Bight in recent years have not resolved this problem.

1.3 Physical circulation in the Mid-Atlantic Bight

The Middle Atlantic Bight continental margin is characterized by a shallow continental shelf region (0-200 m depth spanning 100-200 km) which steepens sharply at the shelfbreak (200-2000 m depth over <50 km). The shelfbreak forms a distinct boundary between coastal and pelagic waters and their contrasting biological systems. Shelf waters are typically fresher than slope and open ocean waters because of the input of rivers, melting ice, and

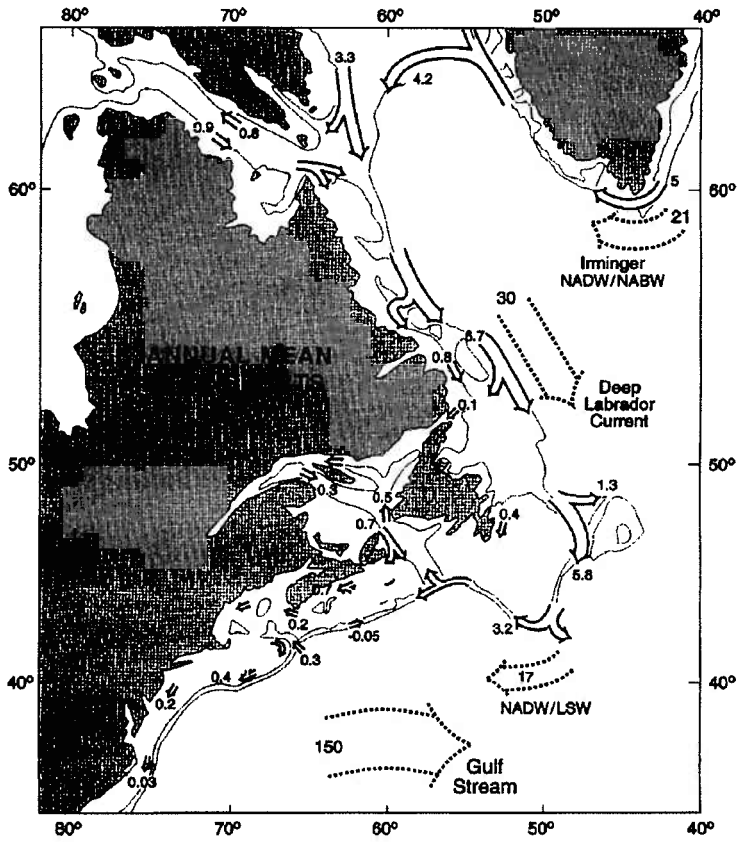

Figure 1.1: Circulation in the Mid-Atlantic Bight as part of the large scale northeastern North American coastal system. From Loder et al. (1998)

groundwater, and may also have strong temperature differences as well, especially in cold winter areas.

The large scale current system in the MAB consists of a broad south-southwestward flow which is most likely dominated by local bouyancy forcing from freshwater inputs, as well as remote buoyancy forcing resulting in a barotropic inflow from the north, as shown in Figure 1.1 (Loder et al. 1998). Mean flow over the shelf is on the order of 10 cm/s (Beardsley et al. 1985; Shearman and Lentz submitted), with substantial temporal variability (standard deviations of the same order as the mean flow). Salinity and temperature gradients across

the shelfbreak can create strong density fronts, as seen in the hydrographic sections in Figure 1.2 (Lyne and Csanady 1984) although they are sometimes density-compensating, resulting in little horizontal stratification. Strong density gradients at the shelfbreak result in the rapid current known as the shelfbreak jet, with velocities as high as 50 cm/s or more.

Density gradients and the shelfbreak jet may inhibit horizontal exchange across the front, but also create frontal eddies whose episodic action could be responsible for significant transport. Frontal eddies are spun off from meanders in the jet on the order of tens of kilometers and form on a timescale of a few days (Garvine et al. 1988). The eddies are deep features around which have been observed shallow plumes of shelf water with strong offshore flow. However calculations of cross-shelf fluxes of heat and salinity showed no significant enhancement of exchange from eddies, unless they become completely detatched from the jet (Garvine et al. 1989). Recent models also suggest the presence of upwelling cells on either side of the jet and advection of water from a shelf bottom boundary layer up along the frontal isopycnals at the shelfbreak, where they then turn downstream (Gawrkiewicz et al. 1992; Houghton 1997; Houghton and Visbeck 1998; Pickart 2000). As a result, surface advection measured seaward of the density front may actually be carrying upwelled deep slope water offshore instead of shallow shelf water. Because of the complexities of shelfbreak circulation, geochemical observations have the potential to provide a useful concrete measure of the physical processes that are occuring and the biogeochemical fluxes that may result.

1.4 Study structure and findings

The final study was comprised of data from 5 cruises, with a total of 8 cross-shelfbreak transects. Two areas were studied, a northern Mid-Atlantic Bight transect south of Nantucket

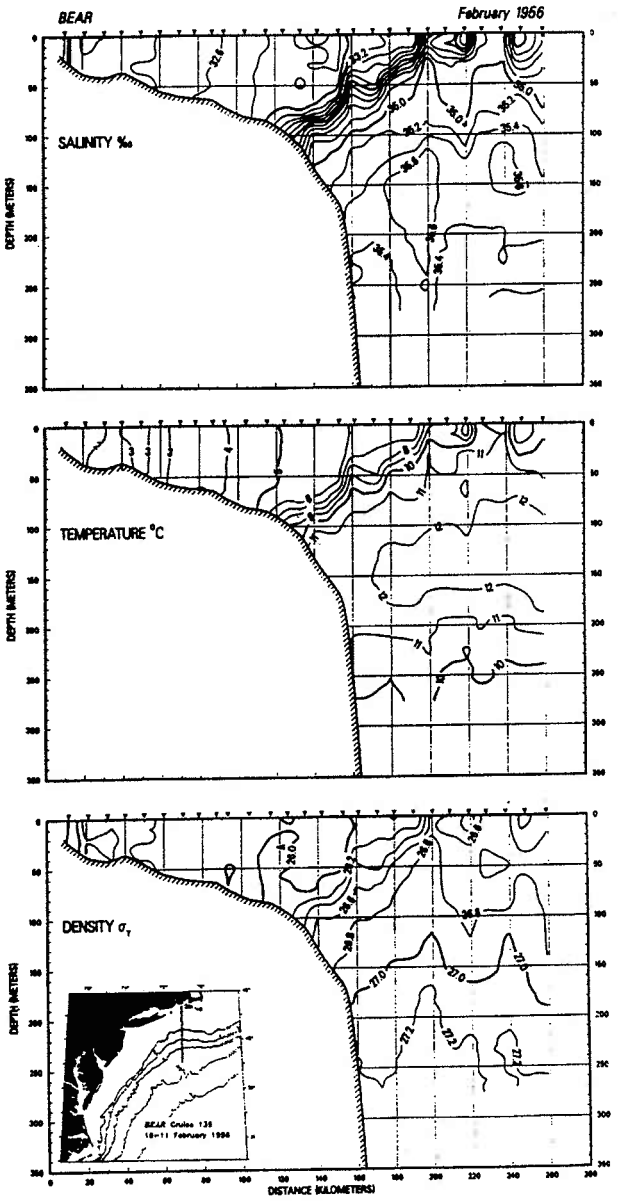

Figure 1.2: Water column structure at the Mid-Atlantic Bight shelfbreak, February 1956. From Lyne and Csanady (1984).

Shoals, and a southern Mid-Atlantic Bight series of transects off the coast of Delaware. In addition, data were collected from the shelfbreak at Cape Hatteras crossing the western wall of the Gulf Stream to help determine sources of anomalous ^{224}Ra which were observed on several of the shelfbreak transects. The results of the shelfbreak crossings were not what was expected. No evidence of recent cross-shelf transport of shelfwater was found (i.e., transport on the scale of weeks to months). On several occasions, unusually high activity of ^{224}Ra was measured beyond the shelfbreak front. However instead of being found in a shelf water mass, the anomalous ^{224}Ra was consistently found in water with high salinity, high temperature, and no characteristics of a coastal source. This appeared to contradict what was known about radium sources, and was additionally perplexing because of the lack of enrichment of the other three isotopes which normally occur together with ^{224}Ra in groundwater and river water. Bottom water sources from the Mid-Atlantic Bight shelf, though enriched in ^{224}Ra, did not supply enough activity to account for the observed ^{224}Ra peaks over the upper slope.

Physical data collected during these surveys pointed to the presence of strong frontal features, often associated with Gulf Stream influences. Transport rates measured in the southern Mid-Atlantic Bight were much higher than expected, on the order of 1-2 Sv, but were found to be consistent with the unusual hydrographic structure which included a large slopewater intrusion and a prominent Gulf Stream water mass. These transport rates, about 1 Sv higher than the most cited estimate from the Nantucket Shoals Flux Experiemtnt (Beardsley et al. 1985) could suggest that there is less cross-shelf export of shelfwater than is inferred from current budgets.

Combined with the hydrographic data, radium measurements suggested a pathway for

exchange in the Mid-Atlantic Bight that was not the direct advection of shelf water toward the slope that we anticipated. Rather, the evidence suggests limited direct exchange of surface shelf water across the shelfbreak front. This provides observational evidence that is consistent with models (e.g., Gawarkiewicz and Chapman, 1991) which predict the shelfbreak front will impede exchange. Furthermore, ^{224}Ra activity on the upper slope points to a rapid transport pathway for bottom water from the Cape Hatteras shelf via the Gulf Stream onto the Mid-Atlantic Bight slope. Although the current data set is limited, the possibility is raised that circulation around the Mid-Atlantic Bight "slope-sea gyre," with intrusions from Gulf Stream meanders and warm-core rings, may be more important for exchange between the shelf, slope and deep ocean than more direct pathways.

This study is divided into four sections which will cover the theory and analytical methods that were used or developed, Chapter 2; the overall results of the radiochemical and nutrient data collected in the Mid-Atlantic Bight, and inferences that can be drawn from them in terms of cross-shelf exchange and nutrient flux, Chapter 3; Gulf Stream and slopewater influences during an intensive hydrographic survey, with evidence of substantial alongshelf transport, Chapter 4; and finally evidence for strong Gulf Stream influence on exchange pathways in the Mid-Atlantic Bight, Chapter 5.

Chapter 2

Radium as a tracer of coastal waters:

Theory and methods of analysis

Radium is an element that has been employed increasingly in recent years to study coastal processes because its unique properties make it especially suitable as a water mass tracer (Levy and Moore 1985; Schmidt and Reyss 1996; Moore 1997; Moore and Shaw 1998; Krest et al. 1999; Moore 2000b). It is not bioactive or particle reactive in seawater, so it can be treated as a conservative tracer, and unlike salinity, it does not affect the physical properties of the water mass. Four radioactive isotopes of radium occur naturally in the environment as decay products from uranium and thorium (Figure 2.2). Radium enters the ocean when terrestrial water that has been in contact with these elements via streambottoms, suspended riverine sediments and aquifers reaches the freshwater-saltwater interface. When particulate radium encounters seawater, it is desorbed through cation exchange with sodium, calcium and magnesium. As a result there is a large input of radium in coastal marshes, estuaries, and aquifer outcrops (Moore 1996; Rama and Moore 1996; Moore and Shaw 1998). It is this nearshore flux that makes radium useful as a tracer for shelfwater circulation.

This chapter will present the theory behind use of radium as a coastal tracer; some of

the traditional methods of analysis of radium data; and finally, some new methods of data analysis that may be useful in coastal settings, particularly where advective processes are signficant. As an example, new data analysis methods will be applied to one of the "classic" data sets from the South Atlantic Bight collected by W. Moore (2000a; 2000b).

2.1 Physical properties and sources of radium

The ultimate sources of radium are rocks and minerals containing uranium and thorium, although they are present in somewhat different quantities in different types of rock (NCRP 1987). In general, rocks that are formed early in the magma cooling process (such as the dark basalts) contain the lowest activities of both isotopes, because they are incompatible with the crystal formation of these minerals. Likewise, quartz minerals contain little of these isotopes. Aluminum-silicate minerals forming late in the cooling process contain the most U and Th. Sedimentary rocks are generally higher in U and Th, especially those such as shales which contain organic material to which reduced forms of U adsorb in addition to the particle reactive Th. Comparable with shales are continental crust and soils. Carbonate rocks created from the shells and skeletons of corals and other marine biota are enriched in uranium but not thorium because of the substitution of uranium for calcium during their formation. Because of this enrichment, the radium isotopes that occur in the uranium series are also enriched in carbonates (i.e., ^{226}Ra from the ^{238}U series, and ^{223}Ra from the ^{235}U series.) Carbonate-rich apatite minerals (including phosphorites) will show similar enrichment in these minerals. It should be noted however that the natural abundance of the two U parents differs significantly, with ^{238}U accounting for over 99% of all naturally occuring uranium by mass. Thus, ^{226}Ra is considerably more abundant than ^{223}Ra, with

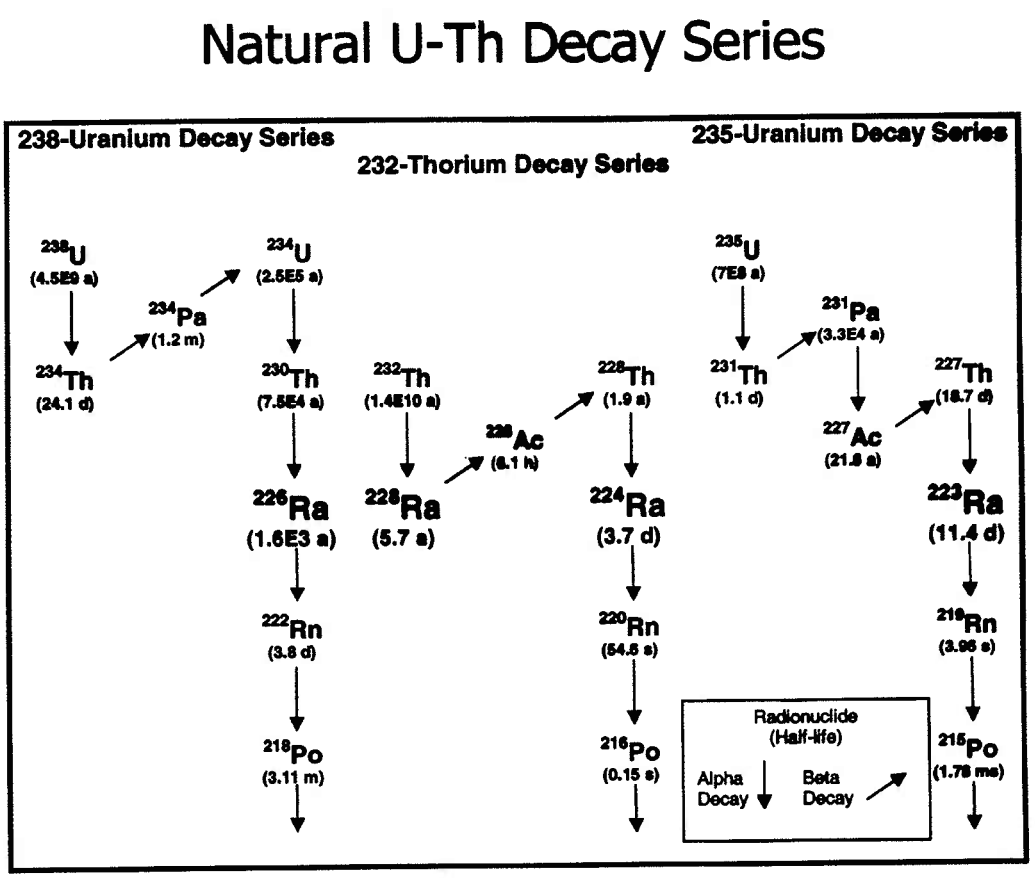

Figure 2.1: Natural uranium and thorium decay series.

activity ratios of approximately 1 : 1 : 0.05 : 1 for ^{226}Ra : ^{228}Ra : ^{223}Ra : ^{224}Ra.

All of the isotopes also have sources in the water column from parent isotopes in the uranium-thorium decay chains that are dissolved in seawater, however only ^{226}Ra is present in substantial activities in the open ocean (Broecker et al. 1967; Moore 1969; Kaufman et al. 1973; Moore 1976). The other three isotopes are less abundant due to a combination of faster radioactive decay, less abundant parent isotopes, and the presence of several particle-reactive precursors (thorium, protactinium and actinium) which are scavenged from the water column. While ^{228}Ra is present in small quantities, the unsupported short-lived

isotopes are virtually absent away from the coast. Open ocean activities of ^{226}Ra and ^{228}Ra for the North Atlantic from Moore (1969) and Kaufman et al. (1973) are shown in Table 3.3 and discussed in more detail in Chapter 3. For the purpose of tracing coastal water masses, it is the "excess" radium over open ocean values that is of interest. For ^{224}Ra this can be determined easily by allowing the initial activity to decay, and making subsequent measurements of the ingrowth from its parent ^{228}Th which is also adsorbed onto the collection fibers. The "supported" ^{224}Ra can then be subtracted from the initial measurements to obtain the "excess" ^{224}Ra. A similar procedure can be used to obtain the excess ^{223}Ra that is unsupported by dissolved ^{227}Ac. Unlike the short-lived isotopes, most of the open ocean ^{228}Ra and ^{226}Ra results from the long half-life of these isotopes which allows them to be mixed well offshore. Because its half-life is of the same order as ocean mixing, ^{226}Ra activities are quite high throughout the Atlantic, around 8 dpm/100L. Mean ^{228}Ra activity in the open Atlantic, approximately 1.5 dpm/100L, reflect its shorter half-life. The mean open ocean activities of these isotopes can be subtracted from coastal activities to estimate the "excess" long-lived activity in a coastal sample.

In addition to freshwater and seawater sources, radium enters the water column from marine sediments which have high activities of thorium plus some uranium that accumulates in sediments with settling particles. Sand and gravel which are composed primarily of quartz have relatively little of these parent isotopes, but fine-grained silts and clays can contribute a significant amount of radium to bottom waters, especially if particle scavenging has been high in the overlying water column. Because most radium on the surface of particles will have desorbed while in the water column, the diffusion of radium from sediments depends on regeneration from the parent isotopes after deposition. This in turn is affected by the

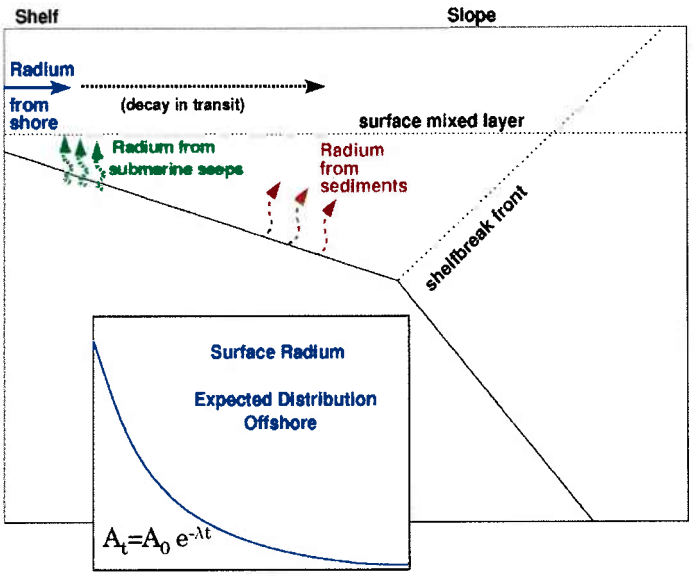

Figure 2.2: Sources of "excess" radium to seawater. Coastal sources include both river and groundwater inputs.

different radium half-lives which determine how long it takes to reach radioactive equilibrium with the parent isotopes. Short-lived isotopes will come into equilibrium with longer lived parents relatively quickly. ^{228}Ra activity, for example, is regenerated about 280 times faster than ^{226}Ra activity (Krest et al. 1999). The very short-lived isotopes ^{223}Ra and ^{224}Ra in particular are generated rapidly from thorium deposited in the sediments. The activity ratio of a short-lived radium isotope to a long-lived isotope could be expected to be higher in waters where sediment resuspension has occurred than in waters where the radium quartet is being introduced from source water that has had a long residence time for all of the isotopes to equilibrate, such as groundwater. Sediment type and environmental conditions may also affect radium flux from sediments. Measurements made by Torgersen et al. (1996) of ^{224}Ra in Long Island Sound revealed that while nearshore water was enriched in this isotope,

bottom water in the middle of the sound was enriched twice as much, possibly due to finer grained sediments. They also point out that in oxygenated water, manganese oxides at the sediment surface can scavenge diffusing Ra before it reaches the water column; hence oxygen levels can also affect relative radium flux. Li et al. (1979) have observed that Ra and salinity do not always follow a simple linear relationship over the shelf in the New York Bight, as would be expected when radium has a freshwater source; this could be an indicator of vertical mixing of radium with sediment sources.

Radium from sediment sources contributes to the coastal enrichment, and can also reach surface water when there is strong vertical mixing, upwelling over the shelf, or currents passing over shallow sills or outcrops. Schmidt and Reyss (1996) observed enrichments of ^{228}Ra in Mediterranean Outflow Water that had contact with sediment over the Straits of Gibraltar. The enrichment was traceable all the way into mid-depth "meddies," eddies in the Atlantic formed from Mediterranean outflow water, where both salinity and ^{228}Ra were considerably elevated over surrounding water outside the eddies. It should be noted that not all radium diffusing from marine sediments is produced in the sediment. Moore (1997) observed Ra enrichments of 3-10 times open ocean activities at the shelf edge off South Carolina 80 km from shore. In this case the isotopic composition was a clue to the origin of the enrichment. Sediments in the area were composed of sand, gravel and phosphorites. Only the phosphorites could be a potential source, but the radium in phosphorites originates from uranium enrichment, so ^{228}Ra, a product of the ^{232}Th decay chain, is not produced. The bottom water observed at the shelf edge was enriched in all four isotopes, typical of an aquifer source.

The four isotopes also have a range of half-lives that make them useful "clocks" for

studying natural phenomena on a wide range of timescales. Two isotopes have fairly long half-lives, ^{226}Ra (half-life 1600 years) and ^{228}Ra (half-life 5.7 years), while two have very short half lives, ^{223}Ra (half-life 11.4 days) and ^{224}Ra (half-life 3.7 days). Any observations made using these isotopes must be considered to be integrations over the appropriate timescale for the isotope half-life. A dynamic process like coastal mixing may not be in "steady state" over any of these time scales however. While limiting in model calculations that require a steady state simplification, this property can also be advantageous for observing transient phenomena such as streamers, plumes, or eddies which can be identified and aged by isotopic decay. In the observations of meddies (Schmidt and Reyss 1996) features which have lifetimes on the order of months to years, ratios of the decaying ^{228}Ra and the relatively "stable" ^{226}Ra were employed to constrain the age of the meddies since formation near the outflow. The time scale of the isotope is then a critical factor when using it to observe physical phenomena. As a general rule, one can consider naturally occuring radioisotopes to be readily measurable for a period of approximately 6 half lives. For ^{224}Ra and ^{223}Ra six half-lives are equal to about 3 weeks and 2 months, respectively, and for ^{228}Ra and ^{226}Ra approximately 35 years and 9600 years.

Finally, in reporting radioisotope levels in seawater an "activity" scale is used rather than concentration. Activity is the rate at which disintegrations occur in a sample. Starting with the exponential law of radioactive decay:

$$\frac{dN}{dt} = -\lambda N, \quad N(t) = N_0\, e^{-\lambda t} \tag{2.1}$$

where N is the number of radioactive nuclei present, the absolute rate of decay is then

$|dN/dt| = \lambda N(t) = \lambda N_0 e^{-\lambda t}$. The rate of decay of a sample is defined as the activity, A, where $A \equiv \lambda N$, and the decay law can then be written as

$$A = A_0\, e^{-\lambda t} \tag{2.2}$$

One advantage in using activity units is that when parent and daughter isotopes are in equilibrium, their concentrations may be quite different but their activities are equal. This is expressed in the Bateman equation for activity of a daughter isotope. When the parent isotope has a very long half-life (as the U and Th parent isotopes of radium do), the Bateman equation simplifies to

$$A_d(t) \approx A_p \left(1 - e^{-\lambda_d t}\right) \tag{2.3}$$

where A_d and A_p are the activities of the daughter and parent isotopes. This goes to $A_d(t) = A_p$ at large values of t and enables one to discern quickly, from activity measurements, whether a system is in equilibrium or if there has been removal or addition of an isotope.

Detection methods count individual decay events in a sample, rather than mass or concentration, which are then averaged over time (decays per minute, or dpm) and divided by the volume of the sample to give units of actvity per unit volume. Traditionally, the units used for radium activity in seawater in the U.S. are dpm/100 L (equivalent to 1/60 Bq/100L).

2.2 Interpretation of Radium Distributions: Physical Mixing

If mixing coefficients can be reliably estimated they can be extremely useful in calculating oceanic fluxes of biologically or environmentally important compounds, particularly when

horizontal gradients of the compounds are measured concurrently. Somayajulu et al., (1996) calculated lateral eddy mixing rates for the eastern Arabian Sea using ^{228}Ra (half life 5.7 years) over a large area bounded on one side by organic-rich anoxic Indian shelf sediments. Using a two-dimensional balance between diffusion and decay, they calculated mixing rates both zonally and meridionally and used these to estimate the horizontal flux of DOC from the shelf to denitrifying regions of the Arabian sea where researchers were puzzled by budget deficits of organic matter. Similar techniques can be used to estimate nutrient and pollutant fluxes in the coastal zone if steady state can be assumed on a decadal time scale.

However, several assumptions are made in these type of calculations that may lead to unreliable results. The assumptions most commonly made are that the system is in steady state on the time scale of the isotope being used, and that advection is negligible. Both of these assumptions are risky in a coastal setting, and as will be shown below, estimates of eddy mixing can have a very broad margin of error if advection is not included in calculations, even if it is a slow flow rate. Mean current data collected during the Nantucket Shoals Flux Experiment (NSFE) shows cross-shelf flow is common in both the offshore and shoreward directions. Data means from the outer 3 current meters over the shelfbreak show mean flow rates in the upper 30 meters ranging from -2.1 cm/s to +1.0 cm/s with standard deviations of 12-15 cm/s. In addition, the correlation time scales of the data range from 2 days over the shelf and shelfbreak, to 7 days over the upper slope, which shows how rapidly conditions can change. High resolution studies of shelf and slope circulation indicate that over the timescale of the short-lived isotopes, conditions over the outer shelf can shift dramatically over a time scale of hours to days (Gawarkiewicz et al. submitted 2002). Near the shelfbreak front, cross-shelf advection is subject to strong variations in both

direction and magnitude due to the influence of density driven currents; similar currents have been observed in the mid-shelf region as well and the variability of these is unknown (see Chapter 4). Moore (2000a) has noted that the shift in Ra activity gradients at mid-shelf could be the effect of more complex processes operating over the outer shelf that are not clearly discernable from the radium data. Caution must especially be exercised when using short-lived Ra data to make estimates using a steady-state assumption.

Methods for using radium distribution to estimate physical mixing and transport processes are based on basic models of advective and diffusive transport of an element with a constant decay rate. The governing equation in one dimension is a balance of these processes:

$$\frac{\partial A}{\partial t} = \kappa \frac{\partial^2 A}{\partial x^2} - w \frac{\partial A}{\partial x} - \lambda A \tag{2.4}$$

where A is the excess activity of the isotope from unsupported coastal sources, κ is the horizontal eddy diffusion coefficient, w is the horizontal advective velocity, and λ is the radioactive decay constant. Figure 2.3 illustrates the theoretical activity curves that would be observed over a 100 km wide shelf under a variety of conditions with a shoreline source of radium. The top curve (A, dotted) shows the distribution with diffusive mixing only, no radioactive decay or advection. On the distance scale used here, decay at the rate of a 1600 year half life (^{226}Ra) can be considered the same as "no decay"; results are identical. The element is well-mixed across the shelf even with a very small eddy diffusion coefficient, $\kappa = 10$ m^2 s^{-1}; the curve of diffusive mixing is a straight line. Increasing the value of κ increases the transport and homogeneity of the tracer and the distribution curve approaches a horizontal line. If the diffusivity κ is high enough, even elements with shorter half-lives will exhibit a flat distribution. The dashed curves (B, C) show the case where the element

is decaying at the rate of ^{228}Ra (5.75 year half life) with no advection. With the same low κ as in curve A, an exponential decay away from shore is clearly visible. Higher diffusion coefficients push the distribution toward the pure diffusive case, i.e., toward a straight flat line, making the signature of decay less apparent. The solid curves (D, contiguous with C, and E) show a case with no decay, but with a slow advection rate, 0.5 cm/s, typical of a large-scale mean flow (Beardsley et al. 1985). The distribution is a similar exponential decrease in activity offshore. If the advective flow was in the offshore direction it would create a convex rather than concave curve. At a moderately high mixing rate ($\kappa = 250$ m^2 s^{-1}) this cross-shelf profile is virtually indistinguishable from the case where there is decay with a low mixing rate (curve C).

These idealized curves can help in interpreting observations, but also illustrate the difficulty in determining the role of advective transport with a decaying tracer since decay and shoreward advection have similar effects on the activity curves, as do diffusion and offshore advection. To obtain estimates of large-scale mixing rates, steady state, a constant κ, and negligible advection are normally assumed. This creates a balance between eddy diffusion and radioactive decay that enables solving for the mixing coefficient κ once the isotope gradient has been measured. (If $\kappa\frac{\partial^2 A}{\partial x^2} = \lambda x$, $m = \sqrt{\lambda/K}$, where m is the slope of the natural log plot of radium as a function of distance. Boundary conditions are $A(\infty) = 0$ and $A(0) = A_0$.) But as seen in the above examples, slow advection that one might consider "negligible" can have a large effect.

As an example, actual radium distributions for the two long-lived istopes are shown in Figure 2.4. Moore (2000a) made measurements along four transects on the shelf of the South Atlantic Bight and then distance-averaged the data to smooth some of the spatial

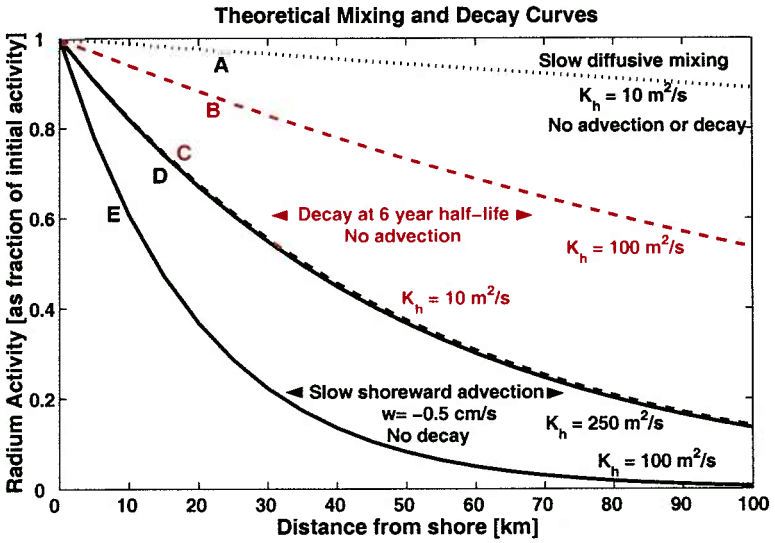

Figure 2.3: Cross-shelf steady-state distribution of radium with diffusive mixing only (top dotted curve), decay plus diffusive mixing (dashed curves), and advection plus diffusive mixing (bottom solid curves). Decay and advection curves are shown with low and high eddy diffusion coefficients.

and temporal variability. As Moore points out, it is possible to interpret the distribution as being the result of two different mixing regimes with a boundary 50 km offshore. Seaward of 50 km ^{226}Ra behaves as expected for an isotope with no measureable decay where eddy mixing is occurring, i.e., a flat distribution. The slope of the ^{228}Ra line is consistent with this interpretation, since we have seen that decay at a 5.7 year half life in the presence of eddy diffusion will steepen the slope of the mixing line. From the idealized diagram, it appears the mixing rate is moderately high seaward of 50 km, corresponding to about $\kappa > 100$ m^2 s^{-1} in Figure 2.3 (curve B). Shoreward of the 50 km boundary, the slope of the ^{228}Ra distribution suggests greatly reduced diffusive mixing, or the presence of slow shoreward advection. The slope of the ^{226}Ra curve is steep for an isotope with little decay however; if there is any realistic eddy diffusivity this could only be explained by shoreward

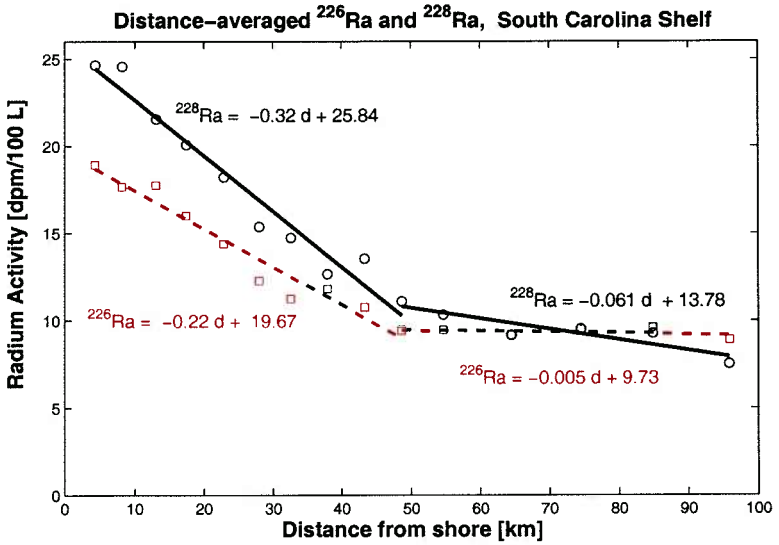

Figure 2.4: Cross-shelf distribution of long-lived radium isotopes in the South Atlantic Bight (data from Moore 2000a). Solid and dashed lines represent first order polynomial fits for the inner and outer shelf.

advection or a very recent pulse of radium from the coast that has not yet mixed, which is an unlikely scenario. The two mixing regime scenario is also only a speculation of what might be occuring in this situation; the Gulf Stream boundary is at the end of the transect, not in the middle.

This example illustrates the difficulties inherent in interpreting data of this type. Slow advection can have a major effect on Ra distribution, as seen in Figure 2.3 in which a very slow mean flow has an effect comparable or greater than decay for isotopes with half-lives on the order of ^{228}Ra or shorter. Yet over a distance of 50 km the curved shape that results from slow advection would be barely distinguishable from a straight mixing line, particularly with the natural scatter of real data. As will be shown later, it is often better to include advection in the calculations; in this case, the result is one curve that can reasonably account for data over the entire transect.

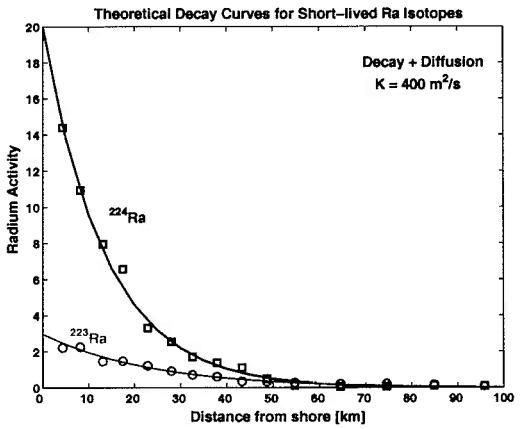

Figure 2.5: Cross-shelf steady-state distribution of short-lived radium isotopes, ^{223}Ra (half-life = 11.4 days) and ^{224}Ra (half-life = 3.7 days), with diffusive mixing. Initial concentrations are typical of MAB nearshore.

Theoretical decay curves for the short-lived isotopes ^{223}Ra and ^{224}Ra are shown in Figure 2.5, plotted with actual distance-averaged data from Moore (2000a). Even with fairly high eddy diffusivity ($\kappa = 400$ m^2 s^{-1}) the cross-shelf activity levels decay rapidly with distance from shore. These curves include only decay and diffusion, with no advection. Cross-shelf advection will alter the steepness of the curves, as with the long-lived isotopes, shoreward advection causing the curves to be steeper near shore with lower activities offshore, and seaward advection resulting in a flatter distribution with higher activity offshore. In this example, a single value of κ fits both data sets without the addition of an advection term. However, it can be shown that this solution is not unique, so therefore not necessarily correct.

The distance-averaged data sets collected by Moore (2000a) are a good test case for examining the relative effects of eddy diffusion, advection and radioactive decay on radium

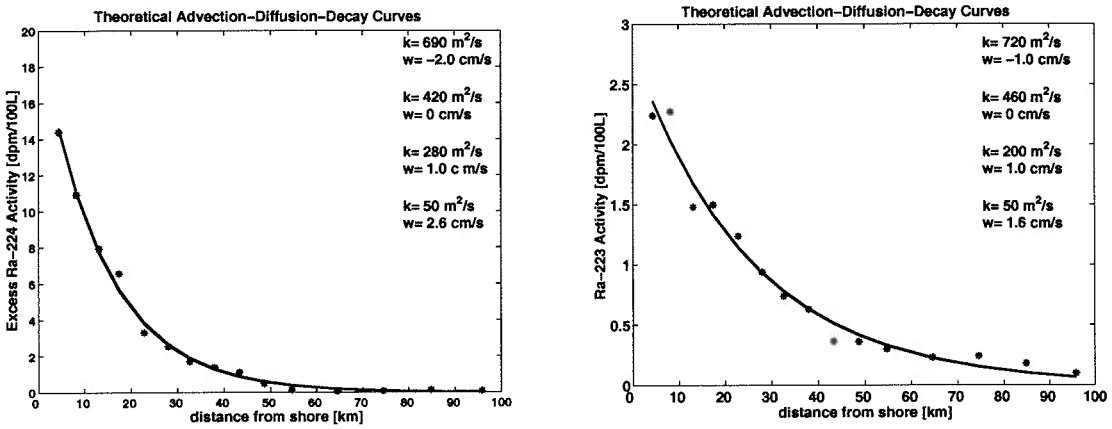

Figure 2.6: Theoretical advection-diffusion-decay solutions for ^{224}Ra and ^{223}Ra. Several solutions for different pairs of κ and w are plotted which identically overlap. The κ and w solution pairs in the upper right hand corner show the range that is plotted. The star-shaped data points on the plot are the actual distance-averaged data points from Moore (2000a).

distributions and eddy diffusion coefficient calculations. With boundary conditions $A(\infty) = 0$ and $A(0) = A_0$, the full steady-state solution to equation 2.4 gives the activity with distance from shore, $A(x)$, as a function of κ, w and λ:

$$A(x) = A_0\, e^{rx}$$

where

$$r = \frac{w - \sqrt{w^2 + 4K\lambda}}{2K} \tag{2.5}$$

Using a nonlinear least squares regression (Levenburg-Marquardt method) a tight best-fit can be obtained for these data sets, with solutions for w and κ. However the uncertainties in w and κ are extremely large, rendering the solutions meaningless.

As it turns out, the range of possible solutions for κ and w for this data set is extremely wide, as illustrated in Figures 2.6 and 2.7. The figures show the actual data (starred

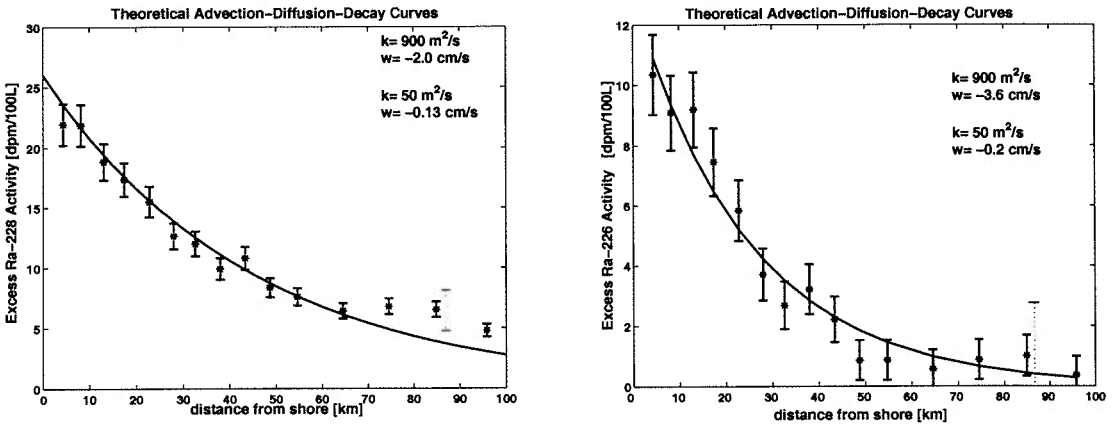

Figure 2.7: Theoretical advection-diffusion-decay solutions for ^{228}Ra and ^{226}Ra. Several solutions for different pairs of κ and w are plotted which identically overlap. The κ and w solution pairs in the upper right hand corner show the range that is plotted. The star-shaped data points on the plot are the actual distance-averaged data points from Moore (2000a). Error bars are included for the long-lived isotopes and are equal to the $\pm 7\%$ estimated counting errors for individual (not distance-averaged) data points. Error bars do not include standard deviations from distance-averaging, however one sample error bar is shown for data at 85 km to illustrate one standard deviation in the mean at that distance. Errors on the open ocean values used to compute the "excess" are ± 0.75 for ^{228}Ra, and ± 0.14 for ^{226}Ra (one standard deviation from the mean).

data points) with several theoretical solutions superimposed on each plot. The ^{228}Ra and ^{226}Ra data shown are "excess" Ra, i.e., in excess of average open ocean values; means from Chapter 3, Table 3.3, North Atlantic Western Gyre are used to compute excess. As with the short-lived isotopes, it is the elevated nearshore activity of ^{228}Ra and ^{226}Ra in excess of open ocean values that allows the isotopes to be used as coastal water mass tracers. Error bars are included for the long-lived data sets where the curves are not as tight a fit. Each curve plotted corresponds to a different κ, w solution, and identically overlaps the others. From this we can discern several important points. First, the range of κ that is possible is extremely large, from 0 to over 1000 m^2/s (solutions $>>$ 1000 m^2/s are also possible, but are not included). Secondly, the range in solutions for w that corresponds to this is

quite small, only a few cm/s. This shows how critical the advection term is in accurately determining κ.

The interaction of the two parameters can be seen graphically when minimizing the sum of squares errors. For each isotope, values of r were computed for a 20×20 array of κ, w pairs in the range $\kappa = 50$ to 1000 m^2/s and $w = -4.5$ to 5.0 cm/s using equation 2.5, and each r was then used to calculate a theoretical activity curve, $A_{calc}(x)$. The sum of squares error between the calculated curves and the actual data, $\Sigma(A_{calc}(x_i) - A_{obs}(x_i))$, was then determined for each curve. Figure 2.8 shows the contours of the sum of squares error for the entire range of κ, w pairs for each data set. For unique solutions (one best fit curve) the contours would be concentric around the κ, w pair that is the best solution for the data. Steep contours would indicate a narrow range of acceptable solutions (small uncertainty) while widely spaced contours indicate a wide range of solutions (large uncertainty). In this case the minimization of the sum of squares error is a zero contour line, not a closed contour, and the contours do not converge to a single solution or set of acceptable solutions. The zero contour lines indicate an extremely broad range of possible eddy diffusivity coefficients, and a narrow range of advection rates. It is interesting to note that for the short-lived isotopes, solutions are possible with both positive (offshore) and negative (shoreward) advection, while the long-lived data sets have solutions only for shoreward advection. A sum of squares error minimization on the data from the inner 50 km shows that the same holds true for that sub-region.

Because the chemical behaviour of the four Ra isotopes is the same and only the decay rates vary, it is possible to use this to better constrain the values of κ, w. In effect, we have four different tracers with identical physical properties, but different internal clocks. By

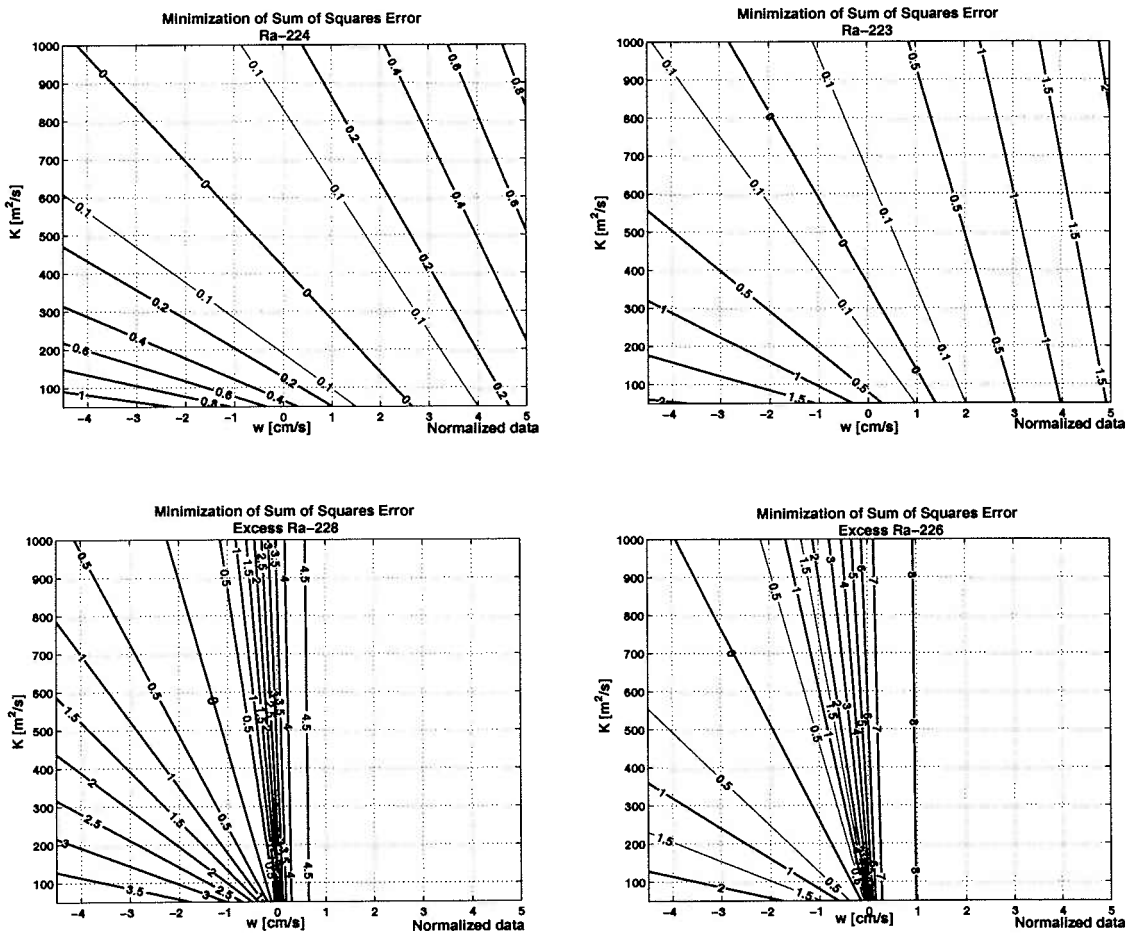

Figure 2.8: Minimization of the sum of squares error for the advection-diffusion-decay equation and distance-averaged coastal radium data from Moore (2000a). Contours show the sum of squares errors as functions of horizontal eddy diffusivity κ and cross-shelf advection w. The zero contour indicates κ, w pairs that result in a "best fit" regression curve for the data.

finding where the minima of the sum of squares error calculations intersect we can limit the range of appropriate values of κ, w. Figure 2.9 shows the zero sum of squares error contours for each isotope. The first thing that is apparent from the figure is that the short-lived and long-lived isotopes seem to have different behaviours with respect to mixing, as the regions of intersection are different for the two pairs. This is really not so suprising when one considers that ^{224}Ra and ^{223}Ra are integrating conditions over a time scale of days and

^{228}Ra and ^{226}Ra are integrating over tens to thousands of years. It should also be noted that this method is based on a steady-state assumption, which is problematic in coastal regions because of the small spatial and temporal scales involved in advective processes. Whether or not the long-lived isotopes can effectively measure long-term mean conditions that reflect a longer scale steady state is a question that is open to debate.

In Figure 2.9 we see that the zero error contours for ^{224}Ra and ^{223}Ra intersect near $\kappa = 500$ m^2/s. Figure 2.10 shows the calculated curves and their fit to the Moore data using identical κ, w values, $\kappa = 510$ m^2/s and $w = -0.7$ cm/s in equation 2.2. Thus on a short time scale, there is a unique solution that works for both tracers, assuming there are not non-steady state processes operating that affect the two isotopes differently. The zero contours for ^{228}Ra and ^{226}Ra do not intersect, but are in closest proximity at about $\kappa = 125$ m^2/s. One value of w does not fit both curves well in this case, but advective rates must differ by only 0.2 cm/s for curves to fit with $\kappa = 50$ m^2/s, a difference in w that is not measureable by any practical means. On longer time scales then, it appears that κ may be lower, approximately 50 m^2/s, with advection averaging -0.2 to -0.4 cm/s (i.e., slightly shoreward cross-shelf flow).

Method	w	κ
^{224}Ra	0	420 m^2/s
^{223}Ra	0	360 m^2/s
^{224}Ra + ^{223}Ra	-0.7 cm/s	510 m^2/s
^{228}Ra + ^{226}Ra	$-0.1 - -0.2$ cm/s	50 m^2/s

Table 2.1 Summary of eddy diffusivity constants for South Atlantic Bight obtained by Moore (2000a) using single isotopes and assuming zero advection, and by the sum of squares error minimization method using two isotopes.

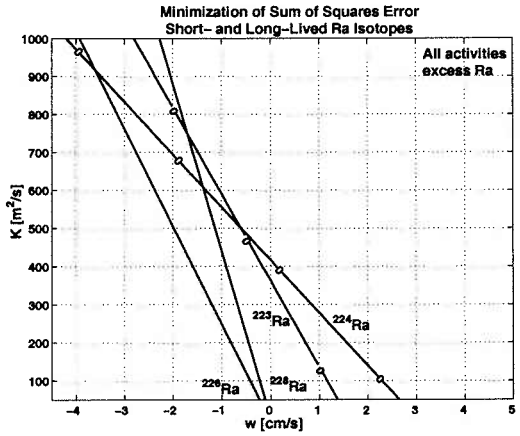

Figure 2.9: Minimum sum of squares errors for advection-diffusion-decay model for all four Ra isotopes.

It is also notable that the advection-diffusion-decay curves fit the data about as well as the two linear regression lines for the inner shelf shown in Figure 2.4 and are a better fit when using data corrected to reflect excess ^{228}Ra and ^{226}Ra. When using excess ^{228}Ra and ^{226}Ra, it also may be unnecessary to divide the shelf into inner and outer mixing regimes since one curve can adequately account for the full data set. Although the outer shelf data still deviates more from the curve than the inner, the fit is better than Moore's method using total Ra and zero advection, and any division between inner and outer shelf is less distinct than with the total Ra data. This analysis shows that a solution for eddy diffusivity with zero advection is possible, but it is by no means unique, and the system is highly sensitive to advection rates as slow as a few centimeters per second.

The implications for neglecting advection in calculations, and thus incorrectly estimating the eddy diffusion coefficient κ, are best illustrated by considering a flux calculation. As an example, let's use a physical setting similar to that above. Over this we will have an element of interest (such as a nutrient) with concentration C and an offshore ΔC = -500

μmol/m^3 (equivalent to 0.5 μmol/L). We can examine two cases with different concentration gradients, one with $\Delta x_1 = 500$ km, $dC/dx = -0.001\mu$mol/m^4, and one with $\Delta x_2 = 5$ km, $dC/dx = -0.1\mu$mol/m^4. The flux of our element can then be calculated at the midpoint of the gradient where C = 250 μmol/m^3, using

$$J_{AD} = wC - K\frac{dC}{dx} \tag{2.6}$$

This equation gives the advective-diffusive flux across the shelf-slope boundary, and not the *total* flux within the region which would include terms for consumption and production of nutrients (primary production, remineralization, nitrogen fixation) as well as inputs and sinks from other sources (such as atmospheric deposition, riverine input, and denitrification). A full flux equation would look something like $J_{tot} = wC - K\frac{dC}{dx} + P$, where P is the combined effect of biological consumption, remineralization, fixation, etc. These other processes can have important effects on the nutrient concentrations and gradient on either side of the boundary, but the advective-diffusive flux we are concerned with here is the physical transport of the resulting nutrient distribution; i.e., we are solving for w and κ. (We are also assuming steady state for this example, and the multitude of processes affecting nutrient concentrations is certainly not steady state, as is evident in the data presented in the next sections.) For a range of κ, w pairs obtained in the sum of squares error minimization for the four isotopes (Figure 2.10) we obtain the fluxes shown in Table 2.1 (with examples for the two different concentration gradients).

Several things should be noted in the flux calculations. First, clearly variations in w are not compensated for by the resulting changes in κ. Neglecting advection does not allow the

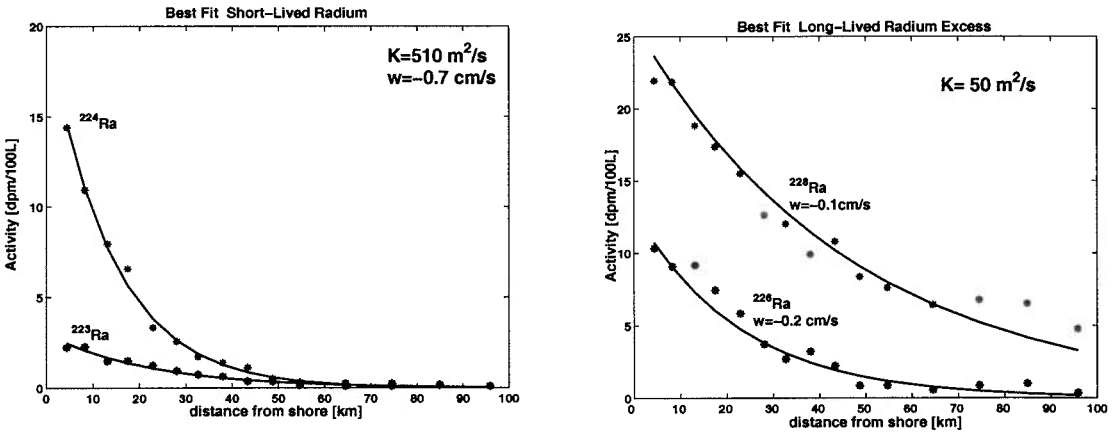

Figure 2.10: Best fit κ, w pairs for short-lived and long-lived isotopes.

estimation of an "effective κ" that includes the effects of advection. When κ is estimated using zero advection, the resulting flux calculation will be in error by a factor of 2-10 if the actual flow is just a couple centimeters per second. In addition, and even more important for nutrient calculations, the direction of the flux may also be in error. It is also worth noting that shoreward flow does not necessarily cause shoreward flux, because of the down-gradient effect of diffusion.

	^{224}Ra					^{223}Ra			^{228}Ra, ^{226}Ra
w [cm/s]	-2	-1	0	1	2	-1	0	1	-0.3
κ [m^2/s]	700	550	400	280	140	600	360	125	50
J_1 [μmol/m^2· s]	65.0	53.0	40.0	30.5	19.0	-58.0	36.0	15.0	4.3
J_2 [μmol/m^2· s]	-4.3	-2.0	0.40	2.8	5.1	-1.9	0.36	2.6	-0.70
J_{adv} [μmol/m^2· s]	-5.0	-2.5	0	2.5	5.0	-2.5	0	2.5	-0.75
Pe_1	0.14	0.09	0	0.18	0.71	0.08	0	0.40	0.30
Pe_2	14	9.1	0	18	71	8.3	0	40	30

Table 2.2. Sample flux calculations based on possible advective rates (w) and eddy diffusion coefficients (κ) calculated from South Atlantic Bight data collected by Moore (2000a). Fluxes J_1 and J_2 differ in the magnitude of their concentration gradients. Both have a $\Delta C = -500\,\mu$mol/m^3 (equivalent to 0.5 μmol/L, decreasing offshore) but the length scales Δx vary, with $\Delta x_1 = 5$ km and $\Delta x_2 = 500$ km. The resulting concentration gradients are -0.1 and -0.001 μmol/m^3· m respectively.

The flux shown for ^{228}Ra and ^{226}Ra is based on the area of convergence for κ and w for both isotopes. This may be viewed as a long-term estimate because the parameters are calculated using isotopes with very long half-lives. However, questions regarding steady state over long time periods as well as the limitations of a 1-D model over any timescale must be considered when interpreting these results. The flux J_1 calculated for ^{224}Ra using zero advection is about a factor of 10 higher than the long-term estimate. Viewed in another way, the difference between the long-lived estimate for J_1 and the flux estimate based on ^{224}Ra and zero advection is equivalent to using a value of κ that is too high by 350 m^2/s. For J_2 one would have to increase κ from 50 to 1150 m^2/s to arrive at the same flux based on ^{224}Ra and zero advection.

The purely advective component of the flux is also shown for comparison and we can see that this is a much larger fraction of J_2 than J_1. The Peclet number, Pe, can be used as a measure of the relative dominance of the advective and diffusive components. $Pe = wL/K$, where L is the length scale associated with the concentration gradient. A $Pe > 1$ indicates dominance of the advective component and results when w or the length scale of the gradient is large relative to κ, the former increasing the advective term, and the latter decreasing the diffusive term. Peclet numbers for the two cases J_1 and J_2 are shown at the bottom of the table. The difference in the two regimes is apparent in the Peclet numbers of $Pe << 1$ in the case of J_1 where diffusion is dominant, and $Pe >> 1$ in the case of J_2 where advective flow accounts for the bulk of the flux.

2.3 Interpretation of Radium Distributions: Transport Times

Radium measurements can also be used to determine water mass ages or transport times (Moore 2000b). The principle behind this method is the simple radioactive decay equation:

$$A(t) = A(0)\, e^{-\lambda t}\, f_{EM} \tag{2.7}$$

where f_{EM} is the fraction of end member remaining in the sample after mixing. Expressing the equation as a ratio of two isotopes solves the problem of the unknown mixing fraction, since f_{EM} is the same for both.

$$\frac{A_{short}(t)}{A_{long}(t)} = \frac{A_{short}(0)}{A_{long}(0)}\, \frac{e^{-\lambda_{short} t}}{e^{-\lambda_{long} t}} \tag{2.8}$$

The variable t then gives the "age" or transit time of the water mass:

$$t = -\frac{\ln\left(\frac{A_{short}(t)/A_{short}(0)}{A_{long}(t)/A_{long}(0)}\right)}{\lambda_{long} - \lambda_{short}} \tag{2.9}$$

When using the ratio of a short-lived isotope to a long-lived isotope, the elapsed time since the water mass left its source is determined from the decreasing isotope ratio, as illustrated in Figure 2.11. Although this method is used to normalize for mixing, some assumptions inherent in this method must be recognized. Using the ratio method to determine water mass transit time assumes that the water mass with the tracer is mixed with a zero activity end member. When this is the case, the method is extremely accurate, and gives the transit time of the tracer as if no dilution had occurred. Although it may appear that the method could be used to correct for any type of mixing, with a slight underestimation of water mass age, the method breaks down when the time elapsed is large or when the difference in ages between the two water masses is large. This is because the method does not actually give an "average" age for the two combined water masses. The problem is discussed by Musgrave (1985) and Jenkins (1987) for other passive tracers such as tritium, and is demonstrated below for radium isotopes.

To illustrate the problem, we can use two theoretical isotopes, I_L and I_S, with half-lives of 1000 days (long) and 10 days (short) respectively, and initial activities of $I_L = 10$ dpm/100L, $I_S = 20$ dpm/100L. As a water mass with these isotopes is removed from its source, it will have these properties, assuming there is no mixing or dilution (ages given in half-lives of the respective isotopes):

Time	0 dy	10 dy	20 dy	30 dy	60 dy	∞
I_L age ($t_{1/2}$)	0	0.01	0.02	0.03	0.06	∞
I_L activity (dpm/100L)	10.0	9.93	9.86	9.79	9.59	0
I_S age ($t_{1/2}$)	0	1.0	2.0	3.0	6.0	∞
I_S activity (dpm/100L)	20.0	10.0	5.0	2.5	0.31	0

Table 2.3 Sample water mass properties during transit.

If we sample a water mass that is a 50-50 mixture of one water mass that is 10 days old (10 days removed from source) and a second water mass that is 20 days old, the isotopes will have the following activities:

$$I_L = \left(50\,\mathrm{L} \times \frac{9.93\,\mathrm{dpm}}{100\,\mathrm{L}}\right) + \left(50\,\mathrm{L} \times \frac{9.86\,\mathrm{dpm}}{100\,\mathrm{L}}\right) = 9.90\,\mathrm{dpm/L}$$

$$I_S = \left(50\,\mathrm{L} \times \frac{10.0\,\mathrm{dpm}}{100\,\mathrm{L}}\right) + \left(50\,\mathrm{L} \times \frac{5.0\,\mathrm{dpm}}{100\mathrm{L}}\right) = 7.5\,\mathrm{dpm/L}$$

Since we know the fraction and age of each endmember, we know that the average age of the mixture is 15 days. However if we did not know that the water mass we sampled was a mixture of two distinct water masses and used the radioactive decay equation (Eq. 2.7) with $f_{EM} = 1$, we would get different ages based on I_L or I_S:

$$t_L = -\frac{\ln(9.90/10)}{\lambda_L} = 15.23\,\mathrm{dy}$$

$$t_S = -\frac{\ln(7.5/20)}{\lambda_S} = 14.15\,\mathrm{dy}$$

If we use the isotope ratio method as shown in equation 2.9 to normalize for mixing, we

then obtain an age that is an underestimation of the average age of the mixed water mass:

$$t_{S:L} = -\frac{\ln\left((7.5/20.0)/(9.90/10.0)\right)}{\lambda_S - \lambda_L} = 14.00\,\mathrm{dy}$$

However, it is only because the time intervals and difference in end member ages are small that the result is close to the average age of the mixed water mass. (In fact the estimate would be closer to the average age had we used either one of the isotopes individually.) The problem is more apparent in the following example, a 50-50 mixture of water masses that are 10 days old and 60 days old, with an average age of 35 days. Now the error from the ratioing method is more apparent:

$$I_L = \left(50\,\mathrm{L} \times \frac{9.93\,\mathrm{dpm}}{100\,\mathrm{L}}\right) + \left(50\,\mathrm{L} \times \frac{9.59\,\mathrm{dpm}}{100\,\mathrm{L}}\right) = 9.76\,\mathrm{dpm/L}$$

$$I_S = \left(50\,\mathrm{L} \times \frac{10.0\,\mathrm{dpm}}{100\,\mathrm{L}}\right) + \left(50\,\mathrm{L} \times \frac{0.31\,\mathrm{dpm}}{100\mathrm{L}}\right) = 5.16\,\mathrm{dpm/L}$$

and

$$t_L = -\frac{\ln(9.76/10)}{\lambda_L} = 35.05\,\mathrm{dy}$$

$$t_S = -\frac{\ln(5.16/20)}{\lambda_S} = 19.56\,\mathrm{dy}$$

$$t_{S:L} = -\frac{\ln\left((5.16/20.0)/(9.76/10.0)\right)}{\lambda_S - \lambda_L} = 19.40\,\mathrm{dy}$$

On the other hand, using a mixture with one end member zero ($t = /infty$) we can calculate an age for the tracer-containing end member within rounding error accuracy. For example, a 50:50 mixture of 30-day old water and a zero activity end member has a diluted activity

of $I_L = 4.8971$ dpm/100L and $I_S = 1.25$ dpm/100L. Ratioing gives an age of 30 days:

$$t_{S:L} = -\frac{\ln[(1.25/20.0)/(4.8971/10.0)]}{\lambda_S - \lambda_L} = 29.\bar{9}\,\mathrm{dy}$$

If the two end members both have non-zero tracer activity (such as water masses from two nearshore sources that travel different paths before combining) the water sample that is measured must be described by combining the decay equations for each end member:

$$A_{measured} = A_{EM1} + A_{EM2} = A(0)\,e^{-\lambda t_1}\,f_{EM1} \;+\; A(0)\,e^{-\lambda t_2}\,f_{EM2}$$

where t_1 and t_2 are the transit times for the two separate water masses, including their transits before mixing. Because of the different time variables, this cannot be simplified by expressing as a ratio, so the fraction of each end member must be known. Fortunately, in many cases we can assume as a first approximation that the predominant form of mixing is between one nearshore end member and one near-zero offshore end member. But the possibility of two nearshore end members mixing after separate transits should be borne in mind.

2.4 Discussion

The method of using two or more isotopes in conjunction with a model that includes the advective term is promising for better constraining a horizontal coastal eddy diffusion coefficient, κ. The importance of considering the advective term is not merely to include the effects of advective solute transport. When w is not significant in flux calculations ($Pe << 1$), it is still crucial in constraining where on the continuum of the zero SOS con-

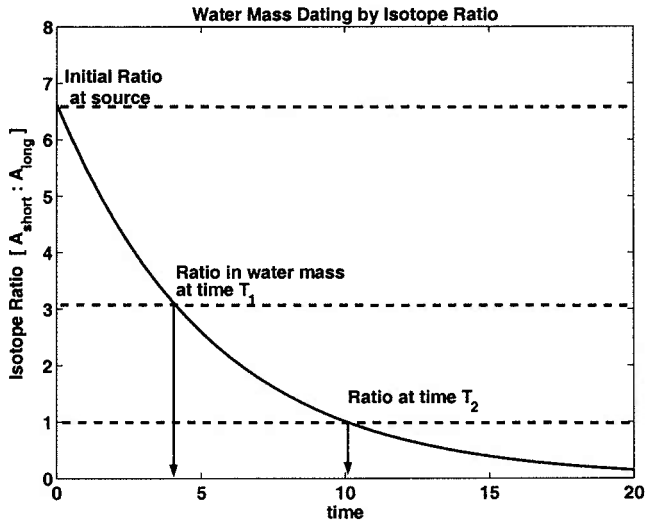

Figure 2.11: Decay of isotope ratios over time, for activity ratio of a short-lived isotope to a longer-lived isotope. Age or transit time is determined by measuring the isotope ratio in transported water mass and in a known source.

tour κ should fall. Regardless of whether or not $w \cdot C$ is large enough to impact the diffusive term in the flux equation, including the term in the basic model (Eqns. 2.4 and 2.5) is what allows one to put limits on κ by finding the intersection or convergence region of two or more zero SOS error contours.

One assumption in using the advection-diffusion equation to establish κ and w is that the system is at steady-state on the time-scale of the isotopes involved. This is a tenuous assumption even for the short-lived isotopes considering conditions over the shelf, and particularly near the shelfbreak, can change on timescales as rapid as days (Gawarkiewicz et al. submitted 2002). This is one of the most potentially problematic limitations in using radiotracers to estimate eddy diffusivity. It was also a major factor in decisions to attempt using radium activity to trace short-lived or episodic plumes of shelfwater, as opposed to using it in the more traditional manner for estimating κ.

Steady state with respect to ^{228}Ra might also be a problem due to seasonality of upwelling inputs near the shelfbreak. Moore's article (1987) on ^{228}Ra in the South Atlantic Bight points out that the activity ratio of ^{228}Ra: ^{226}Ra is affected not only by decay and horizontal mixing, but also by vertical movement of water near the shelfbreak. The ratios are particularly revealing in 2-D vertical contours showing a distinct tongue of high activity ratio water penetrating below the shelfbreak in the winter, and a tongue of low activity ratio water extending up toward the shelfbreak in the spring.

Non-steady state conditions are not necessarily a problem if the measurements reflect long term mean conditions, i.e., if the variability is on a time scale much shorter than what the tracer measures. If variability is on time scales much less than the half life of long-lived isotopes, the isotope activities may average that variability over the time scale of their decay constants. The question is whether or not there is also long-term variability, so that even long-lived isotopes have steady-state problems. Data from the Mid-Atlantic Bight, presented in Chapter 3 suggest that there is some consistency over large time scales in processes affecting the long-lived isotopes. Even so, there is a range of possible solutions for κ, w that is open to considerable variability.

It would seem that variable κ and w are not only possible, but almost inevitable. Surely if we are looking at isotopes with half lives of 6-1600 years these parameters do not remain constant over that range of time scales. Even with short-lived isotope data, one would have to consider whether or not the measurements can be considered a reflection of steady state conditions, and if so, over what period does steady state apply? Time scales for variability in coastal areas are on the order of days. Moored arrays from NSFE (Beardsley et al. 1985) had correlation time scales for subtidal alongshelf currents of 4-10 days, and 3-7

days for cross-shelf currents. More recently, data from the shelfbreak PRIMER experiment (Gawarkiewicz et al., submitted) had correlation time scales of only 0.6 and 1.4 days for alongshelf and cross-shelf currents respectively, and 1.7 days for salinity.

Is it fair to say that data from long-lived tracers is actually measuring long-term mean parameters? Non-steady state is most important to consider are when a system is in flux between one state and another, such that the measurements taken reflect a prior state that has not come into equilibrium with current (or evolving) conditions. This could be a greater problem for the short-lived isotopes than for the long-lived isotopes because their short life span makes them extremely sensitive to conditions changing on a timescale of days; transient events that would not affect a stable element might affect the distribution of a quickly decaying element and therefore create a misrepresentation of the average state of the system. The long-lived isotopes ought to respond more sluggishly, and therefore would be more representative of mean conditions. On the other hand, large scale circulation may contribute to distribution patterns of the longer lived isotopes, so it is still a risky assumption even if some averaging is occuring over these isotopes' integration timescales.

There is also the question of κ itself being inherently non-steady. For eddy diffusivity of discrete patches over time, the diffusivity is a function of the age of the patch:

$$\kappa = Ct^n$$

The numerical values of C and n were derived empirically by Okubo (1974) for radially symmetrical tracer patches. The principle behind this is that over time, as a point source tracer diffuses by turbulent eddy diffusion into a larger and larger patch, a greater range

of eddy sizes are able to diffuse the tracer. At any given time, only eddy sizes less than the patch size are able to act on it in a diffusive manner. Eddies larger than the patch size simply advect the tracer in intact parcels rather than dispersing it. Eventually the patch is larger than all the eddies, and this relationship breaks down, such that κ becomes constant at large t (at least insofar as the total energy of the eddies themselves remains more or less constant). In any case there is no real time dependence once the patch is large; κ may remain constant or it may not depending on the physical processes controlling the eddies.

The theory behind this assumes a normal distribution of concentration radially outward in the patch, such that the length of the patch $L = 4\sigma$. Then equating the diffusion equation with the probability function, one gets $\sigma^2 = 2\kappa t$, and $L = 2\sqrt{2\kappa t}$. This last equation allows estimation of κ from a tracer experiment by measuring the diameter of the patch and the time elapsed since it was released.

Because the tracers were are concerned with here are not introduced as discrete patches, this relationship would probably not apply even on short time scales. Radium is introduced as a line source all along the coastline and so is subject to dispersion by both large and small eddies as soon as it has been dispersed into water deep enough for large eddies to exist. Different behaviour between the two short-lived isotopes would only be expected if one had an effective lifetime so short that it was never dispersed far enough out from shore to be affected by anything but the smallest scale disturbances. With both isotopes found at significant activities tens of kilometers from shore, this is not a problem.

Where these isotopes might be affected differently is on the upper slope where large Gulf Stream eddies are frequently found. If eddies on the shelf are not as large or vigorous as Gulf Stream rings, longer lived isotopes (especially ^{228}Ra and ^{226}Ra) could have a larger

eddy diffusivity when they encounter upper slope processes. It must be taken into account that eddies associated with the shelfbreak jet are also quite vigorous, so it is not clear that there would be a difference between the two regions in terms of horizontal turbulence. This must be considered an unresolved question for both the shelfbreak region and warm-core rings however. Observations by Garvine et al. (1989) showed shelfbreak jet eddies had surprising little *net* effect on horizontal diffusivity and cross-shelf exchange, and this could be true for Gulf Stream rings as well.

The methods described here present an alternative for estimating eddy diffusivity without making assumptions of zero advection which are unrealistic in coastal settings. While there are still many problems inherent in these calculations, particularly with regard to the steady-state assumption, the method does show the different effects of neglecting or including the velocity term. The steady state assumption may in fact severly limit the applicability of radium isotopes in general to determining horizontal mixing rates in settings with even moderate currents and advective variability. The following chapters present data from the Mid-Atlantic Bight that are analysed using methods described here. Horizontal distributions of radium were frequently surpising, however, leading to examination of alternative transport pathways than that of direct cross-shelf advection or diffusion.

Chapter 3

Cross-shelf Distribution of Radium and Nutrients in the Mid-Atlantic Bight

3.1 Introduction

The objective of this field study was to determine radium isotope distribution across the shelf-slope boundary in the Mid-Atlantic Bight in an effort to help understand cross-shelf transport. Earlier studies have been limited to estimating mixing rates and water mass ages for the inner shelf only (Moore 1997; Moore 2000a; Moore 2000b) and do not address the problem of transport across the shelfbreak front. Exchange between ocean margins and the open ocean is a continuing concern for balancing biogeochemical fluxes and carbon budgets in both large scale ocean models and regional ecological studies (Mahadevan and Archer 2000; Nixon et al. 1996; Seitzinger and Giblin 1996; Somayajulu et al. 1996; Michaels et al. 1996; Biscaye et al. 1994b; Falkowski et al. 1994). Problems related to complex physical conditions at the shelfbreak can only be resolved by considering a variety of data sources in order to assist in interpretation of results. I have designed a multi-disciplinary approach, conducting high resolution cross-shelf surveys that include measurement of the quartet of radium isotopes, salinity and nutrients, and interpreting results with the benefit of concurrently collected hydrographic and current data. Interpretation of these results will

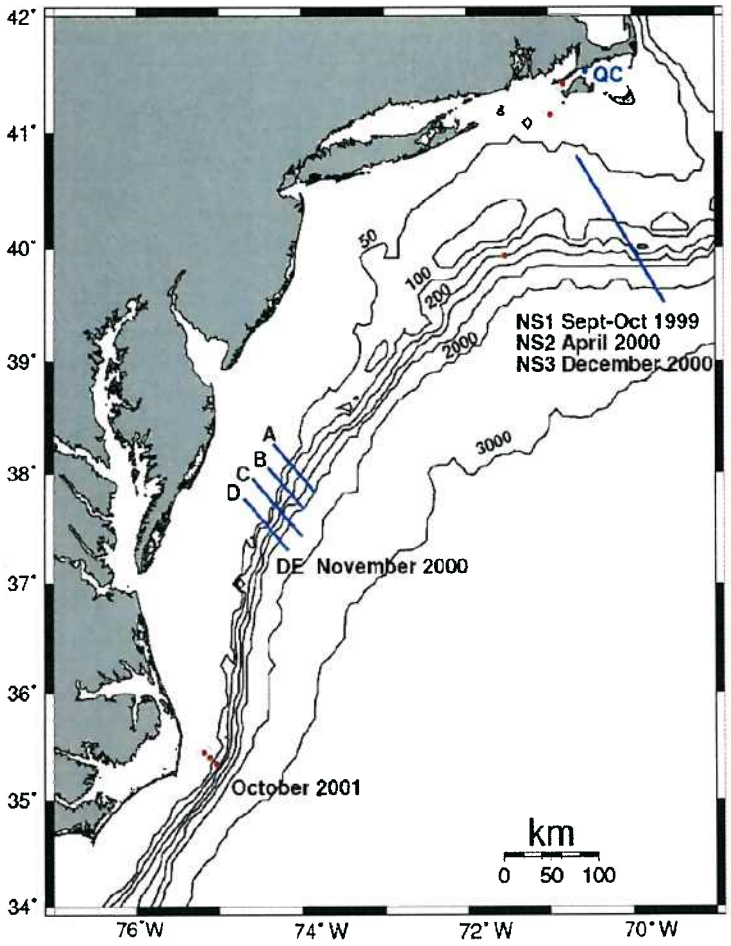

Figure 3.1: Location of sampling transects in Mid-Atlantic Bight.

be aided by methods presented in Chapter 2, but the datasets in the end were problematic for considering direct cross-shelf transport. The anomalies found in the data, the physical settings in which they occurred, and their implications for Mid-Atlantic Bight circulation are discussed further in Chapters 4 and 5.

3.2 Field and Laboratory Methods

The data for this study were collected during five cruises in the Mid-Atlantic Bight (Figure 3.1). Three of these were single transects of the shelfbreak near Nantucket Shoals (which will be referred to as NS1, NS2 and NS3), and one was a shelfbreak survey in the south-central MAB approximately 300 km north of Cape Hatteras, off the Delaware coast (DE). Measurements were made for the four radium isotopes, salinity, and current velocity on all transects, and supplementary nutrient, temperature, and hydrographic data were collected when possible.

3.2.1 Field Sampling

The Nantucket Shoals transect that was sampled is a well studied one, which overlaps the TOPEX satellite sub-track used by Fratantoni et al. (2001) for extensive ADCP studies of the shelfbreak front, and also includes stations from the PRIMER and Coastal Mixing and Optics (CMO) experiements. The three cruises were in fall, early winter, and spring. NS1 data were collected on the *R/V Oceanus* cruise OC349. Radioisotope and salinity samples were collected on 21 September 1999 at 7 stations along a 140 km transect across the shelf and upper slope, ending at the 75 m isobath. Distance from shore spanned approximately 120–260 km. A second crossing was made on the return trip on 7 October 1999, sampling only the inner 4 stations from the first crossing. Stations were spaced at approximately equal 20 km intervals. Shipboard acoustic doppler current profiling (ADCP) data was collected along the transects in both directions from the 60 m isobath to 50 km offshore of the 1500 m isobath.

NS2 data were collected along the same transect on the *R/V Endeavor* cruise EN335.

Radioisotope, nutrient, and salinity samples were collected on 1 April 2000 at 15 stations along a 170 km line starting near the 57 m isobath. Distance from shore spanned approximately 80–250 km. Sampling stations were spaced with higher resolution over the shelfbreak (6–10 km), and lower resolution over the outer shelf and upper slope (10-20 km). Shipboard ADCP data were collected simultaneously, ending 5 km offshore of the 1500 m isobath. Expendable bathythermograph (XBT) temperature data were also collected along the transect at approximately 5 km intervals.

NS3 data were collected on 4-5 December 2000 over 100 km of the Nantucket Shoals transect, from 100–200 km offshore, during cruise EN348 on the *R/V Endeavor*. Surface radiochemical and salinity data was collected with resolution of 6–7 km, as well as mid-depth and bottom samples from three stations. Due to time limitations, the transect ended near the edge of the shelf and a shelfbreak front was not resolved. The salinity at the outer station was only 34.13, indicating that the ship was still in shelf water. Nevertheless, bottom samples from this cruise provided valuable information on radium activity and isotope ratios in bottom water directly overlying MAB shelf sediments.

The survey in the south-central Mid-Atlantic Bight was conducted on the *R/V Cape Hatteras* cruise CH2300 and covered 4 cross-shelfbreak transects, spaced 20 km apart. All transects were sampled at 5 km intervals, with the exception of the most shoreward ends of 3 transects where resolution was lowered to 10 km. Surface radioisotope, nutrient, and salinity data were collected along 3 of the 4 transects (A, B and D). Conductivity, temperature, depth (CTD) profiles were performed at all stations, and ADCP data were collected over all transects. Mid-depth and bottom samples for radioisotopes were also collected at two stations.

3.2.2 Radium Measurement Methods

Seawater was collected in 150-250 L plastic barrels through 10 μm and 1 μm prefilters to remove large particles. Surface samples for the four radium isotopes were collected from 2–3 m depth via the ships' clean seawater lines. Subsurface samples were collected either by attaching a hose to the CTD frame and pumping from selected depths, or by filling multiple large volume Niskin bottles which were then drained into large barrels. The water was then pumped at approximately 1 L min^{-1} through filters made of acrylic fiber coated with manganese oxide to quantitatively remove the radium and preconcentrate it onto the filter column (Moore 1976).

For measurement of ^{223}Ra and ^{224}Ra, the Mn fibers were rinsed in distilled water, partially dried, fluffed, and placed in delayed coincidence alpha counters according to the methods developed by Moore and Arnold (1996). Within the counting apparatus, helium gas is passed through a closed system that includes a 1.1 L alpha scintillation cell. As the gas passes through the fiber columns, ^{219}Rn and ^{220}Rn, created by decay of ^{223}Ra and ^{224}Ra respectively, are flushed out and and circulate through the scintillation cell. Alpha decays of the Rn isotopes and their daughters are recorded by a photo-multiplier tube and routed through an electronic delayed coincidence system. The system differentiates between the ^{223}Ra and ^{224}Ra decay chains by looking for the difference in timing between their decay sequences. ^{219}Rn decays into ^{215}Po which has a 1.78 ms half-life. ^{220}Rn decays into ^{216}Po which has a 150 ms half-life. The first decay detected in the scintillation cell opens an electronic gate for ^{215}Po counts; if a second decay occurs within 5.6 ms, the pair is counted as a product of ^{223}Ra decay. If no decay occurs within this time period, the ^{223}Ra gate closes and a gate opens for 600 ms to register ^{216}Po decays; if a second decay occurs within this

time period the pair is counted as a product of ^{224}Ra decay. When analysis of the counts is done, statistical methods are used to correct for counts that are by chance misdirected into the wrong channel (e.g., a ^{216}Po decay that occurs during the first 5.6 ms when the ^{215}Po channel is open.)

After all short-lived counting is completed (see "Corrections" below), sample fibers were then ashed at high temperature, pulverized, and sealed in vials for ^{226}Ra and ^{228}Ra counting by well-type gamma spectrometers (Charette et al. 2001). ^{226}Ra is counted by way of its daughter isotope, ^{214}Pb, which has a strong gamma emission at 352 keV, while the ^{228}Ra daughter ^{228}Ac has a distinctive emission at 911 keV. To ensure equilibration of the daughter isotopes with their parents, sealed samples are counted after a minimum of 4 weeks.

The reliability of measurements is an important issue when sampling along transects where spatial resolution is necessarily limited and sample volume precludes taking multiple samples per station. Because the mechanics for counting both long- and short-lived radium are so isotope-specific, the chances of "false positive" results are extremely unlikely. A few conditions could result in high counts of short-lived isotopes, but they are simple to detect and correct. Electrical "spikes" that result in false counts occasionally occur despite surge-protection precautions. These spikes are identifiable in the data record because a) counts of both isotopes will be exceptionally high, and b) the data recorded will show a single time interval containing all the excess counts. The data is easily corrected by subtracting the counts and counting time from that interval. Secondly, if many counts are done in sucession with moderate to high levels of ^{224}Ra, its ^{212}Pb daughter can build up in the detectors. This can be prevented by performing the long counts for ^{223}Ra after the ^{224}Ra counts, as well as by flushing the detectors well and checking background between counts. Because

radium isotopes occur naturally in low levels, are not bioreactive, and are not normally found in man-made objects, direct contamination of samples is extremely unlikely. There is speculation that because the thorium parents of radium isotopes are particle-reactive, they could build up within the ship's intake system and release radium into sampled water, but there is no evidence of this actually occuring. A good check for this possibility is the presence of very low Ra measurements within a set of samples, which would not occur if the seawater system itself was introducing Ra. Erroneously low counts can occur if there are leaks in the counting system (the delayed coincidence system, the fiber column, or the counting vial) or if the radium has not been collected with high efficiency. To prevent errors of the first kind, standards are run regularly to test the integrity of the system and calculate counting efficiencies. Collection efficiency errors are suspected when all four sister isotopes are low; the more stable long-lived isotopes should not show great variability, and when both are unusually low it may be an indication that a significant portion of the radium has bypassed the filter fibers.

3.2.3 Corrections and Error Calculation

A small but significant amount of ^{224}Ra that is collected on the fibers will be from decay of its parent ^{228}Th in the water column and not from terrestrial inputs. Because thorium is also extracted onto manganese fibers, a correction for this "supported" ^{224}Ra can be made by performing second counts when ^{228}Th has equilibrated and the original ^{224}Ra has decayed away. This occurs at about 3-4 weeks after collection. All reported ^{224}Ra data is "excess" ^{224}Ra from coastal or sediment sources not supported by parent isotopes in the water column. ^{227}Th and ^{227}Ac, also collected on the fibers, behave similarly with

respect to ^{223}Ra (Figure 3.2). If there are initial ^{227}Th and ^{227}Ac activities on the fibers of 0.025 dpm/100L and 0.050 dpm/100L respectively (disequilibrium from more efficient scavenging of thorium) the decay of ^{223}Ra on the fibers would appear to be normal for the first week or two, but after one month there is a significant ^{223}Ra signal from ingrowth of the parent isotopes. Figure 3.3 shows the ^{223}Ra signal on samples from NS2 as they decay over a period of approximately 3 months; the square symbols indicate the expected activity without ingrowth from parent isotopes. ^{227}Ac activity at 2-3 months does not decay to zero, though it is lower than in the theoretical case shown. ^{227}Ac activity was nearly the same in nearshore samples with much higher initial ^{223}Ra. Measurements from transects NS2, NS3 and DE were corrected for ^{227}Ac-supported ^{223}Ra, which consistently averaged 0.015 dpm/100L over each sampling period. This is in close agreement with the measurements made by Shaw and Moore (2002) in the Southern Ocean southeast of Cape Horn, where activities were 0.01-0.02 dpm/100L in surface water. ^{227}Ac activity in open ocean waters of the Pacific are lower by about half, which they attribute to distance from continental sources of parent isotopes.

The propagated counting error was calculated for each sample to take into account counting error at each step. For the short-lived isotopes, the error for the first counts was calculated at the 2σ level (95% confidence level) using the total number of raw counts from the ^{219}Po and ^{220}Po channels (% error = $2/\sqrt{number\_counts}$). When second counts were done for supported Ra from ^{228}Th or ^{227}Ac, the 2σ errors from both counts were propagated as $\pm\sqrt{(ERR_1)^2 + (ERR_2)^2}$ for the final counting error. Because of the much lower natural abundance of ^{223}Ra, counting errors are generally higher for this isotope than for its short-lived sister ^{224}Ra. The error on the short-lived samples ranged in general from 5–12% for

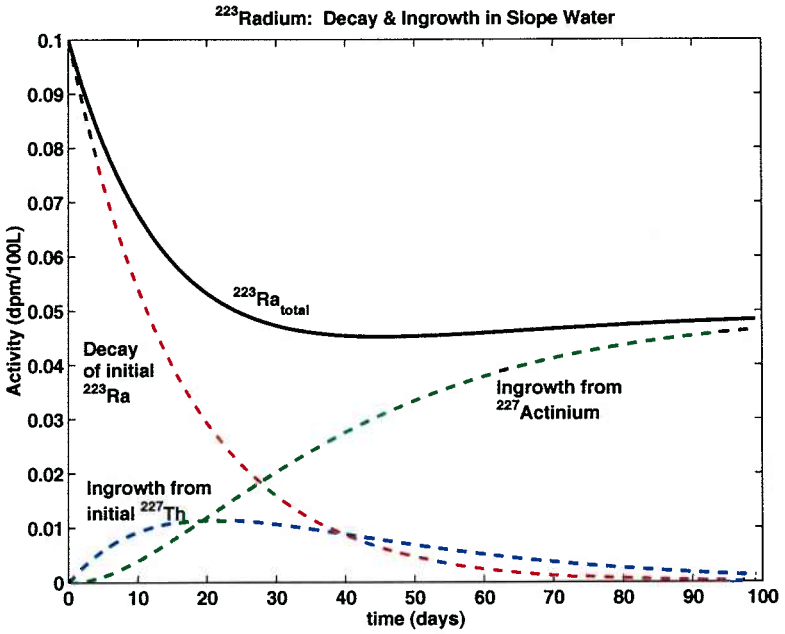

Figure 3.2: Theoretical decay and ingrowth of ^{223}Ra from an initial sample with 0.1 dpm/100L ^{223}Ra, 0.05 dpm/100L ^{227}Ac, and 0.025 dpm/100L ^{227}Th.

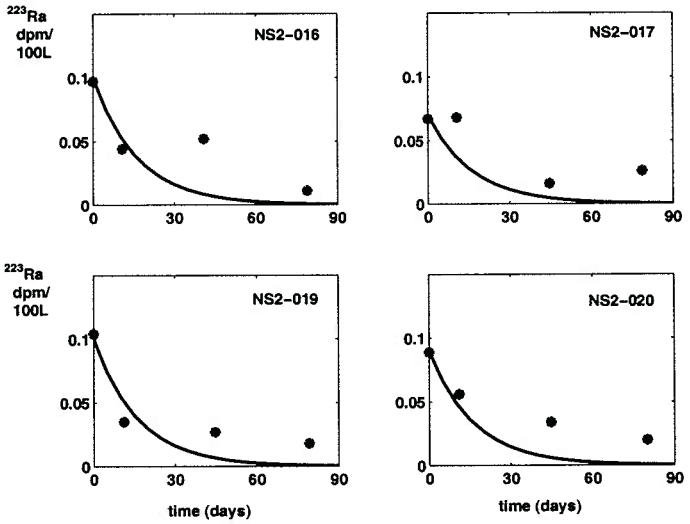

Figure 3.3: Measured ^{223}Ra on sample fibers over a period of 2 months. Stars indicate actual data. Solid lines indicate expected decay without ingrowth from parent isotopes.

^{224}Ra, and 15–30% for ^{223}Ra. In samples where the short-lived isotopes are very depleted the percent counting error can be much higher, but the absolute error is still very small. Counting errors on the long-lived isotopes were maintained at approximately 2–5% for ^{226}Ra, and 7–15% for ^{228}Ra. Because ^{223}Ra has such a low initial activity nearshore, and lower over the outer shelf and slope, count rates are quite low for samples in this region. When these low initial counts are combined with ^{227}Ac corrections, the accumulated counting error makes variations in activity almost insignificant. The low activities and large margin of error in ^{223}Ra beyond mid-shelf thus limits its utility in transport calculations, particularly those involving isotope ratios. It should also be noted that within a large group of samples, counting error can be expected to increase due to decay while a sample is in the queue to be counted (i.e., samples counted last will have fewer counts, and a larger ingrowth correction, and thus higher counting errors).

The efficiency of radium extraction onto the sampling filters was tested using dual filter cartridges placed in series. Mean extraction efficiencies for the short-lived isotopes were near 99% or higher.

Sample No.	^{224}Ra	^{223}Ra	^{228}Ra	^{226}Ra
NS3-113	96%	> 100%	97%	97.30%
QC-01	99%	100%	n/a	n/a
QC-03	98%	100%	n/a	n/a
Mean	98%	100%	97%	97%

Table 3.1. Extraction efficiencies for seawater radium onto manganese-coated filter fibers.

3.2.4 Reproduceability

To test the reproduceability of short-lived radium isotope results with low level samples, 12 replicates were counted from one uniform seawater source using the methods described

above. Nearshore filtered seawater was delivered to four large volume barrels in a rotating fashion so that each barrel had as similar a mixture of water as possible. To reproduce raw counts on fibers similar to those that might be encountered in mid-shelf or slope samples, the large volumes were subdivided into volumes of approximately one-quarter, one-eighth, and one-twentieth of the normal 200 L sample volume (Figure 3.4 a,b). 50 L and 25 L samples were filtered by pump the same as shipboard samples. 10 L sample were gravity filtered because the pump would not fit in the containers.

The standard deviation among eight pumped samples was $\pm 6.9\%$ for ^{224}Ra and $\pm 10.4\%$ for ^{223}Ra (dashed lines in figure). Two of the 10 L samples fell outside one standard deviation of the mean for the pumped samples. Possible reasons for the outliers are the non-standard delivery method, and the very low sample volume (more prone to measurement error when extrapolating to equivalent large volume activities). Among the pumped samples, the total error attributable to sampling and counting (1 standard deviation) is is well within the calculated counting errors which averaged 7.4% and 19.6% respectively. All of the pumped samples, plus or minus counting error, fell within one standard deviation of the mean. Errorbars reported with the study results are counting errors calculated at the 95% confidence level.

3.3 Results

Radium measured on cross-shelf transects in the Middle Atlantic Bight is presented here, followed by concurrently collected nutrient measurements. In order to better interpret radium distributions across the MAB shelf and upper slope, Tables 3.2 and 3.3 present average radium and salinity data for several nearshore sites in the Middle and South Atlantic

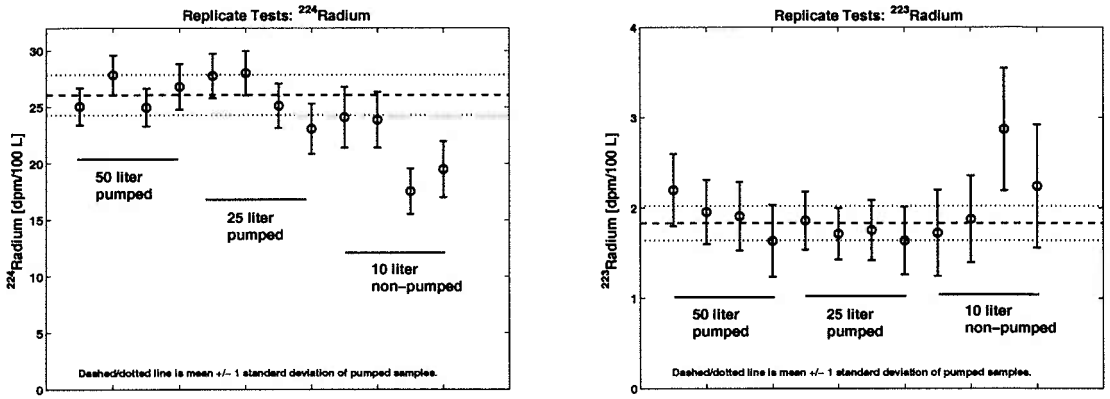

Figure 3.4: Activity of ^{224}Ra and ^{223}Ra in replicate samples taken from a uniform seawater source.

Bight, as well as for sites 100 km offshore, and for the open North Atlantic. Data is taken from several previous studies (Moore 1969; Kaufman et al. 1973; Moore 2000a; Charette et al. 2001) as well as the current one, and unpublished data from C. Gramling. ^{224}Ra activities in the nearshore zone (< 5 km from shore) average 13-26 dpm/100L, with higher means in the north. Nearshore ^{223}Ra averages 1.5-3.5 dpm/100 L, with higher means in the south. Accordingly,^{224}Ra:^{223}Ra ratios are higher in the north, 13-14, compared to about 5 in the south. It should be noted that there is considerable overlap within the data for each region, and the means for all regions are within one standard deviation of each other. An important point to keep in mind is that there is a great deal of variability spatially and temporally. Equally important, and mitigating the variability, processes that mix these isotopes offshore will in effect average them over timescales on the order of their half-lives. Nearshore activities of ^{228}Ra and ^{226}Ra average 21-25 dpm/100L and 7-19 dpm/100L respectively.

At 100 km from shore, ^{224}Ra activities average 0.1-1.0 dpm/100L, again higher in the north. At this distance, however, there is overlap between north and central regions, and

Location	Sample	Distance [km]	Salinity [PSU]	$^{224}Ra_{ex}$ [dpm/ 100L]	^{223}Ra [dpm/ 100L]	^{228}Ra [dpm/ 100L]	^{226}Ra [dpm/ 100L]
Woods Hole, MA							
mean of replicate tests	**QC01-08**	**<1**	**32.00**	**26.08**	**1.83**	**40.21**	**15.06**
Standard Deviation				2.82	0.36	1.43	2.12
Elizabeth Islands, MA							
N. Mid-Atlantic Bight	NS-012	5	32.40	7.05	0.5		
Waquoit Bay Outlet, MA	WB1	<1	31.13	18.3	1.2	26.5	7.5
N. Mid-Atlantic Bight	WB2	<1	31.09	28.5	1.6	27.4	6.2
Charette, et al. (2001)	WB13	<1	31.49	13.1	0.8	11.6	4.3
	WB14	<1	31.43	18.0	2	20.7	6.6
	WB15	<1	31.02	19.9	2.3	21.1	7.8
	WB21	<1	31.46	12.4	1	17.7	7
Mean			**31.27**	**18.4**	**1.5**	**20.8**	**6.6**
Standard Deviation			0.19	5.3	0.5	5.3	1.1
Wilmington, NC	NC228*	<1	36.24	9.6	2.3		
South Atlantic Bight	NC247*	<1	36.29	11.2	3.1		
C. Gramling	NC229*	<1	36.29	10.7	1.7		
(unpublished)	NC231**	<1	36.14	21.6	3.8		
* high tide, ** low tide	NC250**	<1	36.22	24.4	6.4		
	NC232**	<1	36.17	24.3	3.2		
Mean			**36.22**	**17.0**	**3.4**		
Standard Deviation			0.06	7.2	1.7		
Cape Fear-Savannah R.	1A	0.9	33.97	16.51	3.75	24.61	23.37
South Carolina,	1B	0.9	35.53	32.27	4.91	27.94	21.75
South Atlantic Bight	2	1.9	n/a	14.78	4.25	27.49	20.04
Moore (2000)	3	3.7	33.86	3.62	2.11	40.56	27.83
	28	4.0	34.30	5.71	1.75	24.08	6.44
	29	3.0	34.52	10.45	1.88	27.84	18.61
	33	3.0	34.96	15.41	4.34	27.88	20.01
	37	4.8	35.20	14.43	2.93	25.54	20.10
	57	4.8	33.60	20.58	2.44	25.33	17.33
	123	4.6	35.56	5.00	1	15.96	14.07
	150	4.6	32.70	12.84	3.08	24.38	18.98
	163	3.7	35.95	8.04	1.41	14.08	13.53
	209	3.7	33.78	24.59	2.92	40.13	30.75
	239	3.7	36.03	5.04	1.29	14.71	15.26
	242	4.0	35.00	9.02	1.77	17.45	13.61
Mean			**34.64**	**13.22**	**2.65**	**25.20**	**18.78**
Standard Deviation			0.98	8.02	1.22	7.87	6.00

Table 3.2. Average nearshore radium activities on the western North Atlantic coast.

Location	Sample	Distance [km]	Salinity [PSU]	$^{224}Ra_{ex}$ [dpm/ 100L]	^{223}Ra [dpm/ 100L]	^{228}Ra [dpm/ 100L]	^{226}Ra [dpm/ 100L]
Nantucket Shoals	NS2-025	110	33.22	0.66	0.09	8.85	9.71
N. Mid-Atlantic Bight	NS3-119	100	32.55	1.26	0.11	17.18	9.55
	NS3-118	106	32.56	1.15	0.27	12.37	7.39
Mean		**105**	**32.78**	**1.02**	**0.16**	**12.8**	**8.88**
Standard Deviation			0.38	0.32	0.1	4.18	1.3
Delaware Shelf	DEA-009	94	33.68	0.79	0.09	7.05	8.15
Cen. Mid-Atlantic Bight	DEA-010	99	33.72	0.79	0.07	7.26	7.2
	DEA-011	104	34.72	0.4	0.07	6.55	8.94
	DEB-024	95	33.71	1.35	0.03	7.3	7.81
	DED-055	95	33.87	0.19	0.06	8.16	8.73
	DED-054	100	33.86	0.1	0.04	7.73	8.93
	DED-053	105	34.18	0.64	0.04	7.27	7.95
Mean		**99**	**33.96**	**0.61**	**0.06**	**7.33**	**8.24**
Standard Deviation			0.37	0.43	0.02	0.51	0.65
Cape Fear-Savannah R.	11	98	36.26	0.04	0.02	--	--
South Carolina,	136	98	36.29	0.00	0.13	8.16	8.84
South Atlantic Bight	179	95	35.26	0.00	0.15	11.17	9.63
Moore (2000)	180	106	35.96	0.58	0.13	7.53	10.10
	185	102	35.74	--	--	11.03	10.51
	223	100	36.23	0.10	0.05	4.82	8.20
	226	100	35.89	0.00	0.08	6.73	8.73
Mean		**100**	**35.95**	**0.12**	**0.09**	**8.24**	**9.33**
Standard Deviation			0.37	0.23	0.05	2.48	0.89
N. Atlantic, Western Gyre	LV-8	--	--	--	--	2.90	8.29
Moore (1969);	Ra-11	--	--	--	--	1.60	8.42
Kaufman, et al. (1973)	LV-6	--	--	--	--	1.50	8.82
	966	--	--	--	--	2.60	8.67
	965	--	--	--	--	3.50	8.54
	849	--	--	--	--	3.50	8.54
	1007	--	--	--	--	2.90	8.53
	903	--	--	--	--	2.00	8.70
	964	--	--	--	--	3.10	8.38
Mean						**2.73**	**8.60**
Standard Deviation						0.75	0.14
N. Atlantic, Central Gyre	1001	--	--	--	--	1.50	8.33
Kaufman, et al. (1973)	1002	--	--	--	--	1.70	8.95
	1003	--	--	--	--	1.40	8.24
	1004	--	--	--	--	1.30	8.67
	1005	--	--	--	--	1.40	8.24
	1006	--	--	--	--	1.70	8.50
Mean						**1.50**	**8.49**
Standard Deviation						0.17	0.28

Table 3.3. Average offshore radium activities in the North Atlantic.

between central and southern regions, but not between north and south. Activity in the South Atlantic Bight is on average nearly an order of magnitude less than in the northern MAB, an indication that local mixing processes are different in the two regions, and may be more rapid in the north. ^{223}Ra activities average 0.06-0.16 dpm/100L, higher in the north, and all within one standard deviation of the others. If the northern average is not an artifact of sparse sampling, this would also support the idea of more rapid mixing in the north, particularly since the ^{223}Ra activity is initially lower in the north than the south in the nearshore zone. The Gulf Stream, which is much more proximate to shore in the South Atlantic Bight, could also play a role in diluting the coastal signal in that region. Average ^{228}Ra activities at 100 km are 7-13 dpm/100L. Individual activities in the northern MAB (NS2, NS3) and South Atlantic Bight sample sets vary by over a factor of two, while the central region (DE) activities are much more consistent. This is most likely due to the range in times over which the sampling took place, over months in the case of the northern and southern regions, and over a period of a few days in the central region. The very long-lived ^{226}Ra should be much more well mixed, as the ^{226}Ra means at 100 km demonstrate. Average activities of ^{226}Ra at 100 km are 8.2-9.3 dpm/100L, all within one standard deviation of each other.

In the western edge of the North Atlantic gyre, ^{228}Ra decreases to an average of 2.7 dpm/100L; ^{226}Ra is in the same range as it is on the shelf, averaging 8.6 dpm/100L with a standard deviation of only 0.14. In the central gyre ^{228}Ra activities are at their lowest and most consistent, with a mean of 1.5 dpm/100L. ^{226}Ra is steady at 8.5 dpm/100L. No short-lived Ra isotope data exists for the open Atlantic, however with parent isotopes in short supply their supported activities could not be high. ^{224}Ra is a product of the low

activity ^{228}Ra, and is preceded by a particle reactive parent which can be depleted from surface waters. The ^{235}U series of which ^{223}Ra is a member is much less abundant than ^{238}U series isotopes, and ^{223}Ra is preceded by three particle reactive parents as well. "Excess" activities of these isotopes, with no local sources, would of course be zero at great distance from the shore and bottom sediments.

To help determine when sediment disturbances or upwelling had affected surface radium activity, water samples were pumped from mid- and bottom depths on transects DE-A and NS3. Profiles of ^{224}Ra and ^{223}Ra from the pumped samples are shown in Figure 3.5. With the exception of the one shallow water sample at DEA-007, all are elevated in ^{224}Ra over the surface activity. (DEA-007 shows no deep enrichment primarily because it is nearer to shore and the surface ^{224}Ra is higher to begin with.) In three of the profiles, ^{223}Ra is also elevated over the surface activity, but not by as great a percentage as ^{224}Ra. In the four samples where ^{224}Ra is elevated at depth, the ^{224}Ra:^{223}Ra ratios are significantly higher in the bottom samples, ranging from 0.6-8.8 at the surface to 9.1-19.7 at the bottom. Complete isotope, salinity and nutrient data for subsurface profiles are in Tables 3.6-3.8 of the end of the chapter.

In this study, a high degree of variability was seen in radium distribution across the Mid-Atlantic Bight shelf, but there were some recurrent features which will be discussed in the following sections. ^{228}Ra and ^{226}Ra show the most consistency, as might be expected; their distribution reflects the long integration time characteristic of isotopes with long half-lives. In these transects, ^{228}Ra typically decreased by 30-50% from mid-shelf to upper slope, while ^{226}Ra was relatively well mixed over this region, showing little if any decrease away from shore after the mid-shelf. ^{223}Ra was often low across the whole transect, but occasionally

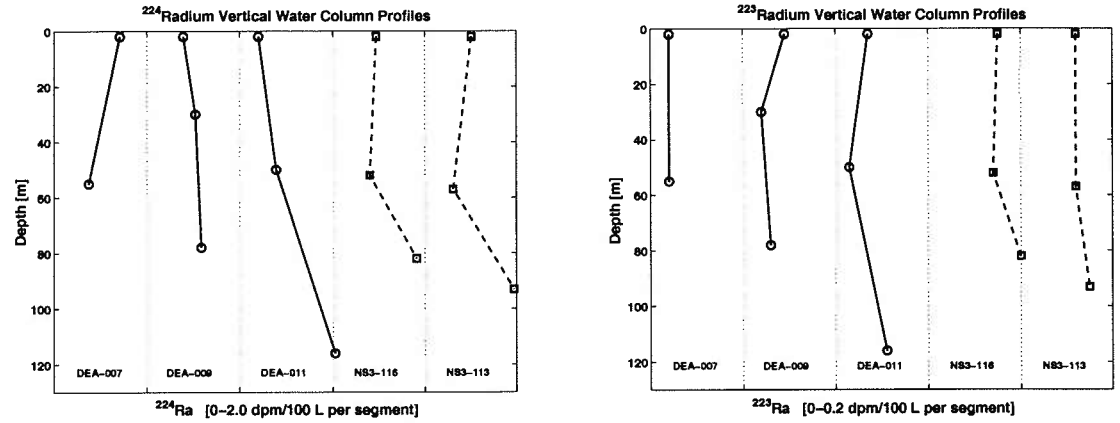

Figure 3.5: Vertical profiles of ^{224}Ra and ^{223}Ra from transects DE-A and NS-3. Each horizontal segment is equivalent to 0-2.0 dpm/100L for ^{224}Ra, and 0-0.2 dpm/100L for ^{223}Ra

was elevated at mid-shelf and decreased to near zero over the upper slope. On the other hand, ^{224}Ra, though frequently elevated at mid-shelf, always decreased to zero before the shelfbreak jet. This indicates that cross-shelf transport may have been occurring on the timescale of the ^{223}Ra (2 months), but not on the timescale of ^{224}Ra (3 weeks). Small-scale features were frequently observed in the short-lived isotope data, which often corresponded to anomalies in salinity and nutrients. Frequently these were associated with Gulf Stream filaments or warm core rings that we observed in the area in hydrographic or satellite sea surface temperature data. The temporal and spatial variability in the short-lived isotope data, particularly ^{224}Ra, meant they were often of limited usefulness in calculating mixing rates that depend on steady-state conditions. However, the same characteristics made these isotopes especially useful as tracers of small-scale water mass movement.

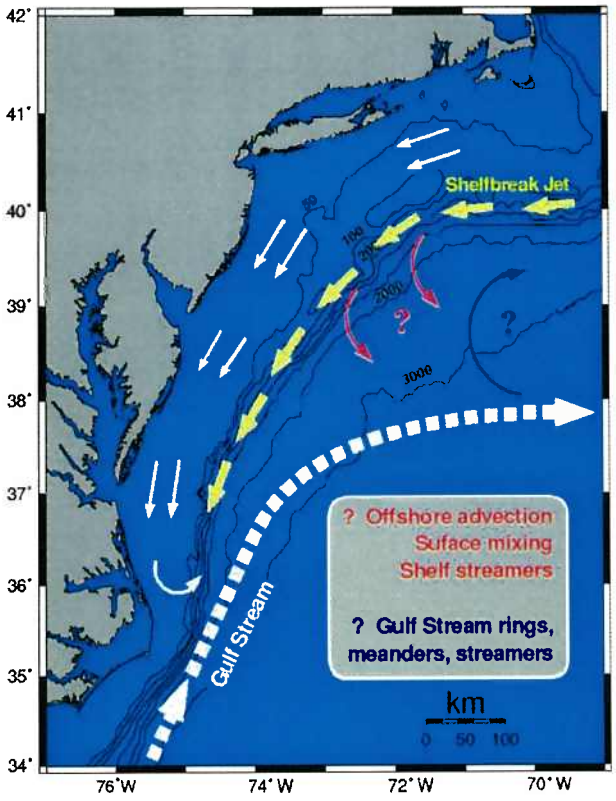

Figure 3.6: Potential pathways of transport in the Mid-Atlantic Bight.

3.3.1 Central Mid-Atlantic Bight

Because the short-lived Ra signal is detectable further offshore in the Mid-Atlantic Bight, it is possible to use these isotopes as a new tool for studying cross-shelf transport in this region. Rapid or transient exchange processes such as shelf streamers, eddy filaments, or short-lived water mass intrusions are therefore within the realm of detection using ^{223}Ra and ^{224}Ra.

The radium and nutrient distributions measured over a 60×70 km outer shelf region

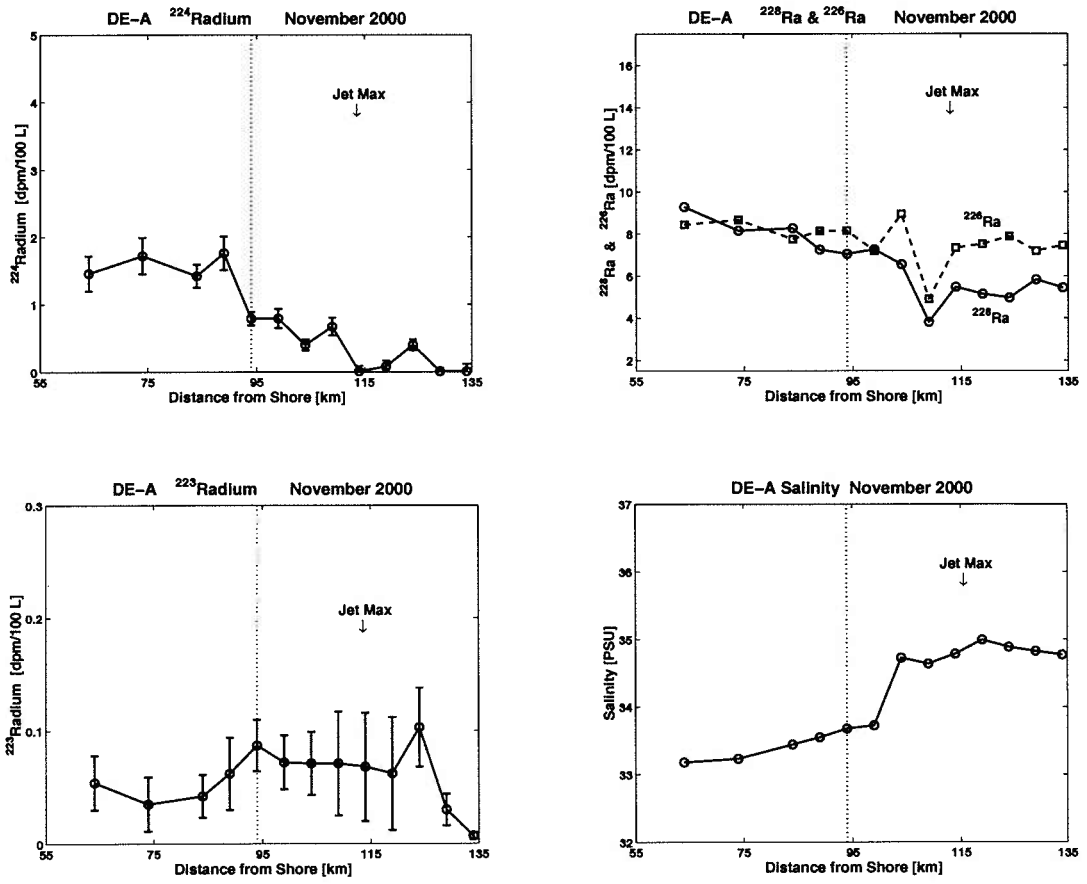

Figure 3.7: Radium and salinity over transect DE-A, Mid-Atlantic Bight Delaware shelf, 3-5 November 2000. Dotted line indicates the position of the 100 m isobath.

over the course of 3 days during the late fall 2000 cruise are illustrative of the small-scale variability that is possible in the coastal zone. Figures 3.7-3.12 show cross-shelf sections of long- and short-lived radium, salinity, nitrate, silicate and phosphate for each of the three transects that were sampled. Complete data tables are located in Tables 3.6 to 3.14 at the end of the chapter. Plots are annotated with the location of the maximum velocity of the shelfbreak jet, and the position of the 100 m isobath which is located here at about 90-95 km from shore. The width of the shelfbreak jet where velocity exceeds 30 cm/s is 10-15 km. Maximum jet velocity at the surface during this period was 40-60 cm/s. A saline surface

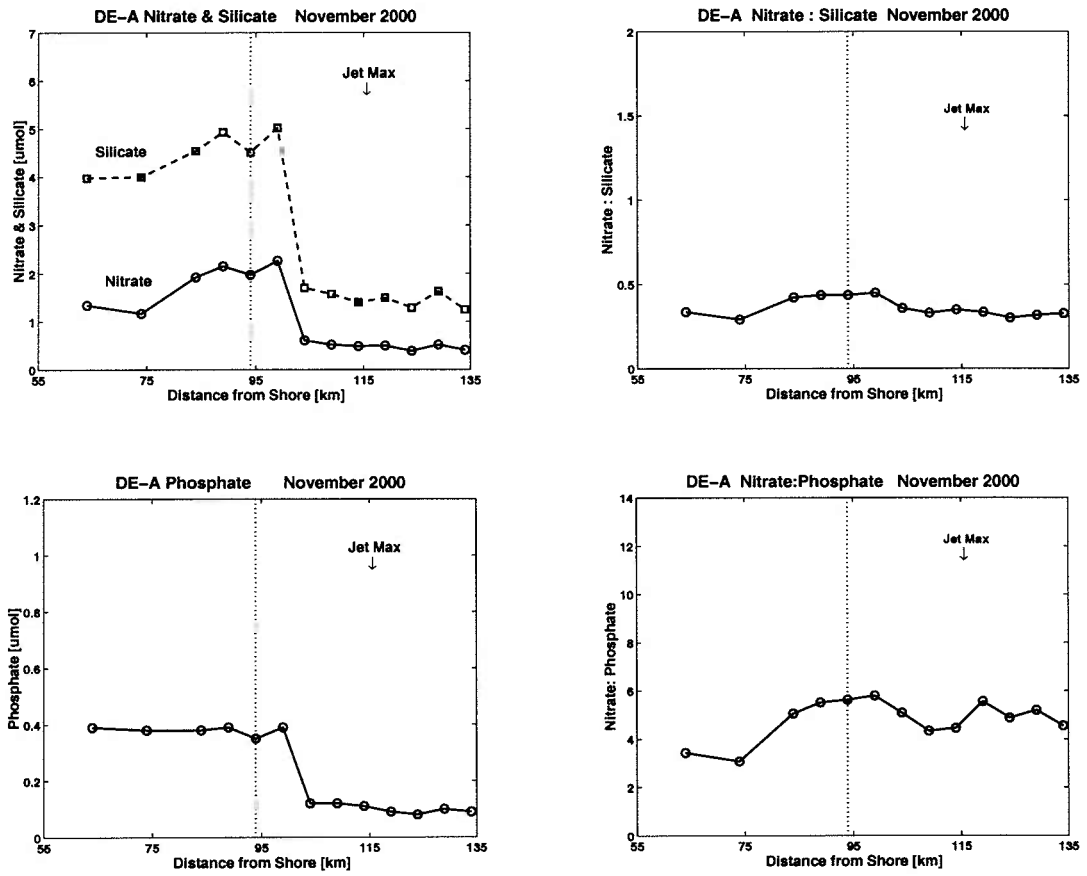

Figure 3.8: Nitrate, silicate and phosphate over transect DE-A, Mid-Atlantic Bight Delaware shelf, 3-5 November 2000. Dotted line indicates the position of the 100 m isobath.

intrusion was present over the outer 10-30 km of the transects, with salinity over 36 PSU at some outermost stations. Satellite imagery shows the presence of streamers extending from the crests of Gulf Stream meanders in this area (see Chapter 4, Figure 4.9). Strong salinity fronts were observed near the shelfbreak at the boundary of the saline intrusion, and weaker fronts were detected at mid-shelf, with surface outcrops 75-80 km offshore near the 60 m isobath.

The activity of the short-lived isotopes shows a great deal of variability, especially over

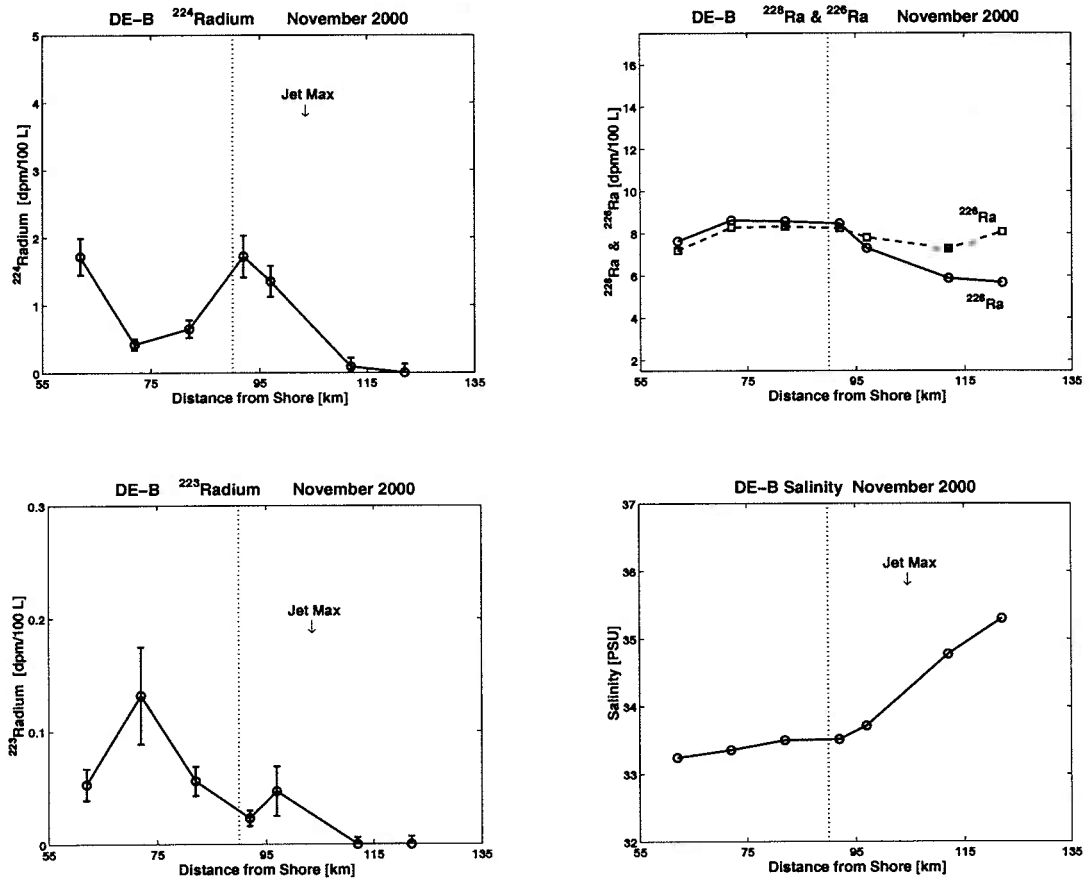

Figure 3.9: Radium and salinity over transect DE-B, Mid-Atlantic Bight Delaware shelf, 3-5 November 2000. Dotted line indicates the position of the 100 m isobath.

transects DE-B and DE-D. Only transect DE-A shows a fairly consistent decrease of ^{224}Ra with distance from shore. ^{223}Ra is very low across all transects, with little discernable trend. However on all transects ^{224}Ra decreases to zero immediately after the shelfbreak jet maximum. Thus it appears that the jet is a barrier to transport on the timescale of this isotope (approximately 3 weeks). On the other hand, ^{223}Ra maintains a more consistent activity on both sides of the jet and may be transported cross-shelf within the span of its useful (measurable) lifetime (approximately 2 months). This gives us some rough guidelines for estimating transport times across the jet boundary. If there was a clear gradient in ^{223}Ra

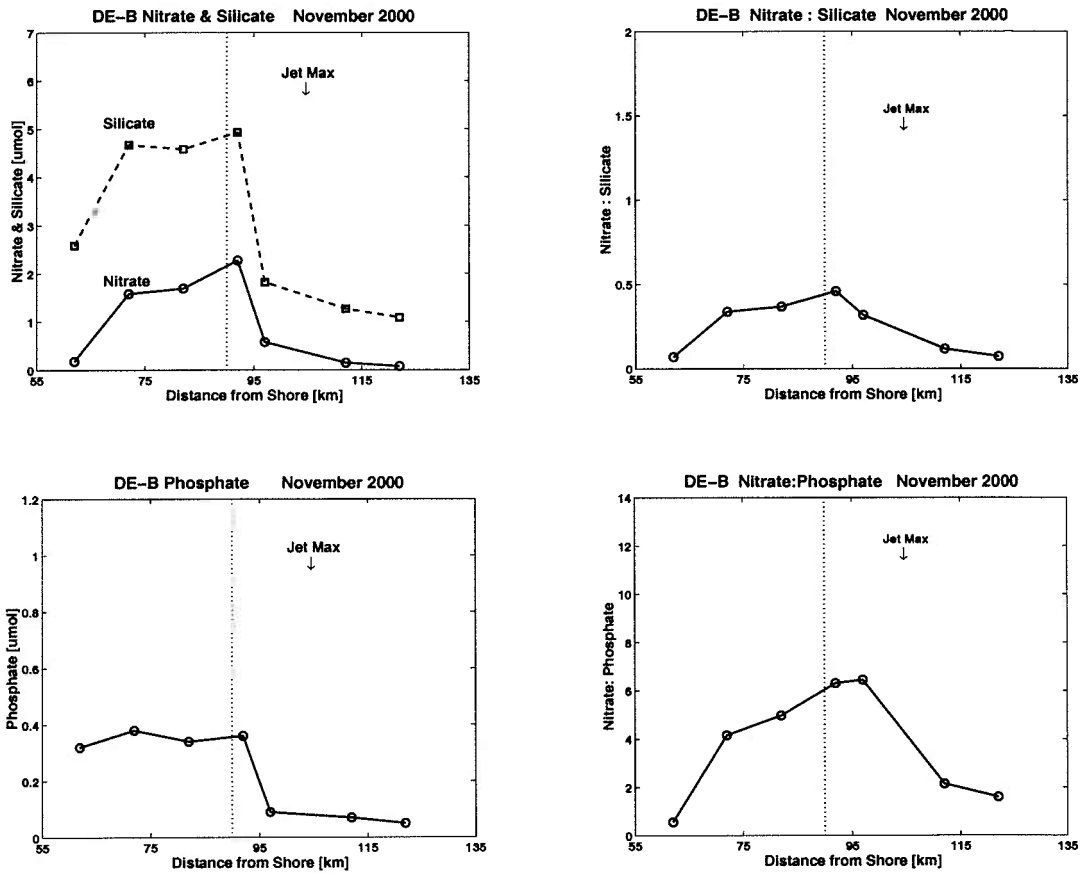

Figure 3.10: Nitrate, silicate and phosphate over transect DE-B, Mid-Atlantic Bight Delaware shelf, 3-5 November 2000. Dotted line indicates the position of the 100 m isobath.

across the shelfbreak it would be possible to use an isotope ratio of ^{223}Ra:^{228}Ra to determine a cross-jet transport time, but none of the transects here have differences in starting and ending activities of ^{223}Ra that are significantly larger than the error associated with the measurements. From this data is is really only possible to say that the transport time is probably greater than 16 days and perhaps less than 50. Activities < 0.1 dpm/100L are extremely low (approximately 1-5% of nearshore activities) so one might argue that ^{223}Ra is effectively zero across most of the transect, especially with the large errors.

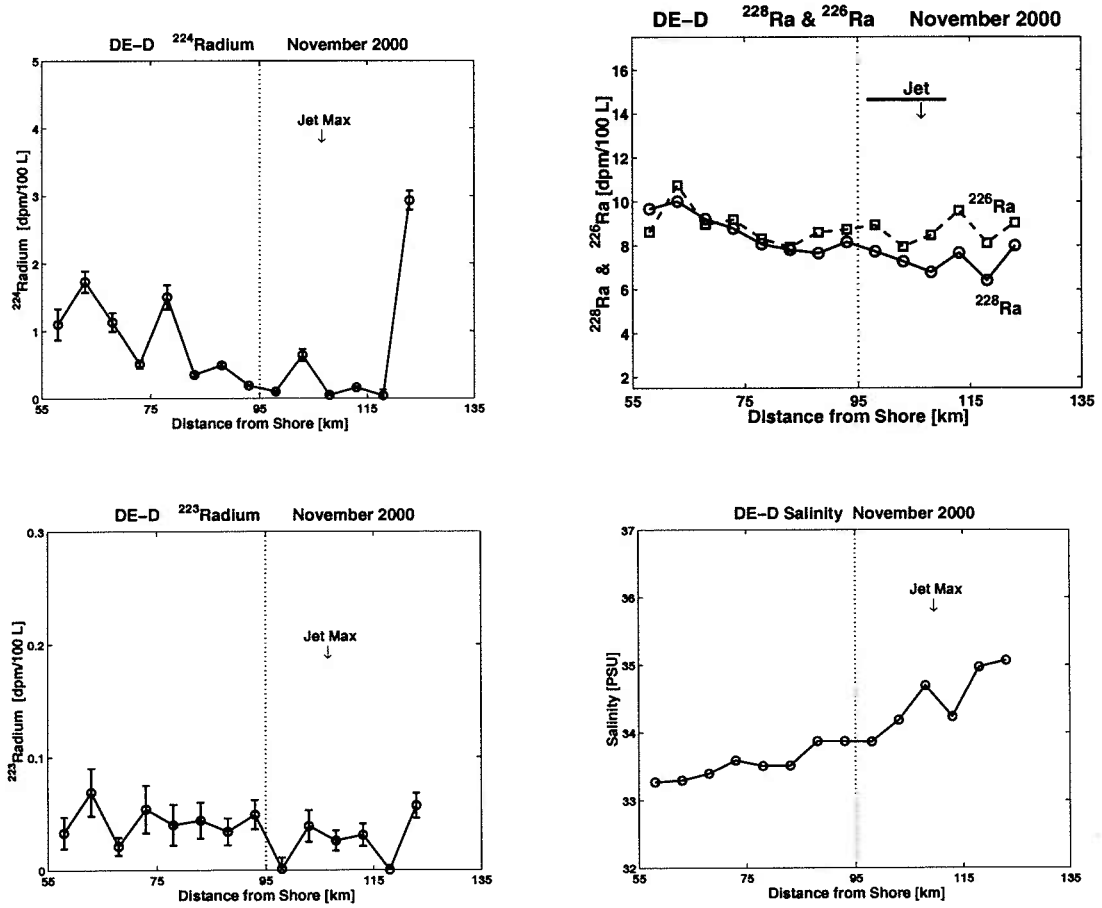

Figure 3.11: Radium and salinity over transect DE-D, Mid-Atlantic Bight Delaware shelf, 3-5 November 2000. Dotted line indicates the position of the 100 m isobath.

Large peaks in ^{224}Ra activity occur on transects DE-B near the shelfbreak and DE-D at the outermost station. Both are accompanied by little or no increase in the other radium isotopes. Other characteristics of the two samples do not match however. The peak in transect DE-B occurs where salinity is still low and where the nutrients are at their highest concentration. The peak ath the end of transect DE-D occurs in very high salinity ($>$ 35 PSU), low nutrient ($NO_3^- = 0\mu M$) water in the midst of the saline incursion. This suggests very different sources for the two. ^{224}Ra activity, salinity and nutrients in bottom

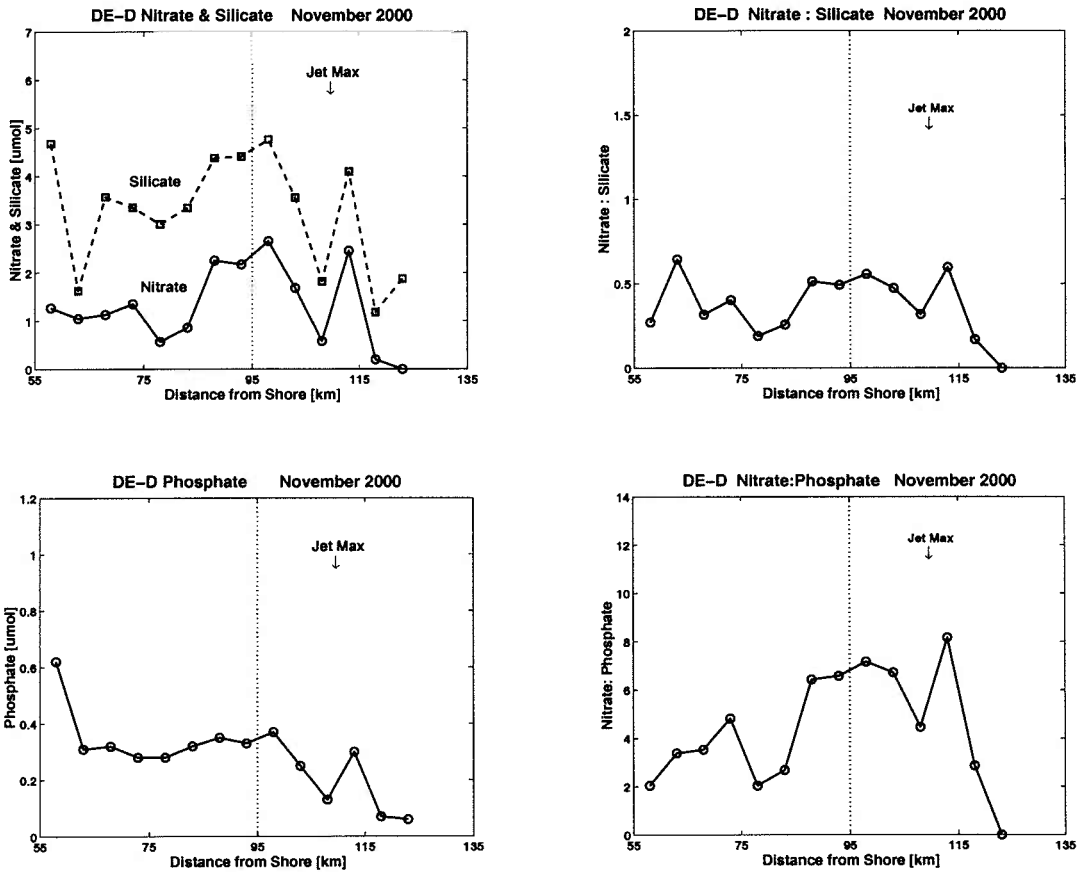

Figure 3.12: Nitrate, silicate and phosphate over transect DE-D, Mid-Atlantic Bight Delaware shelf, 3-5 November 2000. Dotted line indicates the position of the 100 m isobath.

water sampled near the shelfbreak during this survey (Tables 3.9-3.11) are similar to the DE-B sample and this is a possible source if vertical mixing had occurred recently. The possible sources and pathways for high salinity, high ^{224}Ra water were unexpected and will be discussed at length in Chapter 5.

The long-lived isotopes exhibit the expected gradual decrease in activity offshore, with ^{228}Ra decreasing faster than ^{226}Ra. Transect DE-A has the only major anomaly in activity, near the shelfbreak jet maximum. It is possible this could be related to the age of the water

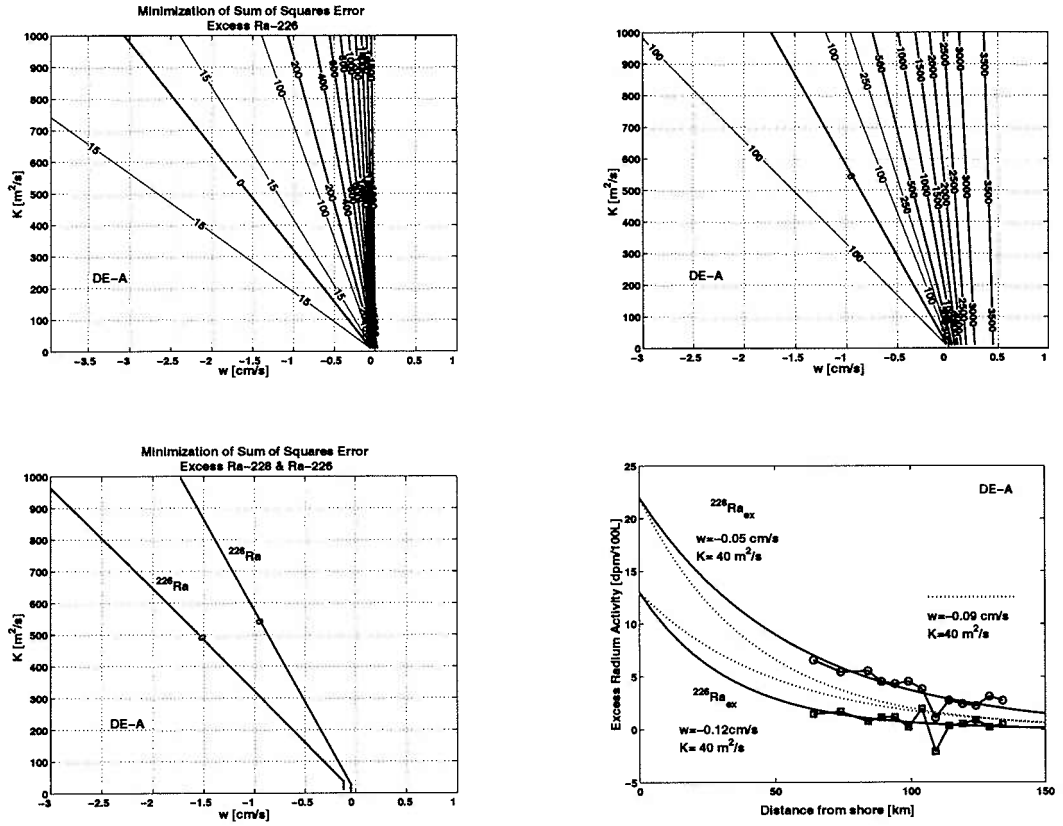

Figure 3.13: Minimization of sum of squares error for advection-diffusion-decay model with "excess" ^{226}Ra and ^{228}Ra data from transect DE-A. Calculated curves (solid lines) are shown in the lower right for the two isotopes with slightly different advective rates. Circle and square markers are actual data points. The dotted lines indicate the curves for the two isotopes if an intermediate value of w is used for both.

in the jet; because it is travelling predominantly along-shelf for large distances from the northeast, water within the jet might have become depleted over time. However this is not seen in measurements taken near the jet on the other transects.

Nutrient concentrations in this region are elevated over the mid- and outer shelf and lower over the upper slope. There is a pronounced peak in concentration just over the shelfbreak near the 100 m isobath, after which concentrations drop dramatically. Transect DE-D has an anomalous peak in nutrients at 115 km, just offshore of the shelfbreak jet.

The nutrient peak is accompanied by a slight elevation in the long-lived isotopes and a drop in salinity. This combination of features could be an indication of a small water mass or streamer from fresher, more nutrient- and isotope-rich shelf water.

The smooth gradients in the long-lived isotopes, particularly those from transect DE-A, make them ideal candidates for calculations of eddy diffusion coefficients using the sum of squares method. Unfortunately the ^{224}Ra data from transect DE-A is not as useful because the ^{223}Ra data does not have a discernable gradient and also has very large error relative to the activity levels. Without a short-lived partner it would be impossible to constrain both κ and w, even though velocity data is available. Velocities from the ADCP and hydrographic data are too large and variable to use as a constraint on w; cross-shelf surface velocity along this transect varies from -10 cm/s (shoreward) to +20 cm/s (seaward). With that kind of variability it is possible that the mean velocities on the timescales of ^{224}Ra and ^{223}Ra could also differ significantly.

Error minimization for an advection-diffusion-decay model is shown in Figure 3.13 for excess ^{226}Ra and ^{228}Ra data from transect DE-A. The closest approach of the two zero contours occurs at about $\kappa = 40$ m^2/s with $w \approx -0.5$ cm/s for ^{228}Ra to -0.12 cm/s for ^{226}Ra. Curves are shown for the two isotopes using their respective best fit value of w (solid lines). The dashed lines indicate the calculated curves for each isotope using an intermediate value of $w = -0.9$ cm/s for both. This shows how very sensitive the calculations are to extremely small variations in advection. It must also be noted that velocities, and variations in velocity, this small could only be realistically measured by moored instruments that can provide a long-term mean.

In conjunction with measured nutrient gradients, these parameters can now be used

to estimate the advective-diffusive nutrient flux across the shelfbreak. Using data from the 100 meter isobath station, and from 20 km beyond the 100 m isobath (95 km and 115 km from shore) we can calculate nutrient gradients across the shelfbreak. At the 200 m isobath, Si= 4.5 μmol/L and the gradient dSi/dx= $-0.15\,\mu$mol/m^3·m. For nitrate and phosphate, N= 2 μmol/L, dN/dx= $-0.08\,\mu$mol/m^3·m and P= 0.4 μmol/L, dP/dx= $-0.015\,\mu$mol/m^3·m. Equation 2.6 gives the following cross-shelfbreak surface fluxes (positive offshore):

Flux [μmol/m^2·s]	Total	Advective	Diffusive
J_{Si}	1.5	-4.5	6.0
$J_{NO_3^-}$	1.2	-2.0	3.2
$J_{PO_4^{3-}}$	0.3	-0.3	0.6

Table 3.4. Nutrient flux across the 200 m isobath of section DE-A. Parameters from long-lived Ra isotope data: $\kappa = 40$ m^2/s, $w = -0.10$ cm/s.

Under these conditions, the advective transport, while not the largest component, is still of the same order as the diffusive transport and plays an important role in scaling back the total flux. Csanady and Hamilton (1988) calculate an average 2-way shelf-slope exchange rate of 0.3 m^3/s per meter coastline over the upper 200 m. Using the shelf-slope concentration difference for nitrate cited in their study, based on Riley (1975), ΔN = +0.86 μmol N/L (12 μg/L), the shoreward flux across the shelfbreak totals 258 μmol/m· s over 200 m depth, or -1.29 μmol/m^2· s. The magnitude of the fluxes derived from the two different methods are similar, lending some support to the κ and w values derived from long-lived Ra data. It must be noted however that nutrient measurements are instantaneous snapshots at one point in time, whereas even the short-lived isotopes integrate over much longer time scales (decadal to thousands of years in the case of ^{228}Ra and ^{226}Ra). This presents one of

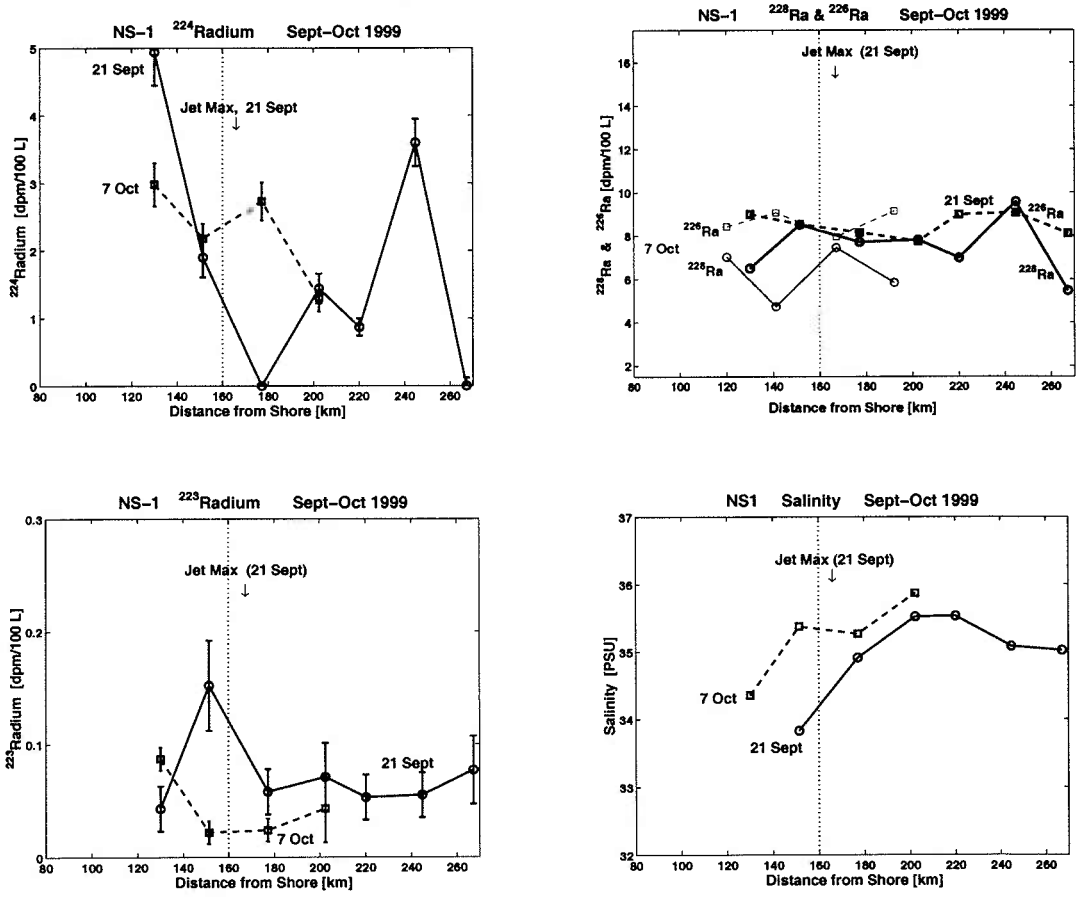

Figure 3.14: Radium and salinity over transect NS-1, Mid-Atlantic Bight Nantucket Shoals shelf, 3-5 21 September 1999 (solid lines) and 7 October 1999 (dashed lines). Vertical dotted line indicates the 100 m isobath position.

the major difficulties of calculating such fluxes based on individual measurements.

3.3.2 Northern Mid-Atlantic Bight

In the northern Mid-Atlantic Bight transects over the Nantucket Shoals shelf region were made during three seasons, fall (NS1), spring (NS2) and early winter (NS3). The shelf is broader in this area, with the 100 m isobath located 160 km from shore. It was not possible to collect detailed hydrographic data on these transects, so only ADCP velocity

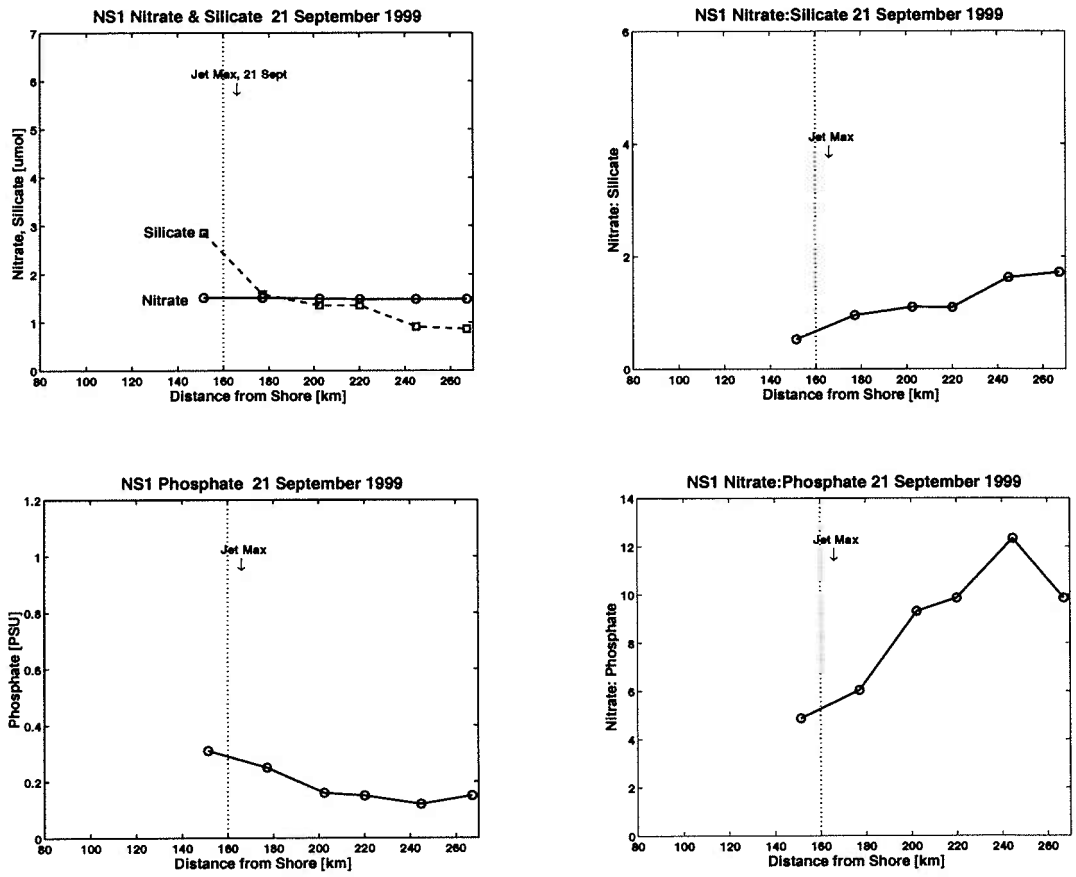

Figure 3.15: Nitrate, silicate and phosphate over transect NS1, Mid-Atlantic Bight, Nantucket Shoals shelf, 21 September 1999. Dotted line indicates the position of the 100 m isobath.

measurements are available along with some bathythermograph data. The shelfbreak jet was a less prominent feature on these surveys, and its velocity was lower than in the southern transects. During surveys NS1 and NS2 large warm core rings dominated the shelfbreak and upper slope region, influencing salinity and temperature as well as the flow magnitude and direction.

Two days prior to the outbound transect of survey NS1 in September 1999, Hurricane Floyd passed by the Northeast U.S. coast. The subsequent ^{224}Ra activity on the shelf during

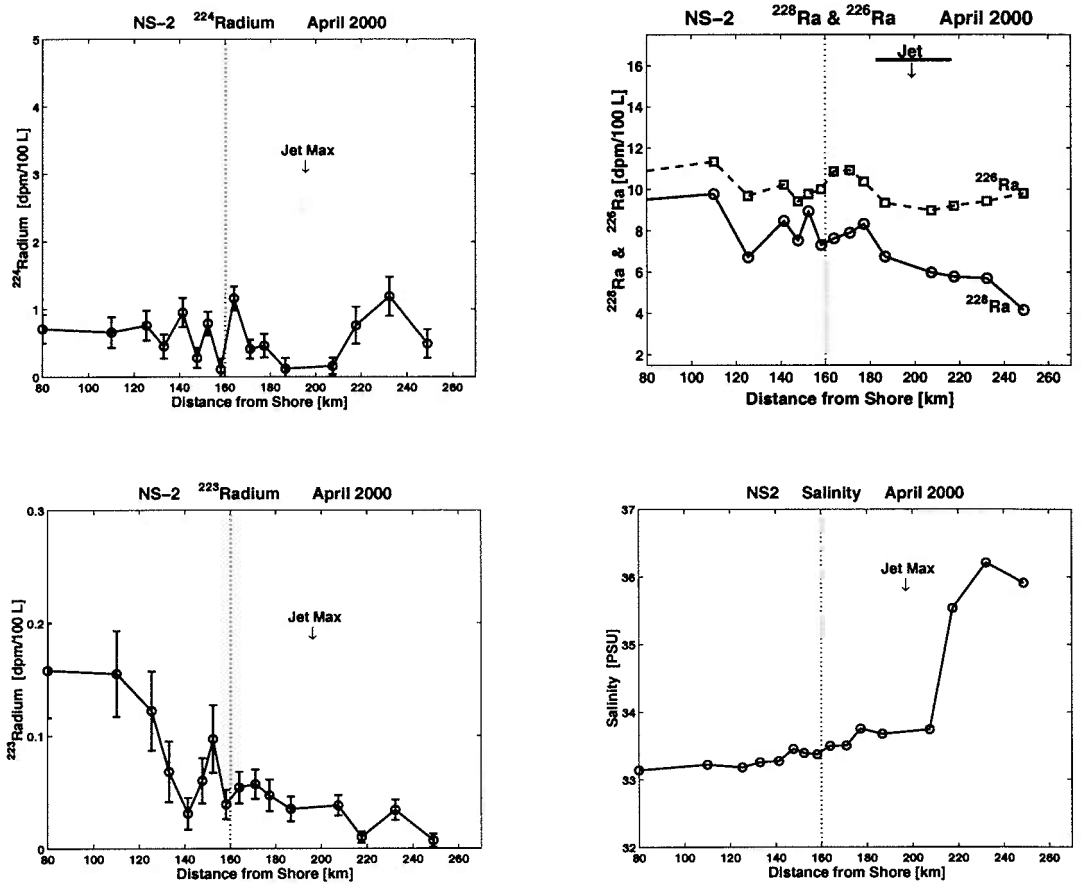

Figure 3.16: Radium and salinity over transect NS-2, Mid-Atlantic Bight, Nantucket Shoals shelf, 1 April 2000. Dotted line indicates the position of the 100 m isobath.

this survey was unusually high (Figures 3.14, 3.15, and Tables 3.12-3.14). The elevated ^{224}Ra relative to the other radium isotopes is characteristic of a local shelf sediment source. Nutrients measured on the outbound leg were also unusually low over the entire transect. An anomalously high ^{224}Ra activity is also seen over the upper slope 240 km offshore. As with the offshore ^{224}Ra peak in transect DE-A, this one also occurs in water with salinity $>$ 35 PSU that is associated with Gulf Stream features. An advancing warm core ring that is visible in AVHRR imagery can also be seen in the shoreward progress of the salinity front between 21 September and 7 October (see Chapter 5, Figure 5.4).

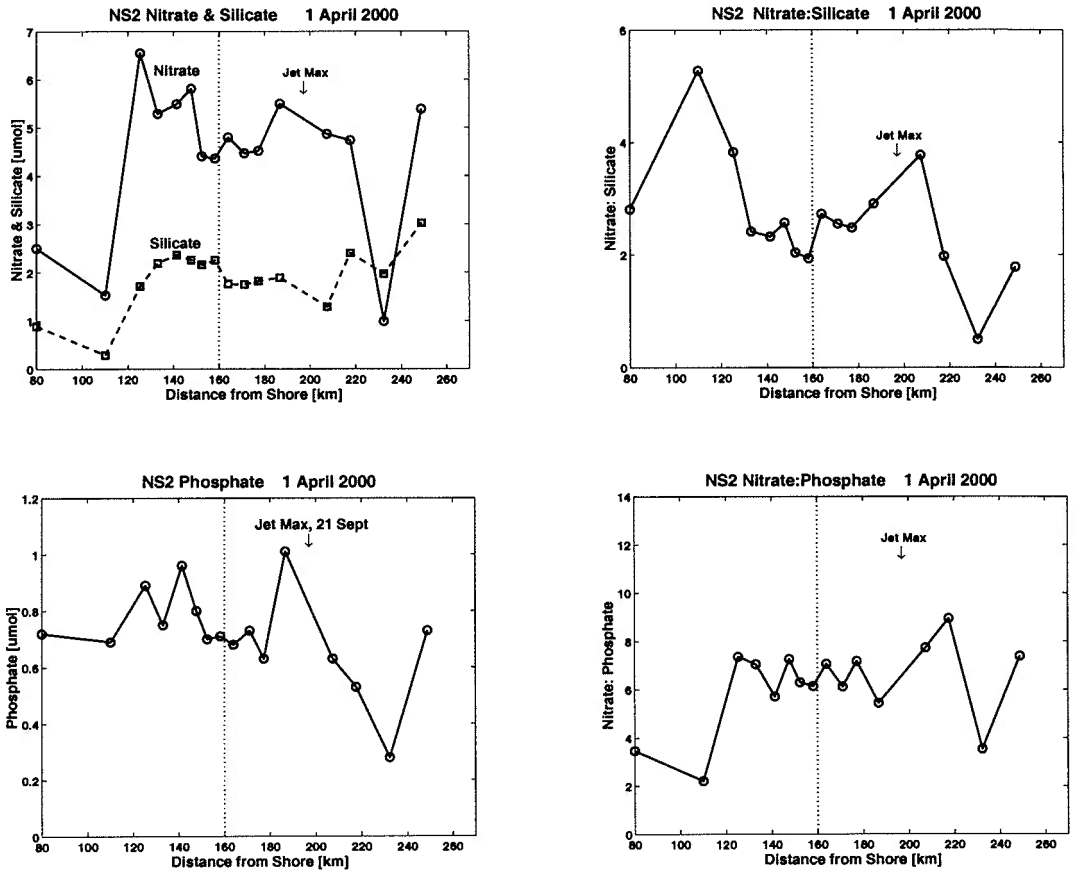

Figure 3.17: Nitrate, silicate and phosphate over transect NS2, Mid-Atlantic Bight, Nantucket Shoals shelf, 1 April 2000. Dotted line indicates the position of the 100 m isobath.

Survey NS2 in April 2000 also encountered a warm core ring at about 210 km offshore, as seen in the steep salinity front in Figure 3.16. ^{223}Ra, ^{228}Ra and ^{226}Ra decrease offshore in a manner consistent with their decay rates. Over this transect ^{224}Ra shows no trend, but does drop to near zero at the shelfbreak jet as in the southern MAB (transects DE-A-D). Also similar to the southern MAB survey, ^{223}Ra extends past the shelfbreak. In this case there is a measureable gradient, which allows calculation of a transit time using the ^{223}Ra:^{228}Ra ratio. We can calculate times for transport up to the shelfbreak jet, as well

as beyond it. The gradient between 110 km and 185 km can represent transport up to the shelfbreak jet, and the gradient between 110 km and 218 km can represent transport past the jet. Equation 2.9 gives transport times of 18 days up to the shoreward side of the jet, and 43 days to reach the seaward side. The jet position will not always be the same, but on the timescale of ^{223}Ra, this should be a fair approximation of its location. If the transport time estimates are correct, it is clear why ^{224}Ra goes to zero at the jet, since 43 days is well beyond the 3 week average lifespan of ^{224}Ra. It is also interesting that it apparently takes as long to cross the 10 km width of the jet as it takes to transit the 80 km before the jet.

Another similarity to the southern MAB is the peak in ^{224}Ra at the end of the transect in high salinity water. As before, ^{223}Ra is only slightly elevated, and ^{226}Ra and ^{228}Ra are not enriched. Salinity in this sample is over 36 PSU. The difference between this water and the adjacent shelf water is most apparent in the nutrient concentrations (Figure 3.17) which decrease sharply where the ^{224}Ra and salinity peak. This is the region where the transect crosses the outer edge of the warm core ring. The presence of such peaks in three surveys that crossed Gulf Stream features suggests that this is not an entirely unusual phenomenon, and will be the basis for additional measurements and transport calculations in Chapter 5.

The cross-shelf distributions of ^{223}Ra, ^{228}Ra and ^{226}Ra can be used to estimate probable values of κ and w using sum of squares error calculations (Figures 3.18 and 3.19. All solutions for the long-lived isotopes give a negative (shoreward) w. But the zero contours do not intersect or converge so it is not possible to identify a unique or even most likely κ, w pair beyond knowing that the range of w is limited to a range within -1.0 to 0 cm/s. The curves shown with the data are merely an example using an arbitrary diffusion coefficient, $\kappa = 100$ m^2/s. ^{223}Ra is not helpful in constraining the parameters either. The zero contour

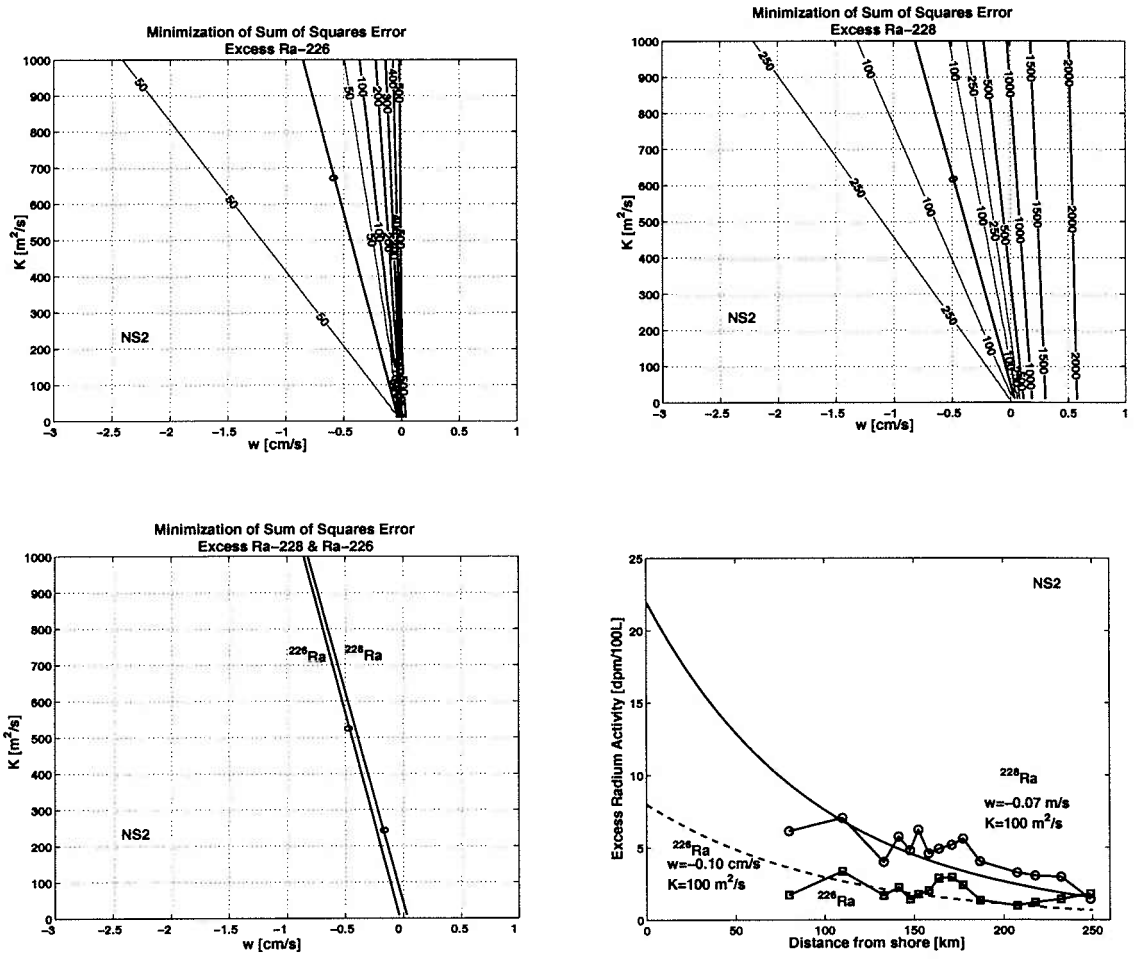

Figure 3.18: Minimization of sum of squares error for advection-diffusion-decay model with long-lived Ra isotope data from transect NS-2, Mid-Atlantic Bight, Nantucket Shoals shelf, 1 April 2000.

of minimized error for the ^{223}Ra falls within a range of all positive (seaward) w, and thus the ^{223}Ra data are clearly integrating over a much smaller timescale during which conditions differed from the long-term mean. ADCP measurements do not assist in this case either because cross-shelf velocity from ADCP measurements ranged from -20 cm/s to +20 cm/s over the length of the transect, with frequent shifts in direction.

The final crossing of this transect took place in early December 2000 and has many

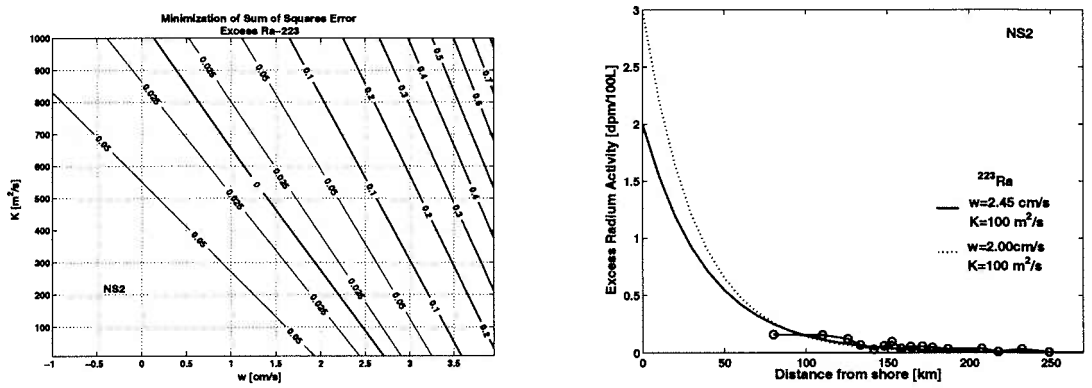

Figure 3.19: Minimization of sum of squares error for advection-diffusion-decay model with short-lived ^{223}Ra isotope data from transect NS-2, Mid-Atlantic Bight, Nantucket Shoals shelf, 1 April 2000.

characteristics in common with the previous survey (Figures 3.20, 3.21). This crossing did not extend far enough to resolve the shelfbreak jet, and salinity remains low (< 34.5) across the transect. However, clear gradients are seen in both ^{223}Ra and ^{228}Ra which are quite high over the shelf. Calculations from ^{223}Ra:^{228}Ra ratios between 100-191 km ($AR_{100} = 0.016$, $AR_{191} = 0.005$) give a cross-shelf transit time of 21 days, similar to the time calculated from survey NS2 for transit up to the shelfbreak jet (18 days from 110-185 km).

^{224}Ra is variable and has no distinguishable trend with distance. Nutrients do show a coherent pattern here, with silicate and nitrate once again peaking at the shelfbreak, while phosphate has the opposite gradient. Sum of square error calculations were done for the two isotopes with cross-shelf gradients, ^{223}Ra and ^{228}Ra. Like the other data sets from this area, the two zero contours (from one short-lived and one long-lived isotope) do not overlap, and solutions to the ^{223}Ra data are all in the positive w domain while solutions to the ^{228}Ra data all have negative w. Curves have again been drawn using an arbitrary $\kappa = 100$ m^2/s to show the difference in w that results from the different isotopes. The selection of A_0

is not always obvious when transects do not extend to the coast. A_0 for ^{223}Ra and ^{228}Ra were selected here by considering highest values observed nearshore (since both isotopes are much higher than normally observed over the mid-shelf) and by optimizing the sum of squares fit for the best A_0.

It should be noted here that in the transects sampled in the Middle Atlantic Bight, ^{228}Ra is quite variable, but the range of κ calculated from sum of squares error minimization is consistently in the negative range of w, between -1.5 and 0, just as it is with the longer-lived ^{226}Ra. This suggests that there is some consistency over large time scales in the processes affecting the long-lived isotope distributions. Even in survey NS3, with an apparently higher coastal input of ^{228}Ra, the range of κ, w solutions is similar to the other transects.

Although data from only one isotope in each long- and short-lived pair was usable, the zero contours do tell us something about the long-term and short-term mean conditions in this area. Data from the Coastal Mixing and Optics Experiment (Shearman and Lentz submitted) was collected from moorings at the shoreward end of the transects. (The data from this survey was collected during mooring deployment for follow-up studies of the same location.) At the 86 m isobath (beginning of transect) cross-isobath subtidal current velocity means are from 0.5 to 3 cm/s at 30 m depth, to 6-8 cm/s at 4 m depth (converting their data to a coordinate system where positive w is in the offshore direction).

The geostrophic component of the current is 2-4 cm/s over the upper 30 m. The portion of the short-lived ^{224}Ra sum of squares minimization zero contour that falls in a range of realistic κ (about 0-600 m^2/s) corresponds to velocities from 2-3.5 cm/s, in excellent agreement with the geostrophic current velocity. More problematic is the ^{228}Ra zero contour, which falls almost entirely in the negative w region, from -0.6 to 0 cm/s. (Note different x-

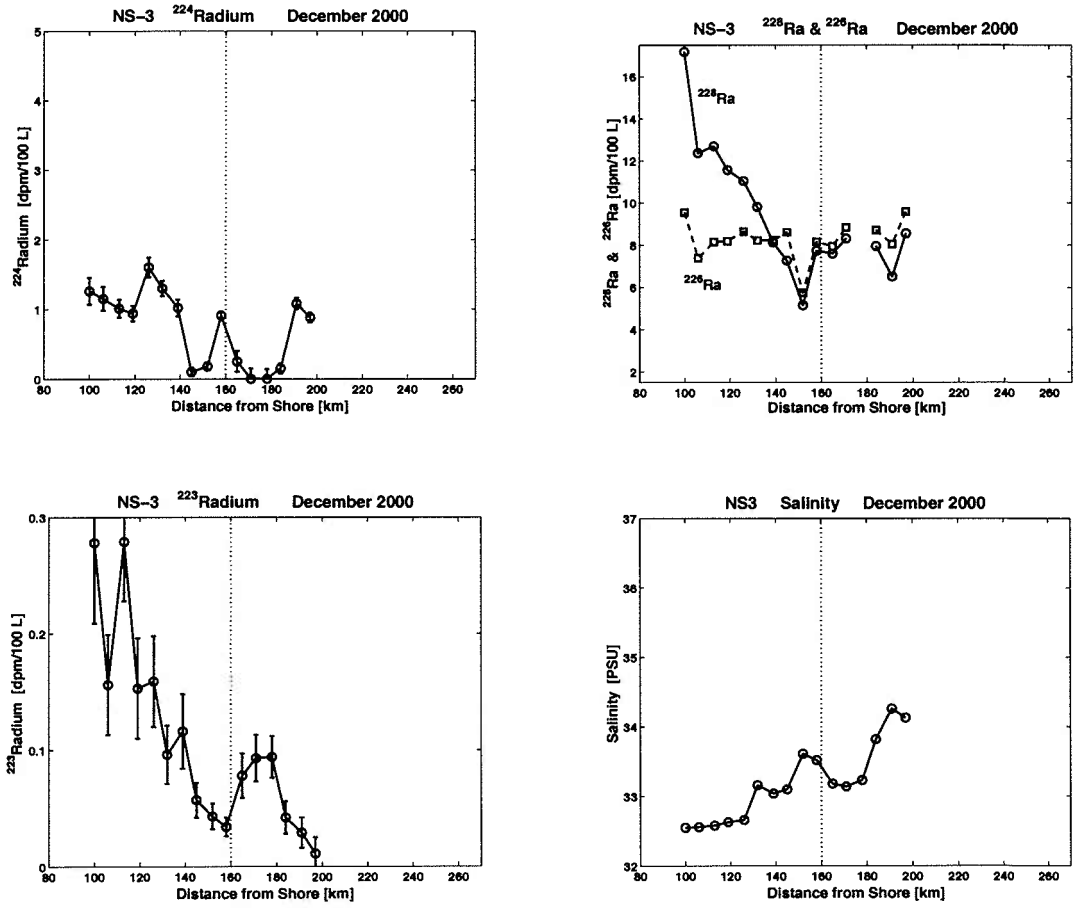

Figure 3.20: Radium and salinity over transect NS-3, Mid-Atlantic Bight, Nantucket Shoals shelf, December 2000. Dotted line indicates the position of the 100 m isobath.

and y-axis limits for this isotope because of the steepness of the contours.) This indicates a long-term mean velocity near zero and slightly negative. It is possible this reflects a long-term trend or variability. The NSFE occupied a slightly longer mooring transect just east of CMO, with data from 1979-80 (Beardsley et al. 1985). The subtidal cross-isobath current means from this experiment were lower, but still in the offshelf direction, 0.5-2.8 cm/s over the upper 10-32 m at the 88 m isobath. The low, slightly negative cross-shelf velocities implied by all of the long-lived Ra isotope data collected on the MAB outer shelf are

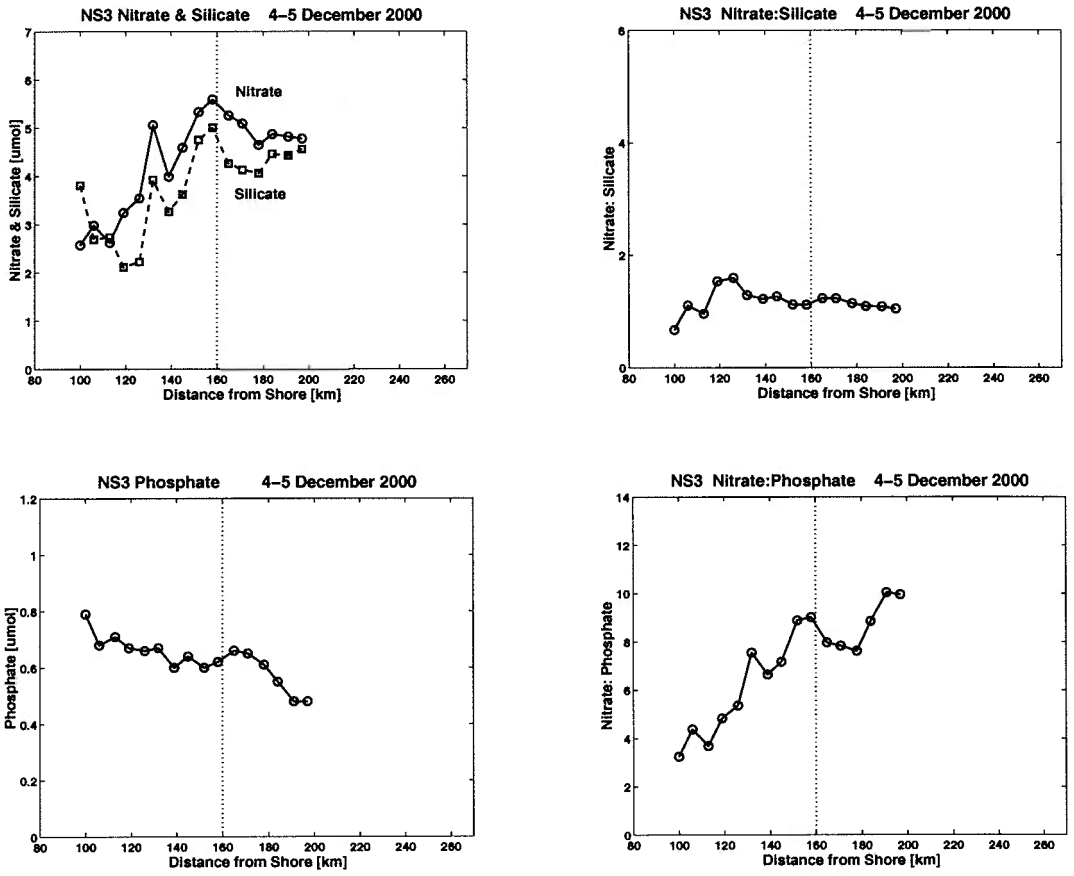

Figure 3.21: Nitrate, silicate and phosphate over transect NS3, Mid-Atlantic Bight, Nantucket Shoals shelf, December2000. Dotted line indicates the position of the 100 m isobath.

an interesting problem that may help reveal information about Ra transport or long-term current means.

3.4 Discussion

In actual data from the Mid-Atlantic Bight we have seen that the advective component in a nutrient flux calculation is of the same order as the diffusive component, so including the advective term in our equations is especially important. Rather than resolving the advective

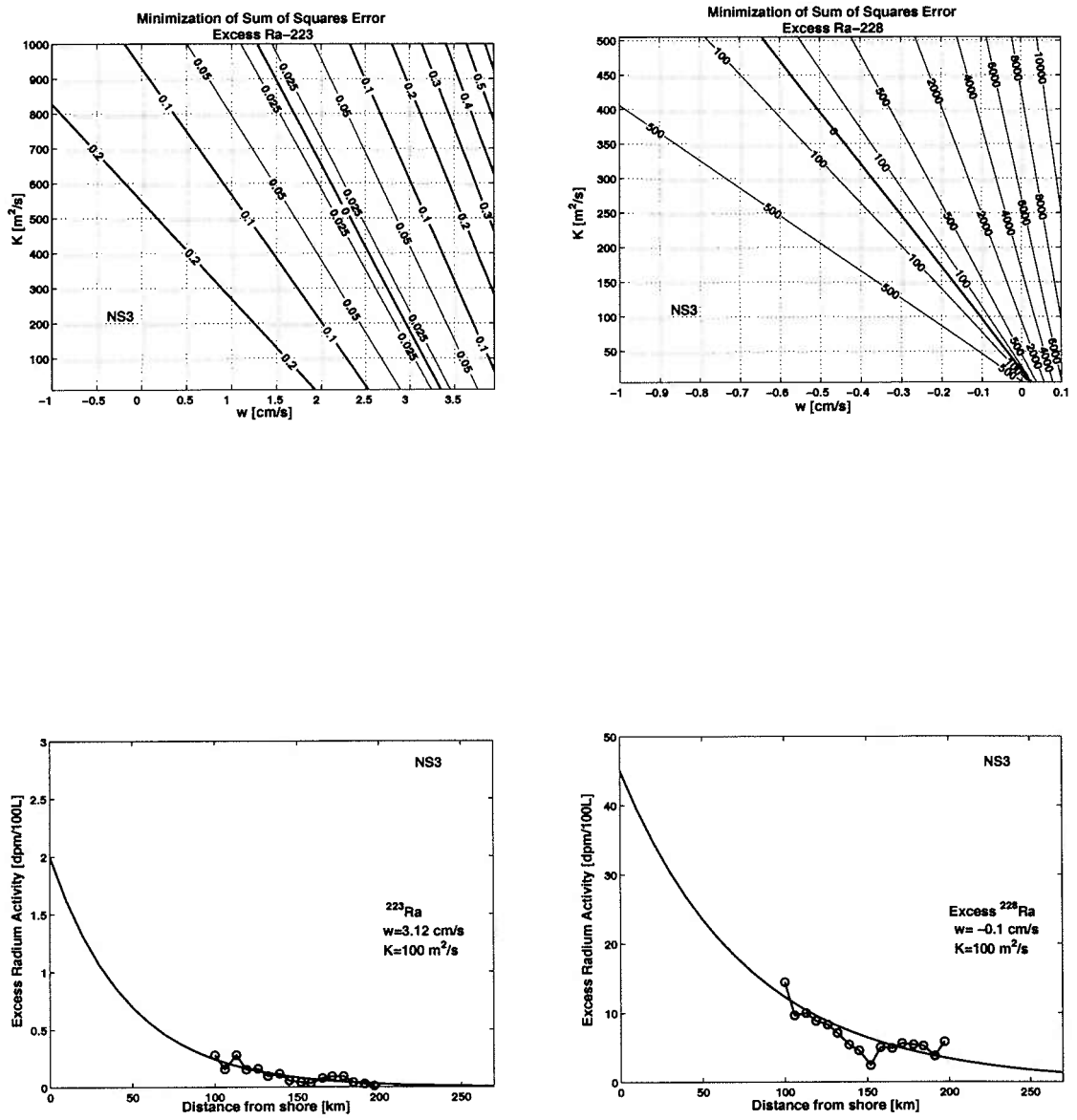

Figure 3.22: Minimization of sum of squares error for advection-diffusion-decay model with ^{223}Ra and ^{228}Ra isotope data from transect NS-3, Mid-Atlantic Bight, Nantucket Shoals shelf, December 2000.

problem, concurrent velocity measurements highlight the difficulty of factoring in advection in the coastal zone. Actual velocities obtained by ADCP or geostrophic current calculations from hydrographic data show that instantaneous cross-shelf velocity is actually much larger than long term means, and can certainly have an effect on distributions of the short-lived isotopes. In addition, time scales of variability are extremely short, so geochemical patterns that are observed may be the result of small scale flow that has already shifted.

Long-term moored velocity means, while less variable and lower in magnitude than instantaneous ADCP velocity, are still of a magnitude and variability that can strongly affect the calculation of mixing coefficients. The Nantucket Shoals Flux Experiment means for cross-shelf flow at the 105 m and 198 m isobaths vary from -1.0 m/s (onshelf) to 2.1 m/s (offshelf) in the upper mixed layer and have subtidal standard deviations of $\pm 7.4 - 8.6$ (Beardsley et al. 1985). The more recent Coastal Mixing and Optics Experiment conducted over 1996-97 has recorded even larger mean flows of 0.5-8.0 m/s (offshelf) in the upper 30 m at their outermost station on the 86 m isobath (Shearman and Lentz submitted). These are of a magnitude that can alter the value of κ considerably. Long-lived Ra distributions cross-shelf must also be reconciled to long-term mean current velocities. The cross-shelf gradients of ^{228}Ra and ^{226}Ra require a slight onshore advective flow to maintain, even with low diffusive mixing. This must be explained either through physical circulation, an incorrect assumption such as steady-state, or some basic flaw in the model such as a spatially variable eddy diffusivity or large scale circulation advecting tracer laterally over large time scales.

Hydrographic data also show the difficulty of interpreting some cross-shelf geochemical measurements. Interleaved water masses, slope intrusions, and shelf streamers can all in-

troduce data points that are not necessarily related to those from adjacent stations. For example, gradients observed across the DE-A-D sections could be affected by the slopewater/GS intrusion in the surface layer over the outer shelf and upper slope. If the water masses have been in contact only recently and are therefore geochemically unrelated, this must be considered when interpreting geochemical gradients. Occasionally individual stations are observed that show abnormally high or low radium, salinity or nutrients. When all of the chemical data is considered together, these anomalies may point to the presence of a distinct, isolated water mass, such as at the end of transects DE-D and NS2. It is important in constructing radium or nutrient gradients for use in flux calculations to consider that such points may not actually be a part of the overall gradient.

Fluxes calculated from Mid-Atlantic Bight radium and nutrient data indicate a net offshore transport. In all but one case (phosphate on NS3) nutrient gradients are negative (decreasing offshelf). With the positive (offshelf) advection suggested by short-lived ^{223}Ra data this results in net advective-diffusive export on short time scales. With the small onshore advection suggested by the long-lived isotope ^{228}Ra, the corresponding eddy diffusion is enough to create a net offshelf flux on longer time scales also, providing the nutrient gradients are applicable.

The question of temporal and spatial variability in nutrient gradients is an important one to consider when calculating cross-shelf fluxes. Instantaneous nutrient data across a sampling transect could be very useful in conjunction with short-lived Ra data to calculate a local nutrient flux that reflects current or at most seasonal conditions. However we can see from the data in the northern MAB that nutrient gradients are quite variable over time. Figure 3.23 shows historical nitrate data from the Mid-Atlantic Bight during the

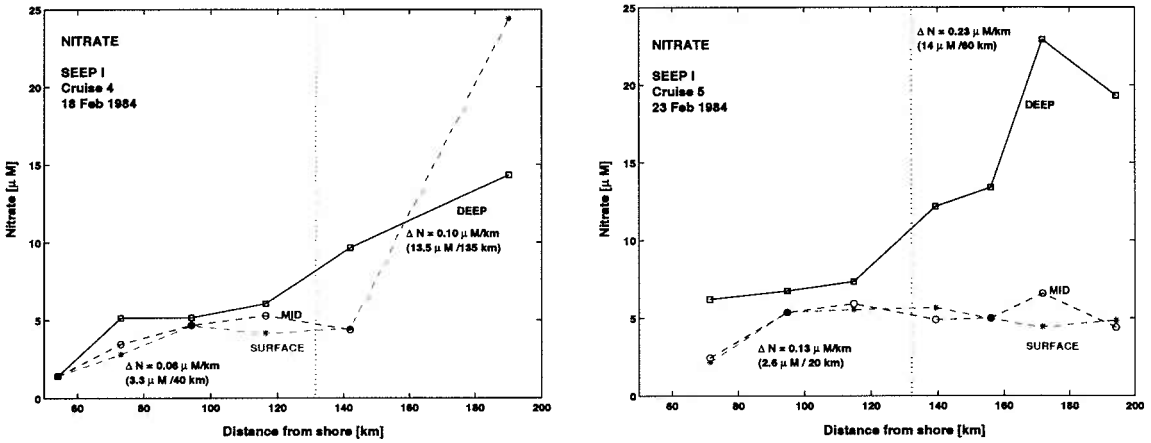

Figure 3.23: Cross-shelf nitrate distribution during SEEP I, Cruises 4 and 5. Red dotted line indicates the location of the 100m isobath.

SEEP experiment of 1984. During these surveys nitrate is low over the shelf and increases beyond the shelfbreak, in a manner more consistent with the traditional concept of high production creating nutrient deficits over the shelf. Yet even in these "classic" nutrient gradients, both the surface and deep water gradients change significantly between the two surveys, just 5 days apart. When using the long-lived isotope data, which likely give more realistic average values of κ and w on a decadal time scale, it would be preferable to obtain long-term time-averaged nutrient gradient data.

Nixon et al (1996) have estimated a net deficit on the northeastern U.S. shelf of 77-147 $\times 10^9$ mol N/yr after considering riverine inputs, denitrification, sediment burial, and atmospheric deposition. To balance this deficit there must be onshelf transport of nitrogen by advective and diffusive processes from deep slopewater, surface slopewater, or both. A comparison of annual advective-diffusive flux estimates along the 900 km shelf-slope boundary of the Mid-Atlantic Bight is shown in Table 3.5, using historical nutrient data from SEEP and data from this survey. For SEEP, an average nitrate gradient of +0.10 μM/km is used for the entire 200 m depth. For this study, the data from DE-A is taken as

a representative nitrate gradient (0.08 μM/km) but only applies to the surface mixed layer; because of this the depth of integration is limited to 50 m for our nutrient data. Exchange rates are taken from long-lived Ra isotope data from the southern MAB survey (DE) and from calculations based on salinity balances in Csanady and Hamilton (1988).

The different nitrate gradients are similar in magnitude but opposite in direction, resulting in a reversal of the flux direction. The SEEP nitrate flux is onshore, while the nitrate flux using data from this study is offshore (positive). Both exchange rates give a total flux that makes a significant contribution to resolving the shelf deficit. Combining SEEP nutrient data with the advection-diffusion rate from long-lived radium isotopes (Survey DE-A) gives an onshore nitrate flux of 51 $\times 10^9$ mol/yr, compared to 85 $\times 10^9$ mol/yr for the exchange rate from salinity balances. For comparison with eddy diffusion calculations that do not account for advective transport, this flux would be equivalent to using $\kappa = 90$ m^2/s with zero advection. The nitrate flux calculated from radium isotope distribution is thus in fairly good agreement with other estimates, and with nutrient budget requirements estimated for the North Atlantic. The key factor in these cases is the magnitude and direction of the cross-shelf nutrient gradient, which appears to be quite variable over time.

It should also be noted that nitrate concentrations are generally higher at depth due to remineralization and lack of primary production, so deep nutrient gradients may differ from surface gradients in both magnitude and direction (as in SEEP data, Figure 3.23). Deep nutrient fluxes may also be subject to entirely different physical processes such as shelfbreak upwelling cells and bottom boundary layer transport, which may penetrate the shelfbreak front, or merely converge there (Pickart 2000; Chapman and Lentz 1994; Houghton 1997; Houghton and Visbeck 1998). Consequently, there may be net onshore transport of nu-

trients via subsurface pathways even if surface transport is offshore, or there may be no penetration of the front at all (Figure 3.24). Thus in addition to temporal variability in nutrient concentrations, spatial differences in the vertical as well as horizontal direction must be taken into account when estimating cross-shelf flux. It is quite possible that surface and deep fluxes must be calculated separately, using different nutrient gradients and different advective-diffusive exchange rates.

Exchange Rate	Nitrate Gradient [μM/km]	J [μmol/m^2·s]	J_{MAB} [10^9 mol/yr]	Integration Depth [m]
MASAR	0.10	-15.0	-85.2	200 m
MASAR	-0.08	$+2.25$	$+12.7$	50 m
Ra isotopes	0.10	-9.0	-51.0	200 m
Ra isotopes	-0.08	$+1.2$	$+1.7$	50 m
Shelf budget requirement			-77-147	200 m

Table 3.5. Comparison of advective-diffusive flux of nitrate across the shelf-slope boundary. Fluxes are calculated using a) the two-way exchange rate calculated in the MASAR publication from salinity balance (Csanady and Hamilton 1988), 0.3 m^3/s per meter coastline, and b) advection and diffusion rates calculated with long-lived radium isotopes in this study, $\kappa = 40$ m^2/s, $w = -0.10$ cm/s. Nitrate gradients are from historical SEEP I data (0.10 μM/km, or ΔN $\approx 10\mu$M between slope and shelf) and from this study (-0.08μ M/km, orΔN $\approx -1.5\mu$M between slope and shelf). The nitrogen flux required to balance North Atlantic budgets is shown for comparison (Nixon et al. 1996). Integration depth is 200 m for SEEP nutrients which include deep samples, and 50 meters for surface nutrient data from this study. Positive flux = offshelf.

Ideally field experiments aimed at determining cross-shelf fluxes or exchange rates should incorporate some type of long-term sampling. Repeated nutrient sampling is important to determine the extent of temporal variability. Within one area we have seen nutrient gradients change significantly in less than one week. Over longer time periods, the direction of the gradient is different, positive offshore during SEEP I (1984) and negative offshore in our surveys (2000-2001). Nutrients should also be measured in at least two depths, surface

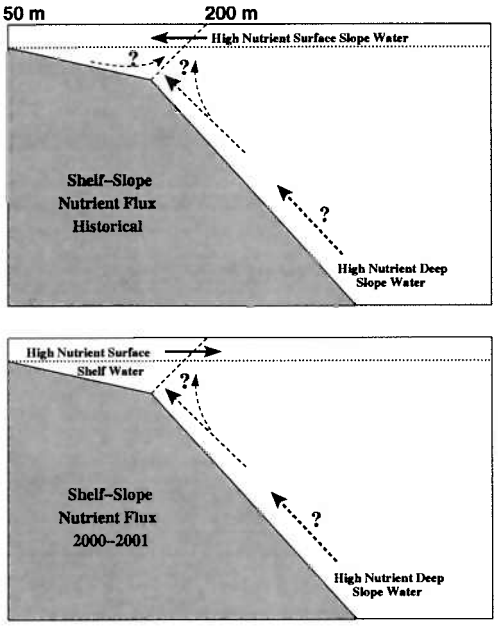

Figure 3.24: Possible pathways for nutrient flux across the shelfbreak with alternative gradient scenarios. Top: Historical nutrient gradients, and Bottom: Gradients measured in this study.

and near bottom, to account for different concentrations at depth from remineralization and lack of uptake. Likewise, radium isotopes would ideally be measured repeatedly across the entire shelf and upper slope, at fairly high resolution ($\leq$ 5 km). This would allow observing both broad gradients and long-term changes, as well as small-scale, short-term physical processes. Concurrent hydrographic sampling is also essential to determine what type of physical structure is underlying and affecting the chemical measurements. Hydrographic and ADCP data would also provide information on the flow regime in place at the time. In order to determine flux of nutrients, it is also necessary to know flow patterns over longer time scales, at the surface and at depth. Moored velocity data would be useful for this purpose.

Combining the best possible data still leaves a difficult task of interpretation. Neither

nutrient nor isotope distributions are in steady-state, and they are subject to different processes that determine those distributions. Nutrient gradients are subject to both biological and physical processes that can alter their concentrations on a timescale of days. Radium isotopes originating from the coast are subject to seasonal input changes and transient physical flow phenomena, as well as longer term changes in mixing across the shelf. Even with ideal sampling opportunities the problem of non-steady state biochemical and physical processes operating on different time scales will make determining fluxes a challenge. It is possible that "average" conditions are meaningless, and that exchange across the shelf-slope boundary occurs primarily as a series of continuous transient conditions that taken individually would be unrepresentative of their cumulative effect.

Sample Location	Station Depth (m)	Sample Depth (m)	$^{224}Ra_{ex}$ (dpm/100L)	$^{223}Ra_{ex}$ (dpm/100L)	^{228}Ra (dpm/100L)	^{226}Ra (dpm/100L)
DEA-007-sfc	61	2	1.42 ± 0.17	0.04 ± 0.02	8.27 ± 0.45	7.75 ± 0.19
DEA-007-bot	61	55	0.75 ± 0.07	0.04 ± 0.01	9.07 ± 0.81	8.26 ± 0.29
DEA-009-sfc	85	2	0.79 ± 0.10	0.09 ± 0.02	7.05 ± 0.40	8.15 ± 0.17
DEA-009-mid	85	30	1.05 ± 0.10	0.04 ± 0.02	7.33 ± 0.67	8.20 ± 0.28
DEA-009-bot	85	78	1.18 ± 0.10	0.06 ± 0.02	8.64 ± 0.64	7.91 ± 0.22
DEA-011-sfc	121	2	0.40 ± 0.08	0.07 ± 0.03	6.55 ± 0.43	8.94 ± 0.19
DEA-011-mid	121	50	0.78 ± 0.09	0.03 ± 0.01	7.04 ± 0.54	8.33 ± 0.31
DEA-011-bot	121	116	2.05 ± 0.21	0.10 ± 0.03	8.86 ± 0.65	8.85 ± 0.24
NS3-116-sfc	83	2	0.94 ± 0.11	0.15 ± 0.04	11.56 ± 0.91	8.19 ± 0.27
NS3-116-mid	83	52	0.80 ± 0.10	0.14 ± 0.04	8.92 ± 0.68	7.77 ± 0.24
NS3-116-bot	83	82	1.82 ± 0.18	0.20 ± 0.06	9.71 ± 0.57	8.78 ± 0.20
NS3-113-sfc	100	2	1.02 ± 0.12	0.12 ± 0.03	8.13 ± 0.56	8.23 ± 0.20
NS3-113-mid	100	57	0.62 ± 0.13	0.12 ± 0.04	7.30 ± 0.69	8.97 ± 0.23
NS3-113-bot	100	93	1.95 ± 0.16	0.15 ± 0.03	6.10 ± 0.50	8.34 ± 0.17

Table 3.6: Subsurface radium isotope activities, Mid-Atlantic Bight. ^{223}Ra and ^{224}Ra activities are "excess," after correcting for supported activity from ^{227}Ac and ^{228}Th in the water column.

Sample Location	Distance (km)	Salinity (PSU)	^{228}Th (dpm/100L)	^{227}Ac (dpm/100L)
DEA-007-sfc	84	33.44	0.35 ± 0.08	N/A
DEA-007-bot	84	33.68	0.53 ± 0.09	0.01 ± 0.00
DEA-009-sfc	94	33.68	0.40 ± 0.03	N/A
DEA-009-mid	94	33.89	0.39 ± 0.04	0.02 ± 0.01
DEA-009-bot	94	33.88	0.58 ± 0.09	0.01 ± 0.00
DEA-011-sfc	104	34.72	0.49 ± 0.04	N/A
DEA-011-mid	104	34.15	0.38 ± 0.04	0.02 ± 0.01
DEA-011-bot	104	34.08	0.2 ± 0.05	0.03 ± 0.01
NS3-116-sfc	119	32.63	0.72 ± 0.05	0.00 ± 0.00
NS3-116-mid	119	32.91	0.80 ± 0.06	0.04 ± 0.01
NS3-116-bot	119	33.02	0.73 ± 0.06	0.02 ± 0.01
NS3-113-sfc	139	33.04	0.52 ± 0.08	0.00 ± 0.00
NS3-113-mid	139	33.74	0.77 ± 0.11	0.03 ± 0.01
NS3-113-bot	139	33.51	0.56 ± 0.10	0.01 ± 0.01

Table 3.7: Subsurface salinity, ^{228}Th, and ^{227}Ac activities, Mid-Atlantic Bight.

Sample Location	Distance (km)	Nitrate (μM)	Phosphate (μM)	Silicate (μM)	Ammonium (μM)	N:P	N:Si
DEA-007-sfc	84	1.92	0.38	4.54	0.54	5.05	0.42
DEA-007-bot	84	1.90	0.34	4.12	0.62	5.59	0.46
DEA-009-sfc	94	1.97	0.35	4.51	0.44	5.63	0.44
DEA-009-mid	94	3.63	0.49	6.16	0.51	7.41	0.59
DEA-009-bot	94	4.87	0.57	7.82	0.36	8.54	0.62
DEA-011-sfc	104	0.61	0.12	1.70	0.58	5.08	0.36
DEA-011-mid	104	3.48	0.42	5.68	0.40	8.29	0.61
DEA-011-bot	104	5.92	0.64	8.34	0.37	9.25	0.71
NS3-116-sfc	119	N/A	N/A	N/A	N/A	N/A	N/A
NS3-116-mid	119	N/A	N/A	N/A	N/A	N/A	N/A
NS3-116-bot	119	N/A	N/A	N/A	N/A	N/A	N/A
NS3-113-sfc	139	N/A	N/A	N/A	N/A	N/A	N/A
NS3-113-mid	139	N/A	N/A	N/A	N/A	N/A	N/A
NS3-113-bot	139	N/A	N/A	N/A	N/A	N/A	N/A

Table 3.8: Subsurface nutrient concentrations, Mid-Atlantic Bight.

Sample Location	Distance (km)	$^{224}Ra_{ex}$ (dpm/100L)	$^{223}Ra_{ex}$ (dpm/100L)	^{228}Ra (dpm/100L)	^{226}Ra (dpm/100L)	Salinity (PSU)
DE-A						
DEA-005	64	1.46 ± 0.26	0.05 ± 0.02	9.28 ± 0.46	8.44 ± 0.19	33.18
DEA-006	74	1.72 ± 0.27	0.04 ± 0.02	8.16 ± 0.56	8.67 ± 0.19	33.23
DEA-007	84	1.42 ± 0.17	0.04 ± 0.02	8.27 ± 0.45	7.75 ± 0.19	33.44
DEA-008	89	1.76 ± 0.25	0.06 ± 0.03	7.25 ± 0.44	8.14 ± 0.20	33.55
DEA-009	94	0.79 ± 0.10	0.09 ± 0.02	7.05 ± 0.40	8.15 ± 0.17	33.68
DEA-010	99	0.79 ± 0.14	0.07 ± 0.02	7.26 ± 0.45	7.20 ± 0.17	33.72
DEA-011	104	0.40 ± 0.08	0.07 ± 0.03	6.55 ± 0.43	8.94 ± 0.19	34.72
DEA-012	109	0.67 ± 0.13	0.07 ± 0.05	3.81 ± 0.27	4.91 ± 0.13	34.64
DEA-013	114	0.00 ± 0.08	0.07 ± 0.05	5.47 ± 0.30	7.33 ± 0.15	34.78
DEA-014	119	0.08 ± 0.09	0.06 ± 0.05	5.14 ± 0.35	7.51 ± 0.16	34.99
DEA-105	124	0.40 ± 0.08	0.10 ± 0.03	4.96 ± 0.39	7.88 ± 0.19	34.88
DEA-016	129	0.00 ± 0.05	0.03 ± 0.01	5.83 ± 0.44	7.20 ± 0.22	34.82
DEA-017	134	0.00 ± 0.11	0.01 ± 0.00	5.45 ± 0.38	7.46 ± 0.18	34.77
DE-B						
DEB-030	60	1.72 ± 0.27	0.05 ± 0.01	7.63 ± 0.70	7.19 ± 0.28	33.24
DEB-029	70	0.42 ± 0.08	0.13 ± 0.04	8.62 ± 0.62	8.28 ± 0.29	33.35
DEB-027	80	0.65 ± 0.13	0.06 ± 0.01	8.57 ± 0.64	8.33 ± 0.26	33.50
DEB-025	90	1.72 ± 0.31	0.02 ± 0.01	8.47 ± 0.68	8.24 ± 0.24	33.51
DEB-024	95	1.35 ± 0.23	0.05 ± 0.02	7.30 ± 0.50	7.81 ± 0.17	33.71
DEB-021	110	0.09 ± 0.13	0.00 ± 0.01	5.87 ± 0.47	7.27 ± 0.18	34.77
DEB-019	120	0.00 ± 0.13	0.00 ± 0.01	5.67 ± 0.59	8.07 ± 0.19	35.30
DE-D						
DED-063	60	1.10 ± 0.23	0.03 ± 0.01	9.67 ± 0.84	8.62 ± 0.34	33.27
DED-061	65	1.73 ± 0.16	0.07 ± 0.02	10.01 ± 0.85	10.75 ± 0.35	33.29
DED-060	70	1.13 ± 0.14	0.02 ± 0.01	9.21 ± 0.62	8.96 ± 0.24	33.40
DED-059	75	0.51 ± 0.06	0.05 ± 0.02	8.78 ± 0.78	9.18 ± 0.32	33.59
DED-058	80	1.50 ± 0.18	0.04 ± 0.02	8.07 ± 0.72	8.32 ± 0.29	33.51
DED-057	85	0.35 ± 0.03	0.04 ± 0.02	7.81 ± 0.64	7.93 ± 0.27	33.51
DED-056	90	0.49 ± 0.04	0.03 ± 0.01	7.65 ± 0.67	8.60 ± 0.29	33.87
DED-055	95	0.19 ± 0.01	0.05 ± 0.01	8.16 ± 0.55	8.73 ± 0.23	33.87
DED-054	100	0.10 ± 0.01	0.00 ± 0.01	7.73 ± 0.49	8.93 ± 0.21	33.86
DED-053	105	0.64 ± 0.09	0.04 ± 0.01	7.27 ± 0.57	7.95 ± 0.24	34.18
DED-052	110	0.05 ± 0.01	0.03 ± 0.01	6.78 ± 0.60	8.47 ± 0.25	34.69
DED-051	115	0.16 ± 0.01	0.03 ± 0.01	7.66 ± 0.57	9.58 ± 0.25	34.24
DED-050	120	0.04 ± 0.09	0.00 ± 0.00	6.41 ± 0.65	8.11 ± 0.27	34.97
DED-049	125	2.93 ± 0.14	0.06 ± 0.01	8.00 ± 0.76	9.04 ± 0.32	35.07
Alongshelf						
DE-066	82	1.42 ± 0.11	0.04 ± 0.01	8.65 ± 0.72	9.01 ± 0.29	33.42
DE-067	86	0.01 ± 0.00	0.03 ± 0.01	8.92 ± 0.83	9.19 ± 0.34	33.51
DE-068	90	0.02 ± 0.00	0.02 ± 0.01	7.83 ± 0.79	9.26 ± 0.34	33.76
DE-069	95	0.77 ± 0.10	0.00 ± 0.02	7.60 ± 0.61	8.98 ± 0.26	34.08

Table 3.9: Radium isotope activities and salinity, Survey DE, November 2000, southern Mid-Atlantic Bight. ^{223}Ra and ^{224}Ra activities are "excess," after correcting for supported activity from ^{227}Ac and ^{228}Th in the water column.

Sample Location	Distance (km)	^{228}Th (dpm/100L)	^{227}Ac (dpm/100L)
DE-A			
DEA-005	64	0.41 ± 0.04	N/A
DEA-006	74	0.33 ± 0.07	N/A
DEA-007	84	0.35 ± 0.08	N/A
DEA-008	89	0.39 ± 0.09	N/A
DEA-009	94	0.40 ± 0.03	N/A
DEA-010	99	0.41 ± 0.03	N/A
DEA-011	104	0.49 ± 0.04	N/A
DEA-012	109	0.52 ± 0.07	N/A
DEA-013	114	0.50 ± 0.08	N/A
DEA-014	119	0.58 ± 0.09	N/A
DEA-105	124	0.59 ± 0.04	N/A
DEA-016	129	0.64 ± 0.05	N/A
DEA-017	134	0.60 ± 0.11	N/A
DE-B			
DEB-030	60	0.45 ± 0.08	0.0138 ± 0.0042
DEB-029	70	0.48 ± 0.04	0.0086 ± 0.0017
DEB-027	80	0.44 ± 0.02	0.0071 ± 0.0017
DEB-025	90	0.28 ± 0.02	0.0123 ± 0.0024
DEB-024	95	0.26 ± 0.03	0.0124 ± 0.0025
DEB-021	110	0.65 ± 0.13	0.0090 ± 0.0029
DEB-019	120	0.64 ± 0.13	0.0196 ± 0.0056
DE-D			
DED-063	60	0.24 ± 0.01	0.0261 ± 0.0077
DED-061	65	0.38 ± 0.03	0.0162 ± 0.0040
DED-060	70	0.47 ± 0.04	0.0107 ± 0.0033
DED-059	75	0.21 ± 0.02	0.0172 ± 0.0045
DED-058	80	0.48 ± 0.05	0.0137 ± 0.0041
DED-057	85	0.54 ± 0.05	0.0145 ± 0.0046
DED-056	90	0.49 ± 0.10	0.0263 ± 0.0069
DED-055	95	0.62 ± 0.11	0.0104 ± 0.0031
DED-054	100	0.50 ± 0.09	0.0441 ± 0.0099
DED-053	105	0.59 ± 0.10	0.0047 ± 0.0017
DED-052	110	0.59 ± 0.10	0.0089 ± 0.0027
DED-051	115	0.45 ± 0.08	0.0107 ± 0.0040
DED-050	120	0.54 ± 0.09	0.0102 ± 0.0035
DED-049	125	0.50 ± 0.08	0.0190 ± 0.0047
Alongshelf			
DE-066	82	0.49 ± 0.02	0.0118 ± 0.0034
DE-067	86	0.72 ± 0.12	0.0093 ± 0.0025
DE-068	90	0.65 ± 0.13	0.0220 ± 0.0053
DE-069	95	0.42 ± 0.04	0.0137 ± 0.0042

Table 3.10: ^{228}Th and ^{227}Ac activities, Survey DE, November 2000, southern Mid-Atlantic Bight.

Sample Location	Distance (km)	Nitrate (μM)	Phosphate (μM)	Silicate (μM)	Ammonium (μM)	N:P	N:Si
DE-A							
DEA-005	64	1.34	0.39	3.98	1.35	3.44	0.34
DEA-006	74	1.17	0.38	4.00	0.88	3.08	0.29
DEA-007	84	1.92	0.38	4.54	0.54	5.05	0.42
DEA-008	89	2.15	0.39	4.93	0.95	5.51	0.44
DEA-009	94	1.97	0.35	4.51	0.44	5.63	0.44
DEA-010	99	2.26	0.39	5.02	0.71	5.79	0.45
DEA-011	104	0.61	0.12	1.70	0.58	5.08	0.36
DEA-012	109	0.52	0.12	1.57	0.97	4.33	0.33
DEA-013	114	0.49	0.11	1.40	0.38	4.45	0.35
DEA-014	119	0.50	0.09	1.49	0.46	5.56	0.34
DEA-105	124	0.39	0.08	1.29	0.40	4.88	0.3
DEA-016	129	0.52	0.10	1.63	0.35	5.2	0.32
DEA-107	134	0.41	0.09	1.25	0.36	4.56	0.33
DE-B							
DEB-030	60	0.18	0.32	2.58	0.49	0.57	0.07
DEB-029	70	1.58	0.38	4.67	0.47	4.20	0.34
DEB-027	80	1.69	0.34	4.58	0.44	4.92	0.37
DEB-025	90	2.27	0.36	4.93	0.45	6.32	0.46
DEB-024	95	0.58	0.09	1.82	0.52	6.14	0.32
DEB-021	110	0.15	0.07	1.27	0.27	2.04	0.12
DEB-019	120	0.08	0.05	1.09	0.31	1.49	0.07
DE-D							
DED-063	60	1.27	0.62	4.68	1.37	2.06	0.27
DED-061	65	1.05	0.31	1.63	0.47	3.41	0.64
DED-060	70	1.13	0.32	3.57	0.41	3.55	0.32
DED-059	75	1.35	0.28	3.35	0.49	4.89	0.40
DED-058	80	0.57	0.28	3.00	0.34	2.00	0.19
DED-057	85	0.86	0.32	3.34	0.50	2.72	0.26
DED-056	90	2.25	0.35	4.38	0.30	6.46	0.51
DED-055	95	2.17	0.33	4.41	0.33	6.49	0.49
DED-054	100	2.65	0.37	4.76	0.36	7.25	0.56
DED-053	105	1.68	0.25	3.55	0.32	6.79	0.47
DED-052	110	0.58	0.13	1.82	0.23	4.41	0.32
DED-051	115	2.45	0.30	4.10	0.28	8.05	0.60
DED-050	120	0.20	0.07	1.18	0.41	2.87	0.17
DED-049	125	0.00	0.06	1.87	0.42	0.00	0.00
Alongshelf							
DE-066	82	1.22	0.33	3.79	0.41	3.70	0.32
DE-067	86	1.78	0.35	4.35	0.33	5.09	0.41
DE-066	90	2.07	0.36	4.81	0.37	5.75	0.43
DE-069	95	1.99	0.31	4.21	0.28	6.42	0.47

Table 3.11: Nutrients, Survey DE, November 2000, southern Mid-Atlantic Bight.

Sample Location	Distance (km)	$^{224}Ra_{ex}$ (dpm/100L)	$^{223}Ra_{ex}$ (dpm/100L)	^{228}Ra (dpm/100L)	^{226}Ra (dpm/100L)	Salinity (PSU)
NS1-01	120	4.94 ± 0.49	0.04 ± 0.02	6.50 ± 0.98	9.00 ± 0.42	N/A
NS1-02	141	1.90 ± 0.29	0.15 ± 0.04	8.51 ± 0.85	8.53 ± 0.37	33.83
NS1-03	167	0.00 ± 0.03	0.06 ± 0.02	7.71 ± 0.85	8.15 ± 0.37	34.91
NS1-04	192	1.44 ± 0.22	0.07 ± 0.03	7.81 ± 0.81	7.75 ± 0.35	35.52
NS1-05	210	0.87 ± 0.13	0.05 ± 0.02	6.98 ± 0.99	8.98 ± 0.40	35.53
NS1-06	234	3.60 ± 0.35	0.05 ± 0.02	9.57 ± 1.04	9.06 ± 0.42	35.08
NS1-07	257	0.00 ± 0.12	0.08 ± 0.03	5.47 ± 0.88	8.11 ± 0.33	35.02
NS1-11	120	1.30 ± 0.20	0.09 ± 0.03	7.04 ± 0.80	8.44 ± 0.31	34.35
NS1-10	141	2.73 ± 0.28	0.02 ± 0.01	4.75 ± 1.05	9.09 ± 0.39	35.37
NS1-09	167	2.18 ± 0.22	0.02 ± 0.01	7.47 ± 0.94	7.98 ± 0.38	35.26
NS1-08	192	2.98 ± 0.32	0.04 ± 0.01	5.86 ± 1.00	9.16 ± 0.40	35.87
NS2-026	80	0.71 ± 0.21	0.16 ± 0.04	N/A	N/A	33.14
NS2-025	110	0.66 ± 0.23	0.15 ± 0.04	8.85 ± 0.66	9.71 ± 0.25	33.22
NS2-024	125	0.76 ± 0.22	0.12 ± 0.04	9.77 ± 0.78	11.34 ± 0.30	33.18
NS2-023	133	0.45 ± 0.18	0.07 ± 0.03	6.71 ± 0.65	9.68 ± 0.26	33.25
NS2-022	141	0.95 ± 0.21	0.03 ± 0.01	8.47 ± 0.62	10.23 ± 0.26	33.27
NS2-021	148	0.28 ± 0.15	0.06 ± 0.02	7.52 ± 0.64	9.41 ± 0.33	33.45
NS2-020	152	0.79 ± 0.17	0.10 ± 0.03	8.94 ± 0.82	9.77 ± 0.42	33.39
NS2-019	158	0.11 ± 0.16	0.04 ± 0.01	7.30 ± 0.91	10.00 ± 0.46	33.37
NS2-018	164	1.16 ± 0.18	0.05 ± 0.01	7.62 ± 0.70	10.86 ± 0.35	33.50
NS2-017	171	0.41 ± 0.14	0.06 ± 0.01	7.89 ± 0.47	10.92 ± 0.22	33.50
NS2-016	177	0.47 ± 0.17	0.05 ± 0.01	8.32 ± 0.68	10.38 ± 0.30	33.75
NS2-015b	187	0.12 ± 0.16	0.04 ± 0.01	6.74 ± 0.78	9.34 ± 0.34	33.67
NS2-015	207	0.16 ± 0.12	0.04 ± 0.01	5.97 ± 0.71	8.97 ± 0.30	33.74
NS2-014	218	0.76 ± 0.28	0.01 ± 0.01	5.77 ± 0.56	9.20 ± 0.21	35.54
NS2-013	232	1.19 ± 0.29	0.03 ± 0.01	5.69 ± 0.54	9.42 ± 0.24	36.21
NS2-012	249	0.49 ± 0.21	0.01 ± 0.01	4.16 ± 0.60	9.80 ± 0.27	35.91
NS3-119	100	1.26 ± 0.19	0.28 ± 0.07	17.18 ± 0.69	9.55 ± 0.23	32.55
NS3-118	106	1.15 ± 0.17	0.16 ± 0.04	12.37 ± 0.53	7.39 ± 0.17	32.56
NS3-117	113	1.01 ± 0.13	0.28 ± 0.05	12.69 ± 0.43	8.15 ± 0.14	32.58
NS3-116	119	0.94 ± 0.11	0.15 ± 0.04	11.56 ± 0.91	8.19 ± 0.27	32.63
NS3-115	126	1.60 ± 0.14	0.16 ± 0.04	11.04 ± 0.61	8.64 ± 0.20	32.66
NS3-114	132	1.30 ± 0.11	0.10 ± 0.03	9.81 ± 0.63	8.22 ± 0.22	33.16
NS3-113	139	1.02 ± 0.12	0.12 ± 0.03	8.13 ± 0.56	8.23 ± 0.20	33.04
NS3-109	145	0.10 ± 0.06	0.06 ± 0.01	7.27 ± 0.65	8.60 ± 0.22	33.10
NS3-108	152	0.18 ± 0.06	0.04 ± 0.01	5.15 ± 0.44	5.74 ± 0.15	33.61
NS3-107	158	0.91 ± 0.06	0.03 ± 0.01	7.73 ± 0.47	8.15 ± 0.17	33.52
NS3-106	165	0.25 ± 0.15	0.08 ± 0.02	7.60 ± 0.36	7.94 ± 0.13	33.18
NS3-105	171	0.00 ± 0.15	0.09 ± 0.02	8.31 ± 0.53	8.84 ± 0.17	33.14
NS3-104	178	0.00 ± 0.14	0.09 ± 0.02	9.47 ± 0.55	8.22 ± 0.21	33.23
NS3-103	184	0.15 ± 0.07	0.04 ± 0.01	7.95 ± 0.65	8.70 ± 0.23	33.82
NS3-102	191	1.08 ± 0.08	0.03 ± 0.01	6.51 ± 0.49	8.05 ± 0.19	34.26
NS3-101	197	0.88 ± 0.07	0.01 ± 0.01	8.55 ± 0.81	9.58 ± 0.31	34.13

Table 3.12: Radium isotope activities and salinity, Surveys NS1 (Sept. 1999), NS2 (April 2000) and NS3 (December 2000), northern Mid-Atlantic Bight. ^{223}Ra and ^{224}Ra activities are "excess," after correcting for supported activity from ^{227}Ac and ^{228}Th.

Sample Location	Distance (km)	^{228}Th (dpm/ 100L)			^{227}Ac (dpm/ 100L)		
NS1-01	120	1.15	±	0.16	N/A		
NS1-02	141	0.76	±	0.13	N/A		
NS1-03	167	1.11	±	0.10	N/A		
NS1-04	192	0.87	±	0.10	N/A		
NS1-05	210	0.83	±	0.05	N/A		
NS1-06	234	0.94	±	0.06	N/A		
NS1-07	257	1.14	±	0.17	N/A		
NS1-11	120	0.80	±	0.09	N/A		
NS1-10	141	0.72	±	0.14	N/A		
NS1-09	167	0.71	±	0.08	N/A		
NS1-08	192	0.88	±	0.16	N/A		
NS2-026	80	0.67	±	0.18	0.0165	±	0.0055
NS2-025	110	0.80	±	0.22	0.0000	±	0.0000
NS2-024	125	0.78	±	0.23	0.0100	±	0.0039
NS2-023	133	0.69	±	0.11	0.0109	±	0.0013
NS2-022	141	0.77	±	0.15	0.0095	±	0.0014
NS2-021	148	0.63	±	0.14	0.0117	±	0.0014
NS2-020	152	0.63	±	0.11	0.0179	±	0.0041
NS2-019	158	0.33	±	0.09	0.0201	±	0.0048
NS2-018	164	0.73	±	0.15	0.0276	±	0.0067
NS2-017	171	0.48	±	0.09	0.0053	±	0.0014
NS2-016	177	0.65	±	0.12	0.0194	±	0.0043
NS2-015b	187	0.49	±	0.11	0.0127	±	0.0033
NS2-015	207	0.62	±	0.12	0.0155	±	0.0035
NS2-014	218	0.49	±	0.14	0.0058	±	0.0017
NS2-013	232	0.73	±	0.16	0.0327	±	0.0065
NS2-012	249	0.68	±	0.14	0.0332	±	0.0065
NS3-119	100	1.09	±	0.16	0.0000	±	0.0156
NS3-118	106	0.86	±	0.13	0.0060	±	0.0021
NS3-117	113	0.87	±	0.11	0.0159	±	0.0070
NS3-116	119	0.72	±	0.05	0.0033	±	0.0014
NS3-115	126	0.61	±	0.05	0.0157	±	0.0081
NS3-114	132	0.59	±	0.05	0.0129	±	0.0042
NS3-113	139	0.52	±	0.08	0.0030	±	0.0014
NS3-109	145	0.61	±	0.06	0.0226	±	0.0064
NS3-108	152	0.66	±	0.06	0.0190	±	0.0053
NS3-107	158	0.31	±	0.03	0.0061	±	0.0022
NS3-106	165	0.74	±	0.15	0.0147	±	0.0047
NS3-105	171	0.83	±	0.15	0.0108	±	0.0033
NS3-104	178	0.85	±	0.14	0.0191	±	0.0056
NS3-103	184	0.81	±	0.07	0.0000	±	0.0059
NS3-102	191	0.48	±	0.05	0.0144	±	0.0109
NS3-101	197	0.39	±	0.04	0.0228	±	0.0133

Table 3.13: ^{228}Th and ^{227}Ac activities, Surveys NS1 (Sept. 1999), NS2 (April 2000) and NS3 (December 2000), northern Mid-Atlantic Bight.

Sample Location	Distance (km)	Nitrate (μM)	Phosphate (μM)	Silicate (μM)	Ammonium (μM)	N:P	N:Si
NS1-01	120	N/A	N/A	N/A	N/A	N/A	N/A
NS1-02	141	1.51	0.31	2.85	N/A	4.87	0.53
NS1-03	167	1.51	0.25	1.58	N/A	6.04	0.96
NS1-04	192	1.49	0.16	1.35	N/A	9.31	1.10
NS1-05	210	1.48	0.15	1.35	N/A	9.87	1.10
NS1-06	234	1.48	0.12	0.91	N/A	12.33	1.63
NS1-07	257	1.48	0.15	0.86	N/A	9.87	1.72
NS1-11	120	N/A	N/A	N/A	N/A	N/A	N/A
NS1-10	141	N/A	N/A	N/A	N/A	N/A	N/A
NS1-09	167	N/A	N/A	N/A	N/A	N/A	N/A
NS1-08	192	N/A	N/A	N/A	N/A	N/A	N/A
NS2-026	80	2.50	0.72	0.89	7.11	3.47	2.81
NS2-025	110	1.53	0.69	0.29	6.16	2.22	5.28
NS2-024	125	6.55	0.89	1.71	7.44	7.36	3.83
NS2-023	133	5.29	0.75	2.19	8.31	7.05	2.42
NS2-022	141	5.49	0.96	2.36	4.60	5.72	2.33
NS2-021	148	5.81	0.80	2.26	3.47	7.26	2.57
NS2-020	152	4.41	0.70	2.16	4.69	6.30	2.04
NS2-019	158	4.36	0.71	2.25	6.74	6.14	1.94
NS2-018	164	4.80	0.68	1.76	5.01	7.06	2.73
NS2-017	171	4.47	0.73	1.75	3.26	6.12	2.55
NS2-016	177	4.52	0.63	1.82	2.98	7.17	2.48
NS2-015b	187	5.50	1.01	1.89	6.26	5.45	2.91
NS2-015	207	4.87	0.63	1.29	5.87	7.73	3.78
NS2-014	218	4.74	0.53	2.40	2.84	8.94	1.98
NS2-013	232	0.99	0.28	1.97	3.18	3.54	0.50
NS2-012	249	5.39	0.73	3.02	4.96	7.38	1.78
NS3-119	100	2.57	0.79	3.81	1.29	3.25	0.67
NS3-118	106	2.98	0.68	2.69	0.66	4.38	1.11
NS3-117	113	2.62	0.71	2.73	0.94	3.69	0.96
NS3-116	119	3.24	0.67	2.11	0.74	4.84	1.54
NS3-115	126	3.54	0.66	2.22	0.66	5.36	1.59
NS3-114	132	5.06	0.67	3.92	1.12	7.55	1.29
NS3-113	139	3.99	0.60	3.26	0.37	6.65	1.22
NS3-109	145	4.59	0.64	3.62	0.40	7.17	1.27
NS3-108	152	5.33	0.60	4.75	0.46	8.88	1.12
NS3-107	158	5.59	0.62	5.00	0.48	9.02	1.12
NS3-106	165	5.26	0.66	4.26	0.45	7.97	1.23
NS3-105	171	5.09	0.65	4.13	0.46	7.83	1.23
NS3-104	178	4.65	0.61	4.06	0.45	7.62	1.15
NS3-103	184	4.87	0.55	4.46	0.44	8.85	1.09
NS3-102	191	4.82	0.48	4.43	0.51	10.04	1.09
NS3-101	197	4.78	0.48	4.56	0.43	9.96	1.05

Table 3.14: Nutrients, Surveys NS1 (Sept. 1999), NS2 (April 2000) and NS3 (December 2000), northern Mid-Atlantic Bight.

Station and depth (m)	Distance km	Salinity	^{238}U dpm/kg	^{234}Th dpm/kg			$\frac{^{234}Th}{^{238}U}$
NS2-012 sfc	249	35.91	2.36	1.35	±	0.03	0.57
NS2-013 sfc	232	36.21	2.36	1.49	±	0.03	0.63
NS2-014 sfc	218	35.54	2.36	1.60	±	0.03	0.68
NS2-015 sfc	207	33.74	2.31	1.03	±	0.02	0.45
NS2-016 sfc	177	33.67	2.31	1.18	±	0.02	0.51
NS2-018 sfc	164	33.49	2.30	0.97	±	0.02	0.42
NS2-020 sfc	152	33.38	2.29	0.81	±	0.02	0.35
NS2-022 sfc	141	33.28	2.28	0.80	±	0.02	0.35
NS2-024 sfc	125	33.18	2.28	0.54	±	0.01	0.24
NS2-025 sfc	110	33.22	2.28	0.42	±	0.01	0.18
NS2-026 sfc	80	33.15	2.27	0.47	±	0.01	0.21
DEB-019 sfc	120	34.00	2.33	1.38	±	0.03	0.59
DEB-021 sfc	110	33.83	2.32	1.64	±	0.03	0.71
DEB-024 sfc	95	33.32	2.29	1.17	±	0.02	0.51
DEB-025 sfc	90	33.10	2.27	1.05	±	0.02	0.46
DEB-027 sfc	80	33.07	2.27	1.13	±	0.02	0.50
DEB-029 sfc	70	33.00	2.26	1.07	±	0.02	0.47
DEB-030 sfc	60	32.82	2.25	0.93	±	0.02	0.41
NS3-101 3m	197	34.13	2.34	1.29	±	0.03	0.55
NS3-101 52m		34.30	2.35	1.75	±	0.03	0.74
NS3-101 100m		34.81	2.39	1.87	±	0.03	0.78
NS3-101 450m		35.11	2.41	2.08	±	0.03	0.86
NS3-102 sfc	191	34.35	2.36	1.49	±	0.03	0.63
NS3-103 sfc	184	34.37	2.36	1.60	±	0.03	0.68
NS3-104 4m	178	33.72	2.31	0.82	±	0.02	0.35
NS3-104 62m		33.91	2.33	1.46	±	0.03	0.63
NS3-104 201m		34.01	2.33	0.62	±	0.02	0.26
NS3-105 sfc	171	33.67	2.31	1.18	±	0.02	0.51
NS3-106 sfc	165	33.49	2.30	0.97	±	0.02	0.42
NS3-107 3m	158	33.38	2.29	0.93	±	0.02	0.41
NS3-107 100m		33.81	2.32	1.33	±	0.03	0.57
NS3-108 sfc	152	33.28	2.28	0.80	±	0.02	0.35
NS3-109 sfc	145	33.18	2.28	0.54	±	0.01	0.24
NS3-113 5m	139	33.04	2.27	0.85	±	0.02	0.37
NS3-113 55m		33.74	2.31	0.22	±	0.01	0.10
NS3-113 93m		33.51	2.30	1.25	±	0.02	0.54
NS3-116 3m	119	32.63	2.24	0.36	±	0.00	0.16
NS3-116 20m		32.91	2.26	0.54	±	0.01	0.24
NS3-116 52m		33.02	2.27	0.61	±	0.02	0.27
NS3-119 3m	100	32.55	2.23	0.35	±	0.01	0.16
NS3-119 25m		32.78	2.25	0.46	±	0.01	0.21
NS3-119 50m		32.85	2.25	0.48	±	0.01	0.22

Table 3.15: ^{234}Th from Surveys NS2 (April 2000), DE-B (November 2000) and NS3 (December 2000), northern Mid-Atlantic Bight. ^{238}U values are calculated by salinity.

Chapter 4

Slope water, Gulf Stream and seasonal influences during the fall-winter transition in the southern Mid-Atlantic Bight

4.1 Introduction

The southern portion of the Mid-Atlantic Bight between Delaware Bay and Chesapeake Bay is complex because of the effects of the narrowing shelf, the proximity of the Gulf Stream after it has detached from the margin, and the convergent Mid-Atlantic Bight and South Atlantic Bight water masses. Gulf Stream effects in this area have been noted by Churchill and Cornillon (1991) who observed fairly frequent intrusions of Gulf Stream water on the upper slope (13-27% of observations) and occasional intrusions onto the outer shelf (3-9% of the time). The influence of the Gulf Stream on shelfbreak currents has been observed by Bane et al. (1988) who demonstrated a relationship between Gulf Stream proximity and shelfbreak current velocity. Pycnocline salinity intrusions, more commonly associated with slope water, have also been shown to have Gulf Stream origins in this region (Gawarkiewicz et al. 1996a). Gulf Stream forcing and effects of Gulf Stream rings and streamers are considered to be some of the possible influences on cross-shelf transport in the Mid-Atlantic Bight, but the magnitude to which these and other porcesses contribute

to cross-shelf exchange is "poorly known in general" (Loder et al. 1998).

The data presented here are from a hydrographic survey taken along 4 closely spaced shelfbreak transects between Delaware Bay and Chesapeake Bay in early November 2000, a particularly under-represented season in Mid-Atlantic Bight studies. This time is characterized by a transition between highly stratified summer conditions and the homogeneous water column over the shelf in winter (Beardsley et al. 1985; Mooers et al. 1976; Wright and Parker 1976). During the fall transition, summer stratification is destroyed by convection as the surface cools, as well as by increased storm activity.

The cruise was designed to provide enough resolution to adequately resolve the structure of the shelfbreak front and shelfbreak jet, as well as small scale features contributing to cross-frontal exchange. Findings included strong interactions of both Gulf Stream and slope water with the shelfbreak front, a very deep bottom intercept of the shelfbreak front, and shelfbreak cold water masses likely unique to the fall-winter transition. A mid-shelf salinity front was also present, which had sizeable transports.

Resolving these features allowed calculations of volume, heat and salt transport across the region that include the contribution of the high-velocity shelfbreak jet, as well as a significant mid-shelf jet. The shelfbreak jet, a relatively small scale feature, was found to account for the majority of alongshelf flux. The resulting volume transport is considerably higher than transport estimates that are typically cited for the Mid-Atlantic Bight (Biscaye et al. 1994a; Beardsley et al. 1985; Ramp et al. 1988), although they are similar to some of the larger estimates that are less frequently used in budget calculations (e.g., Burrage and Garvine, 1988, and Voorhis et al., 1976). The large alongshelf transport was found to be consistent with the unusual hydrographic structure, as predicted by the Yankovsky

and Chapman model (1997). These results contribute to evidence suggesting that Gulf Stream influence on the slope may play a significant role in Mid-Atlantic Bight circulation. Transport estimates such as these also suggest that the "leaky current" model of alongshelf transport in the Mid-Atlantic Bight may need revision.

4.2 Methods

Data were collected from the R/V *Cape Hatteras* in the Mid-Atlantic Bight between Delaware Bay and Chesapeake Bay, approximately 300 km north of Cape Hatteras, on 3-5 November 2000. Four 60-80 km cross-shelf sections were occupied, centered on the shelfbreak, as well as one alongshelf section (Figure 4.1). Conductivity, temperature and depth were measured using a SeaBird CTD at station intervals of 5 km in the cross-shelf direction from approximately the 40 m isobath to the upper slope. Velocity was measured using an RDI 150 kHz ADCP with 8 m bin size, 8 m vertical averaging and an ensemble length of 3 minutes. One of the four ADCP beams was not working, so the entire data set uses 3-beam solutions. No bottom tracking was available for calibration. In this region the M2 barotropic tide has the greatest amplitude (2.4 cm/s at station WQ, 37.92 N, 74.93 W). This is small compared to measured current velocities of over 60 cm/s, therefore ADCP data is not detided (Moody et al. 1984). Wind measurements were taken from the nearest National Data Buoy Center buoy, NDBC 44009, located 26 nmi SE of Cape May, NJ (approximately 30 km NNW of the study area). Winds were steady and moderate from the northwest during the survey, with a mean of 8.7 m/s at 332°, except for a 12 hour period on the second day during which the wind shifted westerly to 231° at 3.7 m/s. The 100 m isobath is used to reference distance from the shelfbreak to facilitate comparison with climatological studies, although

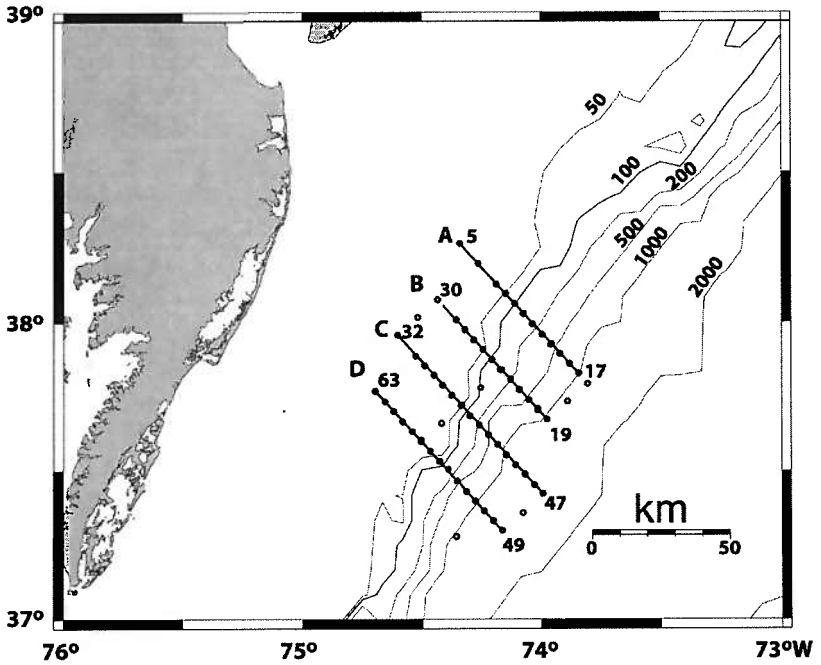

Figure 4.1: Cruise track and station locations for R/V *Cape Hatteras* cruise 2300, 2-6 November 2000.

the actual shelfbreak position varies from 100-140 meters along this region. Velocity is referenced to a cross-shelf/alongshelf coordinate system, constructed by rotating the N-S coordinate system to be perpendicular to the 100 m isobath. The mean deviation of the N-S coordinate system from perpendicular with respect to the 100 m isobath was 50.16°, and varied approximately ±1° between transects. In the rotated coordinate system, **u** is positive to the northeast and **v** positive to the northwest (shoreward). The convention for characterizing shelf water will be defined as salinity < 34.5 PSU.

4.3 Hydrographic Structure

Climatological studies of the Mid-Atlantic Bight have been compiled by Linder and Gawarkiewicz (1998) and S. Lentz (unpublished). Both climatologies show the fall transition between a strong summertime pycnocline in the upper 25-50 meters, and a strong wintertime density front at the shelfbreak. Although the general structure of the climatological sections is similar to sections in our study, they also deviate from mean conditions in significant ways, including the position of the surface outcropping of the shelfbreak front, the depth of the foot of the front, the depth and strength of the shelfbreak jet, and the characteristics of the temperature minimum. Figure 4.2 shows climatological hydrographic sections for the region of this study area during September-November. Mean salinity over the shelf ranges from 31.5-33.5 PSU. Salinities under 34.5 PSU extend offshore beyond the 100 meter isobath, with surface outcrop of the 34.5 PSU isohaline at approximately 50 km beyond the shelfbreak. In the mean sections both the thermocline and halocline have begun to break down over the shelf after summer stratification, although shelfwater is still warm (16-18°C). Minimum temperatures occur over the bottom at the shelfbreak in an area approximately 60 km wide and 20-30 m deep. By late fall, climatological sections compiled for this area from more limited data sets show a well mixed shelf with a mean temperature of 15°C and a minimum temperature of 13°C, now confined to a 15 m pocket over the outer 20 km of the shelfbreak (S. Lentz, unpublished). The Linder and Gawarkiewicz climatology of this region between the New Jersey shelf and Chesapeake Bay (also based on a small number of datasets) shows a moderate baroclinic jet present over the shelfbreak with maximum alongshelf velocity of approximately 18 cm s^{-1}. The 34.5 PSU isohaline is shown to migrate from a flat position in the summer halocline to a more vertical position with a surface

outcropping 40 km beyond the 100 m isobath in October-November, and then to a position over the outer shelf during winter. The foot of the front also migrates shoreward during this period, from near the 100 m isobath to the 75 m isobath.

The hydrographic sections in this study depart quite dramatically from the climatological means. The most striking difference is the presence of well-defined intrusions of high salinity water over the outer shelf in the surface mixed layer (Figure 4.3). These intrusions differ considerably from those observed in summertime (S_{max}) which typically occur where one layer of a deep slope water mass intrudes laterally into a weak layer of the pycnocline over the shelf (Gordon and Aikman 1981; Gawarkiewicz et al. 1990). Although they exhibit similar T-S properties to S_{max} features (salinity, temperature and density nearly uniform with depth and having slope water characteristics) the intrusions observed here are confined to the surface mixed layer and displace or overlay the normal frontal gradients. Above 50 m depth the 34.5 isohaline is much further inshore than in the climatology, outcropping just 4-22 km offshore of the 100 m isobath. On transects A and B, the strongest salinity gradients in the surface mixed layer are located 15-20 km shoreward of those at depths of $>$ 60m. The position of the surface front is displaced towards a more typical offshore position as the transects covered progress southward and in sections C and D the isohalines become nearly vertical in the upper 70-100 m. In addition to the front outcropping closer to shore than in the climatology, the foot of the front is 50-75 m deeper than the climatological average. While the lower half of the front in most sections has a slope of 3-6 $\times 10^{-3}$, similar to those reported by Gawarkiewicz et al (1996a) and Flagg and Beardsley (1978), in the upper 50-70 m of the water column the isohalines are nearly vertical. The horizontal gradients in salinity are particularly strong near the foot of the front directly over the shelfbreak

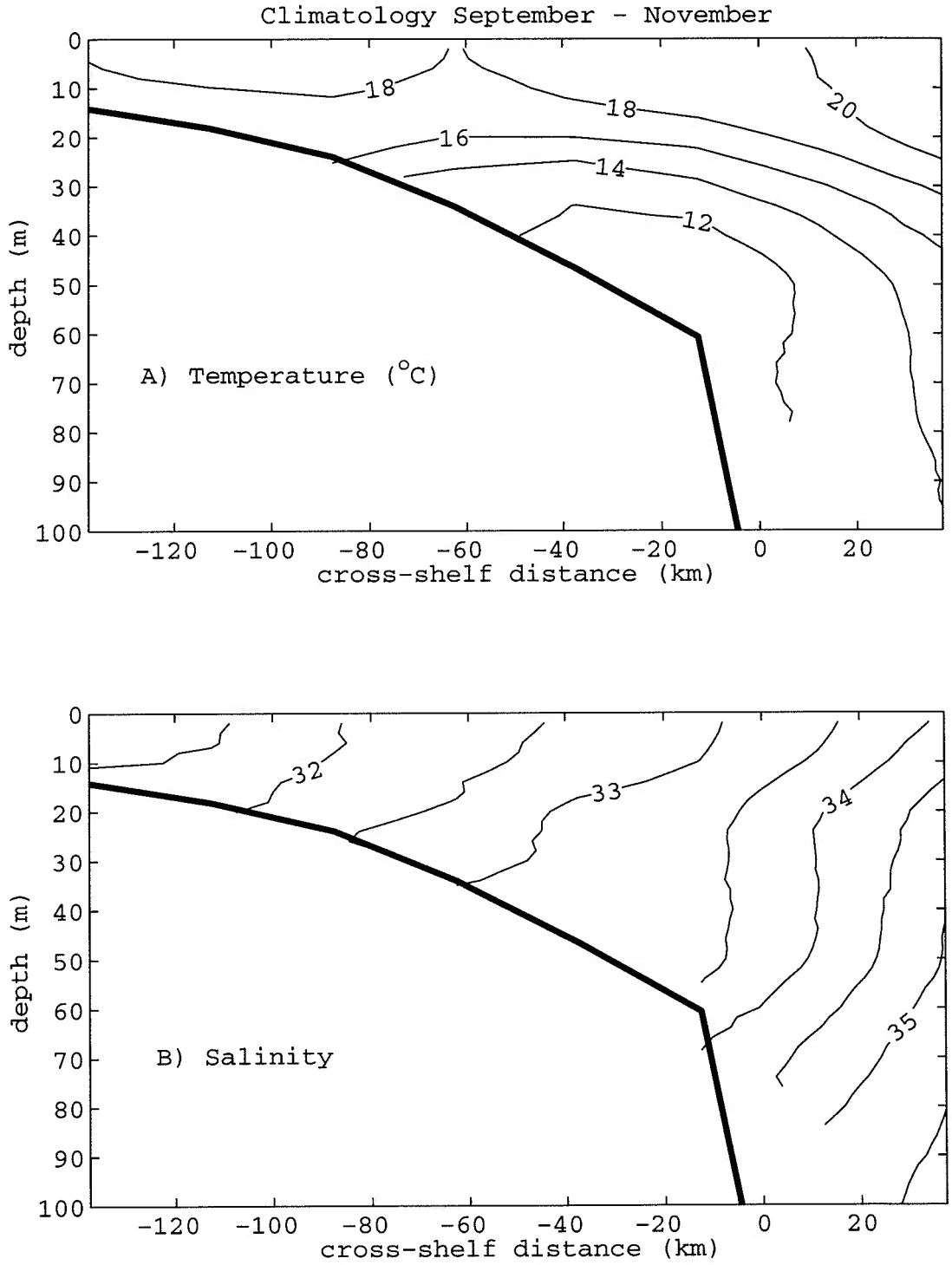

Figure 4.2: Climatology of Mid-Atlantic Bight between Delaware and Chesapeake Bay. A) Temperature, B) Salinity (S. Lentz, unpublished data)

at approximately 60-120 m depth. In the surface mixed layer, strong horizontal salinity gradients are compensated by equally strong temperature gradients and density gradients are thus weak at the surface. Below 50-70 m however, strong horizontal density gradients occur in the subsurface area due to the dominance of a cold, more uniform water mass over the foot of the front. An interesting similarity between present observations and the Linder (1996) climatology is that the mean October-November 34.5 isohaline exhibits a shoreward trend at mid-depth also, raising the question of whether slopewater intrusions are common late fall events.

The slopewater mass in the surface mixed layer extends along the entire alongshelf distance sampled (Figure 4.4) as seen in horizontal maps of temperature, salinity and density contours at 25 m. A sharp front can be seen near the 100 m isobath, and Gulf Stream water in the southeast corner near the end of sections C and D is evident from the high salinities. At the southern end of the survey, shelf water extends further offshore; the southern extent of the shelf water extending onto the slope is not known.

A vertical alongshelf section through all transects at the 1000 m isobath (Figure 4.5, oriented looking towards shore) shows the core of the high salinity water mass along sections A, B, and C, with shelfwater present at section D. ADCP current measurements averaged over the upper water column indicate that an offshore excursion of shelfwater is consistent with surface velocities in the study area which take an offshore turn at the shelfbreak in the south (Figure 4.6). The shift in flow direction could also account for the offshore displacement of the front that is seen in the southern sections.

The Gulf Stream intrusion visible in the horizontal section occurs along the outer 20 km of transect C and the outer 10 km of transect D in a thin layer overlaying the deeper

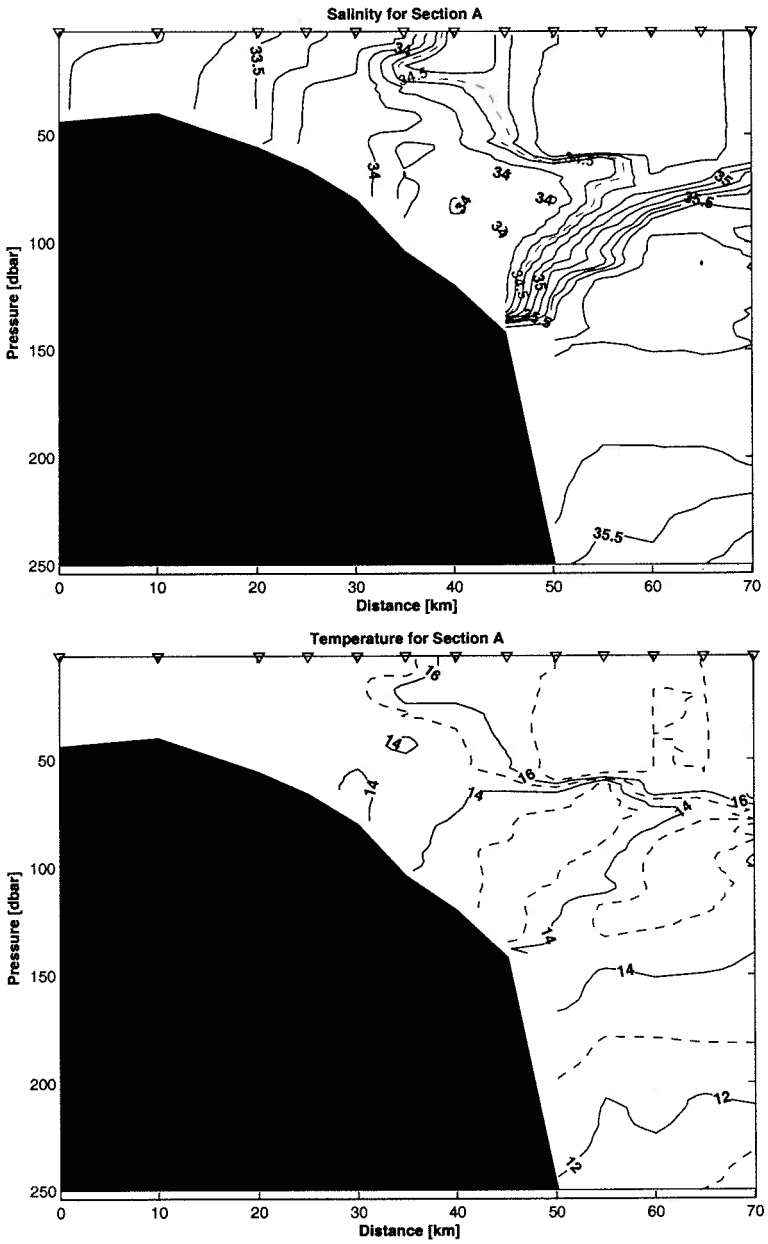

Figure 4.3: A) Salinity, B) Temperature, C) Density, D) Geostrophic Velocity, and E) Barotropic Velocity for the four cross-shelf sections.

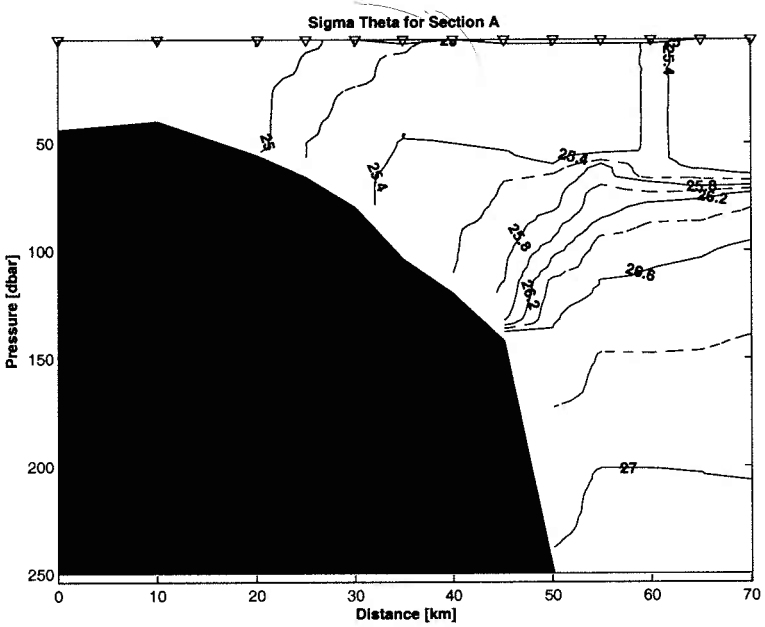
Sigma Theta for Section A
Pressure [dbar]
Distance [km]
25.4
25.4
25.6
26.2
26.4
26.6
27

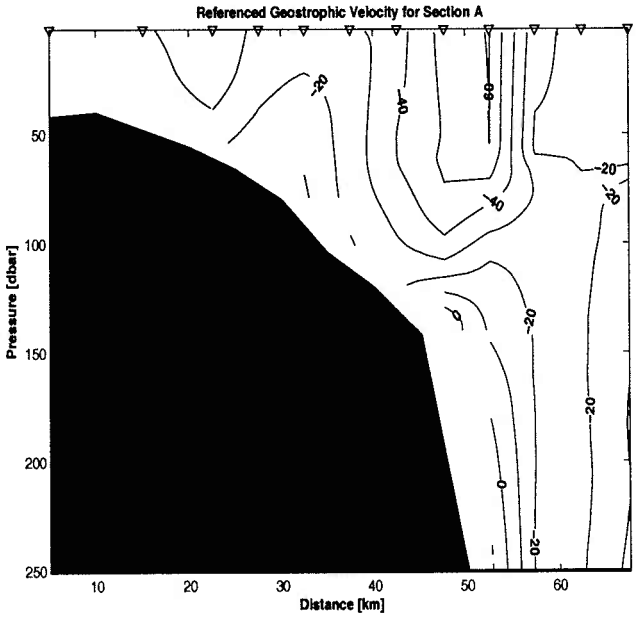
Referenced Geostrophic Velocity for Section A
Pressure [dbar]
Distance [km]
-20
-40
-60
-20
-40
-20
-20
0
-20

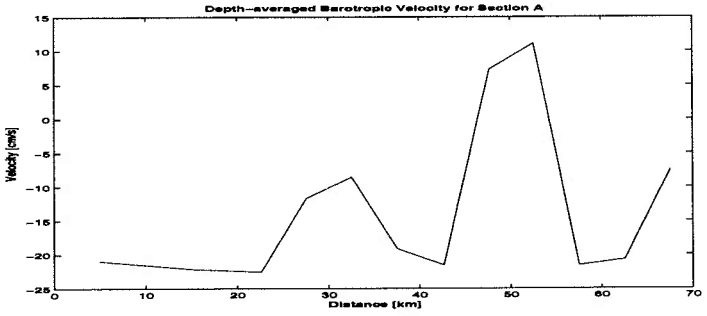
Depth-averaged Barotropic Velocity for Section A
Velocity [cm/s]
Distance [km]

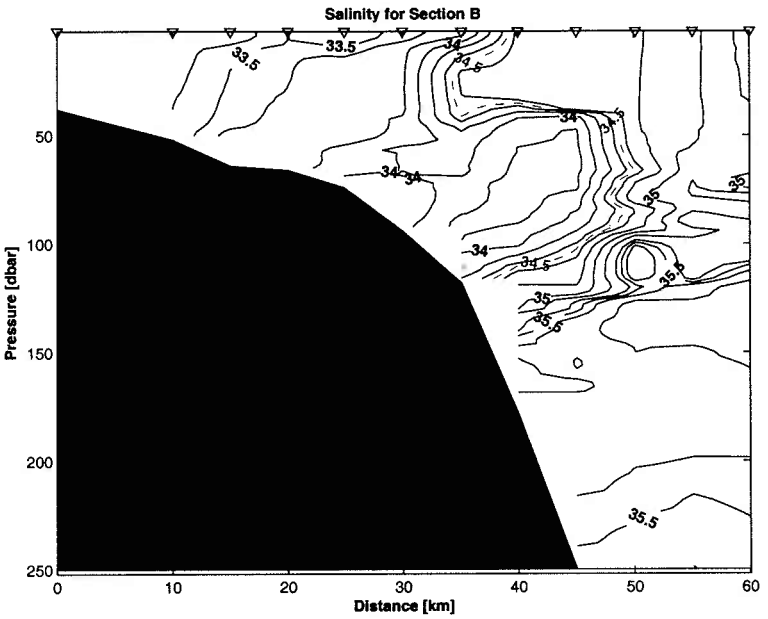
Salinity for Section B
Pressure [dbar]
Distance [km]
33.5
34
34.5
35
35.5
50
100
150
200
250
0
10
20
30
40
50
60

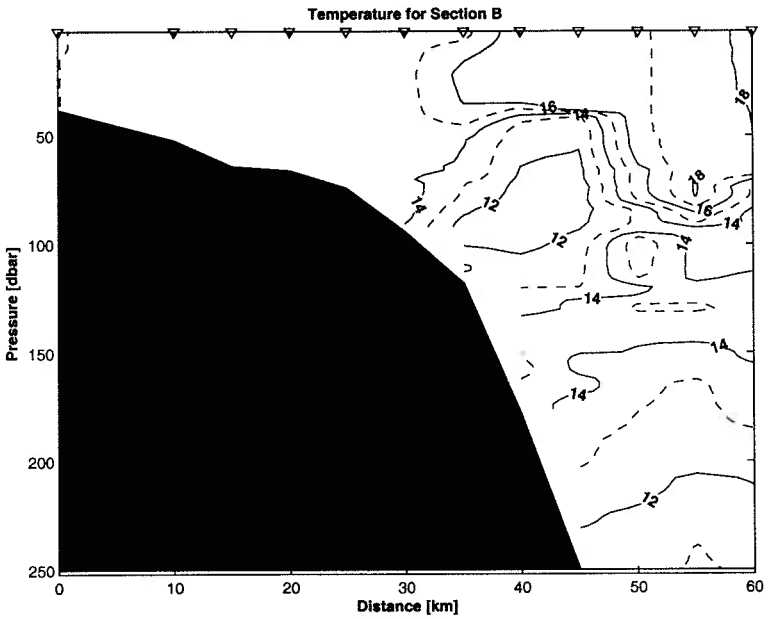
Temperature for Section B
Pressure [dbar]
Distance [km]
12
14
16
18
50
100
150
200
250
0
10
20
30
40
50
60

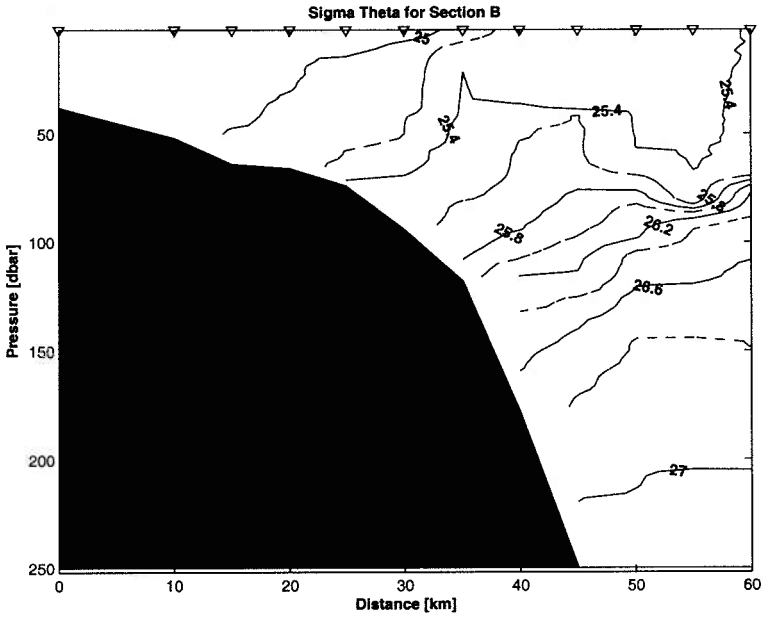
Sigma Theta for Section B
Pressure [dbar]
Distance [km]
25
25.4
25.8
26.2
26.6
27

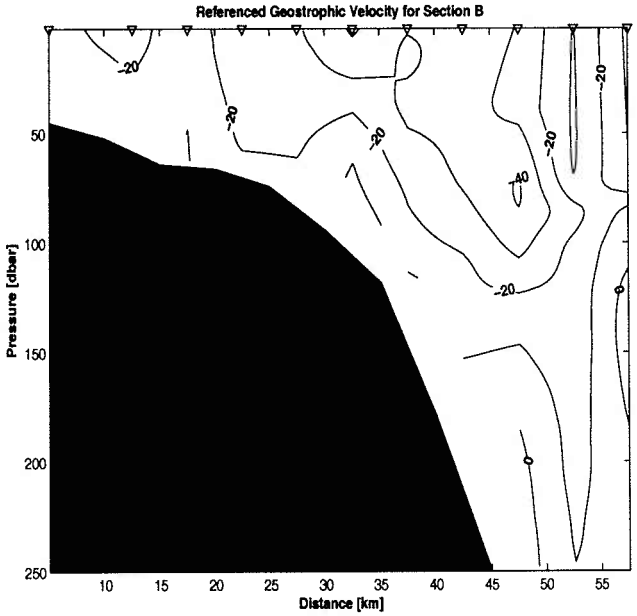
Referenced Geostrophic Velocity for Section B
Pressure [dbar]
Distance [km]
-20
-40
0

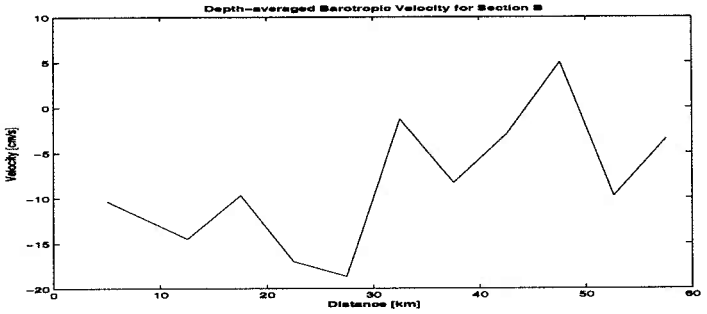
Depth-averaged Barotropic Velocity for Section B
Velocity [cm/s]
Distance [km]

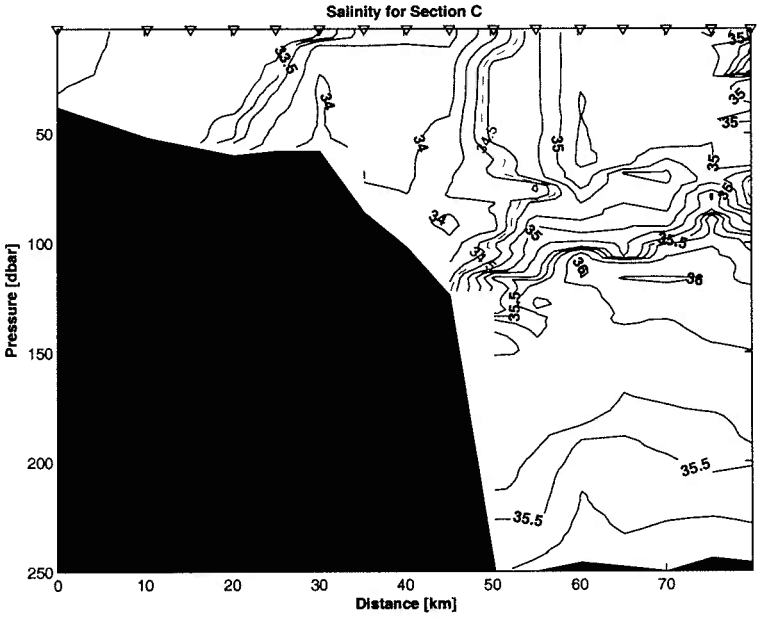
Salinity for Section C
Pressure [dbar]
Distance [km]
50
100
150
200
250
0
10
20
30
40
50
60
70
34
34.5
35
35.5
36

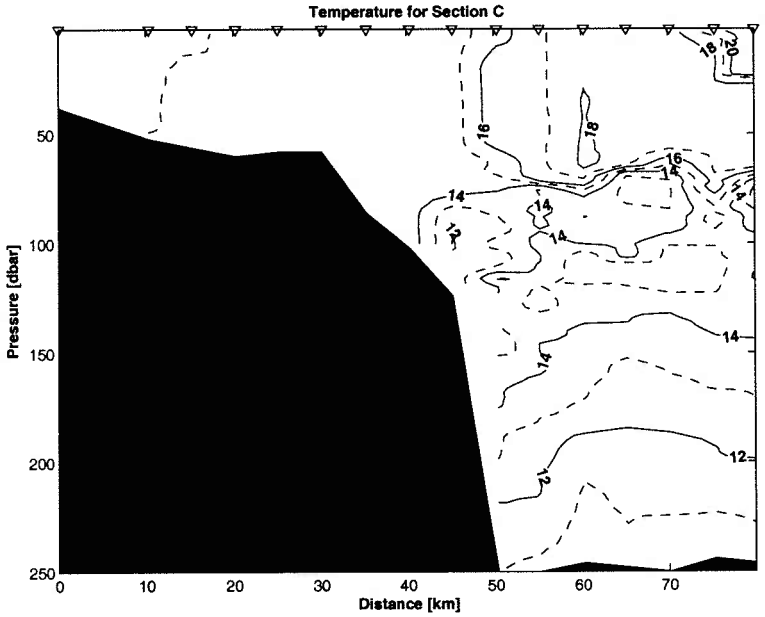
Temperature for Section C
Pressure [dbar]
Distance [km]
50
100
150
200
250
0
10
20
30
40
50
60
70
12
14
16
18
20

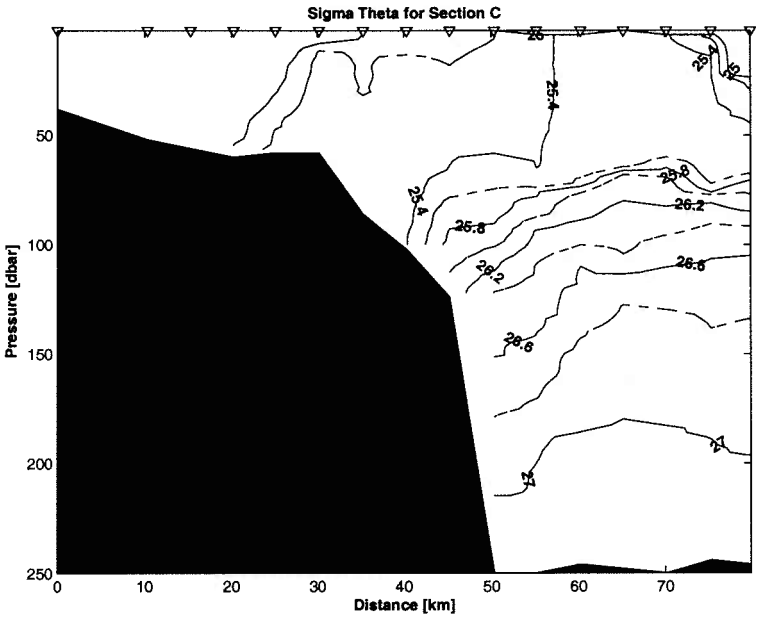
Sigma Theta for Section C
Pressure [dbar]
Distance [km]
50
100
150
200
250
0
10
20
30
40
50
60
70
25.4
25.8
26.2
26.6
26

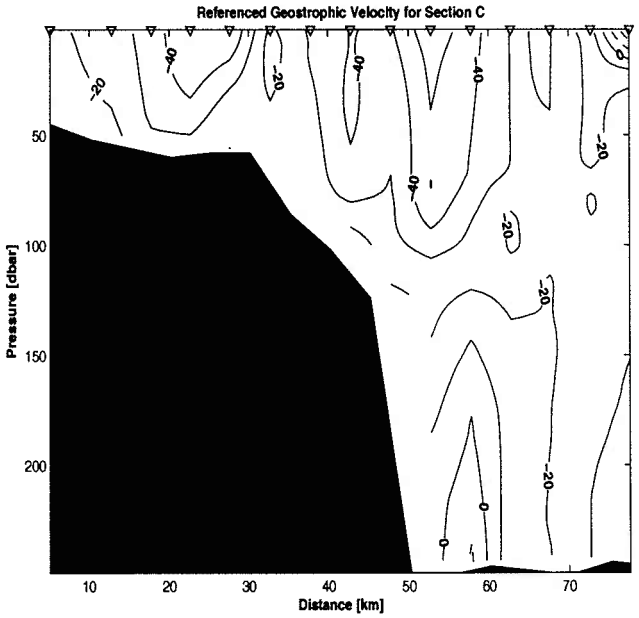
Referenced Geostrophic Velocity for Section C
Pressure [dbar]
Distance [km]
50
100
150
200
10
20
30
40
50
60
70
-20
-40
0

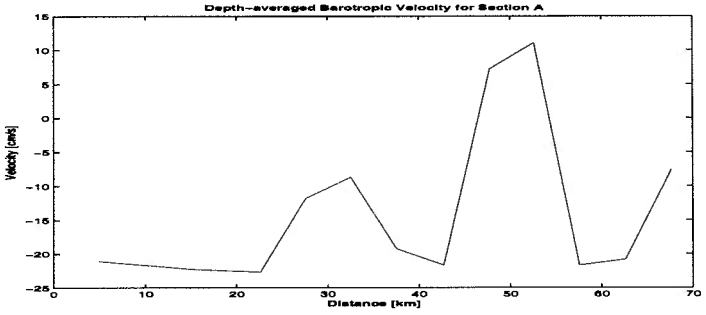
Depth-averaged Barotropic Velocity for Section A
Velocity [cm/s]
Distance [km]
15
10
5
0
-5
-10
-15
-20
-25
0
10
20
30
40
50
60
70

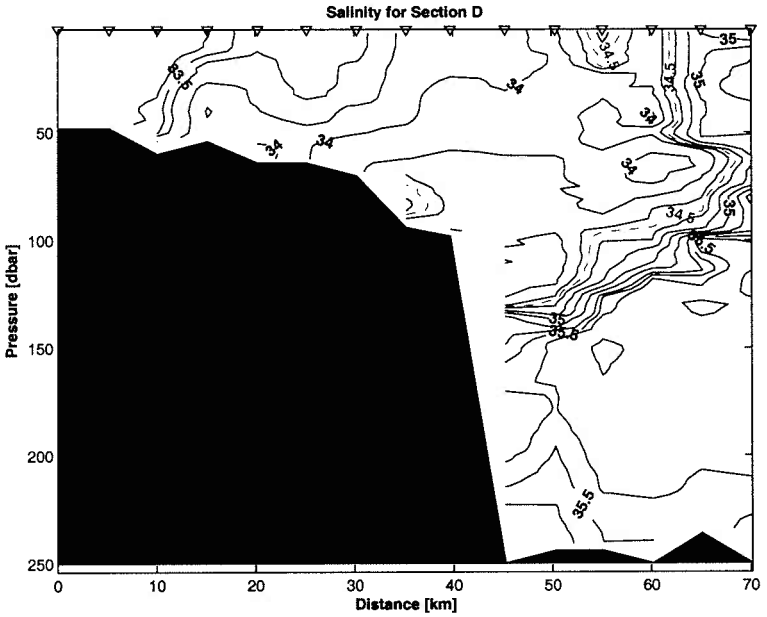
Salinity for Section D
Pressure [dbar]
Distance [km]
50
100
150
200
250
0
10
20
30
40
50
60
70
34
34.5
35
35.5

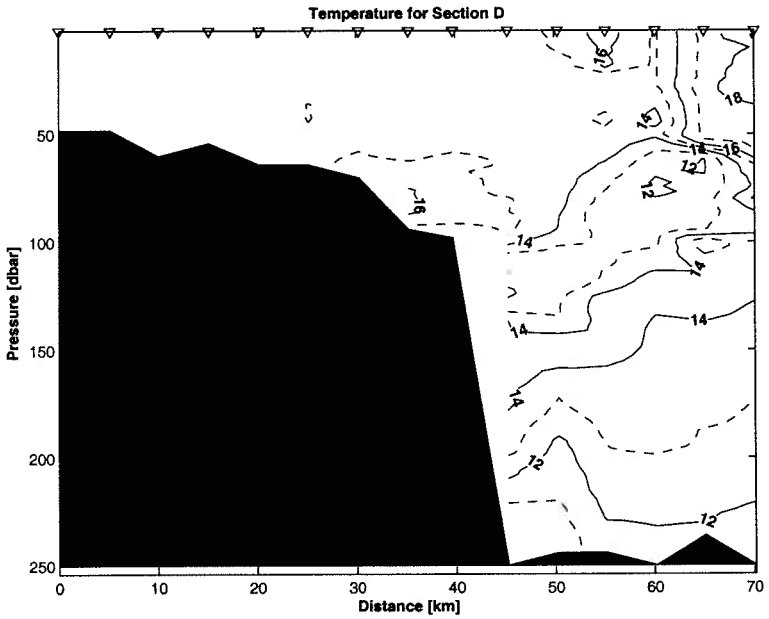
Temperature for Section D
Pressure [dbar]
Distance [km]
50
100
150
200
250
0
10
20
30
40
50
60
70
16
15
14
12

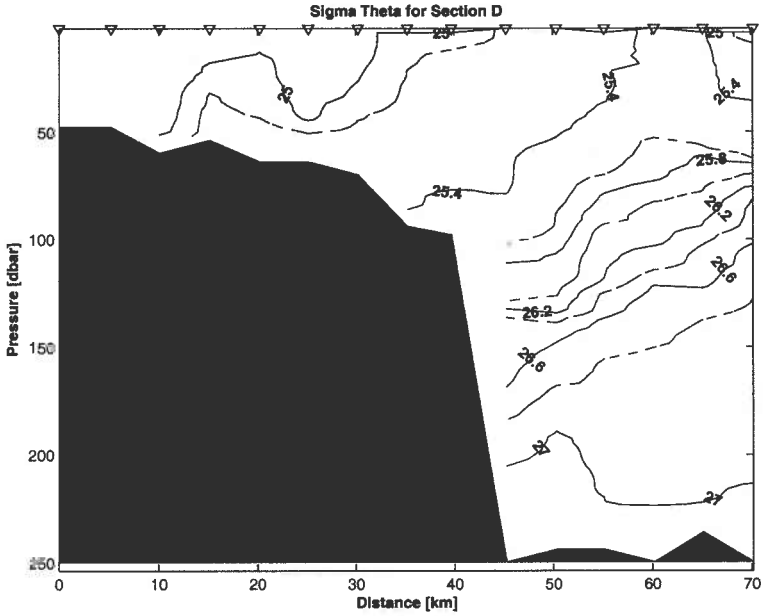
Sigma Theta for Section D
Pressure [dbar]
Distance [km]
25
25.4
25.8
26.2
26.6
27

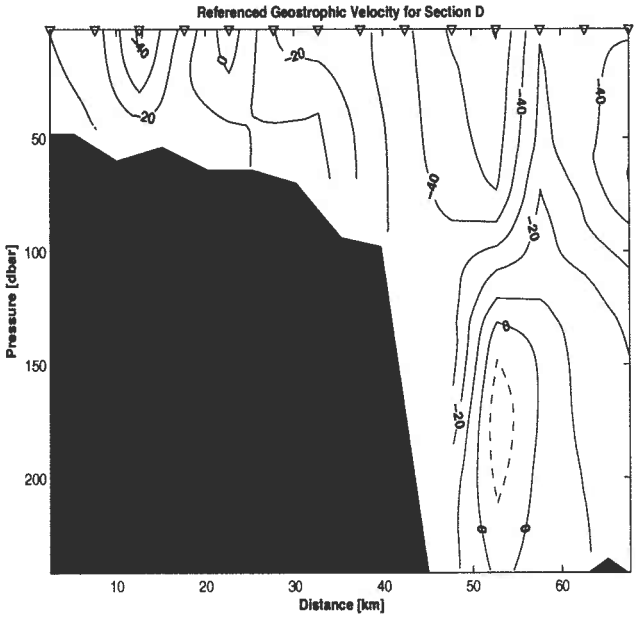
Referenced Geostrophic Velocity for Section D
Pressure [dbar]
Distance [km]

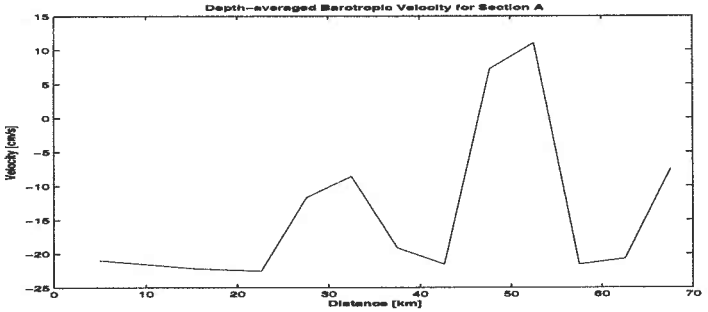
Depth-averaged Barotropic Velocity for Section A
Velocity [cm/s]
Distance [km]

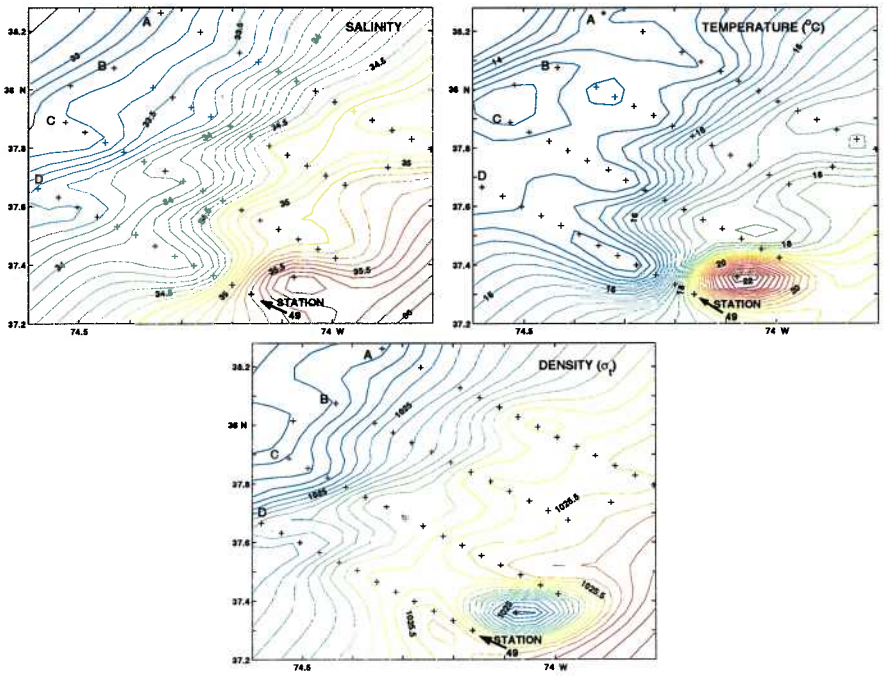

Figure 4.4: Horizontal contours at 25 m depth for A) Salinity; B) Temperature, and C) Density.

slopewater intrusion. The vertical structure and temperature-salinity properties of this layer distinquish it from any of the other water masses in the survey. Vertical profiles alongshelf between the end of transects C and D (including one station between transects) show this water mass occupying a shallow layer in the upper 25 m, with salinity exceeding 36.0 PSU and temperature over 23°C at the core (Figure 4.7).

This layer is visible in the T-S diagrams (Figure 4.10c,d) as the scattering of points along a 24.5 isopycnal at the top of the image, far removed from any other mixing line. The dashed line in the images indicates the normal range of Gulf Stream temperature and salinity. Like the Gulf Stream water commonly found on the upper slope in the analysis by Churchill and Cornillon (1991), this water also has significantly lower density than the

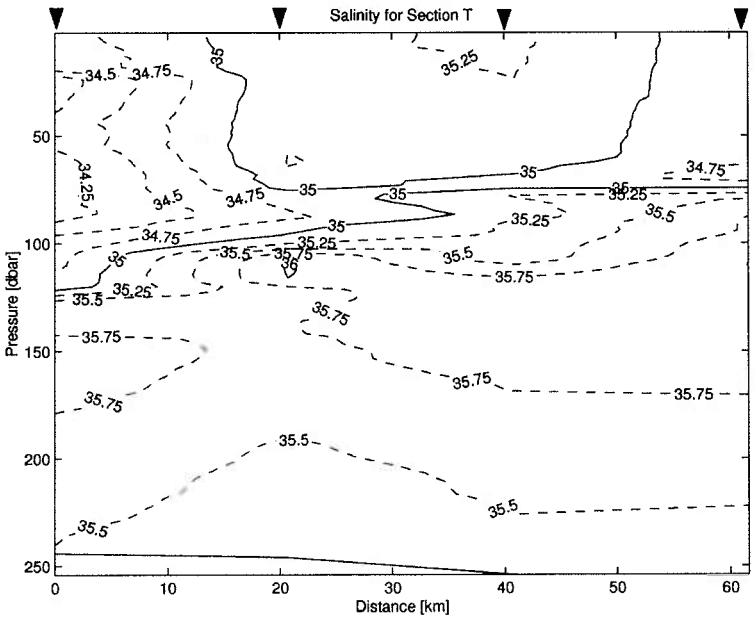

Figure 4.5: Alongshelf section of salinity at 1000 m isobath. Orientation is looking shoreward, with transect D on the left, transect A on the right. Note presence of shelfwater in upper 100 m between x = 0-8 km.

water mass that surrounds it. Temperature of > 23°C also distinguish it as water of recent Gulf Stream origin (see AVHRR image, Figure 4.9) which is significant in the interpretation of its geochemical properties which are discussed at length in Chapter 5.

Local winds may be partly responsible for the observed position and structure of the front. For the two days prior to the cruise (1-2 November) mean wind speed was 11.9 m/s from 327° and decreased in magnitude over the course of the cruise, with a mean of 4.3 m/s from 259° over 5-6 November. The high wind speed with an onshore Ekman transport could have driven surface slope water onto the shelf during the first few days of November. Using the method of Fong (1998) which assumes a momentum equation dominated by the

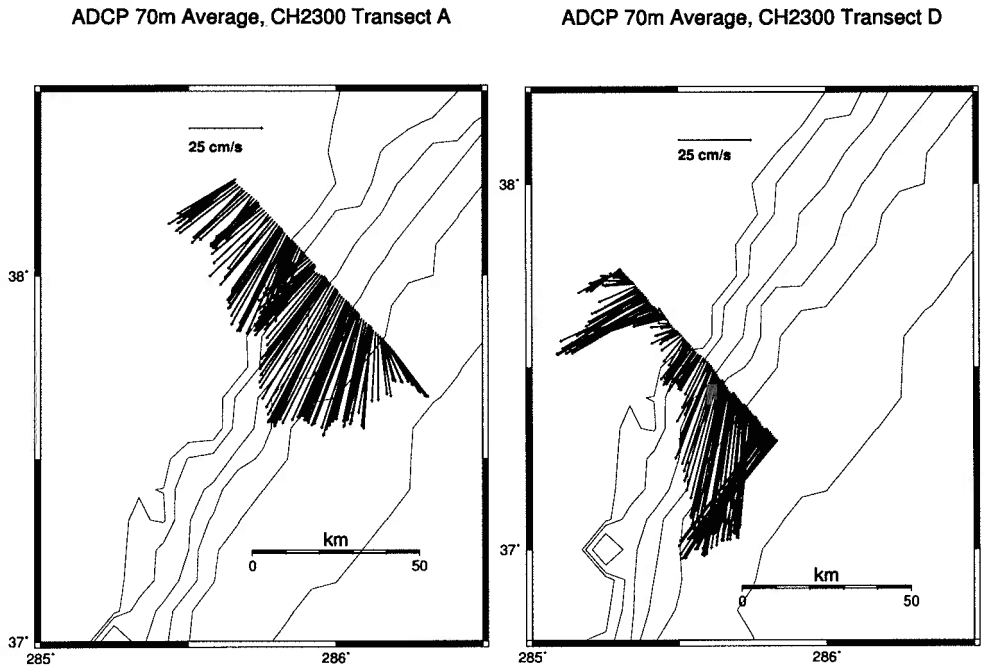

Figure 4.6: ADCP 70m average velocity for sections A and D.

Ekman balance, the distance of an onshore excursion of a surface mixed layer is given by

$$L_e = \int_{t_0}^{t_1} \frac{\tau_x}{\rho h f} dt \tag{4.1}$$

where h is the mixed layer thickness, τ_x is the cross-shelf wind stress, ρ is the layer density, and f is the Coriolis parameter. Figure 4.8 shows the onshore distance the surface mixed layer would travel if exposed to wind stress as observed at the nearest NDBC buoy; three different possible mixed layer depths are shown. By the midpoint of the cruise on 4 November a surface mixed layer 30 m deep, similar to that observed in the tongue of slopewater in section B, would have travelled onshore approximately 25 km, while the 50 m surface mixed layers on sections A, C, and D would have moved only about 15 km. In order for

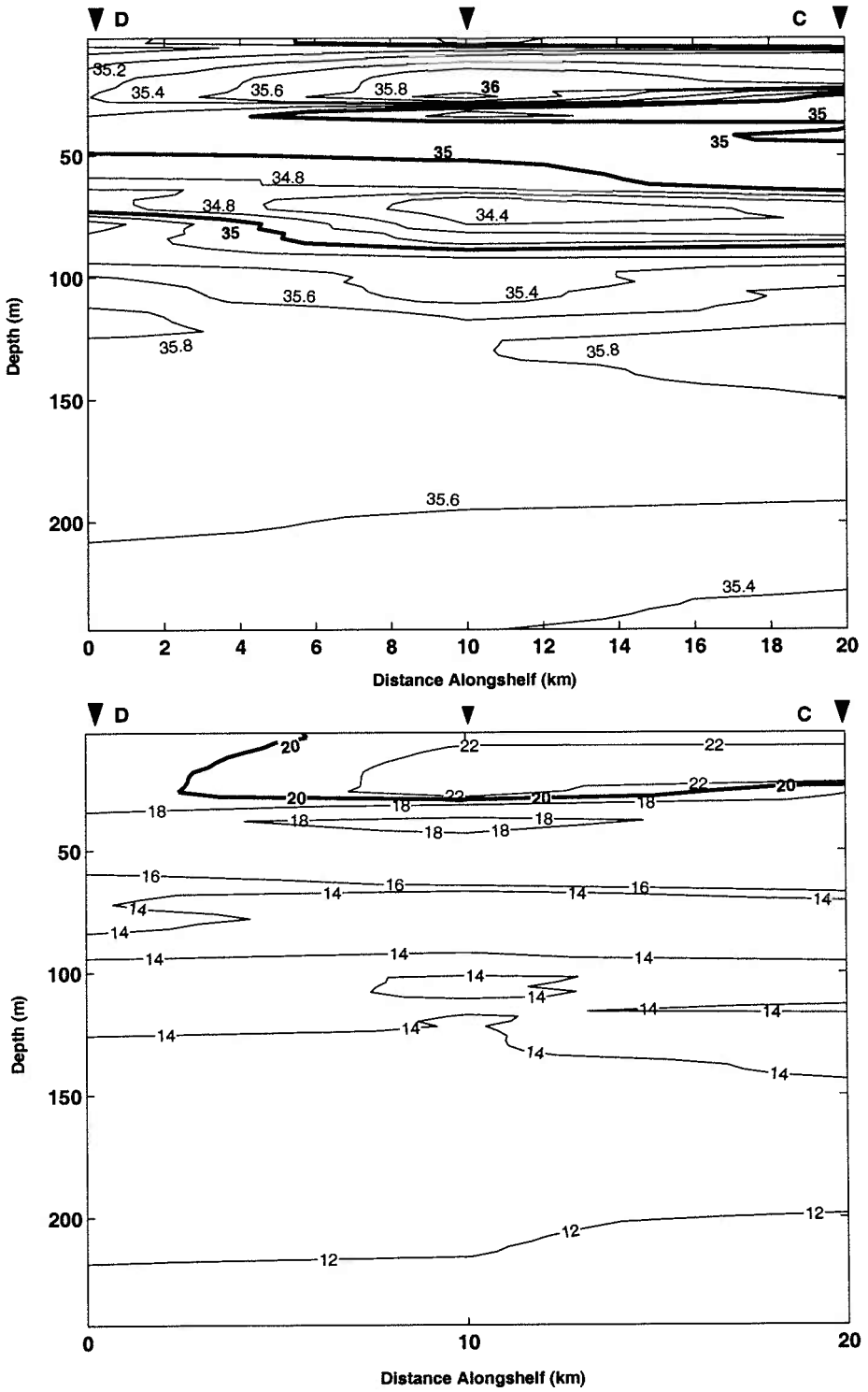

Figure 4.7: Vertical salinity (top) and temperature (bottom) contours for an alongshelf section between transects C and D. Orientation is looking shoreward, with transect D on the left.

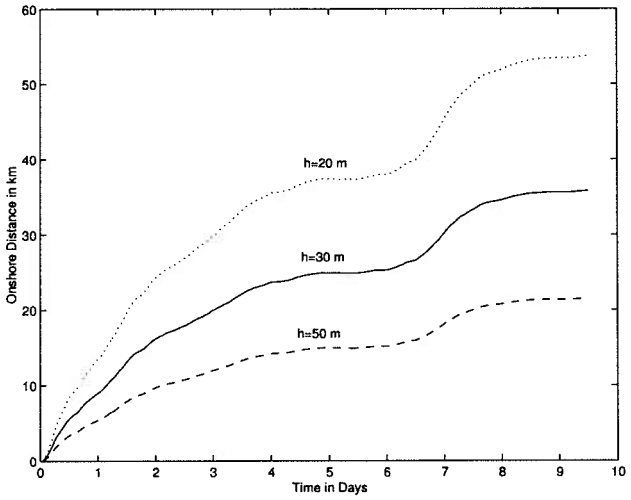

Figure 4.8: Onshore excursion of surface slope water over the front after local wind forcing for mixed layers of 20 m, 30 m, and 50 m. Days start at 30 October 00:00.

this relationship to hold, the near surface water over the slope must be less dense than the shelf water on the shoreward side of the shelfbreak front. A plume from the slope or Gulf Stream, for example, would be expected to flow over the less saline outer shelf providing its temperature were high enough. Given shelf conditions as observed in this survey of 15°C and 34.0 PSU, a slope water mass with salinity $\leq$ 35.0 would be less dense than shelf water if the slope water temperature is at least 3.5°C higher. Gulf Stream water with salinity of 36.0 PSU would require a 6.7°C temperature difference. AVHRR sea surface temperature imagery during this time period (Figure 4.9) shows Gulf Stream temperatures up to 27°C midstream and 20-24°C in streamers expelled from meander crests, more than enough to meet these conditions.

Sea surface temperature images during this time period suggest the influence of Gulf Stream water on the outer shelf. The clearest image for this time period is from 25 October (Figure 4.9) in which there are numerous meanders with expelled Gulf Stream water

extending toward the shelf as far as the outer stations of the survey transects. AVHRR images from 6 November and the 2-7 November composite show these structures continuing throughout the survey period. The major change in SST during this time was a signficant cooling of shelf water from 17-18°C to 14-15°C. The position of the wall of the stream is also anomalously far north. Between 71-73°W, the north wall of the Gulf Stream is approximately 0.25° north of its mean position for the year 2000, and the 2000 mean is itself 0.5° further north than the climatological average over the period 1973-1997 (the second largest northward excursion since 1966)(Drinkwater et al. 1994; Page et al. 2001). The 6 November image and the 2-7 November composite show the Gulf Stream moving slightly north during the two weeks after 25 October. Given the proximity and structure of the Gulf Stream in this region, it is likely that features such as the observed saline intrusion and overlying warm water mass are not isolated events and could have an important impact on shelfbreak processes on timescales of weeks to months. In particular, years in which there are significant northward excursions of the Gulf Stream could be crucial in affecting both the mean state of the shelfbreak front and exchange between the shelf and slope.

In addition to the shelfbreak front, a mid-shelf front is present in all four transects. The foot of this front is near the 50 m isobath, with surface outcrops 10-20 km further offshore, near the 75 m isobath. Seaward of the front is outer shelf water with salinity $\geq$ 34.0 PSU, and shoreward is shelf water with salinities $\leq$ 33.5 PSU. Ullman and Cornillon (1999) also observe mid-shelf fronts throughout the Mid-Atlantic Bight in winter AVHRR sea surface temperature imagery from 1985-1996. These fronts appear around early January, and have surface outcropping at the 50 m isobath. Prior to January a separate temperature front occurs in this region 40 km shoreward of the 50 m isobath and persists until early February;

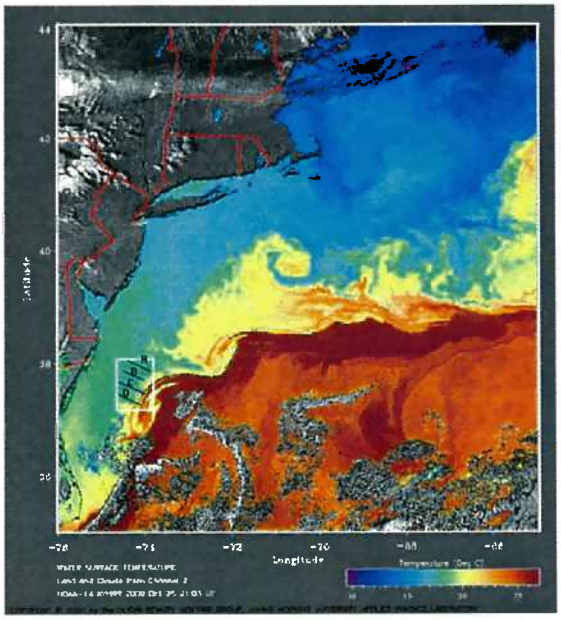

Figure 4.9: AVHRR sea surface temperature for Northern GS region, 25 October 2000. Study area and transect lines indicated for reference only; image is from 1 week previous to survey dates. (Johns Hopkins Applied Physics Laboratory, Ocean Sensing Group.)

the 50 m front appears to develop independently however, and no migration of frontal features is apparent. Unlike these mid-shelf surface temperature fronts, the fronts observed during this survey are slightly further offshore and do not have a corresponding temperature gradient, and thus would not be detectable in AVHRR imagery.

Throughout the survey area minimum temperatures occur near the bottom at the shelfbreak. There appears to be an isolated shelfbreak water mass which is 40-70 m deep and extends 15-20 km in the cross-shelf direction. Within the water mass, temperatures are 12-13°C and salinities are 33.8-34.2 PSU. Bottom temperatures are minimum for only 5-10 km at the outer edge of the shelfbreak, thus this shelfbreak water mass is nearly surrounded by warmer, saltier water. As the sections progress southward from A to D the temperature minimum progresses offshore. A similar 12-13°C temperature minimum occurs in the

September-November climatology, but with some important differences. The climatological minimum occurs well over the shelf, with minimum bottom temperatures extending 50 km over the outer shelf. Also, in the climatology this layer is only 20 m thick in the vertical. In the October-November climatology (not shown) the minimum has shrunk to about 20 km wide by 15 m thick. It appears from the climatological sections that these could be the final stage of the summer "cold pool" as described by Houghton, et al. (1982), as the volume of the cold pool water is diminishing as late fall mixing progresses over the shelf. Salinities in cold pool observations are 33.0-34.0 PSU. Although the temperature, late fall position, and upper limit of the salinity are similar to the shelfbreak water mass observed in the survey, the area covered by the surveyed patches is considerably greater and extends well into the overlying water column; they do not appear to be "shrinking" features. The summertime cold pool observed by Houghton and Marra (1983) exhibits a similar extension across the shelfbreak to the upper slope where it is detatched from the bottom over the outer 30 km of the shelf by a slope water intrusion. The cold pool protrusions are 8-9°C , 33.5-34.0 PSU, covering an area 30-40 m deep by 20-30 km wide and are attached to the main cold pool only tenuously if at all. It is possible that such protrusions become entirely sheared off from the shelf and become cold shelfwater parcels on the slope. The most unusual feature in the observed cold parcels in our survey is that they occur in regions of high alongshelf velocity (see geostrophic velocity sections in Figure 4.3) making it improbable that they are remnants of a local cold pool at all, and raising the question of whether they are instead advective features from much further upstream. The fluctuating shape and cross-shelf position of these cold parcels progressing through the study area also lends support to the conclusion that they do not originate from a local, previously static cold pool.

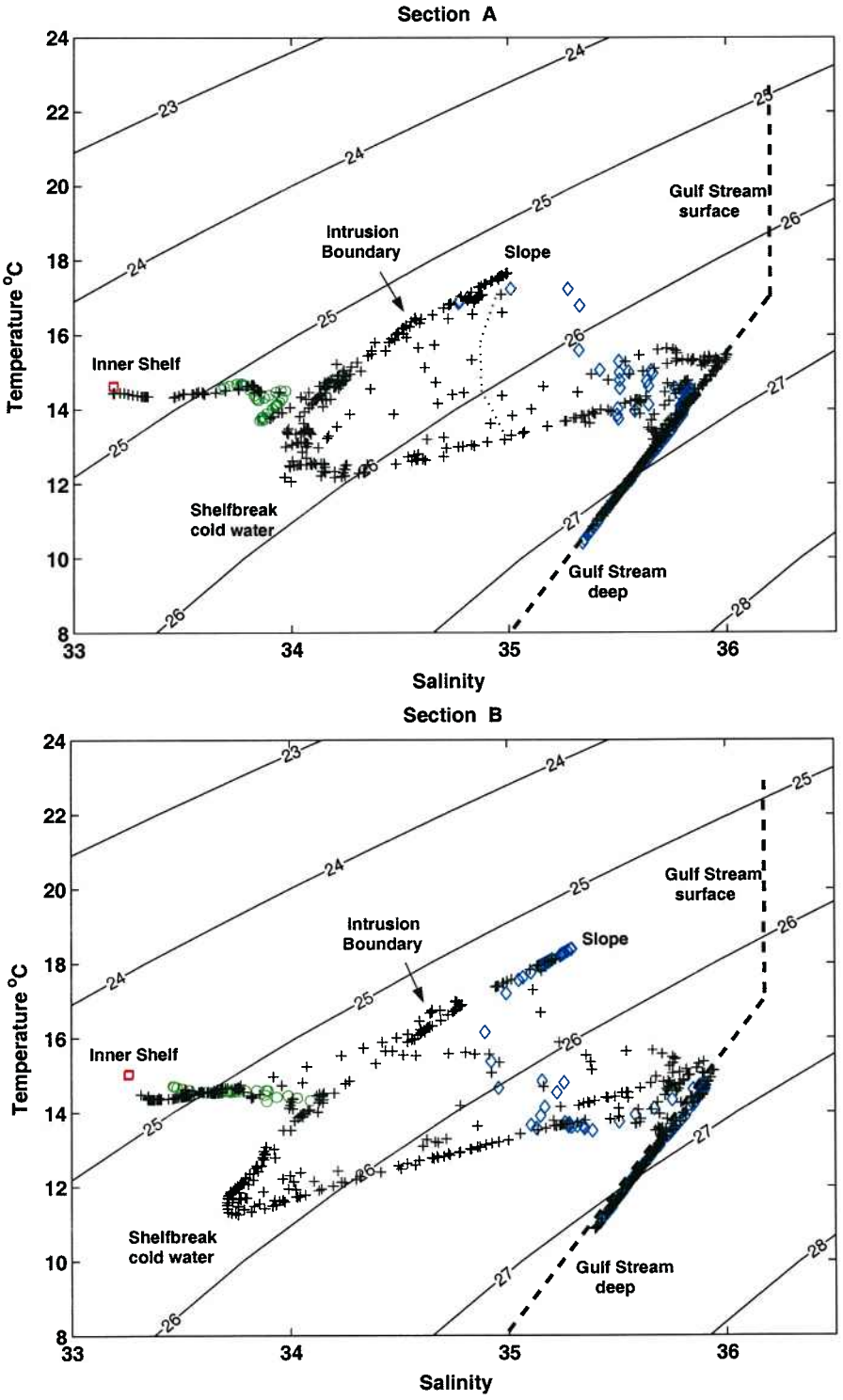

Figure 4.10: T-S Diagrams for Sections A, B, C and D. square=inshore station, diamond=offshore station, o=100m isobath

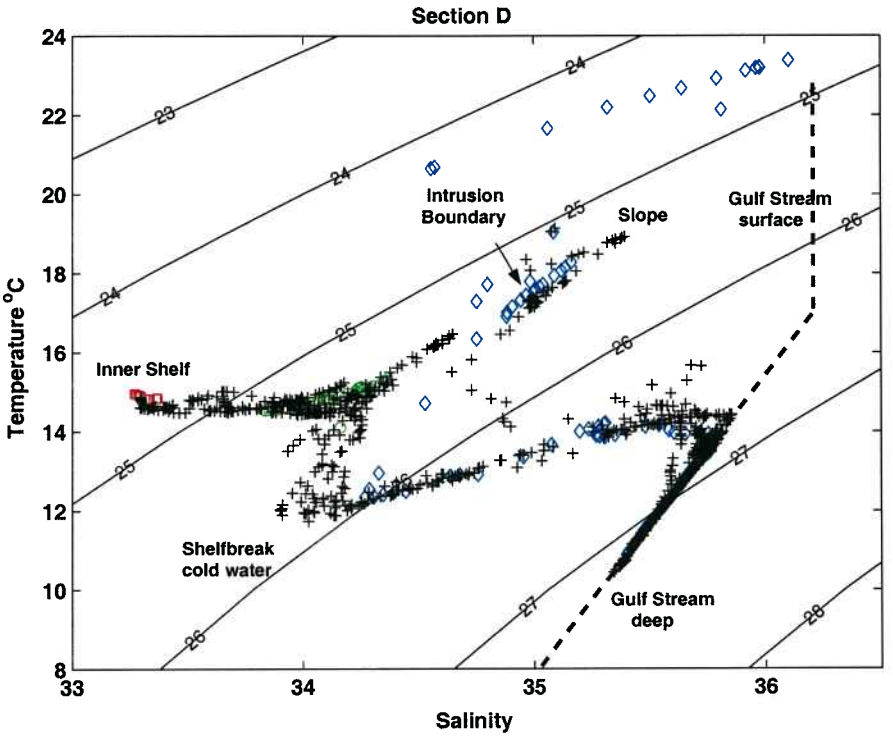
Section D
Temperature °C
Salinity
Intrusion Boundary
Slope
Gulf Stream surface
Inner Shelf
Shelfbreak cold water
Gulf Stream deep

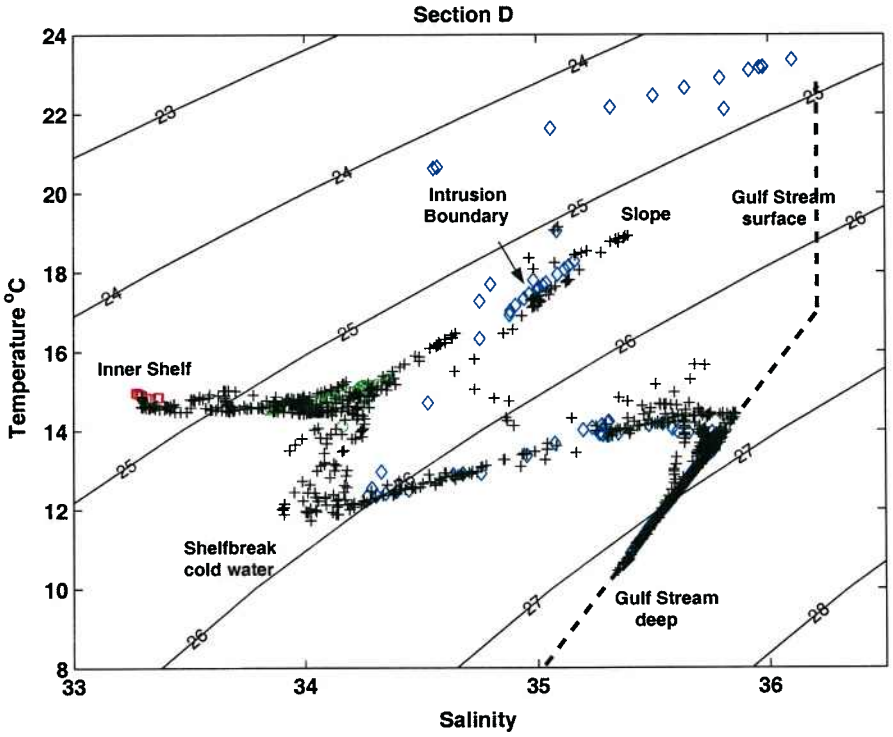
Section D
Temperature °C
Salinity
Intrusion Boundary
Slope
Gulf Stream surface
Inner Shelf
Shelfbreak cold water
Gulf Stream deep

The complex interrelationship of multiple water masses in this region can be seen most clearly in the temperature-salinity diagrams (Figure 4.10) The shape of the T-S relationship is quite different from the classic "inverted V" distribution of the Mid-Atlantic Bight, of which only a vestige is visible here (traced in the section A diagram by the faint dotted line). For comparison, typical Gulf Stream T-S properties are indicated by the dashed line. Shelf water is quite uniform in temperature all the way from the most shoreward stations (red squares) to the 100 m isobath (green circles), presumably having been recently mixed by fall wind events. Along-isopycnal mixing between the surface water of the shelf and upper slope is apparent (part of the classic "inverted V" signature) but with the sharp slopewater intrusion boundary evident in a clustering of points midway along the mixing line. The cold water mass at the shelfbreak forms the hook at the lower left. Above, it mixes across the frontal boundary in the upper water column where the temperature-salinity gradients are density compensating; below, it overlies mid-depth Gulf Stream water. The slope stations at the offshore ends of the transects (blue diamonds) cluster into two distinct water masses, warm slope water and underlying Gulf Stream water. The warm surface intrusion at the outer station of transects C and D is clearly evident as the isolated group in the upper left originating in warm Gulf Stream surface water with T>20, $\sigma_t < 24.5$.

4.4 Velocity Structure

Mean flow along the Mid-Atlantic Bight shelf is to the southwest and is primarily barotropic, with flow rates between 1-10 cm/s (Beardsley et al. 1983). However, density gradients normally present across the shelfbreak front result in a strong jet (Gawarkiewicz et al. 1996a) in the same direction as the mean flow. In the climatology (Linder and Gawarkiewicz 1998)

the highest jet velocity occurs in summer and fall in our study area, with an average maxiumum velocity of approximately 18 cm/s in October-November. Mean cross-shelf position of the jet at this time is 2.5 km offshore of the 100 m isobath, and mean jet width and depth are 25 km by 50 meters (Linder 1996). It should be noted that differences between the climatological and individual measurements are partly due to smoothing effects of climatological averaging, which Linder (1996) estimates can alter dynamical results by a factor of 2-3 (tending to decrease the magnitude of cross-shelf gradients and jet core velocity and increase jet width, for example). The averaged jet is not wide, but shelfbreak jets as narrow as 10 km have been observed in the southern half of the Mid-Atlantic Bight (Gawarkiewicz et al. 1996a), and the width of the jet core is rarely wider than that. So although features may appear to be moderately sized in climatological studies, actual observations underscore the need for high resolution surveys to fully account for the impact of the jet on alongshelf transport as well as other shelfbreak processes.

The effect of the strong horizontal density gradients at the shelfbreak in our survey can be seen in the magnitude of the resulting shelfbreak jet. Velocities measured by the shipboard ADCP are shown in Figure 4.6, averaged over the upper 70 m of the water column. A strong jet is present in all sections, flowing alongshelf until the southern transect (D) where there is a significant offshore component. Alongshelf flow was also computed using the thermal wind equation with zero bottom velocity. It was then adjusted for more realistic non-zero bottom velocities by subtracting out a bottom reference value, taken as the velocity at 250 m depth from ADCP measurements. For water depths < 250 m, the depth averaged ADCP velocity was used to reference the geostrophic velocity. The barotropic component of the flow was included by adding in the difference between the vertically integrated alongshelf component

of the ADCP velocity and the vertically integrated geostrophic velocity. Figure 4.3d shows geostrophic velocity for the four cross-shelf sections. The average barotropic adjustment from the ADCP velocity is 13 cm/s or approximately 20-25 % of the maximum jet velocity (Figure 4.3 e). The maximum velocity computed in the core of the shelfbreak jet is over 60 cm/s in transect A, and ranges from 50-60 cm/s on the other transects, consistent with that measured by ADCP. This velocity maximum is more than three times greater than that of the climatological jet. The jet is also observed to be quite deep (up to 100 m) with a cross-shelf width of 20-30 km. It is the high velocity region of the jet below 50 m in which we find the shelfbreak temperature minima; in transect A the velocity in the temperature minimum reaches 40-50 cm/s.

Despite the fact that the slope water intrusion in the surface mixed layer has moved the surface frontal position well inshore of its average position, the jet cores from the 4 sections are displaced 10-20 km offshore of the 100 m isobath. This is 7-17 km further offshore than the climatological mean. This can be explained by noting that the maximum density gradients are between 50-150 m depth, and as noted earlier the foot of the front in these sections is unusually far offshore. It is interesting to note that the surface mixed layer has little effect on creating the thermal wind shears driving the jet. This is consistent with findings from the climatology, in which the strongest density gradients are at the foot of the front and appear to dominate the jet velocity and position (Linder and Gawarkiewicz 1998). One exception occurs in transect B. A related scenario can be found in the hydrographic survey further south in the Mid-Atlantic Bight where Gawarkiewicz et al. (1996a) note that a pycnocline salinity intrusion split the shelfbreak jet into two by creating two distinct horizontal density gradients, one above and one below the pycnocline. A similar process

appears to be at work in transect B where horizontal density gradients are present both below the surface mixed layer, and within the surface mixed layer, and create two velocity maxima. The resulting jet is double-lobed, with one velocity maximum at the surface above the 100 m isobath and one 20 km past the 100 m isobath at 75 m depth.

Throughout the survey area significant flows also occur at the mid-shelf front with velocities of 30-40 cm/s. Note that the mid-shelf front is almost entirely a salinity front, and may be present for more of the year than the thermal fronts observed by Ullman and Cornillon (1999; 2001). These fronts would not be detectable by thermal imagery, but are in fact responsible for flow rates equal to a moderately strong shelfbreak jet.

Strong horizontal shears are present in the cross-shelf sections (Figure 4.11a). Alongshelf velocity and Rossby number are shown for the surface mixed layer at 32 m. Near-surface waters show pronounced double peaks in relative vorticity (Figure 4.11b) corresponding to the multiple velocity maxima. Rossby numbers (normalized by f) are nearly -0.6f, indicating a strongly nonlinear flow regime. The largest anticyclonic shear occurs on the shoreward side of the double-lobed shelfbreak jet in transect B (-0.58f) while the largest cyclonic shear occurs on its offshore side (0.40f) . In the northern Mid-Atlantic Bight where mean climatological jet velocities are about double that of the southern region, mean relative vorticity in August-September is -0.22f (shoreward side of jet) to 0.16f (offshore side of jet) (Linder and Gawarkiewicz 1998). High Rossby numbers such as this, combined with observed jet velocities of 60 cm/s, are consistent with observations of the shelfbreak frontal structure which showed considerable variability between sections 20 km apart. Models constructed by Lozier et al. (Lozier et al. 2002) demonstrated that horizontal shear was an important energy source for the growth of frontal instabilities, and growth rate of instabilities

in a shelfbreak front was most dependent on jet velocity and Rossby number. The highest growth rates occured as the jet velocity was increased from 30 to 60 cm/s and the Rossby number was increased from 0.37 to 0.96 (Rossby number a function of jet narrowness in the model). The high observed velocity of the jet in these sections, combined with its relatively narrow width, creates conditions of large horizontal shear which are likely related to the observed variability in the structure of the front.

4.5 Volume and Mass Transport

Volume and mass transport are controlled not only by the high jet velocity in the study area, but also by the vertical extent of the jet which is large than previous observations. The total alongshelf transport is given in Table 4.1. The volume transport is calculated in a variety of ways: for the shelfbreak jet, for the barotropic component of the jet alone, for the mid-shelf jet when present, and for the entire shelf section that was sampled. The vertical boundary of the jet is defined by the depth of the central isopycnal at the foot of the density front; this ranges from 120-134 m. Horizontal boundaries are defined by the distance at which velocity drops below 20 cm/s, or by the local velocity minimum in cases where the shelfbreak and mid-shelf jets overlap. Along with each "whole section" estimate is the actual shelf width used in the calculation which varies depending on the cross-shelf data set(s) used.

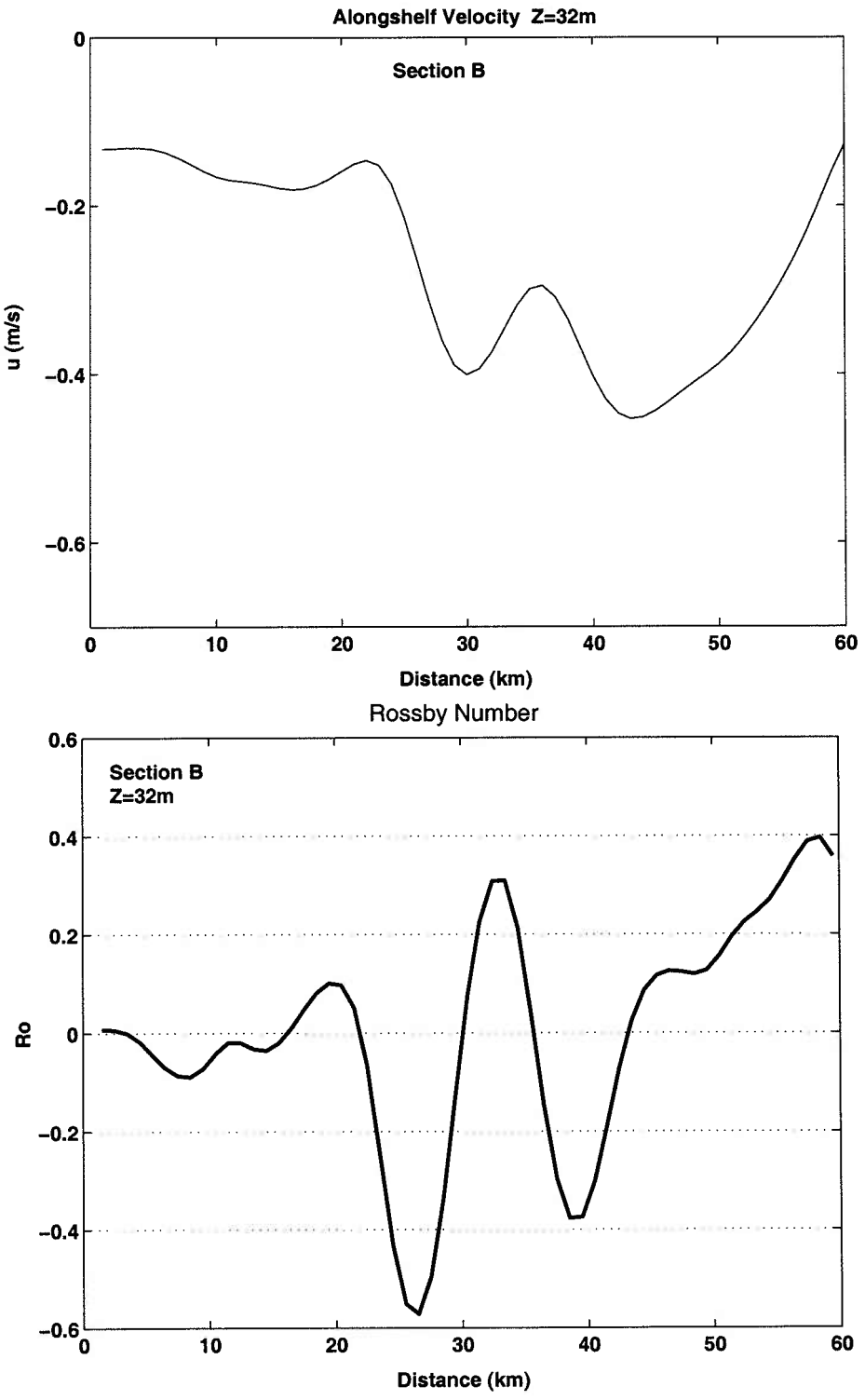

Figure 4.11: A) Alongshelf velocity and B) Rossby number (Relative vorticity $\times f$) for sections B and C, computed at 32m depth.

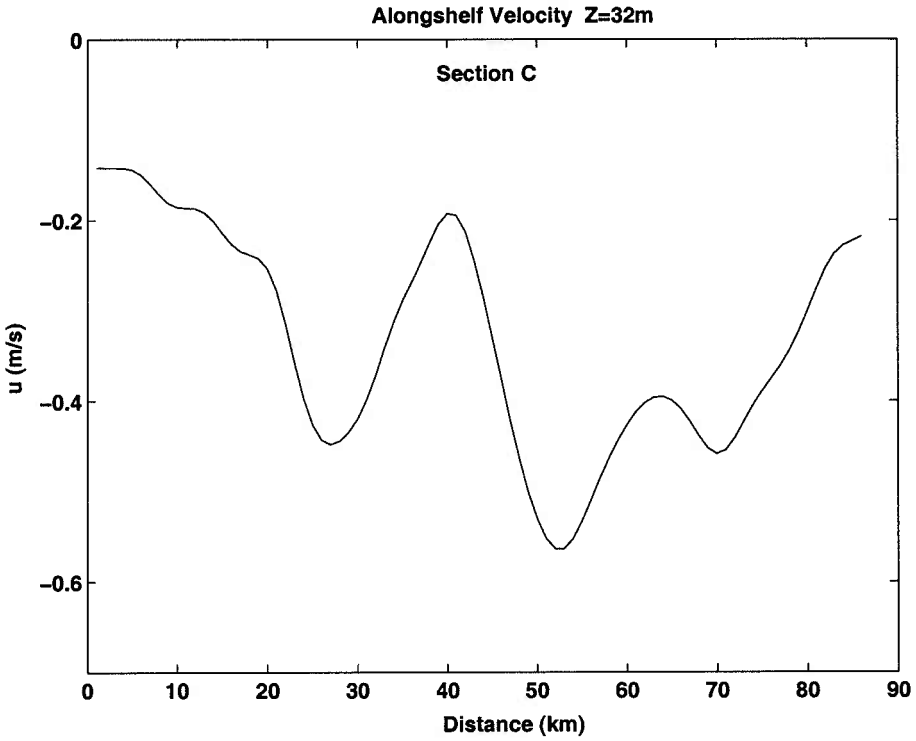
Alongshelf Velocity Z=32m
Section C
u (m/s)
0
-0.2
-0.4
-0.6
0
10
20
30
40
50
60
70
80
90
Distance (km)

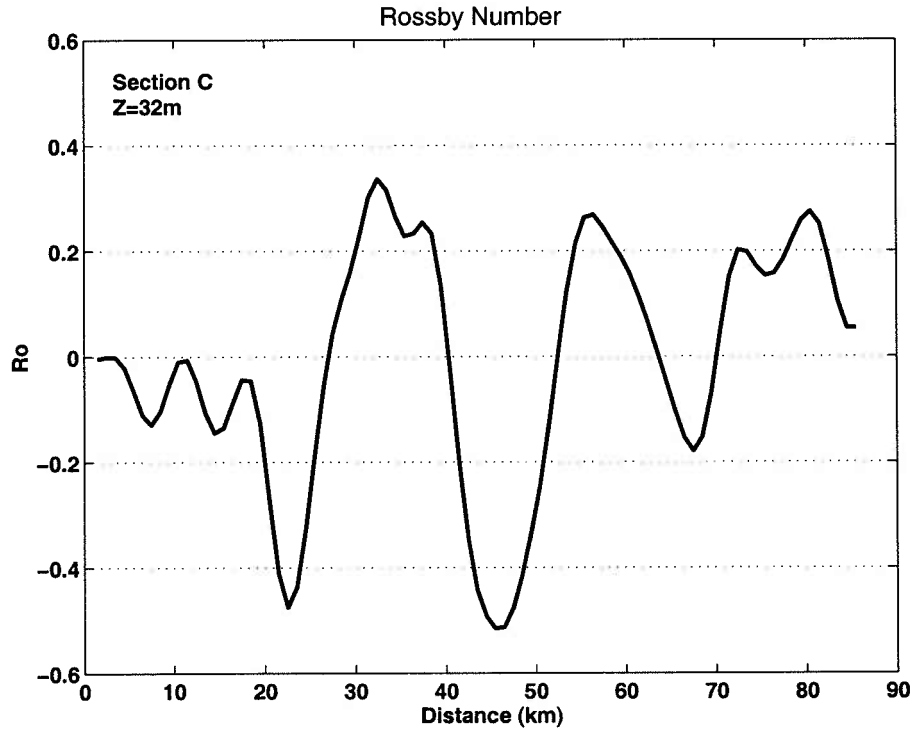
Rossby Number
Section C
Z=32m
Ro
0.6
0.4
0.2
0
-0.2
-0.4
-0.6
0
10
20
30
40
50
60
70
80
90
Distance (km)

Section	Baroclinic Jet	Barotropic Jet	Jet Width	Mid-shelf Jet	Whole Section	Section Width
A	1.17 Sv	0.22 Sv	25 km	–	1.51 Sv	70 km[1]
B	0.69 Sv	0.15 Sv	20 km	–	1.02 Sv	60 km
C	1.27 Sv	0.31 Sv	30 km	0.39 Sv	1.81 Sv	80 km
D	0.94 Sv	0.46 Sv	20 km	0.14 Sv	1.53 Sv	70 km
Mean	1.02 Sv	0.29 Sv	24 km			
Voorhis et al. '76[2]					1 Sv	
Beardsley et al. '85 [3] (M)					0.38 Sv	70 km
Ramp et al '88[3] (M)					0.22 ±0.4 Sv	120 km
Burrage & Garvine '88					1.0 Sv	
Biscaye et al '94 (M)					0.19 Sv	
Schlitz et al. '01 (M)					0.83 ±0.2 Sv	70 km
Gawarkiewicz et al. '96	0.38 Sv		20 km			
Linder & Gawarkiewicz '98	0.16 Sv		30 km			

Table 4.1. Volume transport comparison for Mid-Atlantic Bight Shelf/Slope. [1]Transport is to depth of 100m or bottom. [2]Voorhis et al. transport is calculated from geostrophic velocity between 100m-1000m isobaths (0.7 Sv), plus Beardsley (1976) inner shelf transport. [3]Beardsley et al. and Ramp et al. calculations are from same NSFE data set; the former extends only to the shelfbreak, while the latter includes the upper slope and effects of warm core rings reversing normal flow.) (M) indicates estimates based on moored current meter observations; the remainder are based on geostrophic velocity from hydrographic sections.

For comparison, estimates of volume transport from other studies of the Mid-Atlantic Bight are shown (Burrage and Garvine 1988; Biscaye et al. 1994a; Beardsley et al. 1985; Ramp et al. 1988; Linder and Gawarkiewicz 1998; Gawarkiewicz et al. 1996a). The 0.7-1.3 Sv transport within the shelfbreak jet in these sections is comparable or far exceeds other estimates for whole shelf transport. Transport within the shelfbreak jet accounts for 61-77% of the total transport over each section. Volume transport within the mid-shelf jet is lower,

but comparable to previous estimates of transport over the entire shelf.

The large differences in transport between the sections we observed are largely due to methods of defining the boundaries. Some effect might also result from meandering of the jet in the the along-shelf direction. To make the sections more comparable, Table 4.2 presents transport for similar shelf widths, integrated to a full depth of 250 m (or bottom where the water column depth is less than 250 m). The total transport in each section over the same width differs no more than 4-12% from the mean.

Section	80 km	70 km	60 km
A	–	1.88 Sv	1.46 Sv
B	–	–	1.20 Sv
C	2.61 Sv	2.00 Sv	1.46 Sv
D	–	1.92 Sv	1.30 Sv
Mean			1.36 Sv

Table 4.2. Volume transport for shelf sections of similar length, to full depth of 250 m or bottom. Larger lengths extend further inshore.

Heat and mass transport within the jet are also high, as shown in Table 4.3. Heat and salt transport are calculated as transport through a 2-D section with width spanning the shelfbreak jet and a depth of 100 m. Reference temperature and salinity was set at 12°C and 34.0 PSU.

Section	Heat ($\times 10^{13}$ W)	Salt ($\times 10^{5}$ kg/s)	Jet width (km)
A	1.29	5.30	25
B	0.73	1.80	20
C	1.45	5.02	30
D	1.45	4.41	20
Mean	1.23	4.13	24

Table 4.3: Heat and Salt transport within the shelfbreak jet.

Estimates using 3-dimensional sections are considered more reliable, however the CTD resolution in the alongshelf direction is not sufficient in these sections for that method to be of use. Mass transport across the entire shelf-slope sections are shown in Table 4.4 for depths to 100m. For comparison with the Nantucket Shoals Flux Experiment (Ramp et al. 1988), figures are also included for calculations relative to 0°C and 0 PSU. Cross-shelf widths are shown for each case.

Section	Heat	($\times 10^{13}$ W)	Salt	($\times 10^{5}$ kg/s)	Shelf
	12°C ref.	0°C ref.	34.0 ref.	0.0 PSU ref.	width
A	2.02	9.46	5.48	534	70 km
B	1.23	6.24	5.13	358	60 km
C	2.43	11.38	6.73	636	80 km
D	1.29	6.70	2.14	382	70 km
NSFE		1.32		128	120 km

Table 4.4. Heat and Salt transport across whole shelf sections. All sections begin near the 40 m isobath; the NSFE section extends only to the shelfbreak while the southern sections A-D, on a narrower shelf, extend onto the upper slope.

As with volume transport, alongshelf heat and salt transport are dominated by flow within the shelfbreak jet. Thus, flux estimates from shelf sections that resolve the strong shelfbreak jet are considerably higher than those based on more widely spaced moorings or sampling stations.

4.6 Summary and Discussion

During a short survey in the late fall of 2000 in the southern Mid-Atlantic Bight shelfbreak region, we observed hydrographic features that may be important in the seasonal transition between fall and winter conditions. Gulf Stream and slope water interaction with the front

strongly influenced the thermohaline and velocity structure at the shelfbreak. High volume transport was also observed which appears to be closely tied to the thermohaline structure.

High resolution sampling during the survey was crucial in identifying the complex structure of water masses in this region, as well as for resolving hydrographic gradients that were responsible for a complex velocity structure with multiple jets. Many of these features were small-scale (5−10 km) and/or subsurface. Mid-shelf gradients could have been missed or underestimated by coarser sampling, resulting in erroneous transport etimates. Resolving strong subsurface lateral gradients, as deep as 120-140 m and as narrow as 5 km, was also critical in calculating the baroclinic flow and for accurately estimating volume, heat and mass transport. These observations are relevant not only to understanding the local circulation, but also in understanding shelf circulation and transport along the length of the Mid-Atlantic Bight.

4.6.1 Fall Transition Features

A cold shelfbreak water mass was observed in the area at the foot of the front with characteristics different from the "cold pool" found under the pycnocline on the New England shelf. The summertime cold pool has been understood to result from isolation of the winter mixed layer after summer stratification sets in. The features are assumed to dissipate with the onset of fall and winter wind-driven mixing. Houghton et al. (1982) found a positive association between duration of cold pool isolation in a region and the magnitude of the cross-sectional shelf area. They attribute this to the wide shelf area effectively insulating the cold pool on both sides, thereby minimizing the impact of heat transfer from the adjacent shallow shelf on one side and warm slope water on the other. Compared to the

cross-sectional area of the rest of the Mid-Atlantic Bight, this survey area is in the lowest 25% of the range, with only the shelf to the south towards Cape Hatteras smaller; therefore one would not expect the local cold pool to persist into the fall. Houghton et al. also saw a southward migration of minimum bottom temperature on the shelf from the New York Bight towards Delaware Bay over the course of May-October, with a minimum bottom temperature of 9-10°C reaching the northern part of our study area by the end of October. Given the observed migration of cold pool water from the north, as well as the possibility of cold pool parcels becoming detached and transported into the upper slope (Houghton and Marra 1983), it seems reasonable to speculate that the shelfbreak temperature minima in our sections, with velocities of 30-50 cm/s, could be cold pool water originally from the northern MAB that has been entrained into the shelfbreak jet further south. Travelling at this rate from the New York Bight, total transit time would be 6-10 days. One interesting result of having cold water masses located directly over the foot of the salinity front is that the uniform temperature enables a strong density gradient to be present in the lower half of the water column; it is this density gradient that is primarily responsible for the strong baroclinic jet observed during the survey.

It is possible that the mid-shelf salinity fronts seen in this area are also a late fall seasonal feature. The fronts are within 10-20 km of the surface temperature fronts observed by Ullman and Cornillon (1999) that develop two months later, and may result from freshwater input from nearby bays. Since freshwater input would persist into winter, while the inner shelf cools, eventually the salinity fronts would develop a temperature gradient as well. It would be interesting to see the evolution of both surface temperature and salinity fronts simultaneously to determine if their development is related, or whether the salinity front

remains isolated enough to maintain the density gradient associated with it. The density gradients associated with late fall mid-shelf salinity fronts are responsible for transport rates rivaling previous estimates of the entire shelf. If mid-shelf density fronts persist for long periods of time, their transport would be a significant contribution to annual shelf totals.

4.6.2 Gulf Stream and Slope Influence on Thermohaline and Velocity Structures

A high velocity baroclinic jet with maximum flow rates of up to 60 cm/s was observed at the shelfbreak. Data for climatological averaging in this region and season are scarce, so comparisons to mean shelfbreak jet velocity can be tenuous; additionally, smoothing effects can make means of dynamical features difficult to interpret. Among the factors that could influence seasonal or interannual changes in jet position and velocity is remote forcing from the Gulf Stream, particularly in the southern Mid-Atlantic Bight where the Gulf Stream is proximate enough to have local as well as remote influence. Bane et al. (1988) analysed the potential effect of Gulf Stream position relative to the shelf on shelfbreak current velocity. Average Gulf Stream position during 2000 was at its second most northerly position since 1966, and the location at the time of the survey was 50% further north from its long-term mean than the annual average. Measuring from Bane et al.'s Station B reference, approximately 100 km upstream from our transect A, the north wall of the Gulf Stream was 100 km away during the survey period. Currents at Station B were observed to be at their maximum velocity (30-40 cm/s) when the Gulf Stream position was within 150 km, which would put our observations at the extreme of GS proximity and current velocity.

In their study of mean shelfbreak jet dynamics, Fratantoni et al. (2001) note that the

Bane relationship does not hold further north in the Nantucket Shoals region. However, the Gulf Stream is approximately twice as far from the shelf there, compared to the southern Mid-Atlantic Bight. Further south, Savidge and Bane (2001) found no correlation between Gulf Stream offshore position and current velocity, but they did see a strong correlation between Gulf Stream position and alongshelf velocity convegence, suggesting some relationship between Gulf Stream forcing and cross-shelf transport.

Locally, AVHRR images from this time period show Gulf Stream meanders close to the shelf, with water ejected from meander crests reaching the study area. A high salinity and very warm water mass closely related to Gulf Stream surface water was observed in a thin layer overlying the slopewater intrusion in the southern part of the survey. The local surface salinity intrusions did not create density fronts that affected shelfbreak jet velocity, however, which is consistent with findings by Churchill and Cornillon (1991) but the proximity of the main wall of the Gulf Stream must be considered a factor in jet stregth.

Gulf Stream water such as that observed in the thin surface layers does have potential significance for shelf-slope exchange, since the T-S properties would allow it to flow over outer shelf water. Radiochemical properties that were also measured during this survey tie this water mass closely to water from the north wall of the Gulf Stream at Cape Hatteras; similar signatures have been seen as far north as Nantucket Shoals and bring to light a potentially new pathway for exchange within the shelf-slope gyre.

4.6.3 Relationship between transport and thermohaline structure

The transport rates calculated for the survey area are high, particularly for the southern Mid-Atlantic Bight where a portion of shelf flow is thought to be already detrained onto

the slope. In particular, shelf transport rates are significantly higher than those calculated from lower resolution data sets that do not adequately resolve the shelfbreak jet. Transport within the jet in this survey accounts for 61-77% of the total alongshelf transport.

To test the validity of these transport numbers, one can look at the relationship between transport and the bottom depth of the front. Yankovsky and Chapman (1997) developed a theory for buoyant coastal discharges which includes a length scale for the bottom depth of the plume attachment, h_b, in which the depth of the foot of the front is proportional to the transport and the density difference across the front:

$$h_b = (2Lv_i h_0 f/g')^{1/2} \tag{4.2}$$

where $Lv_i h_0$ is the transport within the plume, f is the Coriolis parameter, and $g' = g\Delta\rho/\rho_0$. We use this to predict the bottom depth of the front, given the jet transport and density difference, $\Delta\rho$. Table 4.5 shows that this relationship holds very well, particularly for the mean conditions seen during the survey.

Section	T_{jet} [Sv]	$\Delta\rho$	h_b [m]	z (actual) [m]
A	1.17	1.2	136	134
B	0.69	1.2	104	126
C	1.27	1.2	131	120
D	0.94	1.4	122	120
Mean	1.02	1.25	124	125

Table 4.5. Relationship between jet transport, T_{jet}, cross-frontal density difference, and depth of the bottom intersection of the front. The bottom depth predicted by the Yankovsky & Chapman relation, h_b, is given as well as the actual depth of the foot of the front.

Mean jet transport over the four sections was 1.02 Sv, with a mean density difference

across the front of 1.2. This gives a predicted depth to the foot of the front of 130 meters, compared to an observed mean depth of 125 meters. This is one of the first observational verifications of the relationship between frontal position and jet transport. It should be noted that because the position of the foot of the front can be defined in a number of different ways and the choice of bounds for the density difference across the front is open to interpretation, these results are not precise. The observed depth of the foot of the front is accurate to within approximately $\pm$ 10 m. The front over which the density difference is calculated could be defined more narrowly or broadly, resulting in $\Delta\rho$ ranging from approximately 0.8-1.4. Over these ranges the mean h_b is 122-160 m, with larger $\Delta\rho$ corresponding to smaller values of h_b. The actual mean depth of the foot of the front, with uncertainty, is approximately 115-135 m.

Figure 4.12 shows the general relationship between density difference across the shelf-break front and jet transport. This relationship also works well for the climatology of the nearby New Jersey shelf, with mean transport of 0.16 Sv and a density difference of 0.5 (based on a very limited number of data sets). The mean depth to the foot of the front is 75 meters, compared to 82 meters predicted by the Yankovsky and Chapman theory.

The thermohaline structure at the front is theoretically consistent with the large volume transport measured during the survey. It is unclear whether hydrographic conditions during this survey are representative of this time period, or if they are anomalous. However, a number of other studies in the Mid-Atlantic Bight have seen slope water intrusions during the fall. During the Nantucket Shoals Flux Experiment (Beardsley et al. 1985) water over the mid-shelf in November and December had higher than normal salinity and was the warmest of the time series. The climatology for the northern Mid-Atlantic Bight also shows

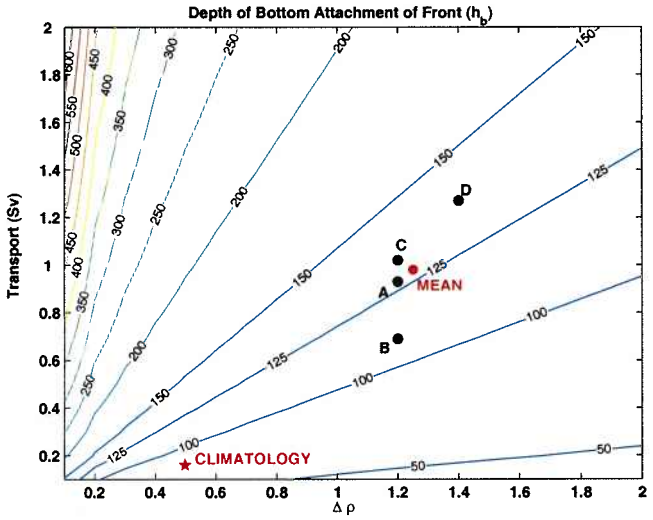

Figure 4.12: Contours of shelfbreak front bottom attachment depth, as predicted by the Yankovsky & Chapman model (1997). Points are plotted for each of the 4 sections surveyed, plus their mean, as well as for the climatology (Linder & Gawarkiewicz 1998). Actual bottom attachment depths are given in Table 4.5.

that the salinity front is at its most shorward position during October-November, however the foot of the front is also at its most shoreward and shallowest position.

Earlier studies have also seen transport on the order of 1 Sv in the Mid-Atlantic Bight (Voorhis et al. 1976; Burrage and Garvine 1988; Schlitz et al. 2001), while others are in the range of 0.2-0.4 Sv (Beardsley et al. 1985; Ramp et al. 1988; Biscaye et al. 1994a). It is interesting to note that most of the former, including this study, are based on geostrophic velocity calculated from hydrographic sections, while the latter are all based on moored current observations. While moored time-series observations might appear more reliable in some respects, in that they can give us more than a short-term snapshot, they are more subject to transport errors from resolution problems. If moorings are not spaced closely

enough to resolve the jet (which is itself often meandering) much of the high current activity will be missed. For example, the Biscaye et al. transport is based on current measurements from three SEEP II moorings spaced at 25-30 km intervals between the 60 m and 130 m isobaths. The more spatially resolved NSFE transport estimate is based on current measurements from 5 moorings with approximately 20 km spacing between the 25 m and 200 m isobaths, and one with surface currents only at the 1000 m isobath. With mean jet widths of 21 km (Linder and Gawarkiewicz 1998) and jet cores of $\leq$ 10 km, a major portion of the transport may not be resolved by current meters at 20-30 km intervals. The moorings in the Schlitz et al. (2001) study were placed at the 60, 100, and 320 m isobaths and had cross-shelf spacing of 40 and 20 km. However, the velocity data clearly shows the presence of the shelfbreak jet at the 100 m mooring, with velocities of up to 50 cm/s, and a mean surface velocity of 27 cm/s.

If higher transport estimates for the Mid-Atlantic Bight are accurate, this would significantly affect transport budget for the northeastern North American coast. Current estimates (Loder et al. 1998) for large scale coastal transport are based on regional transport estimates for seven zones from the Labrador Shelf to Cape Hatteras. Differences between upstream and downstream zones are balanced by cross-shelf export (a "leaky current" model). The NSFE transport estimate (0.38 Sv) is used in this budget for the Mid-Atlantic Bight zone. Substituting one of the higher estimates for MAB transport, 1-2 Sv, significantly alters the balance between alongshore transport and cross-shelf export. It also calls into question the upstream transport estimate of 0.6 Sv for the Halifax section. Loder et al. note that the low implied salinity for export between Halifax and Nantucket shoals "probably reflects an inadequte estimate of along-shelf transport," and that an additional 0.5

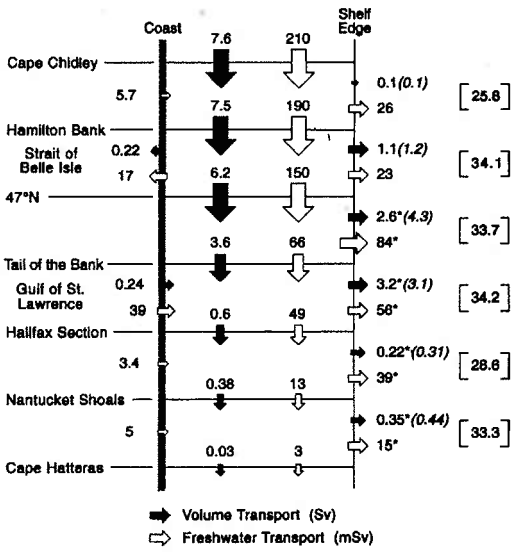

Figure 4.13: Box model for transport in the coastal ocean of northeastern North America. Inferred cross-shelf transport is given on the right boundary, with transport rates in parentheses (in m^2/s) and corresponding inferred salinity of exported shelfwater in brackets. (From Loder et al., 1998).

Sv across the Halifax section into the Mid-Atlantic Bight would make the implied export salinity more reasonable (32.9). This would bring the net transport into the MAB to over 1 Sv, and requires either greater transport inputs from upstream sources, or lower cross-shelf export (a less leaky current).

Little concrete evidence exists for the inferred cross-shelf export of large quantities of shelf water. In light of the lack of data suggesting direct cross-shelf transport, and with increasing evidence of high alongshelf transport, it is possible that a model such as Csanady and Hamilton's slope-sea gyre (1988), with limited direct cross-shelf exchange, may be more applicable. In this model dominant circulation is southwestward along coastal isobaths, and northeastward along the Gulf Stream, with MAB shelf water entering Gulf Stream circulation near Cape Hatteras, and Gulf Stream water re-entering the slope in the

northern Mid-Atlantic Bight, primarily through the effects of warm-core rings and streamers ejected from Gulf Stream meanders. Radiochemical tracer evidence (see Chapter 5) so far shows no signs of cross-shelf export of surface shelf water on timescales of weeks to months, but does support the Gulf Stream recirculation pathway, as do several drifter studies (Hare et al. 2002; Dragos et al. 1998). This area of inquiry, identified in the Loder et al. review as being one of the "key research issues" in the region, still has many unanswered questions.

Chapter 5

Boundary Current Influence on Shelf-Slope Exchange in the Mid-Atlantic Bight: Radiochemical and Hydrographic Evidence

The physical flow regime in the Mid-Atlantic Bight has important implications for the exchange of material between the coastal shelf and open ocean. The processes affected include the transfer of nutrients between deep nutrient-rich waters from the slope and the continental shelf; the transport of anthropogenic materials from urban coastal areas into the shelf sea and Atlantic ocean; and the movement of larval stages of fish, many of which are commercially important, between spawning grounds and feeding grounds (Biscaye et al. 1994a; Houghton et al. 1994; Loder et al. 1998; Dragos et al. 1998; Hare et al. 2002). An open question in this area is how much exchange occurs across the shelfbreak, particularly how much the shelfbreak front is a barrier to exchange because of its strong horizontal stratification and the resulting strong alongshelf flow in the shelfbreak jet. Other questions include what pathways may be important for shelf-ocean exchange.

Studies frequently focus on direct exchange between shelf water and adjacent slope water, through processes such as large scale eddy diffusion; flow of surface shelf water onto the slope through interaction with warm core rings; lateral shearing of cold bottom

water parcels from the shelf; and transport of the shelf bottom boundary layer which may detach and flow up the pycnocline of the shelfbreak front (Joyce et al. 1992; Pickart 2000; Houghton and Marra 1983; Moore 2000a). Compensating flow of slope water onto the shelf is assumed in large-scale mass balance estimations (Nixon et al. 1996), however the processes responsible for a return flow are not well understood. Observations have been made of mid-depth saline intrusions into shelf water, either through interaction with warm core rings or through penetration along isopycnals in the summer pycnocline (Gawarkiewicz et al. 1996b; Gordon and Aikman 1981) but the extent of these processes is not known.

Results from this study suggest that Gulf Stream activity such as warm core rings and large meanders may play an important role both in facilitating movement of open ocean water onto the slope, and in transporting coastal material from the Cape Hatteras shelf onto the northern slope. The physical features found most commonly during this study were strong shelfbreak currents, small scale hydrographic and velocity structures, and frequent influence of Gulf Stream water masses. After a brief description of the field and laboratory methods used in the study, this chapter will present the hydrographic and radiochemical results from the central and northern Mid-Atlantic Bight, radiochemical data from the Gulf Stream near Cape Hatteras, and end with an analysis and discussion of different potential pathways for physical and biogeochemical transport in the Mid-Atlantic Bight.

5.1 Methods

The data for the study were collected during five separate cruises in the Mid-Atlantic Bight (Figure 5.1). Three of these were in the north at the shelfbreak near Nantucket Shoals (which will be referred to as NS1, NS2 and NS3). One was a shelfbreak survey in the

south-central MAB approximately 300 km north of Cape Hatteras, off the Delaware coast, covering 4 cross-shelf transects (DE-A to DE-D). The final survey sampled the west wall of the Gulf Stream 20 km north of Cape Hatteras (CH1). Measurements were made for the four radium isotopes, salinity, and current velocity on all transects, and temperature and hydrographic data were collected when possible.

5.1.1 Field Sampling

The Nantucket Shoals transect overlaps the TOPEX satellite sub-line used by Fratantoni et al. (2001), and also includes stations from the PRIMER and Coastal Mixing and Optics (CMO) experiments. The three cruises were in fall, early winter, and spring. NS1 data were collected on the *R/V Oceanus* cruise OC349. Radioisotope and salinity samples were collected on 21 September 1999 at 7 stations along a 140 km transect across the shelf and upper slope, starting at the 75 m isobath. Distance from shore spanned approximately 120–260 km. A second crossing was made on the return trip on 7 October 1999, sampling only the inner 4 stations from the first crossing. Stations were spaced at approximately equal 20 km intervals. Shipboard acoustic doppler current profiling (ADCP) data were collected along the transects in both directions from the 60 m isobath to 50 km offshore of the 1500 m isobath. NS2 data were collected along the same transect on the *R/V Endeavor* cruise EN335. Radioisotope, nutrient, and salinity samples were collected on 1 April 2000 at 15 stations along a 170 km line starting near the 57 m isobath. Distance from shore spanned approximately 80–250 km. Sampling stations were spaced with higher resolution over the shelfbreak (6–10 km), and lower resolution over the outer shelf and upper slope (10-20 km). Shipboard ADCP data were collected simultaneously, ending 5 km offshore of the 1500 m

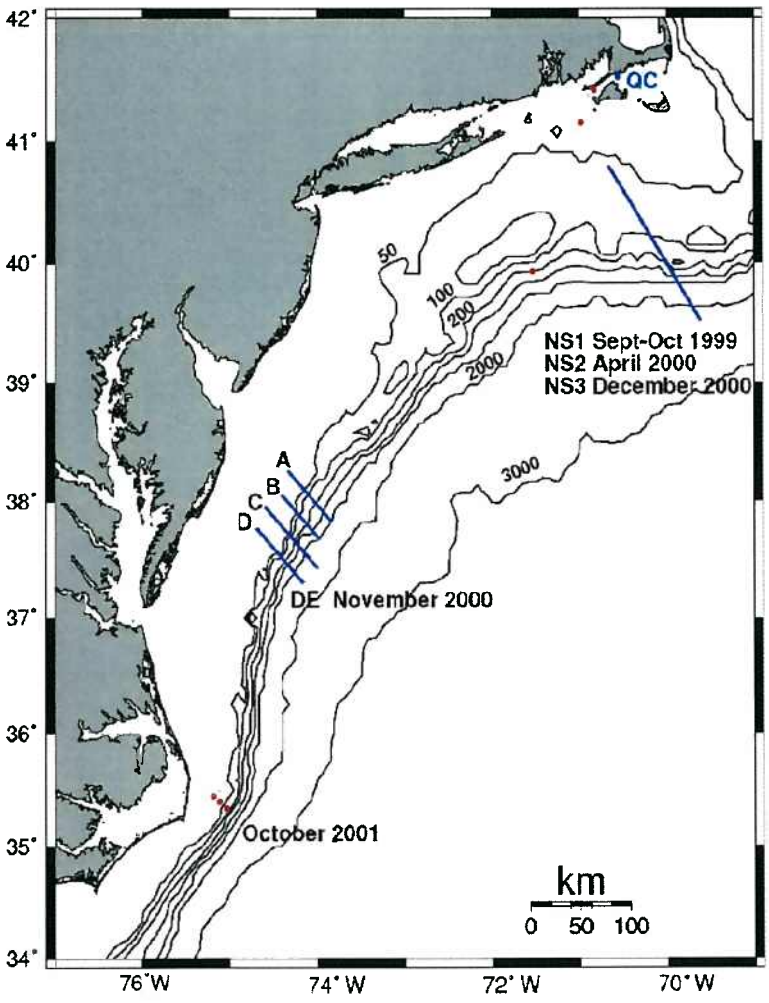

Figure 5.1: Location of sampling transects in Mid-Atlantic Bight.

isobath. Expendable bathythermograph (XBT) temperature data were also collected along the transect at approximately 5 km intervals. NS3 data were collected on 4-5 December 2000 over 100 km of the Nantucket Shoals transect, from 100–200 km offshore, during cruise EN348 on the *R/V Endeavor*. Surface radiochemical and salinity data were collected with resolution of 6–7 km, as well as mid-depth and bottom samples from three stations. Due to time limitations, the transect ended near the edge of the shelf and the shelfbreak front was not resolved. The salinity at the outer station was only 34.13, indicating that the ship was still in shelf water. Nevertheless, bottom samples from this cruise provided valuable information on radium activity and isotope ratios in bottom water directly overlying MAB shelf sediments.

The survey in the southern Mid-Atlantic Bight off the Delaware coast was conducted on 3-5 November 2000 aboard the *R/V Cape Hatteras* cruise CH2300 and covered 4 cross-shelfbreak transects, spaced 20 km apart in the alongshelf direction. All transects were sampled at 5 km intervals, with the exception of the most shoreward ends of 3 transects where resolution was lowered to 10 km. Details of the survey track can be found in Chapter 4. Surface radioisotope, nutrient, and salinity data were collected along 3 of the 4 transects (DE-A, DE-B and DE-D). Conductivity, temperature, depth (CTD) profiles were performed at all stations, and ADCP data were collected over all transects. Mid-depth and bottom samples for radioisotopes were also collected at two stations.

Data from the west wall of the Gulf Stream were collected on a return transit of the *R/V Knorr* cruise KN164 on 24 October 2001. Three stations were sampled 40 km northwest of Cape Hatteras across the Gulf Stream temperature front, between 75.04°W, 35.33°N and 75.19°W, 35.44°N. Surface, mid-depth and bottom radioisotope and salinity data were

collected at these stations.

5.1.2 Radiochemical Methods

Surface samples for the four radium isotopes were collected from 2–3 m depth from the ships' clean surface seawater line. Subsurface samples were collected by pumping through a hose attached and lowered overboard with the CTD frame. 200–250 liters of seawater were collected into plastic barrels through 10 μm and 1 μm prefilters to remove large particles. The water was then pumped at approximately 1 L min^{-1} through filters made of acrylic fiber coated with manganese oxide to quantitatively remove the radium and preconcentrate it onto the filter column (Moore 1976). Extraction efficiencies measured by placing Mn filters in series ranged from 98.2–99.8% (see Chapter 3). For measurement of ^{223}Ra and ^{224}Ra, the Mn fibers were rinsed in distilled water, partially dried, and placed in delayed coincidence alpha counters according to the methods developed by Moore and Arnold (1996). Second counts were performed at 3–4 weeks to correct for ^{224}Ra generated by ^{228}Th in the water column. All reported ^{224}Ra data is "excess" ^{224}Ra from coastal or sediment sources not supported by parent isotopes in the water column. Third counts at 2–3 months to similarly correct for ^{227}Ac-supported ^{223}Ra were conducted on some groups of samples; these corrections are generally quite small (0.015 dpm/100L). Sample fibers were then ashed at high temperature, pulverized, and sealed in vials for ^{226}Ra and ^{228}Ra counting by well-type gamma spectrometers (Charette et al. 2001). The propagated error on these samples is approximately 5–12% for ^{224}Ra, and 15–30% for the lower count-rate ^{223}Ra. For very low level samples where the short-lived isotopes are depleted the percent counting error can be much higher, but the absolute error is still very small. Counting

errors on the long-lived isotopes were maintained at approximately 2–5% for ^{226}Ra, and 7–15% for ^{228}Ra.

5.2 Mid-Atlantic Bight current and hydrographic observations

The hydrography of the southern study area is described in detail in Chapter 4. Superimposed on a mean southwesterly flow were a variety of features that do not appear in climatological studies or in coarser resolution time series or mooring observations. Particularly relevant features that could influence cross-shelf transport of biogeochemical signals included a strong, deep shelfbreak jet, as well as a smaller mid-shelf jet. The width of the jet core, sometimes less than 10 km, illustrates the importance of high resolution hydrography to accurately determine the magnitude of the jet. The transport in the mid-shelf jet alone was comparable to previous estimates of whole-shelf transport (Burrage and Garvine 1988; Biscaye et al. 1994a; Beardsley et al. 1985) and transport in the shelfbreak jet was approximately 3 times larger. Much of the transport occurred in depths greater than 50 m. Subsurface features were important in quantifying jet velocity and transport; the density gradient responsible for the geostrophic flow was the deep horizontal stratification at the foot of the front, also less than 10 km wide in some transects.

At the surface, a strong saline intrusion of slope water was present in the upper mixed layer near the shelfbreak, and Gulf Stream water (T> 22°C, salinity 36 psu) was observed at the outer stations on the upper slope (Figure 5.2). The Gulf Stream water appears to be the result of water expelled from meander crests that appear in the AVHRR sea surface

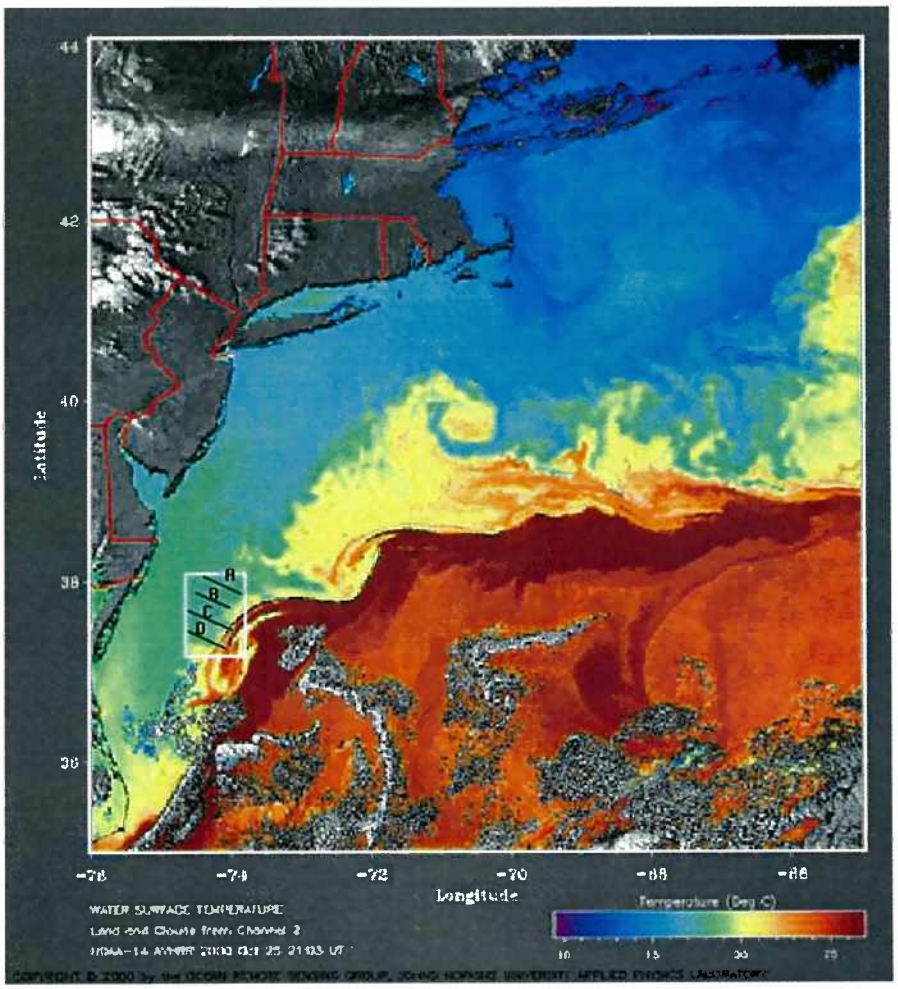

Figure 5.2: Survey DE: AVHRR sea surface temperature for 25 October 2000.

temperature imagery. The Gulf Stream influence is particularly pronounced near the end of transects C and D (Figure 5.3) as seen in a horizontal section of salinity and temperature from the middle of the surface mixed layer at 25 m depth. It appears from the radiochemical data that both the strong frontal-shelfbreak jet system and the Gulf Stream intrusion had an effect on the distribution of radium (see Section 3).

A mean alongshelf, westerly flow was also observed in the northern study area, and Gulf Stream influences were present over the slope during two of the three cruises. AVHRR sea surface temperature images (Figure 5.4) are shown for dates nearest the 1999 crossing dates. Throughout this period there was a large warm water mass present over most of the transect. The mean velocity over the upper 50 meters from ADCP data is shown in Figure 5.5. Flow over the mid-shelf is dominated by winds at this time, with alongshelf winds of 3-8 knots from the east in the 24 hours prior to the September 21 crossing, and alongshelf winds of 6-11 knots from the west-northwest in the 24 hours prior to the October 7 crossing (NDBC station 44008, 54 nm southeast of Nantucket). The shift in winds is visible in the 50 m mean current velocity over the midshelf which has shifted directions from the normal westward flow to an eastward flow on 7 October. The 21 September ADCP data shows a relatively strong shelfbreak jet with maximum velocity 50 cm/s. In the 21 September crossing there was a strong reversal of flow direction over the upper slope from southwest to southeast. The anticyclonic flow is indicative of the presence of a warm core ring. Salinity samples taken on the transect show salinity 35.0-35.5 PSU as far onshore as the 200 m isobath. The ring and jet are readily distinguishable in the vertical ADCP section (Figure 5.6). The deep, barotropic eastward flow in the warm-core ring appears at the right (red), while the shallow 50 m shelfbreak jet appears in blue beneath stations 4-5. A midshelf jet

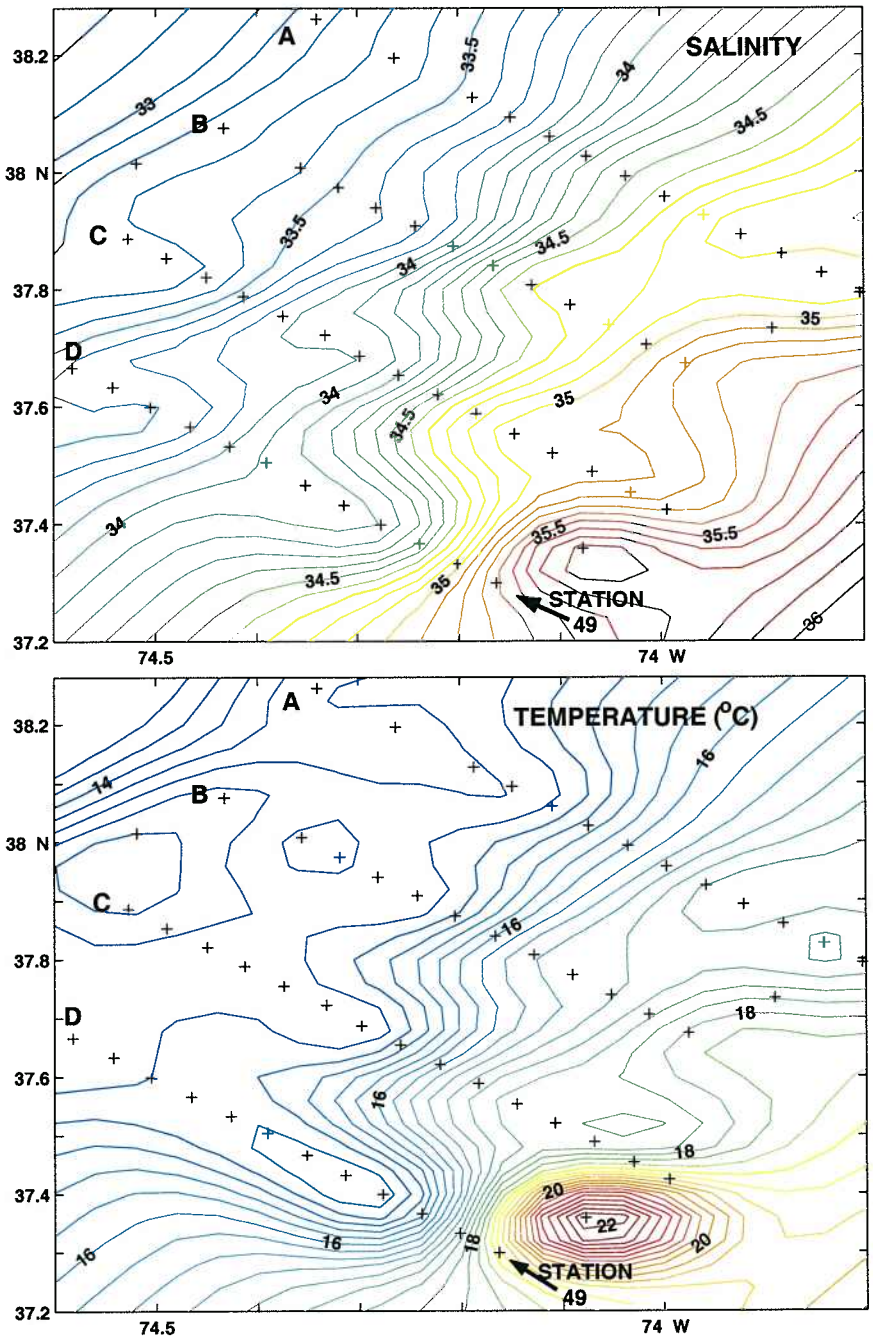

Figure 5.3: Horizontal contours of salinity (top) and temperature (bottom) at 25 m depth for survey DE, southern Mid-Atlantic Bight, Nov.2000. Station 49 is location of high ^{224}Ra.

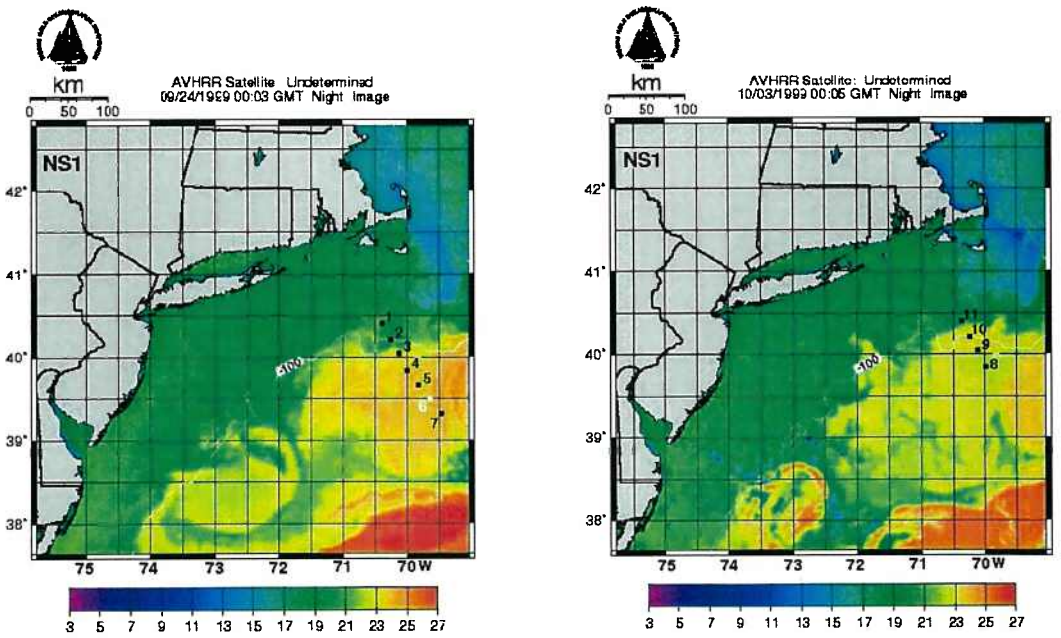

Figure 5.4: AVHRR sea surface temperature for a) 24 September 1999, and b) 3 October 1999. Actual crossing dates were 21 September and 7 October.

similar to that described in the southern Mid-Atlantic Bight (survey DE) in Chapter 4 is also visible at stations 1-2. Station 6, at the edge of the warm-core ring, was the site of unusually high ^{224}Ra, which will be discussed in Section 3. During the return crossing on 7 October, the warm-core ring had moved further north and the currents were dominated by the ring's deep, barotropic easterly and northeasterly flow over the entire upper slope. Strong anticyclonic circulation with velocity up to 1 m/s is visible in the vertical ADCP section, corresponding to the warm, circular water mass in the sea surface temperature imagery. Salinity of > 35.3 PSU was measured as far inshore as the 95 m isobath.

A large warm core ring was also present over the outer quarter of the transect during survey NS2 in April 2000, and is clearly visible in the AVHRR image from the same day (Figure 5.7). A vertical temperature section taken by XBT shows an extremely strong

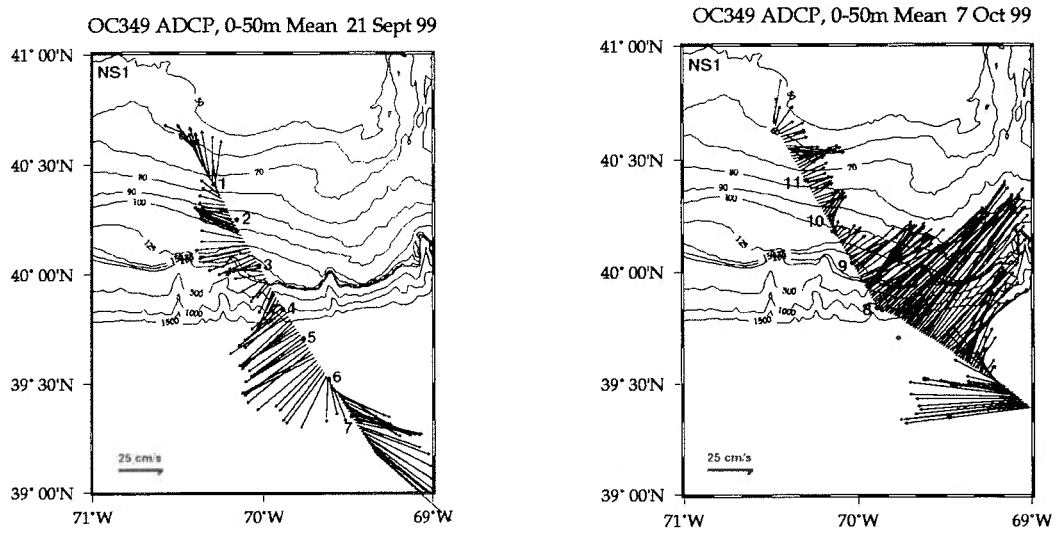

Figure 5.5: NS1: ADCP mean current velocity for upper 50 m, Nantucket Shoals transect, a) 21 September 1999, b) 7 October 1999.

temperature gradient of 6.5°C/10 km across the edge of the ring down to approximately 40 m depth (Figure 5.8). Shelf water appears to have overflown the surface edge of the ring (see "N" shape of salinity front between 180-210 km). Across this front the salinity dropped from > 36 to 33.7 PSU (Figure 5.10). The flow across the outer shelf is disorganized, especially in the area of maximum alongshelf velocity. In this area there is also a 90 degree shift in flow direction (Figure 5.9). Over the upper slope there is a strong (> 50 cm/s) offshore flow where the transect appears to cross the outer edge a warm core ring filament. Unfortunately ADCP data is only available from Station 14 shoreward, so the vertical structure of this ring is not available.

In both the fall and spring northern MAB surveys, anomalously elevated ^{224}Ra activity was detected where the transect crossed the outer edge of the warm core rings. In the southern survey, even more elevated ^{224}Ra activity was seen where the transect crossed

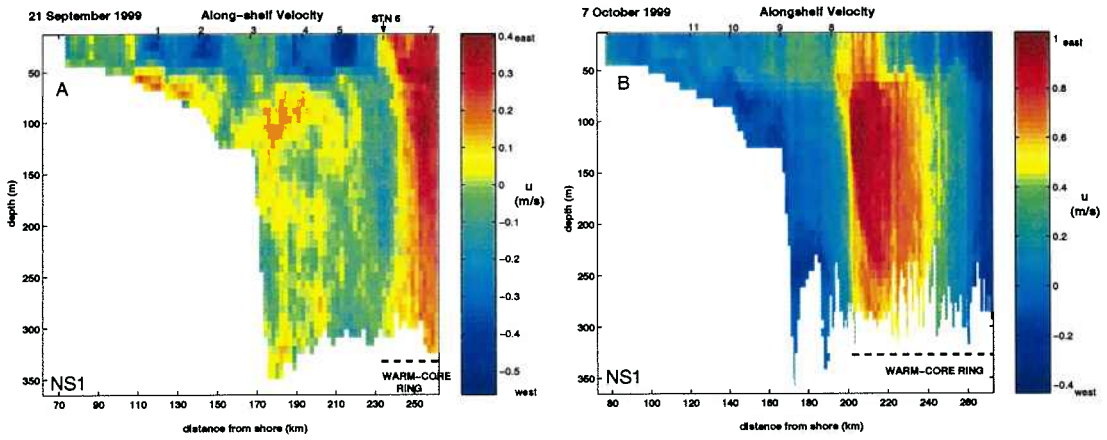

Figure 5.6: NS1: ADCP alongshelf velocity profiles. a) 21 September 1999, b) 7 October 1999. Warm core ring over shelf on 21 Sept has moved 30 km inshore by 7 October. Shelfbreak jet in 21 Sept image is visible as the 40-50 cm/s westward flow beneath stations 4-5. By 7 October, the jet has been disrupted by eastward flow from the upper half of the ring. Note also different velocity scales; eastward flow on 7 October is approximately double that on 21 September.

the Gulf Stream intrusion. Warm core rings are seen on the MAB slope regularly, and data from drifters analysed by Hare et al. (2002) indicated a 19% probability of drifters from the southern MAB being entrained by warm core rings and transported onto the shelf (see Discussion). Radium distributions across the shelfbreak suggest that this pathway for exchange may be more important than direct cross-shelf transport to slope water.

5.3 Cross-shelf Radium Distribution

Cross-shelf radium measurements of the full quartet of radium isotopes have been made previously only in the South Atlantic Bight (Moore 1997; Moore 2000a; Moore 2000b) where the shelf is narrow (100 km) and flow is dominated by the close proximity of the Gulf Stream at the shelfbreak. Estimates from short-lived radium distributions indicated rapid

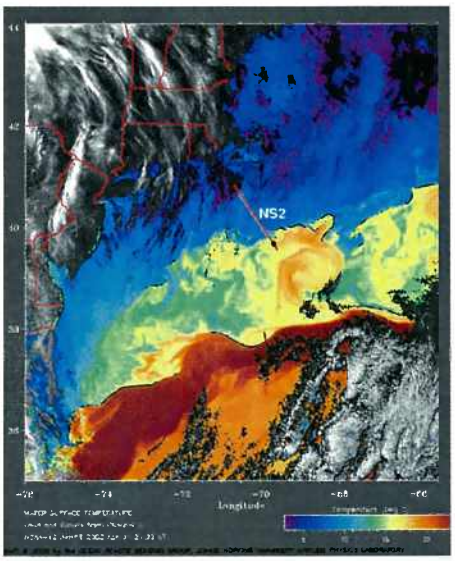

Figure 5.7: AVHRR sea surface temperature for 1 April 2000. Station 13, the site of high ^{224}Ra activity, is indicated by the black circle. (Johns Hopkins Applied Physics Laboratory, Ocean Sensing Group)

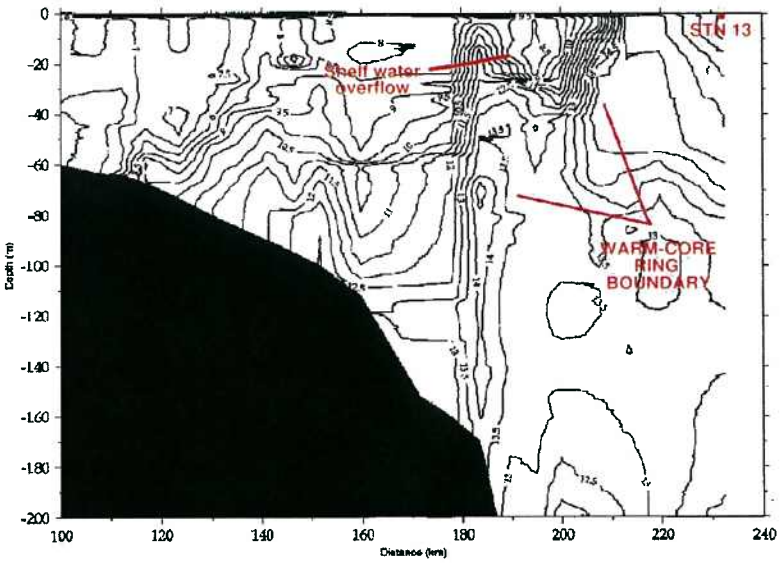

Figure 5.8: Temperature profile, 1 April 2000, Nantucket Shoals transect.

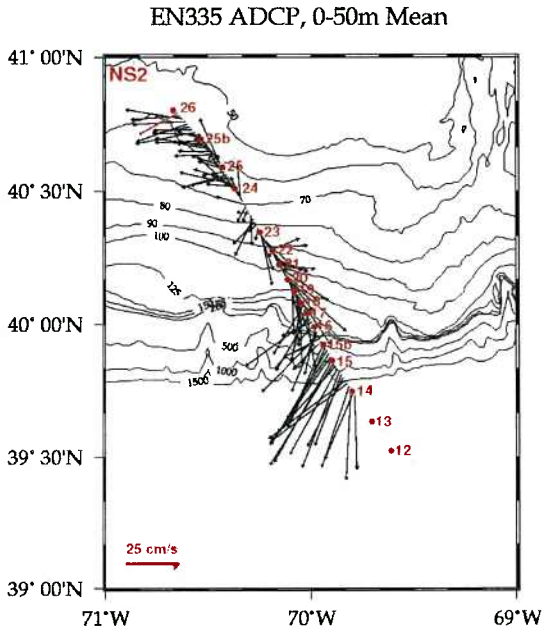

Figure 5.9: ADCP mean current velocity for upper 50 m, Nantucket Shoals transect, 1 April 2000.

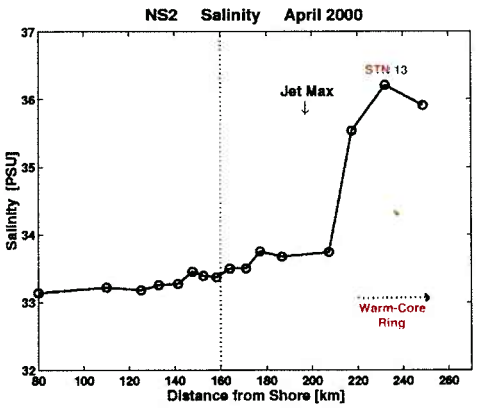

Figure 5.10: NS2 Surface salinity. Nantucket Shoals transect, 1 April 2000.

mixing over the inner 50 km of the shelf, dominated by eddy diffusion. Water mass ages determined from radium isotope ratios were approximately 2-4 weeks for outer shelf water, approximately 80-100 km from shore. The wider Mid-Atlantic Bight shelf presents several new challenges for using radium tracers. If cross-shelf transport is slow, the short-lived isotopes, particularly ^{224}Ra with its 3.7 day half life, could be of limited use because they will have decayed in the very early stages of transport. An area of particular interest to us is the effect of the shelfbreak front and jet on cross-shelf transport. If short-lived radium has already decayed before reaching the shelfbreak, it will only be possible to put a lower limit on transport time. On the other hand, since ^{223}Ra and ^{224}Ra occur naturally in the open ocean only in minute concentrations (Rama and Moore 1996), they provide a unique tool for detecting water masses very recently upwelled or transported from the coast.

A further challenge in the Mid-Atlantic Bight is that ideal conditions for using short-lived radium tracers are where there is strong vertical stratification, isolating shallow coastal water in the upper mixed layer as it is transported off-shelf. With the exception of mid-summer, conditions in the MAB are generally less than ideal. At least some vertical mixing will have occured in most areas, and where depths are shallow, ^{223}Ra and ^{224}Ra can be mixed into the overlying water by diffusion from sediments, possibly giving an erroneously "young" age. Further off-shelf, coastal radium can be diluted as it mixes into deeper waters, making mixed water appear "older" than the mean of its component ages. The use of isotope ratios can help correct for the latter problem (although see caveats in Chapter 2). Local input of radium from shallow sediments on the shelf appears to be only a small problem. Samples of bottom water taken from 50-120 m depths on one southern and one northern transect have short-lived radium activities an order of magnitude or less smaller than nearshore sources

(nearshore ^{224}Ra ~25 compared to bottom ^{224}Ra ~1–2, and nearshore ^{223}Ra ~2 compared to bottom ^{223}Ra ~0.05–0.15). In addition, samples from the bottom, mid-depth and surface have shown that the highest activities are at the bottom and surface, indicating a lack of complete vertical mixing. For reference, nearshore and open ocean end member activities for all four isotopes are shown in Table 5.1.

Location	^{226}Ra	^{228}Ra	^{223}Ra	^{224}Ra
Nearshore SAB[1]	10-20	10-40	0.5-3.0	5-25
Nearshore MAB:				
Vineyard Sound [2]	15.1	40.2	1.8	26.1
Waquoit Bay Outlet [4]	6.6	20.8	1.5	18.4
Open Atlantic[3]	7.5-8.5	1.5-4.0	~ 0	~ 0
MAB Bottom Water[2]	7.9-8.8	6.1-9.7	0.04-0.20	0.75-1.95

Table 5.1. End member activities of the 4 radium isotopes. [1]Moore 2000a; [2]Rasmussen et al., this study; [3]Kaufman et al., 1973 and Moore 1969; [4]Charette, et al. (2001)

Samples of the long-lived isotopes ^{226}Ra (half-life 1600 years) and ^{228}Ra (half-life 5.7 years) are shown for a northern (NS2) and southern (DE-D) transect (Figure 5.11) for comparison with the short-lived isotopes. The long-lived isotopes are well mixed in the ocean on the time scales of their radioactive decay, so activities should never decrease to zero. In the northern transect there is little overall trend in ^{226}Ra, which is consistent with its long half-life; variability should be expected to reflect mixing and not radioactive decay. ^{228}Ra similarly shows little trend until the end of the transect where the warm core ring water mass begins. Within the ring, activity is significantly lower and more characteristic

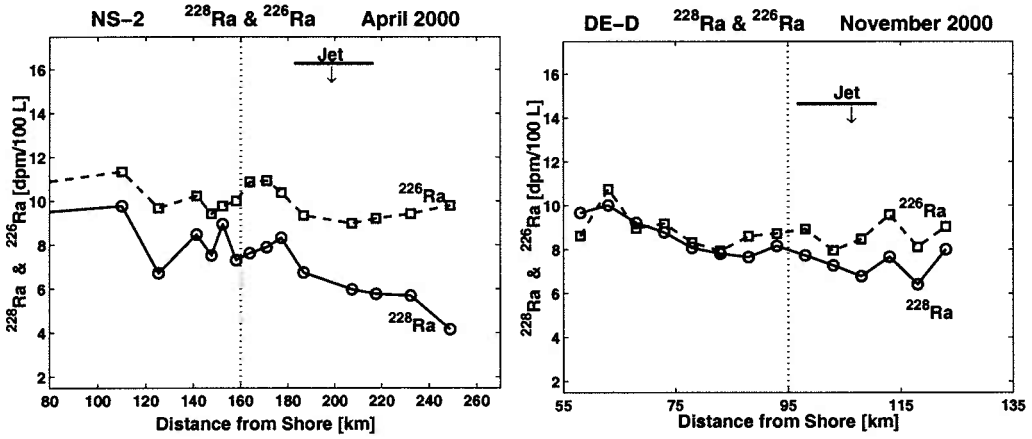

Figure 5.11: Cross-shelf measurements of the long-lived isotopes ^{226}Ra (half-life 1600 years) and ^{228}Ra (half-life 5.7 years) are shown for a northern and southern transect. A) Nantucket Shoals transect NS2, April 2000; B) Southern MAB transect DE-D, November 2000. Arrows indicate position of jet maximum velocity, and vertical dashed line is the position of the 100 m isobath. Errors on ^{228}Ra are $\leq \pm 0.91$ dpm/100 L and on ^{226}Ra are $\leq \pm 0.46$ dpm/100 L.

of open ocean waters off the northeastern U.S. (2.9-3.5 dpm/100L) measured by Moore (1969). This is consistent with a distinct water mass that has not yet mixed with the adjacent slopewater. As in the north, ^{226}Ra across the southern transect exhibits no overall trend, just spatial variability within a range that is characteristic for the outer shelf; many of these values are within the range of the open ocean end member. ^{228}Ra does show a slight decrease with distance from shore. This may be due to mixing rather than decay, since the shape is more or less linear and ^{228}Ra decay (half-life = 5.7 years) occurs over a long time scale.

Two cross-shelf transects of the short-lived isotopes are shown for the northern region (Figure 5.12 a,b) and the southern region (Figure 5.13 a,b). Although activities of ^{224}Ra at the beginning of the transects are the equivalent of 3-4 half-lives (11-15 days) lower than nearshore values, some interesting features can still be observed. Activities shoreward of

the shelfbreak jet are variable, but decrease to zero at the jet core. This indicates that the shelfbreak jet could be a barrier to transport on the timescale of ^{224}Ra decay (3 mean-lives or $\sim$ 22 days). ^{223}Ra activities start quite low at mid-shelf, so timescales of decay are difficult to determine. In the southern surveys (see Chapter 4, Figures 3.7, 3.11) ^{223}Ra activity is very low, flat and noisy across the entire transect, suggesting that values $<<$ 0.1 dpm/100L are approaching the limits of this method; the noise in the data in this case is exacerbated by the time elapsed between the crossing of the first transect (DE-A) and the counting of the samples after the cruise, which resulted in low raw counts and large error bars.

Another recurring feature is the presence of anomalously high ^{224}Ra beyond the shelfbreak front on three of the transects, after decreasing to zero within the jet. High offshore ^{224}Ra occurs on two northern transects in virtually the same location several months apart, in both cases exceeding levels recorded over 100 km inshore on the mid-shelf. In the southern region, the ^{224}Ra measured at the offshore end of transect D was the highest level seen in the entire survey. The sample location (Station 49) was at the edge of a high salinity, high temperature plume with Gulf Stream origin (Figure 5.3). (No samples were taken on transect C or between transect C and D). By comparing offshore sites with high ^{224}Ra and potential sources of high ^{224}Ra, it becomes clear that the offshore ^{224}Ra is related to an entirely different water mass (Table 5.2):

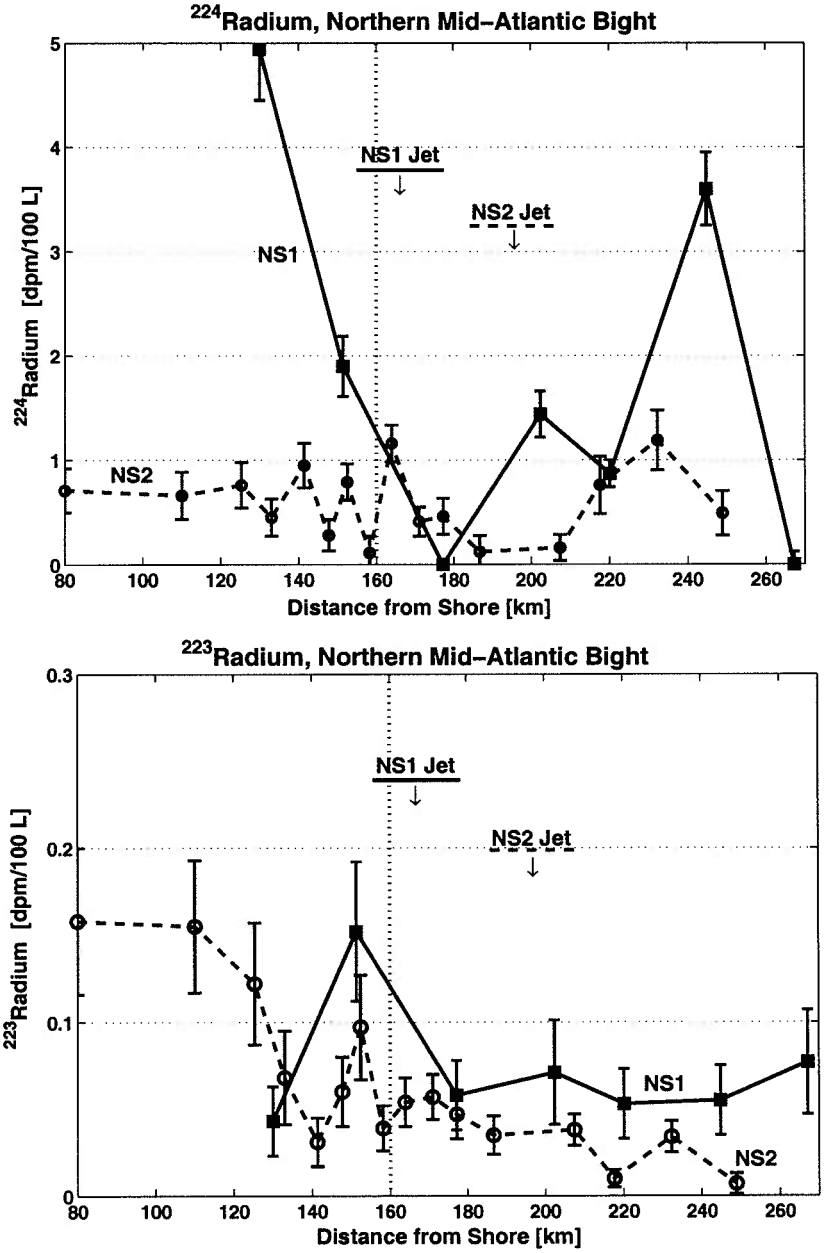

Figure 5.12: ^{224}Ra (top) and ^{223}Ra (bottom) in the northern Mid-Atlantic Bight from surveys NS1 (September 1999) and NS2 (April 2000). Position of maximum jet velocity is indicated by the arrows. Vertical dashed line indicates the position of the 100 m isobath.

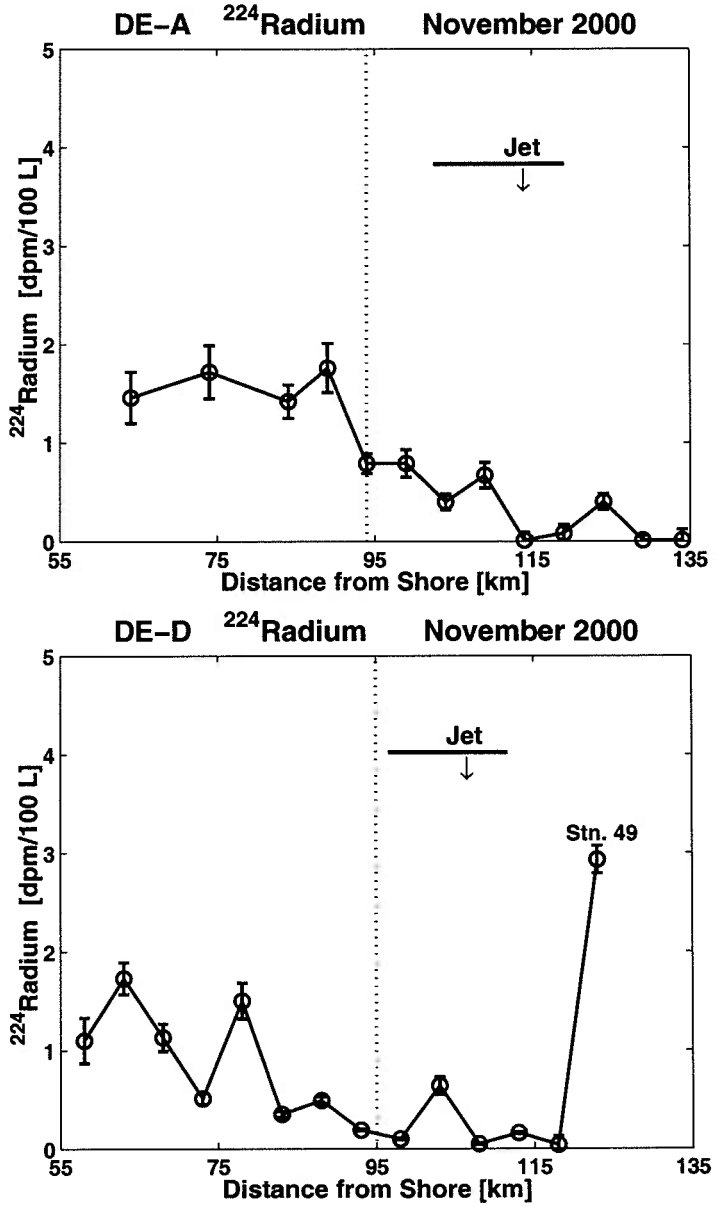

Figure 5.13: ^{224}Ra in the south-central Mid-Atlantic Bight. a) Transect DE-A; b) transect DE-D. Position of maximum jet velocity is indicated by the arrow. Dashed vertical line indicates the position of the 100 m isobath.

Source Waters	224:223	224:228	Salinity
MAB Nearshore[1,3]	12–14	0.7–0.9	31.35
SAB Nearshore[2]	4	0.5	
MAB Bottom Water [3]	23	0.1–0.3	33.53
Offshore ^{224}Ra Peaks	224:223	224:228	Salinity
Southern MAB (DE-D)	49	0.4	35.07
Northern MAB (NS1)	66	0.4	35.08
Northern MAB (NS2)	40	0.2	36.21

Table 5.2. Mean ^{224}Ra:^{223}Ra activity ratios and salinity for source waters, and ratios for observed offshore ^{224}Ra hot spots. Offshore distances for samples in transects DE-D, NS1, and NS2 are 125 km, 234 km, and 232 km respectively. [1] Charette et al., 2001; [2] Moore, 1997; [3] Rasmussen et al., this study.

Upwelling cannot account for the large offshore enrichment of ^{224}Ra because the highest ^{224}Ra levels measured in bottom water are 2.2 dpm/100L, with a higher proportion of ^{223}Ra than is seen in the offshore samples. ^{224}Ra:^{223}Ra activity ratios are approximately half than that seen in the northern offshore samples, and ^{223}Ra activities are in the same range as adjacent stations. Clearly another source must be involved, with a combination of high ^{224}Ra, low ^{223}Ra, and high salinity.

Although there was no prior record of high radium in Gulf Stream water, the strong influence of Gulf Stream warm core rings and streamers on these stations raised the question of whether radium could be transported via this pathway. A location was chosen just off Cape Hatteras to test the hypothesis that the western edge of the rapidly moving current could pick up a significant amount of radium near shore while in the shallow waters at the

Cape and begin to transport it northward. This pathway would be the one most likely to have contact with sediments, transport water onto the MAB slope, and have salinities in the correct range. Stations were selected along a 25 km section at the boundary of the west wall just north of Cape Hatteras, in salinities ranging from 34.2 to 36.5 PSU, and depths of 40-80 m.

The ^{224}Ra activities measured here are unlike any others recorded on the eastern U.S. continental shelf (Figure 5.14). ^{224}Ra activity at the highest salinity station was nearly 18 dpm/100 L, a degree of enrichment normally seen only in very nearshore waters or estuaries. Towards shore and fresher water, ^{224}Ra drops rapidly to levels more representative of shelf regions. ^{223}Ra is slightly enriched over MAB shelf water to the north, but it is exactly the same as SAB shelf water to the south that averages ~0.3-0.6 at distances 40-60 km from shore (Moore 2000a). No enrichment of^{223}Ra at all is seen in the location with high ^{224}Ra. Table 5.3 summarizes the properties of the high ^{224}Ra station surface water for comparison to other source waters. Complete data from from the three stations on this survey are given in Table 5.5 at the end of the chapter.

Location	^{226}Ra	^{228}Ra	^{223}Ra	^{224}Ra	224:226	224:228	Salinity
GS, sfc	8.27 ±0.15	6.44 ±0.33	0.32 ±0.05	17.9±0.76	2.2	2.8	36.32
GS, bot	9.66 ±0.12	7.97 ±0.27	0.27 ±0.06	12.0±0.70	1.2	1.5	36.36

Table 5.3. Radium isotope activities in Gulf Stream water from the west wall near Cape Hatteras. Depth at this station was approximately 80m.

The long-lived isotopes are likewise unenriched. Other offshore ^{224}Ra enrichments have

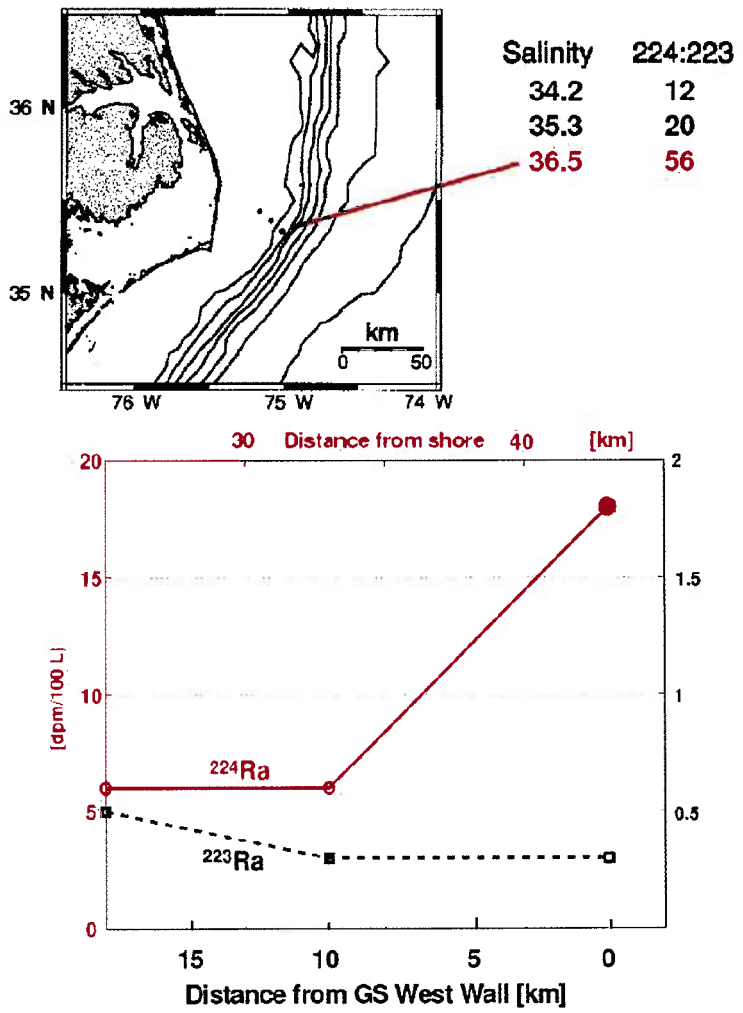

Figure 5.14: Station locations, salinity and ^{224}Ra:^{223}Ra ratios at the Cape Hatteras transect (top) and activities of the short-lived radium isotopes across the west wall of the Gulf Stream (bottom).

been seen on the eastern U.S. shelf, in bottom waters off South Carolina, 40-80 km from shore at a depth of 30-50 m (Moore and Shaw 1998). However, all four isotopes were highly enriched in this area, pointing to a groundwater source and a different type of water mass than we have sampled at Cape Hatteras. It is probable that the sediments near Cape Hatteras are the source of the high ^{224}Ra. When collecting the sample, filters that normally last for dozens of filtrations (typically through 5000 liters or more) became clogged with particulates after the first station (approximately 400 liters pumped), where the high ^{224}Ra was found, and surface water at this station was just as turbid as the bottom water.

5.4 Transport of Radium-224 in GS water

In order to determine the likelihood of ^{224}Ra from Cape Hatteras being transported via the Gulf Stream onto the Mid-Atlantic Bight outer shelf/upper slope, we can utilize isotope ratios. Of particular relevance for transport studies is the activity ratio of one short- and one long-lived isotope which not only helps correct for mixing, but also enables calculation of transport times based on the decay of the short-lived isotope. Because we are dealing with a ^{224}Ra enrichment, a good choice of activity ratio is ^{224}Ra:^{228}Ra. Although ^{226}Ra is more robust in terms of decay stability than ^{228}Ra, the difference between coastal levels of ^{226}Ra and its open ocean activity are often small so it is not as effective as a tracer of coastal water. The very low open ocean activity of ^{228}Ra makes it less prone to differencing errors when calculating "excess" activity because its coastal signal is stronger.

The "age" of a particular water mass can be estimated using the equations for radioactive decay for each isotope, expressed as a ratio:

$$\left(\frac{^{224}Ra_{ex}}{^{228}Ra_{ex}}\right)_{obs} = \left(\frac{^{224}Ra_{ex}}{^{228}Ra_{ex}}\right)_{init} \frac{f_{em}}{f_{em}} \frac{e^{-\lambda_{224}t}}{e^{-\lambda_{228}t}}$$

where λ is the decay constant for each isotope and f_{em} is the fraction of each end member remaining in the sample after mixing. Because the isotopes are travelling together in the same water mass f_{em} is the same for both, so there is no need to estimate mixing coefficients. (For caveats about mixed water masses, Chapter 2.)

In the sample at the west wall of the Gulf Stream at Cape Hatteras, ^{224}Ra:^{228}Ra = 2.8, compared to 0.65 for nearshore Mid-Atlantic Bight water. By plotting the functions for these two initial ratios, one can determine the time a parcel would have been removed from its initial source given a specific observed end ratio. In Figure 5.15, these two ratios are plotted, with horizontal dashed lines indicating the observed isotope ratios of the high ^{224}Ra stations in the northern and southern Mid-Atlantic Bight (ratios from NS1 station 6 and NS2 station 13 in the north, and DE-D station 49 in the south). The travel time required for nearshore water to reach an observed activity ratio equal to that seen in the high ^{224}Ra stations is 1.5–3 days, clearly improbable for water travelling 120-240 km offshore in a cross-shelf direction. The time required for enriched Cape Hatteras water to reach the same observed ratios is 9-11 days, a much more realistic travel time which is consistent with the velocity and dynamics of Gulf Stream transport. It must be noted here that these transit times are estimates based on tracer samples taken from different water masses at different times, and do not follow the same water mass over time. They are therefore only probable estimates for transport and decay, based on ^{224}Ra measured in Gulf Stream-influenced

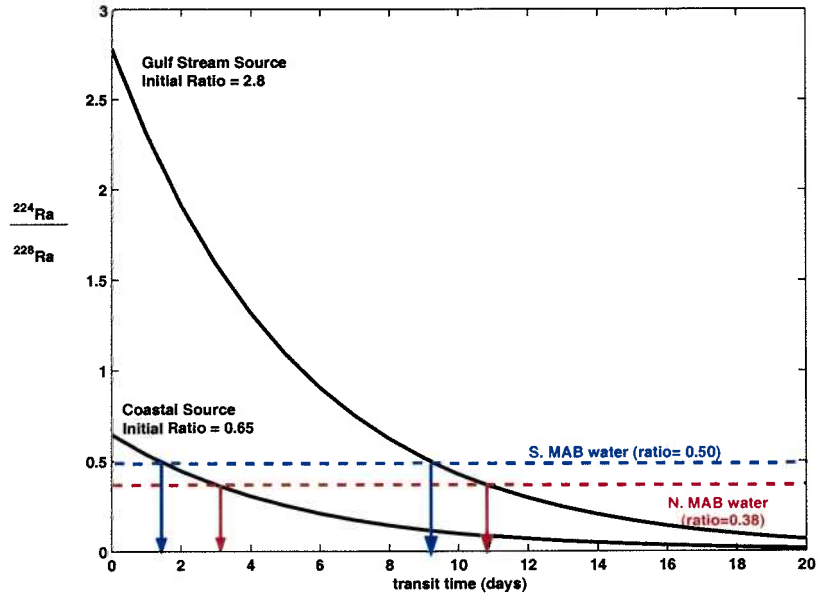

Figure 5.15: Water mass transit time as a function of initial ^{224}Ra:^{228}Ra activity ratios. Dashed lines indicate ratios of observed ^{224}Ra-enriched samples. Arrows indicate transit times required for different source water to reach the observed ratio.

water masses, and in water from the most probable source. The results are consistent with transport via the proposed pathway. Exact transit times may vary depending upon the activity of the source water at any given time, which is likely a function of Gulf Stream strength and position (see Discussion), and on the velocity of the Gulf Stream and presence of slope intrusions.

5.5 Discussion

5.5.1 ^{224}Ra enrichment in sediments and water of the Continental Shelf

If water along the west wall of the Gulf Stream is preferentially rich in ^{224}Ra, this begs the question of what the source could be. Levy and Moore (1985) present three alternatives

for enrichment of ^{224}Ra away from the usual sources in groundwater, salt marshes, and estuaries. In these sources, freshwater in contact with stream bed or aquifer sediments contains both particulate radium as well as radium parent isotopes. Upon mixing with higher salinity water, particulate radium may be desorbed, thus accounting for inputs of radium isotopes – in proportion to their content in soils and sediments – into coastal areas. The nearshore signature is thus an enrichment in all four Ra isotopes. Away from nearshore sources, ^{224}Ra can enter the water column via dissolved or particulate ^{228}Th in the water column, advection by longshore currents, or by release from ^{228}Th adsorbed onto bottom or suspended sediments. ^{224}Ra from dissolved ^{228}Th is subtracted when calculating the unsupported ^{224}Ra, so does not contribute to the high "excess" activity we are concerned with. Particulate ^{228}Th in the water column (i.e., particulates from biogenic detritus, not suspended sediments) is generally not high enough to support the high activity of ^{224}Ra seen at the edge of the Gulf Stream. Total ^{228}Th activities measured in the NW Atlantic and Pacific are no more than 2-3 dpm/100 L, of which only 7-25% is particulate (Nozaki et al. 1987; Cochran et al. 1987). There are other mechanisms, however, that can result in enrichment of ^{228}Th, and its daughter ^{224}Ra.

In their sampling areas in the South Atlantic Bight, Levy and Moore found significant enrichment of ^{224}Ra up to 70 km offshore, especially in bottom water when the water column was stratified. There was no evidence of a large component of dissolved ^{228}Th in the water column, nor any evidence of longshore transport between the two transects over 200 km apart. (One would expect to see lower activity levels in the downstream site, due to decay in transit.) They conclude that the dominant source of ^{224}Ra in these samples was shelf sediments high in ^{228}Th from biogenic particle settling. Furthermore, ^{228}Th production in

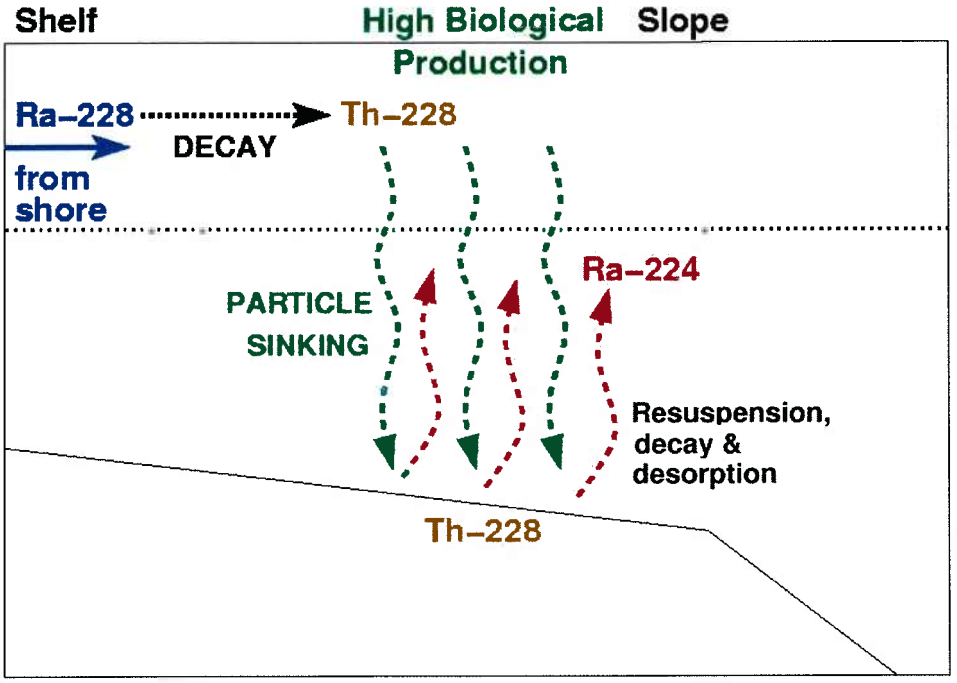

Figure 5.16: Pathways for transport of ^{224}Ra into shelf water.

the water column should be elevated over the shelf because of excess ^{228}Ra from the usual nearshore sources. This creates a situation over continental shelves where there is both high production and high removal, resulting in enrichment of ^{228}Th, the ^{224}Ra parent isotope, in shelf sediments, as illustrated in Figure 5.16. Levy and Moore consider this to provide a "significant input of ^{224}Ra in the mid shelf region." The same is not true for the other isotopes because ^{224}Ra is the only one with another Ra-Th isotope pair preceding it in the radioactive decay chain (see Chapter 2, Figure 2.2). Because the radium from the other series disintegrates by alpha decay, they do not produce thorium which in turn can produce another radium isotope. In effect, it is the beta decay of ^{228}Ra that makes this situation possible.

Rapid removal of the ^{228}Th that is produced by ^{228}Ra decay in the water column was

observed in the New York Bight by Li et al. (1979) who found that the removal rate of ^{228}Th was approximately 4-6 times faster from surface waters of the shelf than from the slope. Disequilibrium between ^{228}Th and its parent ^{228}Ra was greater over the shelf, with ^{228}Th:^{228}Ra ratios of only 0.015-0.022, compared to ratios as high as 0.090-0.110 over the slope. Because of the enhanced removal of ^{228}Th from the water column, shelf sediments are thus a potentially rich source of ^{224}Ra.

Enrichment of ^{224}Ra offshore in Long Island Sound was also observed by Torgersen et al. (1996), who noted that ^{224}Ra in surface and deep waters operated as separate systems. They attributed the enrichment to one of three possible scenarios: high quantities of fine-grained (i.e., non-sandy) sediments in the central Sound, enhanced bioturbation increasing diffusion from sediments, or lack of a MnO_2 scavenging layer in the sediment due to low oxygen levels. The exact source was not determined in this study. MnO_2 layers can form in organic-rich marine sediments by diffusion of reduced Mn from depth reaching the oxic-anoxic boundary; if the upper layers of sediment are frequently disturbed by strong currents, as is likely at the outer shelf near Cape Hatteras, it is possible this layer is absent there as well. ^{224}Ra enrichments observed in these other studies suggest a similar source as the ^{224}Ra enrichment at Cape Hatteras, in both the magnitude of the activity and the activity ratio. Average surface and deep ^{224}Ra activity and ^{224}Ra:^{226}Ra ratios are shown in Table 5.4 for stations with anomalously high ^{224}Ra activity from Levy and Moore (1985) and Li et al. (1979), compared to the activities measured at the west wall of the Gulf Stream at Cape Hatteras.

Location	^{224}Ra	^{224}Ra range	^{226}Ra	^{224}Ra: ^{226}Ra	^{224}Ra:^{226}Ra range	^{224}Ra: ^{228}Ra
So. Atlantic Bight[1]						
(N=3) Surface mean	6.7	1.6 – 9.0	12.2	0.53	0.15 – 0.77	0.5
Deep mean	11.6	11.2 – 12.3	12.2	0.96	0.90 – 1.07	1.0
Long Island Sound[2]						
(N=11) Surface mean	14.9	8.2 – 23.2	16.6	0.81	0.46 – 1.42	n/a
Deep mean	19.2	8.1 – 27.7	14.1	1.36	0.88 – 1.98	n/a
Cape Hatteras[3]						
Surface	17.9	–	8.3	2.17	–	2.8
Deep	12.1	–	9.7	1.24	–	1.5

Table 5.4. ^{224}Ra and ^{226}Ra activities at offshore stations with ahigh ^{224}Ra. Figures for So. Atlantic Bight and Long Island Sound are means (n=3 and n=9 respectively). Ra activity is in dpm/100L. [1]Levy and Moore (1985); [2]Torgersen, et al. (1996) [3]This study.

Samples from the South Atlantic Bight, which is in close proximity to the Gulf Stream like Cape Hatteras, also had salinities close to or exceeding 36 PSU (mean of 36.03) like that seen in the Cape Hatteras samples as well as the high ^{224}Ra samples from the offshore stations in the Mid-Atlantic Bight. In Long Island Sound, no relationship between ^{224}Ra activity and salinity was found despite its closer proximity to groundwater sources. ^{224}Ra vs. salinity did group into different clusters, however, with bottom samples and surface samples appearing to occupy distinct regimes (Torgersen et al. 1996).

Conditions at the intersection of the Gulf Stream and Cape Hatteras are also conducive to release of ^{224}Ra because of turbulence and sediment load in the water column. At the high ^{224}Ra stations from the South Atlantic Bight and Long Island Sound, conditions were vertically stratified and non-turbulent, and ^{224}Ra activity, ^{224}Ra:^{226}Ra ratios, and salinity were often significantly higher at depth than at the surface. At the Cape Hatteras station on the west wall of the Gulf Stream conditions were unstratified (surface salinity is approximately equal to bottom salinity, see Table 5.5). The amount of suspended sediment

in the water column was observed visually and by filtration problems to be very high, suggesting a large amount of turbulence as well. (By contrast, the other two stations shoreward of the GS had salinity increases of 0.58 PSU and 2.28 PSU between the surface and bottom, and comparatively little suspended sediment.)

In radium desorption experiments, Webster, et al. (1995) found that proportionately more ^{224}Ra is desorbed from fine grained sediments (such as those found in suspension) than from coarse grained sediments (which would remain near the bottom under turbulent conditions). Experiments were conducted on freshwater sediments (i.e., sediments with fully adsorbed radium) which were exposed to water up to 100% seawater proportions. The experiment was designed to model the behaviour of riverine sediments exposed to saline esturary conditions, as well as the desorption behaviour in continental shelf sediments. In shelf sediments, "this process continues, with the desorbed radium being continuously replaced by the decay of the sediment-bound thorium parents." The desorbable proportion was found to be similar for all 4 isotopes when only salinity varied, but differed when grain size was changed. The desorbable proportion of ^{224}Ra increases more than two-fold, from 24% to 59%, when grain size decreases from 125-500 μm to $< 63\mu$m. In addition, the desorbable proportion of ^{224}Ra exceeds that of the other radium isotopes by 14-33%.

Turbulent suspension of sediments is likely to be of greater magnitude at Cape Hatteras than at other points on the Eastern U.S. coastline even without the effect of the Gulf Stream. In models constructed by Harris and Wiberg (2002) of cross-shelf sediment transport and deposition, sediment resuspension and transport was greater on narrow, steep shelves than on wide, flat shelves, due to large gradients in bottom shear stress. Furthermore, wave action in these regions created coarse, eroded areas over the inner shelf, while depositing

fine-grained sediment on the mid-outer shelf. Thus the physical flow created by the topography alone creates a distribution of sediment types that is conducive to both suspension of sediment and desorption of ^{224}Ra in regions like the Cape Hatteras shelf.

Another explanation for high ^{224}Ra could be a situation where recent processes (such as a spike in biological activity) have stripped out ^{228}Th from the water column, such that the measured dissolved ^{228}Th is not actually representative of the amount that has contributed to recent production of ^{224}Ra. If this were the case, the ^{228}Th activity that is subtracted from the total ^{224}Ra activity to determine "excess" (i.e., unsupported) ^{224}Ra is actually too low, and the ^{224}Ra activity consequently appears too high. However, the ^{228}Th correction would have to be unrealistically high to support the ^{224}Ra activity measured at the west wall of the GS. The 18 dpm/100 L activity required is about an order of magnitude higher than that measured in surface waters by Nozaki, et al. (1987) and Cochran, et al. (1987). As it is, the measured dissolved ^{228}Th may actually be too high due to contributions from sub-micron particulates. Overall, our measured dissolved ^{228}Th is in good agreement with that measured by both Li, et al. (1979) and Levy and Moore (1985).

Lateral transport and deposition of sediment can also enhance ^{228}Th concentrations on the particulate matter itself, through the processes of boundary scavenging and repeated sediment resuspension. Smoak et al. (2000) collected samples from sediment traps in the Santa Barbara basin that demonstrated the effects of advection on particle-reactive elements ^{234}Th, ^{228}Th, and ^{210}Pb. This area is different in many respects from the Mid-Atlantic Bight, but has some interesting parallels to the region adjacent and just north of Cape Hatteras. The Santa Barbara basin, like Cape Hatteras, is a meeting point of a warm, saline current (Southern California Countercurrent) and colder water from the north (California

Current) which converge near a topographic outcropping (Point Conception). Although the California Current is mild compared to the Gulf Stream, the converging circulation in this area is characterized by strong flow (20-50 cm/s) and it is an imporant transition zone between northern and southern ecological zones. (Hickey 1993; Harms and Winant 1998). Sediment deposited here had ^{228}Th activities 1.5-22 times the values expected from direct water column scavenging as estimated by the methods of Moore et al. (1981). Particles advected in currents can continue adsorbing particle-reactive elements, such that the time and the area over which they can potentially scavenge is increased. Regions with rapid boundary currents are thus likely to have more ^{228}Th attached to particles than would be expected by measuring ^{228}Th in the immediate water column. When these particles ultimately settle, ^{228}Th from a large area is left in the deposition area. A similar process occurs when deposited sediment is repeatedly resuspended in the water column, where it can continue to accumulate ^{228}Th.

The conditions necessary to enrich ^{224}Ra in Gulf Stream water regularly to the degree observed during the Cape Hatteras cruise are a) enrichment of bottom sediments with ^{228}Th from local or remote sources; b) resuspension of bottom sediments into the water column; c) a high enough sediment load in the water column to provide sufficient particulate ^{228}Th parent; and d) transit of the Gulf Stream through these conditions for a long enough period of time to accumulate excess ^{224}Ra activity of a magnitude 10-20 dpm/100L. The following example illustrates a possible scenario under which these conditions are met, using parameters that are conservative enough to be applicable to a range of actual circumstances. As illustrated in Figure 5.17, Gulf Stream water entering the turbid zone has no initial enrichment of ^{224}Ra and picks up resuspended bottom sediment along Cape Hatteras, from

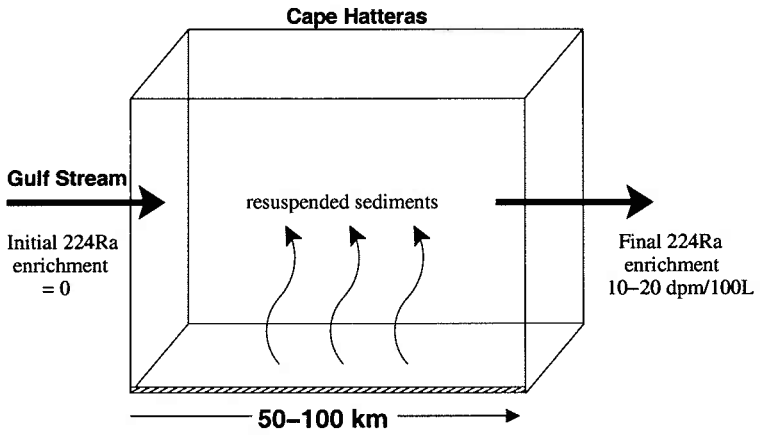

Figure 5.17: Schematic for enrichment of Gulf Stream water by suspended sediment near Cape Hatteras.

which ^{224}Ra is enriched by decay of particulate ^{228}Th while in transit. After the Gulf Stream passes Cape Hatteras and detaches from the shelf, it is assumed that the particulate matter would settle out of the water column and enrichment would cease.

^{228}Th has been measured on marine sediments at activities of approximately 2-3 dpm/g on continental shelves of the New York Bight, the Gulf of Thailand, and Taiwan (Li et al. 1979; Srisuksawad et al. 1997; Chung and Chang 1996) and as high as 30-100 dpm/g in Bay of Bengal sediment trap material (Sarin et al. 2000; Smoak et al. 1999). Smoak et al. measured activities of ^{228}Th on sediment trap material of 1-9 dpm/g in the Guaymas Basin, and particulate activities as high as 20-50 dpm/g that were associated with higher than normal scavenging efficiency there during episodic El Nino events. Suspended sediment concentration in shelf waters with bottom currents of 8-10 cm/s have been measured at 1.5-2.5 g/L (Wright et al. 2001).

Taking conservative estimates of 2 dpm/g ^{228}Th on sediments, and a suspended sedi-

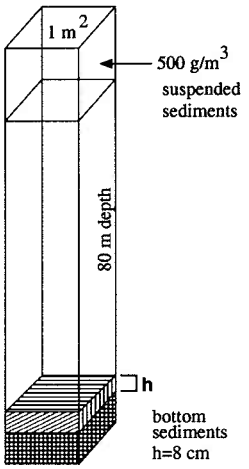

Figure 5.18: Example of a vertical 1-meter square section of water column at west wall of Gulf Stream with average resuspended sediment concentration for the 50-100 km transit past Cape Hatteras. Depth h is the equivalent depth of bottom sediments to equal the sediment load in the overlying water column.

ment concentration of 0.5 g/L, the particulate activity of ^{228}Th would be 100 dpm/100L seawater. When integrated over an 80 m water column (Figure 5.18) this suspended sediment concentration is equivalent to resuspension of an 8 cm deep layer, assuming a low surface sediment density of 0.5 g/cm^3. The length of the shelf over which the west wall of the Gulf Stream passes close inshore near Cape Hatteras may be estimated at 30-100 km. At a Gulf Stream average velocity of 1 m/s, the time elapsed during this passage would be approximately 8-24 hours. Figure 5.19 shows the ingrowth of ^{224}Ra from particulate ^{228}Th in the water column that would occur in transit under these conditions. Initial ^{224}Ra in Gulf Stream inflow water is assumed to be low ($\leq$ 1 dpm/100L) and ^{228}Ra activity is set at 8 dpm/100L as measured in the Gulf Stream samples.

In this example, 8-24 hours of transit would result in an enrichment of ^{224}Ra by approximately 10-20 dpm/100L, enough to support the observed enrichment at Cape Hatteras.

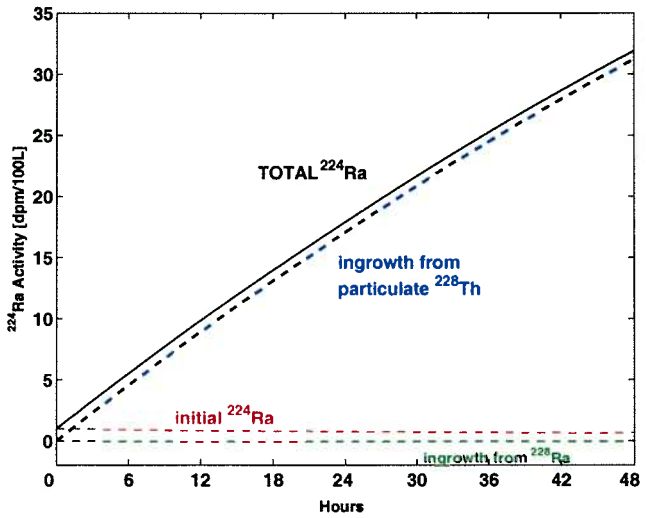

Figure 5.19: Example of ingrowth of ^{224}Ra from particulate ^{228}Th on resuspended sediments in the water column. Particulate ^{228}Th = 2 dpm/g, sediment load is 0.5 g/L, initial ^{224}Ra = 1 dpm/100L and ^{228}Ra = 8 dpm/100L.

Under actual conditions, many of these parameters could vary. A higher particulate ^{228}Th activity or a higher sediment concentration, both of which are possible, would result in greater enrichment of ^{224}Ra during transit. This would then require less transit time (and therefore a shorter distance in contact with sediments) to achieve the same ^{224}Ra activity.

In summary, there are numerous ways that ^{224}Ra can become enriched in Cape Hatteras waters. Bottom and suspended sediments are likely rich in ^{228}Th, and both currents and topographic effects favor a large sediment load in the water column on the outer shelf. ^{228}Ra will be high on the shelf from nearshore inputs, and its particle reactive daughter ^{228}Th will be removed by high productivity such as that which occurs at strong fronts such as the wall of the Gulf Stream. Finally, boundary scavenging plus lateral transport of particles may occur in this region, which would make particles advected here, or deposited here and resuspended in the water column, even more enriched in ^{228}Th than the local seawater alone

could support.

5.5.2 Transport of Radium via Gulf Stream water to the Mid-Atlantic Bight

In the radium data from the Mid-Atlantic Bight and Cape Hatteras there is evidence of ^{224}Ra enrichment offshore from several non-nearshore sources. In the transects sampled by Levy and Moore (1985) in the South Atlantic Bight there was no indication of longshore transport, the third major potential source of radium enrichment. However, data from the Mid-Atlantic Bight does support the conclusion that longshore transport is responsible for enrichment of northern waters over the upper slope. At Cape Hatteras, Gulf Stream water that has been close to the shelf all along the South Atlantic Bight becomes detatched from that potential radium source. Before it departs northeastward, its western wall passes a shallow but steep region at the Cape that has a high probability of being a very rich sedimentary source of ^{224}Ra. As the Gulf Stream progresses northward, these sources are absent, which creates a ^{224}Ra "clock" in the water mass. ^{224}Ra enriched water with high salinity sampled at the outer stations of transects in the southern and northern Mid-Atlantic Bight indicate that this water may originate near Cape Hatteras, with transit times on the order of 10 days. Figure 5.20 illustrates the proposed path.

How often can we expect such enrichments to be detectable, particularly if the warm-core rings that can bring Gulf Stream water to the slope and outer shelf are far removed from the source and persist for long periods of time? In Joyce's review of Gulf Stream warm-core rings (Joyce 1991), the combined data of Auer (1987) and Brown et al. (1986) compiled over 10 years shows distinct groupings of long-lived and short-lived warm-core

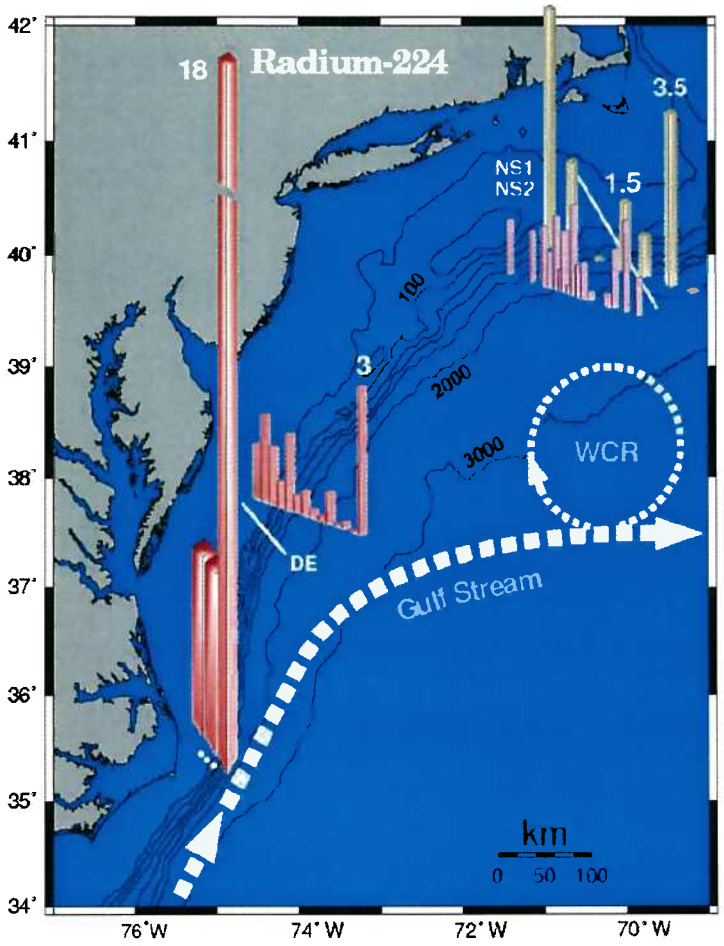

Figure 5.20: Pathways for transport of ^{224}Ra in the Mid-Atlantic Bight via the Gulf Stream.

rings with mean lifespans of 229 days and 54 days respectively. Water masses associated with a ring that has existed for 1-7 months or more would be in the range of 7-50 half-lives of ^{224}Ra (half-life 3.7 days). Thus any high ^{224}Ra signal from Cape Hatteras would have decayed beyond detection. More recent Gulf Stream water is frequently found along the edges of warm-core rings however. Nof (1986; 1988) found in his non-linear model that streamers form around the upstream side of a ring when there is even slight contact with the Gulf Stream (e.g., when a GS meander touches a previously detatched ring). The streamer propagates around the edge at approximately one-half the speed of the Gulf Stream where the streamer originated. Given Gulf Stream velocities of 1-2 m/s, this rapid propagation would propel Gulf Stream water half way around a 200 km ring in 3.6-7.2 days. This result is independent of both the size of the ring and its azimuthal velocity, so is widely applicable, and shows how the streamer flow is largely independent of the ring. Observational evidence for GS streamers can be seen in moored observations near warm-core ring 82B in which Ramp (1989) found a warm streamer of Gulf Stream water around the western edge of the ring. A similar feature can be seen in ring 81D (Joyce 1984) where surface temperature is highest ($> 26°$C) in a streamer extending around the western edge of the ring, and lowest in the ring center ($< 23°$C), indicating that water along the edge has been more recently entrained into the ring system than the water at the core. Thus, advection of southern GS water into the Mid-Atlantic Bight by way of warm-core rings depends only on the presence of a ring that is interacting with the Gulf Stream, not on the presence of a "young" or new ring.

In an unusual finding concurrent with other observations of warm-core ring 81D, Orr et al. (1985) detected elevated activity of ^{222}Rn, the short-lived daughter of ^{226}Ra. The

half-life of ^{222}Rn is 3.8 days, almost identical to ^{224}Ra. The normal source of ^{222}Rn away from coastal or sedimentary inputs is production in the water column from ^{226}Ra which typically has a mean activity of 8.6 dpm/100 L in the western portion of the North Atlantic gyre (Moore 1969; Kaufman et al. 1973) and is well mixed due to its long half-life (1600 yr). ^{222}Rn in equilibrium with its parent would show the same activity. The other sources, as with radium isotopes, are coastal inputs and diffusion from bottom or suspended marine sediments. Activity of ^{226}Ra in vertical profiles in and near WCR 81D fall as expected within a very narrow range between 8-9 dpm/100 L. Because ^{222}Rn is an inert gas, profiles are typically depleted near the surface due to atmospheric exchange; this is seen in 81D, where surface activity is between 3-6 dpm/100 L. At the center of the ring, subsurface ($z > 20$ m) activities are close to equilibrium with ^{226}Ra. However two profiles at the ring edge show activities of ^{222}Rn elevated to approximately 10.5 dpm/100 L, up to 2 dpm/100 L or more in excess of ^{226}Ra. Slope water adjacent to the ring is depleted at the surface as far down as 150 m, except for isolated pockets of elevated ^{222}Rn around 50-70 m depth. The ^{222}Rn in these layers is 1-5 dpm/100L greater than the ^{226}Ra activity, and 4-7 dpm/100 L in excess of the expected surface-depleted ^{222}Rn profile at that depth. ^{222}Rn excesses of this magnitude must come from recent contact with sedimentary sources, or have been advected rapidly from an area with recent sedimentary inputs.

This ring was surveyed when the western edge was at approximately 66°W, or about 200 km east of the ring crossed by transect NS2 on 1 April 2000. Given similar transit times as those calculated for ^{224}Ra to reach the NS2 transect, and adding 200 km at a mean GS velocity of 101 cm/s (Hare et al. 2002) one could estimate a transit time of approximately 13 days. Given the decay rate of ^{222}Rn and an observed "excess" activity of 7 dpm/100 L, we

can calculate an approximate starting activity of 75 dpm/100 L. ^{222}Rn has been measured 24 km offshore in Florida at activities of 100-400 dpm/100 L, but a considerable amount of this is due to groundwater inputs (Cable et al. 1996). In marine sediment porewater from the same area (equilibration studies not subject to groundwater inputs) ^{222}Rn activity is 169 ± 62 dpm *per liter* porewater (Cable et al. 1996), so areas subject to sediment stirring and resuspension could have a very large input of ^{222}Rn activity.

Although the reason for excess ^{222}Rn in warm-core rings was perplexing to Orr et al. at the time, the observations are consistent with the new data acquired during this study. High ^{222}Rn and ^{224}Ra, with nearly identical half lives, have now both been detected along Gulf Stream features. Highest activity at the edge of warm-core rings is also consistent with what we know of warm-core ring entrainment of new water from the edge of the Gulf Stream. The distribution of ^{222}Rn across the edge of ring 81D similar to that of ^{224}Ra across the outer edge of the NS2 ring.

A similar estimate using decay time scales in observations of Gulf Stream transport made use of larval fish from the South Atlantic Bight that are frequently found on the Mid-Atlantic Bight shelf. Hare et al. (2002) conducted a study analysing drifter tracks to determine the probabilities of larval fish spawned south of Cape Hatteras reaching nursery grounds on the northern shelf of the Mid-Atlantic Bight where they have been observed as juveniles. The pathway is the same from Cape Hatteras northward as the proposed ^{224}Ra pathway, as shown in Figure 5.21. Average downstream velocities in the Gulf Stream were 101 cm/s after leaving Cape Hatteras, and drifters were observed to make the trip to the area south of Nantucket Shoals in 5.4 days. When drifters were entrained into warm core rings moving into the slope, their cross-slope velocity averaged 50.9 cm/s and a trip along

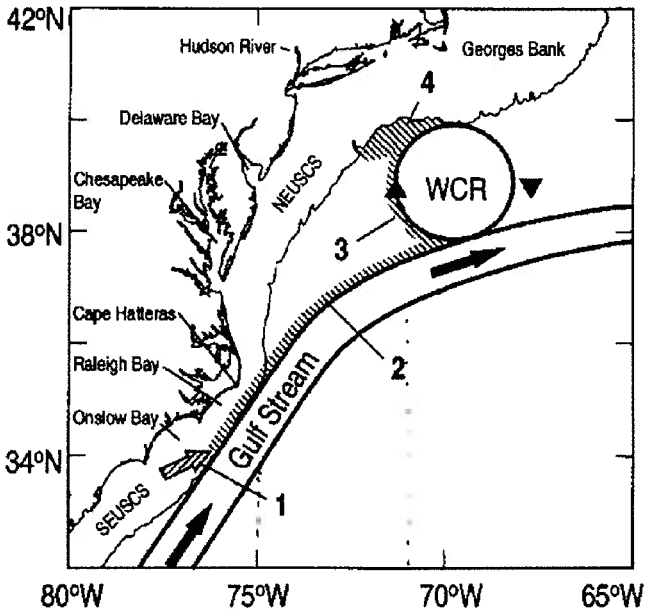

Figure 5.21: Proposed transport route for larval fish (and ^{224}Ra). Hatched area on the shoreward side of the Gulf Stream and warm-core ring is the proposed pathway. From Hare et al. 2002.

the side of a ring to the edge of the shelf took about 8 days. The total travel time of ~13 days is of the same order of magnitude as the the ~10 day travel time for ^{224}Ra-enriched Gulf Stream water to reach the northern Mid-Atlantic Bight. It is thus plausible that the same transport pathways are involved.

Hare et al. then constructed a model to determine the probability of larval species being transported by this pathway onto the MAB shelf, using a larval mortality function identical to an exponential radioactive decay function, i.e., $N(t) = N_0 e^{-zt}$, where z is the larval mortality rate. The larval mortality rate was based on two species of interest; if converted into a "half-life" for larvae, the rates correspond to half-lives of 5.8-6.3 days, and mortality rates slightly higher (slightly shorter half-lives) were in closest agreement with the

observed larval distributions. The model predicted that based on drifter transport data, the observed age distributions of South Atlantic Bight larvae in the MAB were reasonable. The distribution was highly dependent on the probability of entrainment into a warm-core ring, just as one would expect with ^{224}Ra tracer picked up in the northern wall of the stream. Because of the similarities of decay rates, this model would apply equally well to ^{224}Ra enrichment in the Gulf Stream at Cape Hatteras as it travels northward. The agreement between independently derived transit times from drifters, larval fish, and radium suggests that conclusions about the "routes and rates" involved in this transport pathway are not anomalies. It is also notable that the average transit times around the edge of a WCR determined by drifters agrees exactly with that predicted theoretically by Nof (1988), i.e., the mean WCR streamer velocity as measured by drifters (50.9 cm/s) is one-half the adjacent mean Gulf Stream velocity (101 cm/s). This could be a reliable rule-of-thumb to use in future tracer or larval transport studies.

5.5.3 Summary

In their review article on the coastal ocean of northeastern North America, Loder et al. (1998) point out that even after intensive study during the 1990's only "crude estimates" of cross-shelf exchange rates exist, and those do not identify mechanisms of exchange, where the exchange takes place, and how seasonal or longer variability affects the estimates. Gulf Stream ring effects on the slope and outer shelf are considered to be possibly important, but the magnitude of the contribution of each component in the system is described as "poorly known in general." When direct cross-shelf flow does occur, it may be directly related to Gulf Stream dynamics. Joyce et al. (1992) observed that Gulf Stream warm-core

rings can entrain large amounts of shelf water onto the slope, and in the other direction intrusions of Gulf Stream water have been observed to penetrate as far as the MAB shelf (Gawarkiewicz et al. 1990; Gawrkiewicz et al. 1992) In a study of Gulf Stream influence on cross-shelf export near Cape Hatteras, Savidge and Bane (2001) found that contrary to some expectations, Gulf Stream position does not appear to impact along-shelf transport, even in a region where it is in close proximity to the shelf; however it does correlate with transport convergence which they hypothesize may be responsible for cross-shelf, seaward flux of shelf water.

Drifter studies conducted by Dragos et al. (1998) south of Hudson Canyon in the Mid-Atlantic Bight revealed that over a two-year period surface exchange across the shelf-slope front was nil. The drifters were launced on the upper slope side, and all made their way down to the north wall of the Gulf Stream just north of Cape Hatteras, all were entrained, and as with the Hare et al. drifters, 20% became engaged in Gulf Stream rings and recirculated into the Mid-Atlantic Bight. Transit times for these pathways were remarkably rapid; transit to the north wall of the Gulf Stream occured in once case in as little as 4 days, with a mean of only 27 days. Recirculation back to the launch region took as little as 28 days, with a mean of 62 days. This pattern of circulation is consistent with results from radium tracers, which show evidence of transport up the Gulf Stream and onto the slope, but not of cross-shelf transport of shelf water.

Together, observations such as those by Dragos et al. and Hare et al., earlier radiochemical evidence from ^{222}Rn, and ^{224}Ra from this study, combine to present some compelling evidence that circulation in the Mid-Atlantic Bight may be dominated by Gulf Stream influence, whether direct or remote. The observations in this study indicate that Gulf Stream

warm-core rings and streamers from the edges of meander crests can directly deposit Gulf Stream water onto the upper slope and outer shelf of the MAB and may do so at a rate and frequency that is higher than was previously believed. Time series data are not available, but 3 of 4 cruises resulted in measurements of high offshore ^{224}Ra associated with Gulf Stream or slope water, suggesting that this phenomenon is not unusual. On the other hand, the lack of a coastal ^{224}Ra signal beyond the shelfbreak indicates that the direct cross-shelf pathway is not common. Steady and rapid transit of drifters along the shelf-slope front, and entrainment/recirculation of a large percentage of these via the Gulf Stream may be indications that the traditional "leaky current" model of Mid-Atlantic Bight transport (Loder et al. 1998) needs revisiting. In this conceptual model, alongshore transport on the eastern North American coast decreases southward as cross-shelf export removes water from the coastal current. Early alongshore transport estimates were used to construct this model such that lower transport in southern segments is balanced by offshore removal in northern segments. However, there is little direct evidence of "leakage" in the form of cross-shelf transport, and transport may be higher in the southern segments than the estimates this model is based on. At least two other transport measurements have resulted in estimates of larger volumes (1-2 Sv) that would significantly alter the balance of offshore export (Burrage and Garvine 1988; Voorhis et al. 1976). High shelf transport rates measured during this study in the southern Mid-Atlantic Bight (Chapter 4), if they are not anomalous, support this view. It is apparent at least that transport volumes vary tremendously, and until this is resolved the uncertainty in calculations of cross-shelf export by differencing must be large.

That there can be inputs of an isolated radium isotope into high salinity water also introduces an important new facet to our understanding of the radium quartet tracer sys-

Distance (depth)	^{224}Ra excess (dpm/ 100L)	^{223}Ra excess (dpm/ 100L)	^{228}Ra (dpm/ 100L)	^{226}Ra (dpm/ 100L)	^{228}Th (dpm/ 100L)	$\frac{^{224}Ra}{^{226}Ra}$	Salinity (PSU)
60 km							
(sfc)	6.02 ± 0.49	0.49 ± 0.08	13.07 ± 0.42	6.14 ± 0.13	0.41 ± 0.11	0.98	34.09
(15 m)	2.53 ± 0.28	0.31 ± 0.07	2.25 ± 0.13	7.07 ± 0.16	0.26 ± 0.08	0.36	36.06
(25 m)	2.60 ± 0.27	0.25 ± 0.07	6.82 ± 0.40	7.19 ± 0.16	0.07 ± 0.03	0.36	36.37
69 km							
(sfc)	5.97 ± 0.50	0.28 ± 0.06	6.75 ± 0.34	5.86 ± 0.13	0.36 ± 0.10	1.02	35.76
(13 m)	6.68 ± 0.59	0.52 ± 0.10	6.50 ± 0.42	7.52 ± 0.17	0.58 ± 0.17	0.89	36.31
(23 m)	1.63 ± 0.31	0.19 ± 0.07	4.76 ± 0.34	5.76 ± 0.14	0.38 ± 0.13	0.28	36.34
78 km							
(sfc)	17.91 ± 0.76	0.32 ± 0.05	6.44 ± 0.33	8.27 ± 0.15	1.93 ± 0.25	2.17	36.32
(53 m)	12.01 ± 0.70	0.27 ± 0.06	7.97 ± 0.27	9.66 ± 0.12	0.82 ± 0.19	1.24	36.36

Table 5.5 Radium and salinity data for Cape Hatteras stations. Distances are in km from shore.

tem. Currents and topography, even hundreds of kilometers remote, must be considered in analysis of cross-shelf radium distributions and estimates of horizontal mixing taken from cross-shelf radium measurements must be carefully examined for alongshore advective effects. As with the physical model, in some environments it may be necessary to pay more attention to circuitous alongshore transport pathways instead of focusing primarily on export directly across the shelfbreak.

Chapter 6

Conclusions

The purpose of this study was to examine circulation in the Mid-Atlantic Bight, and particularly the process of cross-shelf exchange, with the aid of the naturally occuring radiotracers ^{223}Ra, ^{224}Ra, ^{226}Ra,and ^{228}Ra. These isotopes have coastal sources and a range of half-lives that make them especially suitable for tracing nearshore shelf water as it is mixed or advected onto the outer shelf and slope. In addition, they are non-reactive in seawater, and conservative with respect to biological processes. Concurrent hydrographic measurements were included to put the radium distributions in the most understandable context. Previous studies of this type had little information available on the physical flow at the time of collection; most work had focused on the shelf alone, and neglected advective processes that could influence radium distribution. Correctly determining cross-shelf exchange is considered crucial for understanding fluxes of heat, salt and nutrients between the continental margins and the open ocean.

6.1 Summary of field study and expected results

Data were collected from 5 cruises with 8 cross shelf transects in both the northern and southern Mid-Atlantic Bight, as well as at the west wall of the Gulf Stream at Cape Hat-

teras. Cross-shelf radium activities, surface nutrient concentrations, salinity, XBT temperature profiles, and ADCP current velocities were measured with 10 km resolution along the northern transect. Detailed hydrography was also included over the southern MAB transects, with 5 km resolution. In the laboratory, tests were conducted to determine replicability and extraction efficiencies for the radium measurements.

We expected to find evidence of cross-shelf advection by small-scale or episodic processes, if they were occuring, or evidence of cross-shelf exchange by large-scale eddy mixing. The short-lived radium isotopes, ^{223}Ra and ^{224}Ra, are ideal for such measurements because of their mean lives on the order of days to weeks.

6.2 Major findings and significance for Mid-Atlantic Bight circulation and shelf-slope exchange

Contrary to expectations, we found little evidence of direct cross-shelf transport of shelf water, but did see evidence for strong influence from the Gulf Stream and adjacent slopewater on Mid-Atlantic Bight circulation. The most important findings include:

- Advection is an important consideration in radiotracer estimates of horizontal mixing, even with extremely low flow rates on the order of a centimeter per second. Determinations of κ from cross-shelf radium distributions using an advection-diffusion-decay model were highly dependent on precise estimates of the cross-shelf velocity w. Even in cases with $Pe << 1$ (diffusion dominant) flux calculations vary significantly depending on the choice of κ which can only be accurately determined if w is known precisely.

- The only evidence for cross-shelf transport of shelf water was in surveys NS2 and NS3 in which ^{223}Ra activities were high enough to employ ^{223}Ra:^{228}Ra ratios for water mass age estimates. Transport of nearshore water to the shelf edge was estimated to be about 20 days in both cases. From survey NS2, an additional 23 days was estimated for shelf water to cross the shelf-break jet, giving a cross-shelf transport time of approximately 43 days. The water on the seaward side of the jet is not expected to be from the same locale as the adjacent shelf water however, as it would have been advected down and through the shelfbreak jet. At an average jet velocity of 30 cm/s shelf water would travel approximately 1000 km alongshelf while making the cross-frontal transit.

- Cross-shelf nutrient flux calculations as they currently exist are subject to large errors. In addition to the difficulty of defining an accurate mixing coefficient κ, flux calculations are subject to large uncertainties from the lack of reliable long-term means for cross-shelf velocity and nutrient gradients, both of which can vary on time-scales as short as days. In our surveys during 1999-2000, nutrient gradients were of the same order of magnitude as previous studies such as SEEP I, but in the opposite direction. This presents an interesting situation for determining the magnitude and direction of nutrient flux across the shelf-slope boundary.

- Large volume transport of 1-2 Sv was measured across the southern Mid-Atlantic Bight shelf and shelfbreak. In this region there was a strong influence from the Gulf Stream and slope water. The resulting hydrographic structure, in particular the deep shelfbreak front, were consistent with large transport calculated across the shelf and shelfbreak. Transport numbers such as this have been found in other hydrographic

surveys where geostrophic velocity was calculated, but are significantly larger than estimates based on more broadly space moored time-series observations. Jet transport is a major component of the total that may be missed by moorings. If the larger transport numbers are accurate for the Mid-Atlantic Bight, inferred cross-shelf export of slopewater may be less than previously estimated in shelf transport budgets.

- Gulf Stream rings or meanders were present on 3 of 4 surveys and in all 3 cases anomalously high ^{224}Ra was found in high salinity water at the seaward end of the transect over the upper slope. These features complicate the traditional picture of exponential decrease of coastal radium with distance from shore, and introduce a potentially new source of ^{224}Ra from the vicinity of Cape Hatteras. Transport times based on ^{224}Ra:^{228}Ra ratios are similar to those recently published which are based on drifter data and South Atlantic Bight larval fish age distributions in the Mid-Atlantic Bight. Earlier findings of ^{222}Rn at the edge of a Gulf Stream ring in 1981 are also consistent with this transport scenario. Evidence suggesting a frequent transport route from Cape Hatteras onto the Mid-Atlantic Bight upper slope, combined with other data indicating direct cross-shelf exchange is perhaps smaller than previously estimated, points to the possibility that the dominant circulation in the Mid-Atlantic Bight is more similar to a "slope sea gyre" model than a "leaky current" model.

6.3 Recommendations for future work

Some of the most pressing needs during analysis of radiotracer, nutrient and hydrographic data during this study were for reliable long-term means that could be used to calculate volume fluxes and transport of heat, salt, and nutrients. Up to this point, the common

trade-off has been between spatial resolution and temporal resolution. The detailed time-series data that are available only describe physical properties (e.g. current velocity) and are limited by spatial resolution that may not capture essential features such as the shelfbreak jet. Even poorly resolved long-term means for cross-shelf nutrient gradients do not exist. Highly resolved hydrographic surveys are more common, but present only snapshots of water column structure, and most do not include chemical data for nutrients or tracers. With circulation and chemical gradients varying on timescales as short as days to weeks, it is difficult to determine how representative these snapshots are of either short-term (weeks to years) or long-term (decadal) means. Real progress in estimating overall budgets for the region may only be possible if high resolution time series data is obtainable for both physical and chemical properties. To achieve this, efforts of individual researchers may best be served by strategic long-term planning and both intra- and interdisciplinary collaboration, and may well require a type of early involvement and coordination with funding agencies that is not currently common.

References

Auer, S. J., 1987: Five-year climatological survey of the Gulf Stream system and its associated rings, *Journal of Geophysical Research*, **92**, 11709–11726.

Bacon, M., R. Belastock and M. Bothner, 1994: ^{210}Pb balance and implications for particle transport on the continental shelf, U.S. Middle Atlantic Bight, *Deep Sea Research II*, **41**(2/3), 511–536.

Bane, J. M., O. Brown and R. Evans, 1988: Gulf Stream remote forcing of shelfbreak currents in the Mid-Atlantic Bight, *Geophysical Research Letters*, **15**(5), 405–407.

Beardsley, R., W. Boicourt and D. Hansen, 1976: Physical oceanography of the Middle Atlantic Bight, *Limnology and Oceanography, Special Symposium*, **2**, 20–34.

Beardsley, R., D. Chapman, K. Brink, S. Ramp and R. Schlitz, 1985: The Nantucket Shoals Flux Experiment, I, A basic description of the current and temperature variability., *J. Phys. Oceanography*, **15**, 713–748.

Beardsley, R., C. Mills, J. A. Jermersch, W. Brown, N. Pettigrew, J. Irish, S. Ramp, R. Schlitz and B. Butman, 1983: The Nantucket Shoals Flux Experiment Part 2: Moored array data report., *WHOI Technical Report No. WHOI-83-13.*

Biscaye, P. E., C. Flagg and P. Falkowski, 1994a: The Shelf Edge Exchange Process Experiment, SEEP II: An introduction to hypotheses, results and conclusions., *Deep Sea Research, Part II*, **41**, 231–252.

Biscaye, P., C. Flagg and P. Falkowski, 1994b: The Shelf Edge Exchange Procceses experiment, SEEP-II: an introduction to hypotheses, results, and conclusions, *Deep Sea Research II*, **41**(2/3), 231–252.

Broecker, W., Y.-H. Li and J. Cromwell, 1967: Radium-226 and radon-222: Concentration in Atlantic and Pacific Oceans, *Science*, **158**, 1307.

Brown, O. B., P. C. C. adn S. R. Emerson and H. M. Carle, 1986: Gulf Stream Warm-Core Rings: A statistical study of their behavior, *Deep Sea Research*, **33**, 1459–1473.

Burrage, D., and R. Garvine, 1988: Summertime hydrography at the shelfbreak front in the Middle

Atlantic Bight, *J. Physical Oceanography*, **18**, 1309–1319.

Cable, J. E., W. C. Burnett, J. P. Chanton and G. L. Weatherly, 1996: Estimating groundwater discharge into the northeastern Gulf of Mexico using Radon-222, *Earth and Planetary Sciences Letters*, **144**(3-4), 591–604.

Chapman, D., and S. Lentz, 1994: Trapping of a coastal density front by the bottom boundary layer, *J. Physical Oceanography*, **24**(7), 1464–1479.

Charette, M. A., K. O. Buesseler and J. E. Andrews, 2001: Utility of radium isotopes for evaluating the input and transport of groundwater-derived nitrogen to a Cape Cod estuary, *Limnology and Oceanography*, **46**(2), 465–470.

Chung, Y., and W. Chang, 1996: Uranium and thorium isotopes in marine sediments off northeastern Taiwan, *Marine Geology*, **133**, 89–102.

Churchill, J. H., and P. C. Cornillon, 1991: Gulf Stream water on the shelf and upper slope north of Cape Hatteras, *Continental Shelf Research*, **11**(5), 409–431.

Cochran, J., H. Livingston, D. Hirschberg and L. Surprenant, 1987: Natural and anthropogenic radionuclide distributions in the northwest Atlantic ocean, *Earth Planet. Sci. Letters*, **84**, 135–152.

Csanady, G. T., and P. Hamilton, 1988: Circulation of slopewater, *Continental Shelf Research*, **8**(5-7), 565–624.

Dragos, P., F. A. III and D. Redford, 1998: Lagrangian statistics and kinematics from drifter observations pertaining to dispersion of sludge from the 106-Mile site, *Journal of Marine Environmental Engineering*, **2**, 21–41.

Drinkwater, K. F., R. A. Myers, R. G. Pettipas and T. L. Wright, 1994: Cimatic data for the Northwest Atlantic: The position of the shelf/slope front and the northern boundary of the Gulf Stream between 50°W and 75°W, 1973-1992, *Canadian Data Report Fisheries and Oceans Science*, **125**.

Eppley, R. W., and B. J. Peterson, 1979: Particulate organic matter flux and planktonic new

productionin the deep ocean, *Nature*, **282**, 670–680.

Falkowski, P., P. Biscaye and C. Sancetta, 1994: The lateral flux of biogenic particles from the eastern North American continental margin to the North Atlantic Ocean, *Deep Sea Research II*, **41**(2/3), 583–601.

Flagg, C., and R. Beardsley, 1978: On the stability of the shelf water/slope water front south of New England., *J. Geophysical Research*, **81**, 4623–4630.

Fong, D. A., 1998: Dynamics of Freshwater Plumes: Observations and Numerical Modeling of the Wind-forced Response and Alongshore Freshwater Transport, Ph.D. thesis, Massachusetts Institute of Technology/Woods Hole Oceanographic Institution.

Fratantoni, P. S., R. S. Pickart, D. J. Torres and A. Scotti, 2001: Mean structure and dynamics of the shelfbreak jet in the Middle Atlantic Bight during fall and winter, *Journal of Physical Oceanography*.

Garvine, R., K. Wong and G. Gawarkiewicz, 1989: Quantitative properties of shelbreak eddies, *J. Geophys. Res.*, **94**(C10), 14,475–14,483.

Garvine, R. W., K. C. Wong and G. G. Gawarkiewicz, 1988: Morphology of shelfbreak eddies, *J. Geophys. Res.*, **93**(C12), 15,593–15,607.

Gawarkiewicz, G., K. Brink, F. Bahr, R. Beardsley, M. Caruso, J. Lynch and C.-S. Chiu, submitted, 2002: A large amplitude meander of the shelfbreak front in the Middle Atlantic Bight: Observations from the Shelfbreak PRIMER Experiment, *Journal of Geophysical Resarch – Oceans*.

Gawarkiewicz, G., and D. Chapman, 1991: Formation and maintenance of shelf-break fronts, *Journal of Physical Oceanography*, **21**(8), 1225–1239.

Gawarkiewicz, G., T. Ferdelman, T. Church and G. Luther III, 1996a: Shelfbreak frontal structure on the continental shelf north of Cape Hatteras, *Continental Shelf Research*, **16**, 1751–1773.

Gawarkiewicz, G., C. Linder, J. Lynch, A. Newhall and J. Bisagni, 1996b: A surface-trapped intrusion of slope water onto the continental shelf in the mid-Atlantic bight, *Geophysical Research Letters*, **23**(25), 3763–3766.

Gawarkiewicz, G., R. McCarthy, K. Barton, A. Masse and T. Church, 1990: A Gulf Stream-Derived Pycnocline Intrusion on the Middle Atlantic Bight Shelf, *Journal of Geophysical Research*, **95**(C12), 22,305–22,313.

Gawrkiewicz, G., T. Church, G. Luther III, T. Ferdelman and M. Caruso, 1992: Large-scale penetration of Gulf Stream water onto the continental shelf north of Cape Hatteras, *Geophysical Research Letters*, **19**(4), 373–376.

Gordon, A. L., and F. Aikman, 1981: Salinity maximum in the pycnocline of the Middle Atlantic Bight, *Limnology and Oceanography*, **26**, 123–130.

Hare, J. A., J. H. Churchill, R. Cowen, T. J. Berger, P. C. Cornillon, P. Dragos, S. M. glenn, J. J. Govoni and T. N. Lee, 2002: Routes and rates of larval fish transport from the southeastern to the northeastern United States continental shelf, *Limnology and Oceanography*, **47**(6).

Harms, S., and C. D. Winant, 1998: Characteristic patterns of the circulation in the Santa Barbara Channel, *Journal of Geophysical Research*, **103**(C2), 3041–3065.

Harris, C. K., and P. Wiberg, 2002: Across-shelf sediment transport: Interactions between suspended sediment and bed sediment, *Journal of Geophysical Research*, **107**(C1), 8/0.531–8/12.

Hickey, B. M., 1993: Physical Oceanography., in *Ecology of the Southern California Bight: A Synthesis and Interpretation.*, edited by M. Dailey, D. Reish, , and J. Anderson, pp. 19–70, University of California Press, Berkeley, CA.

Houghton, R. W., 1997: Lagrangian flow at the foot of a shelfbreak front using a dye tracer injected into the bottom boundary layer., *Geophysical Research Letters*, **24**, 2035–2038.

Houghton, R. W., C. N. Flagg and C. J. Pietrafesa, 1994: Shelf-slope frontal structure, motion, and eddy heat flux in the southern Middle Atlantic Bight, *Deep Sea Research*, **41**(2/3), 273–306.

Houghton, R. W., and J. Marra, 1983: Physical/biological Structure and Exchange Across the Thermohaline Shelf/Slope Front in the New York Bight, *Journal of Geophysical Research*, **88**(C7), 4467–4481.

Houghton, R. W., R. Schlitz, R. C. Beardsley, B. butman and J. L. Chamberlain, 1982: The Middle

Atlantic Bight Cold Pool: Evolution of the Temperature Structure During Summer 1979, *Journal of Physical Oceanography*, **12**, 1019–1029.

Houghton, R. W., and M. Visbeck, 1998: Upwelling and convergence in the Middle Atlantic Bight shelf break front, *Geophysical Research Letters*, **25**, 2765–2768.

Jenkins, W. J., 1987: ^{3}H and ^{3}He in the Beta Triangle: observations of gyre ventilation and oxygen consumption rates., *J. Phys. Oceanogr.*, **17**, 763–783.

Joyce, T. M., 1984: Velocity and hydrographic structure of a Gulf Stream warm-core ring, *Journal of Physical Oceanography*, **14**, 936–947.

Joyce, T. M., 1991: Review of U.S. Contributions to Warm-Core Rings, *Review of Geophysics, Supplement*, pp. 610–616.

Joyce, T. M., J. K. B. Bishop and O. B. Brown, 1992: Observations of offshore shelf-water transport induced by a warm-core ring, *Deep-Sea Research*, **39 Suppl.1**, S97–S113.

Kaufman, A., R. Trier, W. Broecker and H. Feely, 1973: Distribution of ^{228}Ra in the World Ocean, *Journal of Geophysical Research*, **78**(36), 8827–8848.

Kemp, P., 1994: Microbial carbon utilization on the continental shelf and slope during the SEEP II experiment, *Deep Sea Research II*, **41**(2/3), 563–581.

Krest, J. M., W. S. Moore and Rama, 1999: ^{226}Ra and ^{228}Ra in the mixing zones of the Mississippi and Atchafalaya Rivers: indicators of groundwater input, *Marine Chemistry*, **64**, 129–152.

Levy, D. M., and W. S. Moore, 1985: ^{224}Ra in Continental Shelf waters, *Earth and Planetary Science Letters*, **73**, 226–230.

Li, Y., H. Feely and P. Santschi, 1979: ^{228}Th–^{228}Ra disequilibrium in the New York Bight and its implications for coastal pollution, *Earth and Planetary Science Letters*, **42**, 13–26.

Linder, C., and G. Gawarkiewicz, 1998: A climatology of the shelfbreak front in the Middle Atlantic Bight, *J. Geophysical Research*, **103**(C9), 18,405–18,423.

Linder, C. A., 1996: A Climatology of the Middle Atlantic Bight Shelfbreak Front, Master's thesis, MIT/Woods Hole Oceanographic Institution.

Loder, J., B. Petrie and G. Gawrkiewicz, 1998: in *The Sea*, vol. 11, edited by A. Robinson, and K. Brink, chapter 5. The Coastal Ocean off Northeastern North America: A Large Scale View, pp. 105–133, John Wiley & Sons, Inc.

Lozier, M. S., M. S. C. Reed and G. Gawarkiewicz, 2002: Instability of a shelfbreak front, *Journal of Physical Oceanography*, **32**, 924–944.

Lyne, V., and G. Csanady, 1984: A compilation and description of hydrographic transects of the Mid Atlantic Bight shelfbreak front, *WHOI Technical Report 84-19.*

Mahadevan, A., and D. Archer, 2000: Modeling the impact of fronts and mesoscale circulation on the nutrient supply and biogeochemistry of the upper ocean, *Journal of Geophysical Research*, **105**(C1), 1209–1225.

Michaels, A., D. Olson, J. Sarmiento, J. Ammerman, K. Fanning, R. Jahnke, A. Knap, F. Lipschultz and J. Prospero, 1996: Inputs, losses and transformations of nitrogen and phosporous in the pelagic North Atlantic Ocean, *Biogeochemistry*, **35**(1), 181–226.

Moody, J. A., B. Butman, R. C. Beardsley, W. S. Brown, P. Daifuku, J. D. Irish, D. A. Mayer, H. O. Mofjeld, B. Petrie, S. Ramp, P. Smith and W. R. Wright, 1984: *Atlas of tidal elevation and current observations on the northeast American Continental shelf and slope*, p. 100, U. S. Geological Survey Bulletin 1611.

Mooers, C., J. Fernandez-Partagas and J. Price, 1976: Meteorological forcing fields of the New York Bight (First Year's Progress Report, *Tech. Rep. TR76-8*, , Rosensteil School of Marine and Atmospheric Science, University of Miami.

Moore, W., 1997: ^{226}Ra, ^{228}Ra, ^{223}Ra, and ^{224}Ra in coastal waters with application to coastal dynamics and groundwater input, *Radioprotection — Colloques*, **32**(C2), 137–146.

Moore, W. S., 1996: Large groundwater inputs to coastal waters revealed by ^{226}Ra enrichments, *Nature*, **380**, 612–614.

Moore, W. S., and R. Arnold, 1996: Measurement of ^{223}Ra and ^{224}Ra in coastal waters using a delayed coincidence counter, *Journal of Geophysical Research*, **101**, 1321–1329.

Moore, W. S., K. W. Bruland and J. Michel, 1981: Fluxes of uranium and thorium series isotopes in the Santa Barbara Basin, *Earth and Planetary Science Letters*, **53**, 391–399.

Moore, W. S., and T. J. Shaw, 1998: Chemical signals from submarine fluid advection onto the continental shelf, *Journal of Geophysical Research*, **103**(C10), 21,543–21,552.

Moore, W. S., 1969: Oceanic concentrations of ^{228}Ra, *Earth and Planetary Science Letters*, **6**, 437–446.

Moore, W. S., 1976: Sampling ^{228}Ra in the deep ocean, *Deep Sea Research*, **23**, 647–651.

Moore, W. S., 2000a: Determining coastal mixing rates using radium isotopes, *Continental Shelf Research*, **20**, 1993–2007.

Moore, W. S., 2000b: Ages of continental shelf waters determined from ^{223}Ra and ^{224}Ra, *Journal of Geophysical Research*, **105**(C9), 22,117–22,122.

Musgrave, D. L., 1985: A numerical study of the roles of subgyre-scale mixing and the western boundary current on homogenization of a passive tracer, *J. Geophys. Res.*, **90**, 7037–7043.

NCRP, 1987: NCRP Report No. 94: Exposure of the Population in the United States and Canada from Natural BackgroundRadiation, *Tech. rep.*, , National Council on Radiation Protection and Measurements.

Nixon, S., J. Ammerman, L. Atkinson, V. Berounsky, G. Billen, W. Boicort, W. Boynton, T. Church, D. Ditoro, R. Elmgren, J. Garber, A. Giblin, R. Jahnke, N. Owens, M. Pilson and S. Seitzinger, 1996: The fate of nitrogen and phosphorus at the land-sea margin of the North Atlantic Ocean, *Biogeochemistry*, **35**, 141–180.

Nof, D., 1986: The collision between the Gulf Stream and warm-core rings, *Deep Sea Research*, **33**(3), 359–378.

Nof, D., 1988: The propagation of "streamers" along the periphery of warm-core rings, *Deep Sea Research*, **35**(9), 1483–1498.

Nozaki, Y., H.-S. Yang and M. Yamada, 1987: Scavenging of thorium in the ocean, *J. Geophys. Res.*, **92**(C1), 772–778.

Orr, J. C., N. L. G. Jr. and D. R. Schink, 1985: ^{222}Rn Surpluses in Warm-Core Rings, *Journal of Geophysical Research*, **90**(C5), 8903–8916.

Page, F., R. Losier, K. Drinkwater, B. Petrie, G. Harrison and D. Sameoto, 2001: Overview of Physical and Biological Oceanographic Conditions on Georges Bank, *Tech. rep.*, , Canadian Science Advisory Secretariat, Fisheries and Oceans Science.

Pickart, R. S., 2000: Bottom boundary layer structure and detachment in the shelfbreak jet of the Middle Atlantic Bight, *Journal of Physical Oceanography*, **30**(11), 2669–2686.

Rama, and W. S. Moore, 1996: Using the radium quarter for evaluating groundwater input and water exchange in salt marshes, *Geochim. Cosmochim. Acta.*, **60**, 4645–4652.

Ramp, S. R., 1989: Moored observations of current and temperature on the shelf and upper slope near Ring 82B, *Journal of Geophysical Research*, **94**, 18071–18087.

Ramp, S. R., W. S. Brown and R. C. Beardsley, 1988: The Nantucket Shoals Flux Experiment 3. The Alongshelf Transport of Volume, Heat, Salt and Nitrogen, *Journal of Geophysical Research*, **93**(C11), 14,039–14,054.

Sarin, M., S. Krishnaswami, R. Dalai, V. Ramaswamy and V. Ittekkot, 2000: Settling fluxes of U- and Th-series nuclides in the Bay of Bengal: results from time-series sediment trap studies, *Deep-Sea Research I*, **47**, 1961–1985.

Savidge, D., and J. Bane, 2001: Wind and Gulf Stream influences on along-shelf transport and off-shelf export at Cape Hatteras, North Carolina, *J. Geophysical Research*, **106**(C6), 11,505–11,527.

Schlitz, R., J. P. Manning and K. W. Smith, 2001: Structure and transport of alongshelf currents across the southern flank of Georges Bank during late summer, 1982, *Deep Sea Research II*, **48**(1-3), 341–372.

Schmidt, S., and J.-L. Reyss, 1996: Radium as internal tracer of Mediterranean Outflow Water, *Journal of Geophysical Research*, **101**(C2), 3589–3596.

Seitzinger, S., and A. Giblin, 1996: Estimating denitrification in North American continental shelf sediments, *Biogeochemistry*, **35**(1), 235–260.

Shaw, T. J., and W. S. Moore, 2002: Analysis of ^{227}Ac in seawater by delayed coincidence counting, *Marine Chemistry*, **78**(4), 197–203.

Shearman, R. K., and S. J. Lentz, submitted: Mean and subtidal currents on the New England Shelf during the Coastal Mixing and Optics Experiment, August 1996-June 1997, *Journal of Geophysical Research.*

Smoak, J., W. Moore, R. Thunell and T. Shaw, 1999: Comparison of ^{234}Th, ^{238}Th, and ^{210}Pb fluxes with fluxes of major sediment components in the Guaymas Basin, Gulf of California, *Marine Chemistry*, **65**(3-4), 177–194.

Smoak, J., W. S. Moore and R. C. Thunell, 2000: Influence of boundary scavenging and sediment focusing on ^{234}Th, ^{228}Th and ^{210}Pb fluxes in the Santa Barbara basin, *Estuarine, Coastal and Shelf Science*, **51**, 373–384.

Somayajulu, B. L. K., M. M. Sarin and R. Ramesh, 1996: Denitrification in the eastern Arabian Sea: Evaluation of the role of continental margins using Ra isotopes, *Deep-Sea Research II*, **43**(1), 111–117.

Srisuksawad, K., B. Porntepkasemsan, S. Nouchpromool, P. Yamkate, R. Carpenter, M. Peterson and T. Hamilton, 1997: Radionuclide activities, geochemistry and accumulation rates of sediments in the Gulf of Thailand, *Continental Shelf Research*, **17**(8), 925–965.

Torgersen, T., K. Turekian, V. Turekian, N. Tanaka, E. DeAngelo and J. O'Donnell, 1996: ^{224}Ra distribution in surface and deep water of Long Island Sound: sources and horizontal transport rates, *Continental Shelf Research*, **16**(12), 1545–1559.

Ullman, D., and P. Cornillon, 2001: Continental shelf surface thermal fronts in winter off the northeast US coast, *Continental Shelf Research*, **21**, 1139–1156.

Ullman, D., and P. Cornillon, 1999: Satellite-derived sea surface temperature fronts on the continental shelf off the northeast U.S. coast, *Journal of Geophysical Research*, **104**(C10), 23,459–23,478.

Voorhis, A. D., D. Webb and R. C. Millard, 1976: Current Structure and Mixing in the Shelf/Slope Waterfront South of New England., *Journal of Geophysical Research*, **81**(21), 3695–3708.

Webster, I. T., G. J. Hancock and A. S. Murray, 1995: Modelling the effect of salinity on radium desorption from sediments, *Geochimica and Cosmochimica Acta*, **59**(12), 2469–2476.

Wright, L., C. Friedrichs, S. Kim and M. Scully, 2001: Effects of ambient currents and waves on gravity-driven sediment transport on continental shelves, *Marine Geology*, **175**, 25–45.

Wright, W. R., and C. E. Parker, 1976: A volumetric temperature/salinity census for the Middle Atlantic Bight, *Journal of Marine Research*, **34**, 1–14.

Yankovsky, A., and D. Chapman, 1997: A simple theory for the fate of buoyant coastal discharges, *Journal of Physical Oceanography*, **27**, 1386–1401.